Chemistry of the Lanthanides with Pyrazolylborate Ligands

Graham Maunder

Thesis submitted in part fulfilment of the requirements of
University College London for the degree of Doctor of Philosophy

Christopher Ingold Laboratories
Department of Chemistry

June 1996

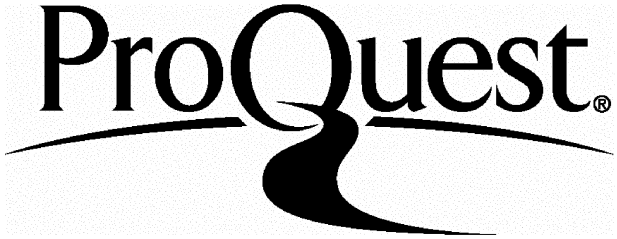

Abstract

In the work presented in this thesis we have established the utility of the substituted *tris*-(pyrazolyl)borates as ancillary ligands for the lanthanides.

Compounds of formula $(Tp^{Me2})_2LnOTf$ have been synthesised.[1,2] For the larger lanthanides, the triflate group is coordinated to the metal, $[(Tp^{Me2})_2LnOTf]$ (Ln = La and Nd), whilst for the smaller elements ion pair complexes are formed, $[(Tp^{Me2})_2Ln]^+[OTf]^-$ (Ln = Y, Dy and Yb); the structures of the Nd and Yb complexes have been determined. For lanthanides of intermediate ionic radius (Ln = Sm), there are good indications that these two structural forms coexist in $CDCl_3$. Attempts to derivatise these complexes were not successful.

Reduction of $(Tp^{Me2})_2LnOTf$ (Ln = Sm, Eu and Yb) gave $[(Tp^{Me2})_2Ln]$;[1] the related $[(Tp^{Me2\text{-}4\text{-}Et})_2Ln]$ complexes were also prepared. $[(Tp^{Me2})_2Ln]$ (Ln = Eu and Yb) were characterised by X-ray crystallography and found to be isomorphous. Initial reactivity studies showed that $[(Tp^{Me2})_2Ln]$ and $[(Tp^{Me2\text{-}4\text{-}Et})_2Ln]$ were significantly less reactive than the decamethyllanthanocenes. They were found to react with TCNQ and TCNE and in the case of the Yb complexes, the products were simple charge transfer salts; the X-ray crystal structure of $[(Tp^{Me2})_2Yb]^+[TCNE]^-$ was determined. The hydrolysis product $[(Tp^{Me2})Sm\{(pz^{Me2})_2B(H)(\mu\text{-}O)\}]_2.(THF)_2$ was also characterised crystallographically. Reaction of $[(Tp^{Me2\text{-}4\text{-}Et})_2Ln]$ with NO gave nitrito complexes and the structure of $[(Tp^{Me2\text{-}4\text{-}Et})_2Sm(\eta^2\text{-}O_2N)]$ was determined by X-ray crystallography. It was not possible to isolate stable half sandwich complexes of the divalent lanthanides with these 3-Me substituted *tris*-(pyrazolyl)borates.

In contrast, the stable monomeric complexes $[Tp^{3\text{-}t\text{-}Bu\text{-}5\text{-}Me}SmI(THF)_2].(Et_2O)_{0.5}$ and $[Tp^{3\text{-}t\text{-}Bu\text{-}5\text{-}Me}YbI(THF)]$ were prepared and characterised crystallographically.[3] These compounds could be desolvated, and pyridine and isonitrile adducts were prepared; the X-ray crystal structures of $[Tp^{3\text{-}t\text{-}Bu\text{-}5\text{-}Me}LnI(3,5\text{-}Me_2py)_2]$ and $[Tp^{3\text{-}t\text{-}Bu\text{-}5\text{-}Me}LnI(CNBu^t)]$ have been determined. $[Tp^{3\text{-}t\text{-}Bu\text{-}5\text{-}Me}YbBH_4(THF)]$ was prepared by reaction of $[Tp^{3\text{-}t\text{-}Bu\text{-}5\text{-}Me}YbI(THF)]$ with $NaBH_4$. This compound decomposes on heating to give at least two new products, the nature of which remains to be established.

Contents

Figures and Tables

Acknowledgements

In time honoured tradition, I firstly thank my supervisor, Dr Andrea Sella, for his support, encouragement, expertise and unfailing enthusiasm in all aspects of chemistry. I am also indebted to Dr Graeme Hogarth (for invaluable use of his glove box), Dr Derek Tocher (for his encouragement in all things crystallographic), Dr Nik Kaltsoyannis (for very useful discussions) and Dr Ivan Parkin (for his help with X-ray powder diffraction) of the Christopher Ingold Laboratories. I am fortunate to have been involved in a number of collaborative projects: with Dr Jennifer Green, Kathryn Longley and Richard Parkin of the University of Oxford (PE spectroscopy of $[(Tp^{Me_2})_2Ln]$ and $[(Tp^{Me_2\text{-}4\text{-}Et})_2Ln]$), Dr Norman Edelstein of the Lawrence Berkeley Laboratories, California (optical and magnetic measurements on $[(Tp^{Me_2})_2Ln]$ and $[(Tp^{Me_2\text{-}4\text{-}Et})_2Ln]$) and Dr Mark Elsegood of the University of Newcastle (X-ray crystal structures of complexes **3.15** and **3.18**) - I thank them for their support and interest in my work.

My thanks are due to Alan Stones for his cooperation and expertise in obtaining elemental analyses on air sensitive samples. In addition, I thank Chris Cooksey and Jill Maxwell (for their help with NMR), Dr Dave Humphrey (for useful discussions on vibrational spectroscopy and many other topics), Dr Patrick Barrie and Dave Butler (for running solid state CP MAS NMR spectra), Dr Christopher Dobson of the University of Oxford (for discussions on the NMR spectroscopy of paramagnetic complexes) and Dave Knapp and Joe Nolan (for keeping our failing laboratory equipment up and running and replacing it, when necessary, at knock-down prices).

Some of my work on the divalent lanthanide pyrazolylborates was carried out simultaneously by Professor Josef Takats and Dr Xing Zhang of the University of Alberta, and I am grateful for the fruitful collaboration which has resulted from our common interests.

I thank my peers in the laboratory - Tiz Coffey, Simon Redmond, Andy Pateman, Dr Mark Lavender, Dr Tim Norman, Dr Glyn Forster, Maya Stevenson and Danya Corby - for their friendship and support over the years. I am especially grateful to Sung-Ying Liu for enlightening discussions on lanthanide pyrazolylborate chemistry and much more.

Finally, I would like to thank Rebecca for her love, encouragement and latterly, financial backing; I dedicate this thesis to her.

Abbreviations and Symbols

A	ancillary ligand
acac	acetylacetonate
acacH	acetylacetone
a_N	electron-nucleus hyperfine splitting constant
as	antisymmetric mode
bd	bending mode
BM	Bohr magneton
Bp	dihydrido-*bis*-(pyrazol-1-yl)borate
Bp^{Me2}	dihydrido-*bis*-(3,5-dimethylpyrazol-1-yl)borate
br	broad
Bu^n	*n*-butyl
Bu^t or *t*-Bu	*tert*-butyl
Bu^t_2DAB	1,4-di-*tert*-butyldiazabutadiene
χ	bulk magnetic susceptibility
COT	cyclooctatetraenyl (C_8H_8)
CP MAS	cross-polarised magic angle spinning
Cp	cyclopentadienyl (C_5H_5)
Cp^*	pentamethylcyclopentadienyl (C_5Me_5)
δ	chemical shift (ppm)
d	doublet
D', D''	molecular susceptibility anisotropies
Δ_c	contact (Fermi) shift
Δ_e	exchange broadening of nuclear magnetic resonance peak
$\Delta G^{\ddagger}$	free energy of activation (kJ mol^{-1})
$\Delta H^{\ddagger}$	enthalpy of activation (kJ mol^{-1})
DME	dimethoxyethane
DMEN	*N,N*-dimethylethylenediamine
Δ_p	dipolar (pseudocontact) shift
$\Delta S^{\ddagger}$	entropy of activation (J mol^{-1})
ε	molar absorption coefficient (M^{-1} cm^{-1})
en	ethylenediamine
EPR	electron paramagnetic resonance
esd	estimated standard deviation
Et	ethyl
E°	standard electrode potential
FAB	fast atom bombardment

g	electron g-factor
γ	magnetogyric ratio
g_e	free electron g-factor (2.0023)
HMPA	hexamethylphosphoramide
HOMO	highest occupied molecular orbital
I	nuclear spin
In^*	permethylindenyl (C_9Me_7)
IR	infrared
J	coupling constant
J	spin-orbital angular momentum
k	Boltzmann constant (1.38066×10^{-23} J K^{-1})
k_A	rate constant
k_c	rate constant at the coalescence temperature
L	neutral ligand
L	total orbital angular momentum
Ln	lanthanide (La to Lu and Y)
M	metal
m/z	mass to charge ratio
μ_B	Bohr magneton (9.27408×10^{-24} J T^{-1})
Me	methyl
μ_{eff}	effective magnetic moment
m_l	electron orbital angular momentum
MO	molecular orbital
m_s	electron spin quantum number
N-MeIm	*N*-methylimidazole
N_A	Avogadro constant (6.023×10^{23} mol^{-1})
NMR	nuclear magnetic resonance
$\nu_{X\text{-}Y(mode)}$	infrared X-Y stretching frequency (type of vibrational mode in parentheses)
OTf	trifluoromethanesulphonate (triflate; O_3SCF_3)
PE	photoelectron
Ph	phenyl
Pr^i or *i*-Pr	*iso*-propyl
py	pyridine
pz	pyrazolyl
pzTp	*tetrakis*-(pyrazol-1-yl)borate
Θ	temperature correction term in the Curie-Weiss equation
θ	cone angle (°)
q	quartet
R, R', R'', R'''	alkyl or aryl groups

S	total electron spin quantum number
s	singlet
s	symmetric mode
sh	shoulder
SP	square pyramidal
st	stretching mode
T	temperature (K)
t	triplet
TBP	trigonal bipyramidal
T_c	coalescence temperature (K)
TCNE	tetracyanoethylene
TCNQ	tetracyanoquinodimethane
THF	tetrahydrofuran
TMEDA	tetramethylethylenediamine
Tp	hydrido-*tris*-(pyrazol-1-yl)borate
Tp'	*tris*-(pyrazolyl)borate
$Tp^{3\text{-a-5-Me}}$	hydrido-*tris*-(3-methyl-2-*H*-benz[g]-4,5-dihydroindazol-2-yl)borate
$Tp^{3\text{-}i\text{-Pr-4-Br}}$	hydrido-*tris*-(3-*i*-propyl-4-bromopyrazol-1-yl)borate
$Tp^{3\text{-}i\text{-Pr-5-Me}}$	hydrido-*tris*-(3-*iso*-propyl-5-methylpyrazol-1-yl)borate
$Tp^{3\text{-Ph-5-Me}}$	hydrido-*tris*-(3-phenyl-5-methylpyrazol-1-yl)borate
$Tp^{3\text{-}t\text{-Bu-5-Me}}$	hydrido-*tris*-(3-*tert*-butyl-5-methylpyrazol-1-yl)borate
Tp^{a}	hydrido-*tris*-(2-*H*-benz[g]-4,5-dihydroindazol-2-yl)borate
Tp^{Me_2}	hydrido-*tris*-(3,5-dimethylpyrazol-1-yl)borate
$Tp^{Me_2\text{-4-Et}}$	hydrido-*tris*-(3,5-dimethyl-4-ethylpyrazol-1-yl)borate
Tp^{Ph}	hydrido-*tris*-(3-phenylpyrazol-1-yl)borate
$Tp^{pyridyl}$	hydrido-*tris*-(3-(2'-pyridyl)pyrazol-1-yl)borate
$Tp^{t\text{-Bu}}$	hydrido-*tris*-(3-*tert*-butylpyrazol-1-yl)borate
Tp^{Tn}	hydrido-*tris*-(3-(2'-thienyl)pyrazol-1-yl)borate
triflate	trifluoromethanesulphonate (OTf; O_3SCF_3)
triflic acid	trifluoromethanesulphonic acid (HOTf; HO_3SCF_3)
UV	ultraviolet
vis	visible
ω	wedge angle (°)
$w_{1/2}$	width at half height
X	anionic ligand

Chapter 1 - Review of the Chemistry of the Lanthanides and of *Poly*-(pyrazolyl)borate Ligands

Introduction[4,5]

The lanthanides are the 14 elements that follow lanthanum in the periodic table. The most characteristic feature of these elements is that they have very similar chemical properties which they share with scandium, yttrium and lanthanum of Group 3. Indeed, when the mineral ceria was isolated in 1803 (independently by Klaproth and Berzelius & Hisinger) it was thought to be the oxide of a single element, and it was not until 1839 that Mosander showed that both ceria and yttria (first reported by Gadolin in 1794) were different mixtures of what turned out to be the 13 non-radioactive lanthanides, together with scandium, yttrium and lanthanum. The problems encountered in early studies of these elements were quite considerable - the almost identical chemistries of the lanthanides meant that repeated fractional recrystallisations were typically required in order to obtain pure compounds - and consequently, the elements remained chemical curiosities.

Two events led to rapid advances in lanthanide chemistry. The first was the development in the late 19th century of the Thoria Coal Gas Mantle (99 % ThO_2 and 1 % CeO_2) by von Welsbach.[6] The large scale mining of thorium containing ores which followed, produced large quantities of lanthanide oxides as by-products and caused renewed interest in the chemistry and potential applications of these elements. More significantly, research into f element chemistry was an important aspect of the Manhattan Project during the Second World War. This work led to the development of ion exchange (by the groups of Cohn[7] and Spedding[8]) and solvent extraction[9] techniques, which at last provided the means of separating the lanthanides efficiently and economically. In addition, these elements were a major product of many of the nuclear fission processes under investigation, and the 14th lanthanide, radioactive promethium, was identified in 1947 by Coryell and coworkers as one of the products of ^{235}U disintegration.[10]

It is now well established that the lanthanide elements exhibit properties that are quite distinct from those of typical transition metals. Their unique chemistry is a consequence of the fact that their valence electrons lie in 4f orbitals which are both poorly shielding and have small radial extension.[11] This has a direct

effect both on the relative stabilities of the oxidation states of these elements and the bonding which is found in their compounds.

The remainder of this chapter provides an overview of the properties and chemistry of the lanthanides and of the *poly*-(pyrazolyl)borate ligand system. This includes a survey of lanthanide *tris*-(pyrazolyl)borate complexes reported in the literature prior to 1993. As is usual, the symbol Ln has been used throughout this thesis to denote some or all of the elements lanthanum to lutetium inclusive, and yttrium.

Oxidation States of the Lanthanides[12]

For all of the lanthanides, removal of the first three electrons from the atom is relatively facile and is easily compensated for by the high lattice and solvation energies of the trivalent ions.[13] In this, the most stable oxidation state of these elements, the 4f electrons are buried deep in the core of the ion,[14] and their poor shielding properties cause the 'closed shell' outer electrons (5p, 5s) to experience a steady increase in relative nuclear charge as the series is traversed. This manifests itself in a regular contraction in the radii of the ions from La^{3+} (1.032 Å) to Lu^{3+} (0.861 Å), and is responsible for the ionic radius of Y^{3+} (0.900 Å) being almost exactly the same as that of Ho^{3+} (0.901 Å); Sc^{3+} is somewhat smaller with an ionic radius of 0.745 Å.[15] The 'lanthanide contraction' has the effect of making the removal of a fourth electron progressively more difficult with increasing atomic number, and as a result, the only well characterised solution chemistry of a tetravalent lanthanide is that of Ce^{4+} ($[Xe]4f^0$). It should be noted that despite the contraction in ionic radius which occurs across the series, the lanthanides are comparatively large with respect to the d block metals, for example, Fe^{3+} and Rh^{3+} have ionic radii of 0.645 and 0.665 Å, respectively.[15]

Divalent ions have been detected for all the lanthanides upon γ-irradiation of the trivalent ions doped into CaF_2[16] and also in $Ln/LnCl_3$ melts.[17] In addition, several divalent lanthanides have been observed as poorly characterised species in aprotic solvents.[18] Standard electrode potentials (E°) between the trivalent and divalent oxidation states have been measured for all of the lanthanides (Table 1.1).[17,19]

Table 1.1 Standard Electrode Potentials (E°) for the Couple Ln^{3+}/Ln^{2+}

Couple	Potential (V)
$E°(Y^{3+}/Y^{2+})$	-
$E°(La^{3+}/La^{2+})$	-2.94
$E°(Ce^{3+}/Ce^{2+})$	-2.92
$E°(Pr^{3+}/Pr^{2+})$	-2.84
$E°(Nd^{3+}/Nd^{2+})$	-2.62
$E°(Pm^{3+}/Pm^{2+})$	-2.44
$E°(Sm^{3+}/Sm^{2+})$	-1.50
$E°(Eu^{3+}/Eu^{2+})$	-0.34

Couple	Potential (V)
$E°(Gd^{3+}/Gd^{2+})$	-2.85
$E°(Tb^{3+}/Tb^{2+})$	-2.83
$E°(Dy^{3+}/Dy^{2+})$	-2.56
$E°(Ho^{3+}/Ho^{2+})$	-2.79
$E°(Er^{3+}/Er^{2+})$	-2.87
$E°(Tm^{3+}/Tm^{2+})$	-2.22
$E°(Yb^{3+}/Yb^{2+})$	-1.18
$E°(Lu^{3+}/Lu^{2+})$	-2.72

By far the most stable divalent species are Sm^{2+}, Eu^{2+} and Yb^{2+}, and it is only these that have a well established solution chemistry and for which crystallographic characterisation has been obtained in this oxidation state. Divalent compounds of these three lanthanides, particularly Sm^{2+}, are widely used to perform one electron reductions in organic synthesis.[20]

The relative stabilities of the trivalent and divalent ions is expected to parallel the third ionisation energy of the lanthanides (Figure 1.1), since other thermodynamic factors such as solvation and lattice energies of the ions vary smoothly across the series on account of the regular lanthanide contraction. Hence, in order to understand the observed variations in the stability of the divalent ions, it is first necessary to consider what influences the size of the third ionisation energy of these elements.

The magnitude of the third ionisation energy is determined by three terms: the coulombic attraction between the nucleus and the electrons, the interelectron repulsion, and the change in exchange energy which accompanies the removal of the electron. The first two of these vary smoothly as the ionic radius changes, hence, the observed irregularities in the third ionisation energy have their origins in the exchange energy term. This quantity rises from zero upon removal of the single electron from a $[Xe]4f^1$ ion ($La^{2+} \rightarrow La^{3+} + e^-$) to a maximum for a $[Xe]4f^7$ configuration ($Eu^{2+} \rightarrow Eu^{3+} + e^-$). Removal of a third electron from Gd^{2+} ($[Xe]4f^8$) breaks this trend because the ionisation is not subject to any exchange energy loss and is therefore relatively facile. Thereafter the pattern is repeated: the third ionisation energy increases to a

maximum for Yb before dropping back sharply again for Lu. Whilst this explains the general trends observed in the third ionisation energy, it fails to account for the somewhat irregular behaviour at the quarter and three-quarter full 4f shell configurations. These arise because electrons which are rotating in the same sense (*ie* their angular momenta have the same sign) do not repel each other as much as those which rotate in opposite senses. This means that the third ionisation of Pr (for Pr^{2+}, $[Xe]4f^3$, $m_l = 3, 2$ and 1) removes an electron which is repelled to a lesser degree by those which remain than in the corresponding ionisation for Pm (for Pm^{2+}, $[Xe]4f^5$, $m_l = 3, 2, 1, 0$ and -1). Hence, the process $Pm^{2+} \rightarrow Pm^{3+} + e^-$ is easier than expected, and $Pr^{2+} \rightarrow Pr^{3+} + e^-$ is more difficult. A similar argument applies to the third ionisation potentials in the second half of the series, where the effect is more marked due to the increased interelectron repulsion caused by the contraction of the 4f orbitals.

Figure 1.1 A Comparison of the Third Ionisation Energy of the Lanthanides with the Relative Stability of the Trivalent and Divalent Ions[12,17]

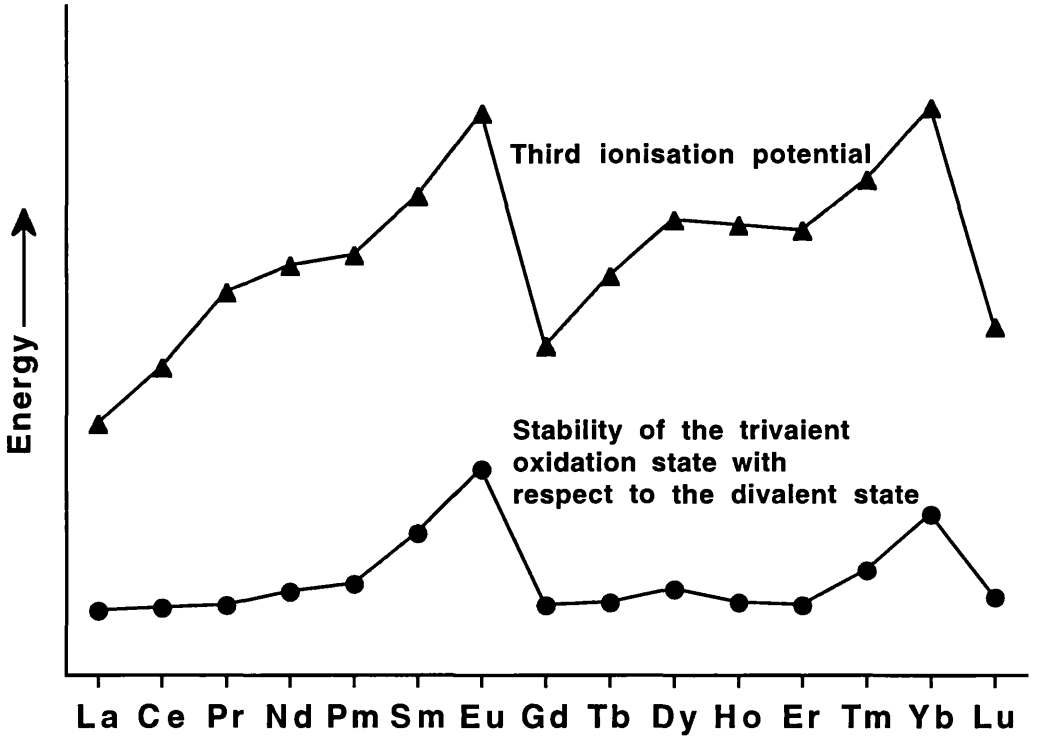

We can now consider the relative stabilities of the divalent ions. These do broadly follow the trend observed in the third ionisation energy of the

lanthanides (Figure 1.1), the principal exceptions being the divalent ions of La, Ce, Gd and Tb which are all found to have greater stability than expected. This is caused by the preferential occupancy of a 5d orbital by one of the valence electrons, where it becomes stabilised by the ligand field. For the free La^{2+} ion the 5d orbitals lie below the 4f in energy, and hence, the ground state electron configuration is $[Xe]5d^1$ anyway. This situation is reversed for the next element, Ce, due to the rapid contraction of the 4f orbitals with increasing atomic number. Nevertheless, when the Ce^{2+} ion is placed in a ligand field, it becomes energetically advantageous to promote one electron to a 5d orbital where it is stabilised. However, for Pr^{2+} the stabilisation of the 4f orbitals is so far advanced that a similar rearrangement of electrons is no longer energetically favourable, and this situation remains true until we reach Gd^{2+} which has eight valence electrons. The onset of electron pairing, which must occur for a $4f^8$ configuration, instead causes the ground state for Gd^{2+} to be $[Xe]4f^75d^1$. Finally, in a similar manner to Ce^{2+}, when Tb^{2+} ($4f^9$) is placed in a ligand field it is thermodynamically favourable to promote one electron to a 5d orbital.

For practical purposes, most of the divalent lanthanide ions are extremely unstable, with disproportionation or electron transfer to other substrates providing facile decomposition routes. Well defined coordination chemistry is restricted to the compounds of Sm, Eu and Yb. There has been one report of a formally divalent Ce complex, $\{K(DME)\}_2Ce(COT)_2$ (DME = dimethoxyethane; COT = cyclooctatetraenyl (dianion), C_8H_8), formed by the reduction of $[Ce(COT)_2]$ with an excess of K metal.[21] However, the only characterising data reported were elemental analysis and infrared (IR) absorptions. Considering the very negative redox potential of the Ce^{3+}/Ce^{2+} couple (-2.92 V), it seems unlikely that this is a genuine Ce^{2+} compound. Furthermore, the green colour of the complex is more consistent with it being a trivalent compound containing the $[(COT)_2Ce]^-$ ion.[22] There has also been a report of a formally divalent organoneodymium complex, $\{K(THF)_n\}_2Cp^*_2NdCl_2$ (THF = tetrahydrofuran; Cp^* = pentamethylcyclopentadienyl, C_5Me_5), although once again the characterising data are insufficient to determine whether this species contains Nd^{2+}.[23]

Finally, a number of zerovalent lanthanide compounds have been reported, generally being synthesised by condensation of the metal vapour with the appropriate ligand. They include poorly characterised carbonyl species $Ln(CO)_n$ (n = 1 to 6) which are stable only at very low temperatures, and a

series of compounds with unsaturated hydrocarbons such as hex-3-yne and butadiene.[24] Complexes in the latter class displayed very different properties from typical trivalent compounds in their colours, apparently low coordination numbers, magnetic moments and nuclear magnetic resonance (NMR) behaviour; whether this was due to the presence of a zerovalent metal or a highly reduced ligand is not clear, as no structural analysis was possible due to oligomerisation in solution.[24] Formally zerovalent lanthanide complexes have been synthesised by the condensation of lanthanide metals (Ln = Y, Nd, Sm, Eu, Gd, Ho and Yb) with 1,4-di-*tert*-butyldiazabutadiene (Bu^t_2DAB, $Bu^tN{=}CHCH{=}NBu^t$).[25] However, most of these were shown to be trivalent complexes of the butadiene radical anion, $[Ln^{3+}(Bu^t_2DAB^{\cdot-})_3]$. The Eu compound was reported to be better formulated as $[Eu^{2+}(Bu^t_2DAB^{\cdot-})_2(Bu^t_2DAB)]$, with the Yb analogue adopting this divalent composition at low temperatures and the trivalent one at higher temperatures.[26,27] In contrast, the condensation of lanthanide metals with bulky arenes such as 1,3,5-tri-(*tert*-butyl)benzene has given the first unquestionably zerovalent lanthanide complexes.[28-30] The Gd and Y species are particularly stable (being sublimable at 100 °C) and [Gd(1,3,5-tri-(*tert*-butyl)benzene)$_2$] has been characterised by X-ray crystallography and found to adopt a monomeric 'sandwich' structure in which the *tert*-butyl groups are staggered.

Thus, many of the lanthanides have the potential to exist in more than one oxidation state. However, two electron redox reactions at these metal centres are unlikely: for example, although well characterised divalent ions of Sm, Eu and Yb are known, the corresponding zerovalent species are among the most unstable. Hence, oxidative addition and reductive elimination mechanisms, which are so prevalent for the d block elements, are absent in lanthanide chemistry.

Bonding Considerations in Lanthanide Compounds

In all oxidation states the 4f electrons of a lanthanide element do not extend beyond the 5s and 5p closed shell.[11,14] Inevitably, this has consequences for the bonding in lanthanide complexes, which is generally agreed to be almost entirely ionic in non-zero oxidation states.[31] Evidence for this ranges from general chemical observations to theoretical considerations.

The *tris*-cyclopentadienyl lanthanides, Cp_3Ln (Cp = cyclopentadienyl, C_5H_5), react readily in solution with $FeCl_2$ to give ferrocene, $[Cp_2Fe]$, indicating the presence of Cp^- ions in solution.[32,33] In addition, crystallographically determined lanthanide to ligand-atom bond lengths are found to be in close agreement with the sum of the ionic radii of the atoms in question, provided a standard correction for the coordination number of the metal is made.[34] Additional evidence that the 4f electrons are not involved in covalent bonding comes from the observation that the ligand field splitting of the 4f orbitals is only some 2 to 3 % of that found in the d block elements, and that the electronic and magnetic properties of trivalent complexes are generally independent of the ligand field (*vide infra*).

A study by Rösch & Green involving quasi-relativistic scattered-wave Xα calculations on $[Cp_2Ln]$ (Ln = Eu, Sm and Yb), in conjunction with photoelectron (PE) spectroscopy of the decamethyllanthanocenes, $[Cp^*_2Ln]$, revealed a very high degree of ionicity in the bonding.[35,36] This was shown in part by the onset of ionisations from the Cp rings some 0.5 to 0.7 eV lower than in the analogous transition metal complexes. A quantitative estimate of the ionicity in the $[Cp^*_2Ln]$ system (*ca* 90 %) has also been made.[37] Similarly, a high degree of ionicity has been reported for the trivalent complexes $[(MeC_5H_4)_3Ln]$ (Ln = Pr and Dy) and $[(C_5H_5)_2Ln(\mu\text{-}Cl)]_2$ (Ln = Gd and Y),[38] although there are indications that there may be more covalency in this higher oxidation state.[39-42] It is worth noting that the actinides show a greater degree of covalency in their chemistry than the lanthanides, but still less than is found for d block systems.[38,43]

Thus, in contrast to transition metal chemistry, in which ligand field effects are an important consideration, we would expect molecular geometry not to be orbitally controlled, but rather to be determined by the maximisation of electrostatic interactions between the metal and the ligand, and the minimisation of interligand repulsions.[34] In this context, it should be noted that the lanthanide contraction frequently causes changes in structure and coordination number to occur across the series in order to maintain optimal metal-ligand interactions. For example, in the anhydrous tribromides, the metal is nine coordinate for the largest lanthanides (Ln = La, Ce and Pr), eight coordinate for Ln = Nd, Pm, Sm and Eu, and only six coordinate for Ln = Gd, Tb, Dy, Ho, Er, Tm, Yb, Lu and Y.[44]

However, even without the directional influence of covalent interactions, there are still some lanthanide compounds which adopt rather unexpected geometries. For example, the low coordinate species $[Ln\{N(SiMe_3)_2\}_3]$[45] and $[Ln\{CH(SiMe_3)_2\}_3]$[46,47] are pyramidal, rather than trigonal planar. Repulsive interligand non-bonding overlap is thought to be minimised in the pyramidal structure, whilst intermolecular agostic interactions (C–H→M), which stabilise the coordinatively unsaturated and electron deficient metal centre, are maximised. Also somewhat surprising is the observation that the divalent decamethyllanthanocenes, $[Cp^*_2Ln]$ (Ln = Sm, Eu and Yb), deviate from a parallel sandwich structure by bending (Figure 1.2).

Figure 1.2 The Bent Structures of the Divalent Decamethyllanthanocenes

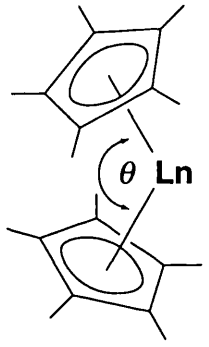

Complex	θ° by Gas Phase Electron Diffraction	θ° by X-Ray Crystallography
$[Cp^*_2Sm]$	-	140.1[48,49]
$[Cp^*_2Eu]$	-	140.3[49]
$[Cp^*_2Yb]$	158[50]	145.7, 145.0[51†]

This phenomenon, which is not predicted by the scattered-wave calculations of Rösch & Green[35,36] (*vide supra*), is not restricted to the lanthanides, also being found in the decamethylmetallocenes, $[Cp^*_2M]$, of Ca,[50,52] Sr[53] and Ba,[52,53] and of Si,[54] Sn[55] and Pb.[56] In the case of the Group 14 compounds, a stereochemically active lone pair argument can be invoked to explain the observation.[55,57] However, for the lanthanide and alkaline earth complexes, no such simple electronic explanation exists. Calculations based on the polarisable ion model of Rittner[58] have been used to account for the bent geometry of the alkaline earth halides in the gas phase.[59] This theory postulates that if a polarisable cation is surrounded by relatively non-polarisable anions, then upon lowering the symmetry (*ie* bending the ligands towards each other) a favourable interaction between the anions and the cation will occur which offsets the interanion repulsions for small bending angles (Figure 1.3).

† Two independent molecules in the unit cell

Figure 1.3 The Polarisable Ion Model[58]

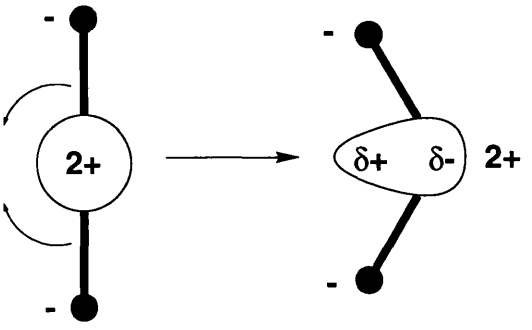

More thorough calculations based on molecular mechanics force fields show that the bent geometry in many metallocene complexes is probably due to Van der Waals attractions between the cyclopentadienyl ligands.[60,61] This starts to become energetically favourable when the metal-carbon bond length exceeds 2.0 Å for $[Cp_2M]$ and 2.2 Å for the Cp^* derivatives.[62] Earlier *ab initio* calculations on the unsubstituted lanthanocenes[63] failed to predict their bent geometries because they neglected to take electron correlation into account. All of the approaches agree that the potential surface for bending the metallocenes is very shallow and hence, the energy difference between the bent and linear structures is very small (<2.1 kcal mol^{-1}).[60] Thus, despite the seemingly straightforward combination of steric and electrostatic factors which determine the coordination geometry of lanthanide complexes, unexpected structures can and do occur. However, such conformations are perfectly consistent with a high degree of ionicity in the bonding and are not caused by covalent interactions between the metal and ligand.

It should be stressed that the above refers to non-zero oxidation states only. The bonding in the zerovalent lanthanide complexes [Ln(1,3,5-tri-(*tert*-butyl)benzene)$_2$] has also been addressed.[29,64,65] The stable Y complex has no available f orbitals and hence, a $5s^24d^1$ electron configuration was postulated as being necessary for covalent interaction with the arene rings.[29] Consistent with this, the 4f → 5d promotion energies of the elemental lanthanides correlate well with the observed stabilities of the zerovalent complexes: Gd has the ground state configuration $[Xe]4f^75d^16s^2$ and [Gd(1,3,5-tri-(*tert*-butyl)benzene)$_2$] is one of the most stable of this series, whilst Eu, Er and Yb have the highest promotion energies and their complexes are too unstable to be isolated.

Magnetic Properties and Electronic Spectroscopy of Lanthanide Compounds[5,66]

The electronic structure of the lanthanides can be described by the Russell-Saunders coupling scheme.[5] Thus, the individual electron spins ($m_s = {}^1/_2$) combine to give a total spin quantum number S, and the individual orbital angular momenta (m_l = +3, +2,...., -2, -3) add to give a total orbital angular momentum L. In contrast to the valence electrons of the d block elements, the radially contracted 4f orbitals of the lanthanides do not interact greatly with the ligand set around the metal - crystal field splitting for the lanthanides is only of the order of 100 cm^{-1} compared with *ca* 20000 cm^{-1} for transition metals - whilst spin-orbit coupling is relatively large (*ca* 2000 cm^{-1}). Thus, S and L couple to give an overall quantum number, J, which takes values $S+L$, $S+L-1$,...., $S-L$ (or $L-S$ if $L>S$)). The ground state configuration has $J = L-S$ for 4f shells which are less than half full, and $J = S+L$ for $4f^8$ configurations onwards (for $4f^7$ configurations S = 0).

The bulk magnetic susceptibility (χ) of a paramagnetic molecule which obeys the Russell-Saunders coupling scheme is given by the Curie law[66] in which N_A is the Avogadro constant, g_e is the free-electron g-factor, μ_B the Bohr Magneton, k the Boltzmann constant and T the temperature of the measurement (in K):

$$\chi = \frac{N_A g_e^2 \mu_B^2}{4kT} J(J+1)$$

This only applies to a magnetically dilute sample and predicts that a plot of magnetic susceptibility against reciprocal temperature will be linear, with χ tending to zero as the temperature approaches infinity. The more general Curie-Weiss law is used to describe non-magnetically dilute samples for which χ tends to a non-zero value by subtracting a constant term (Θ) from the temperature:

$$\chi = \frac{C}{T - \Theta}$$

$$\text{where} \quad C = \frac{N_A g_e^2 \mu_B^2}{4k} J(J+1)$$

The paramagnetism of a complex is more normally quoted as its effective magnetic moment, μ_{eff},(in Bohr magnetons) which is defined as:

$$\mu_{eff} = \left(\frac{3}{2} + \frac{S(S+1) - L(L+1)}{2J(J+1)}\right)\sqrt{J(J+1)}$$

Excited states in lanthanide ions are generally too high in energy to be significantly populated at room temperature, the exceptions being in Sm^{3+}, Sm^{2+} and Eu^{3+}. Hence, calculated magnetic moments (given by the above formulae) predict accurately the observed moments for most lanthanide complexes.

For trivalent complexes, absorption of visible radiation generally corresponds to excitation to electronic states which arise from the same $4f^n$ configuration as the ground state, *ie* a rearrangement of electrons between 4f orbitals.[5] These transitions are orbitally or Laporte forbidden since they break the selection rule $\Delta L = \pm 1$. Furthermore, this rule is not relaxed to any great extent by vibronic coupling in lanthanide complexes, since the crystal field effect exerted by the ligands on the 4f orbitals is small. Consequently, the intensity of these absorptions is weak. The absence of an interaction between the ligand and the 4f electrons also causes the absorptions to be relatively sharp and to occur at wavelengths which are characteristic of the lanthanide ion in question.

For the divalent ions, the 4f orbitals are closer in energy to the 5d than they are in the higher oxidation states, and absorption of visible radiation generally corresponds to 4f $\rightarrow$ 5d transitions. These bands are much more intense since they are orbitally allowed. They are also much broader and the transition energy much more sensitive to the ligand environment of the metal, since the 5d orbitals have a far greater radial extension than the 4f orbitals. Absorption of visible radiation in divalent (and tetravalent) complexes is often also due to charge transfer between the ligand and metal.

It should be noted that in some trivalent complexes the ligand field stabilisation of the 5d orbitals is sufficient to cause a much more intense orbitally allowed 4f $\rightarrow$ 5d transition in the visible region of the spectrum. This is particularly pronounced at the beginning of the lanthanide series where the marked stabilisation of the 4f orbitals with increasing atomic number is yet to begin in earnest. Thus, whilst the $4f^1 \rightarrow 5d^1$ transition energy in the free Ce^{3+}

ion is 49000 cm^{-1}, this falls dramatically to only 17650 cm^{-1} in $[\{C_5H_3(SiMe_3)_2\}_3Ce]$; the results of theoretical calculations on $[Cp_3Ce]$ are in good agreement with this observation, predicting a transition energy of 16500 cm^{-1}.[67]

Nuclear Magnetic Resonance Spectroscopy of Lanthanide Compounds[68,69]

The use of NMR spectroscopy in lanthanide chemistry is complicated by the intrinsic paramagnetism of most of these elements. The only known diamagnetic species are Ce^{4+} ($[Xe]4f^0$), Y^{3+} ($[Kr]4d^0$), La^{3+} ($[Xe]4f^0$), Lu^{3+} ($[Xe]4f^{14}$) and Yb^{2+} ($[Xe]4f^{14}$). It has already been noted that for ions with 4f shells less than half full, the spin and orbital contributions to the magnetic moment partially cancel each other out, whereas for $4f^8$ to $4f^{13}$ electron configurations they are additive. For this reason, compounds of the lighter elements tend to be more suited to investigation by NMR than complexes of the heavier lanthanides. In practice, given favourable conditions and with sufficient care, NMR spectra of most lanthanide compounds can be observed, although the resonances are often highly shifted and extremely broad.

The isotropic shift of a resonance (*ie* the chemical shift difference between a resonance in a paramagnetic complex and the same resonance in an analogous diamagnetic system) is determined principally by two factors. The first of these is the contact (or Fermi) contribution, Δ_C, which is a consequence of unpaired electron density residing at the ligand nucleus of interest. The magnitude of this effect is given by the equation below, where a_N is the electron-nucleus hyperfine splitting constant (*ie* the degree to which the two interact), g is the electron g-factor (not equal to g_e if spin-orbit coupling occurs), μ_B is the Bohr Magneton and γ is the magnetogyric ratio of the observed nucleus:[70]

$$\Delta_C = \frac{-2\pi g(g-1)J(J+1)\mu_B a_N}{3kT\gamma}$$

It might be expected that the electron and nuclear spins would couple, causing the resonance to split in much the same way that adjacent nuclear spins do, although the effect would be far greater due the much larger magnetic moment of the electron. However, because the relaxation time for

electrons is very short (typically 10^{-13} to 10^{-7} s compared with *ca* 10^{-3} to 10^{3} s for nuclear spins), but not fast enough to cause the resonance to collapse completely, a single, rather broad peak is usually observed. In addition, because the energy difference between the electron spin states is large, the Boltzmann populations of these are very uneven (*cf.* nuclear spin states which are almost equally populated) and the resonance shifts from its diamagnetic position. For the lanthanides, the contact effect is normally small due to the limited radial extension of the 4f orbitals. In addition, being a 'through bond' interaction, it is most important for nuclei directly attached to the paramagnetic centre.

The pseudocontact (or dipolar) contribution, Δ_p, is a 'through space' interaction between the magnetic moment of the unpaired electrons and the magnetic moment of the nucleus. It is given by the formula below, where D' and D'' are the molecular susceptibility anisotropies, and r, θ and ϕ are the polar coordinates of the observed nucleus with respect to the paramagnetic centre:[71]

$$\Delta_p = D'\left(\frac{3\cos^2\theta}{r^3}\right) - D''\left(\frac{3\sin^2\theta\cos 2\phi}{r^3}\right)$$

The magnitude of Δ_p is highly dependent upon the symmetry of the lanthanide environment (becoming zero in a cubic field) and falls off rapidly with distance from the paramagnetic centre.

Using the above equations, it is possible to calculate theoretical isotropic shifts and hence, the expected positions of the peaks in the NMR spectrum of a compound of known structure. This approach has been used to investigate the structures of lanthanide complexes in solution.[72,73] The isotropic shift induced by paramagnetic metal ions also finds application in the NMR of organic molecules, for which ^{1}H spectra will frequently contain a number of overlapping peaks: by adding a small quantity of a 'shift reagent' (normally a lanthanide β-diketonate compound), with which the molecule being studied interacts, these resonances are spread out and fully separated.

The isotropic shift of a peak will depend upon the temperature at which the spectrum is measured. If the species is monomeric (*ie* the isotropic shift of each resonance is dependent upon just one paramagnetic nucleus) and there is no temperature dependent structural equilibrium (*eg* involving dissociation

of one of the ligands), then a plot of reciprocal temperature against chemical shift will be linear; this is known as the Curie-Weiss relationship.[66,74] In addition, the chemical shifts of nuclei in paramagnetic molecules which undergo partial dissociation in solution frequently exhibit a significant concentration dependence.

Synthetic Lanthanide Chemistry[24,47]

The two most important considerations in preparative lanthanide chemistry are the high degree of ionicity in the bonding and the relatively large size of the ions. Ancillary ligands should therefore be sterically demanding and capable of forming strong ionic bonds (*ie* not requiring covalent interactions such as back bonding for stability) if tractable complexes are to be synthesised. Since the lanthanides are highly oxophilic and lack directional bonding, their aqueous chemistry is frequently complicated by extensive solvation. In addition, all the divalent lanthanide ions except Eu^{2+} rapidly reduce water.[5] For this reason, studies of the coordination chemistry of the lanthanides have tended to concentrate on the use of ancillary ligands which are compatible with non-aqueous solvents. Of these, the most ubiquitous is the cyclopentadienyl class of ligands.

The trivalent complexes Cp_3Ln [32,33,75] were isolated soon after ferrocene, and preparation of the heteroleptic species $[Cp_2Ln(\mu\text{-}Cl)]_2$ (Figure 1.4**a**) was found to be possible for the smaller lanthanides (Ln = Sm, Gd, Dy, Ho, Er, Yb and Lu). However, this combination of ligands was insufficiently bulky to sterically saturate the larger metals, and for Ln = La, Ce, Pr and Nd, only the formation of Cp_3Ln was observed.[76,77] The synthesis of analogous dimeric metallocene halide complexes of the lighter lanthanides was made possible by the use of the sterically demanding *bis*-(trimethylsilyl)cyclopentadienyl ligand ($C_5H_3(SiMe_3)_2$, Figure 1.4**b**).[78]

Two further examples serve to underline the importance of steric considerations in lanthanide chemistry. The first is the observation that the complexes Cp^*_2LnMe (Ln = Yb and Lu) will activate C–H bonds in methane and are extremely efficient olefin polymerisation catalysts.[79] In contrast, the less sterically encumbered derivatives Cp_2LnMe[80] and $(Me_2C_5H_4)_2LnMe$[81] show no such activity. This distinction is attributed to the inability of the

Figure 1.4 The Structures of $[Cp_2Ln(\mu\text{-}Cl)]_2$ (**a**)[76,77] and $[\{C_5H_3(SiMe_3)_2\}_2Ln(\mu\text{-}Cl)]_2$ (**b**)[78]

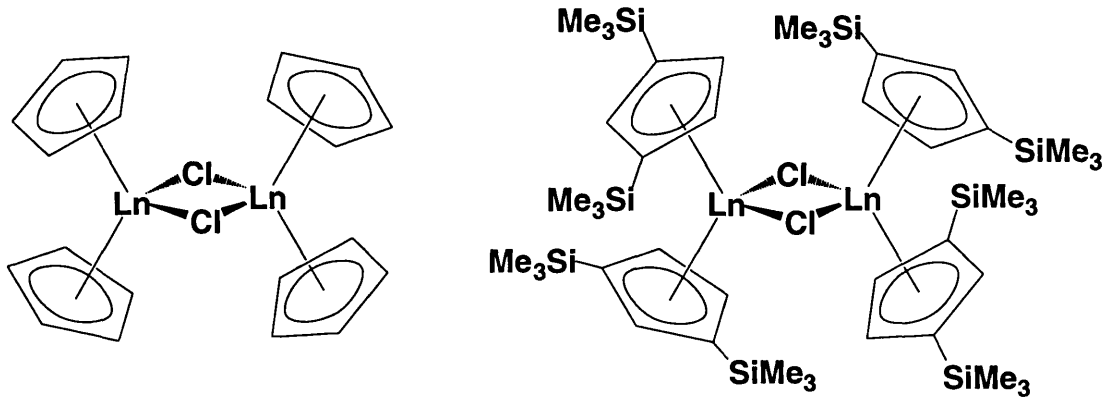

Ln ≠ La, Ce, Pr and Nd **Ln = La, Ce, Pr and Nd**

a **b**

pentamethylcyclopentadienyl complexes to form a symmetrically bridged μ-alkyl dimer analogous to that observed for the less substituted derivatives (Figure 1.5**a**). Instead, a weakly bonded asymmetric dimer is formed in the solid state (Figure 1.5**b**) which exists in rapid equilibrium in solution with the sterically unsaturated monomer.

Figure 1.5 The Structures of $[(C_5H_3R_2)_2Ln(\mu\text{-}Me)]_2$ (**a**)[80,81] and $[Cp^*_2Ln(\mu\text{-}Me)LnCp^*_2Me]$ (**b**)[79]

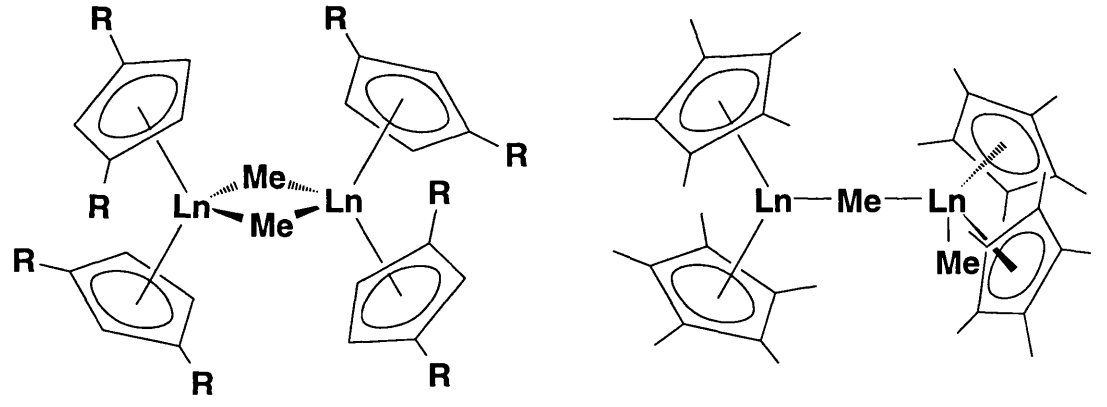

R = H and Me; Ln = Y and Yb **Ln = Yb and Lu**

a **b**

It is this monomer which is thought to be the species responsible for the extraordinary activity of these compounds.[79] In contrast, the stable dimeric structure of the complexes with the less bulky cyclopentadienyls is retained in solution, and these compounds are far less reactive.

The second example concerns the synthesis of divalent cyclopentadienyl derivatives. Compounds of the type Cp_2LnL_n (Ln = Sm, Eu and Yb; L = THF, Et_2O, DME *etc.*; n = 0, 1 or 2) have been prepared by a variety of routes, for example, Equations 1.1, 1.2 and 1.3.[24]

Equation 1.1[75]

$$Eu + C_5H_6 \xrightarrow{\text{Liquid } NH_3} C_5H_8 + Cp_2Eu(NH_3) \xrightarrow[\text{Vacuum}]{120 - 200\ ^\circ C} Cp_2Eu$$

Equation 1.2[82]

$$2\ CpNa + SmI_2(THF)_n \xrightarrow{THF} Cp_2Sm(THF)_2 + 2\ NaI$$

Equation 1.3[83]

$$6\ CpTl + 3\ Yb \xrightarrow{THF} 3\ Cp_2Yb(THF)_2 + 6\ Tl$$

Such complexes are thought to be oligomeric due to their insolubility in most solvents; no crystal structures have been determined and their reactivity has been little studied. The use of the bulkier methylcyclopentadienyl ligand (MeC_5H_4) gives slightly more soluble complexes, but the crystal structure of $[(MeC_5H_4)_2Yb(THF)]_\infty$ indicates that this compound adopts a polymeric structure in the solid state, presumably in order to achieve steric saturation of the metal centre.[84] For both unsubstituted cyclopentadienyl and methylcyclopentadienyl lanthanide complexes, attempts to prepare solvent free species of Yb and Sm result in decomposition. In contrast, the use of the sterically demanding pentamethylcyclopentadienyl ligand enabled the isolation of complexes $[Cp^*_2LnL_n]$ (L = a Lewis base) which were readily desolvated. For example, $[Cp^*_2Sm(THF)_2]$ loses THF on heating to 75 °C

under vacuum to give [Cp^*_2Sm] as a lipophilic crystalline solid.[48] The molecular structure of this complex revealed that it was monomeric with a bent sandwich structure (*vide supra*).

These two examples have highlighted the steric control which can be achieved at a lanthanide centre by the use of the bulky pentamethylcyclopentadienyl ligand. This, together with the robust nature of the ligand (*ie* its resistance to highly oxidising and reducing conditions, and good thermal stability) and its ability to confer solubility and crystallinity on its compounds, has made Cp^* the most prevalent ancillary ligand in lanthanide coordination chemistry. Among the numerous compounds which it has been possible to isolate using this ligand are complexes of dinitrogen, $[(Cp^*_2Sm)_2(\mu\text{-}\eta^2\text{-}\eta^2\text{-}N_2)]$,[85] alkenes, $[Cp^*_2Yb(\mu\text{-}\eta^2\text{-}\eta^2\text{-}H_2C{=}CH_2)PtPh_3]$,[86] and alkynes, $[Cp^*_2Yb(\eta^2\text{-}MeC{\equiv}CMe)]$.[87]

The use of bulky substituents to generate a sterically demanding ligand is not restricted to the cyclopentadienyls. Other ligands have been used with success in trivalent lanthanide chemistry, and there is increasing interest in developing this area further and extending it to the divalent state of these elements.[88,89] Examples of new ancillary ligands for divalent lanthanides (Figure 1.6) include amides (**a**[90]), aryloxides and alkoxides (**b**[91] and **c**[92]), aryl and alkyl chalcogenolates (**d**[93] and **e**[94]), trialkylstannyls (**f**[95]), triarylsilyls and -germyls (**g**, M = Si and Ge[96]), phospholyls (**h**[97]), and alkyls (**i**[98]).

Poly-(pyrazolyl)borate Ligands[99-102]

Pyrazolylborate ligands were first reported by Trofimenko in 1966.[103] They are borohydride anions in which two, three or four of the hydrides have been replaced either with pyrazolyl (pz) groups alone or with a combination of pyrazolyl groups and other substituents (Figure 1.7).

The abbreviations used for these ligands are Bp for dihydrido-*bis*-(pyrazol-1-yl)borate, Tp for hydrido-*tris*-(pyrazol-1-yl)borate, and pzTp for *tetrakis*-(pyrazol-1-yl)borate.[102] Substituents on the pyrazolyl ring are indicated by a superscript giving the nature of the group(s) and their position on the ring (the nitrogen bonded to boron being numbered 1-, the second nitrogen 2- *etc.*). Where two identical groups are indicated but no position is given (*eg* Tp^{Me_2}), the pyrazolyl ring is substituted at the 3-(R) and 5-(R") positions.

Figure 1.6 Some Divalent Lanthanide Complexes with Non-cyclopentadienyl Ancillary Ligands

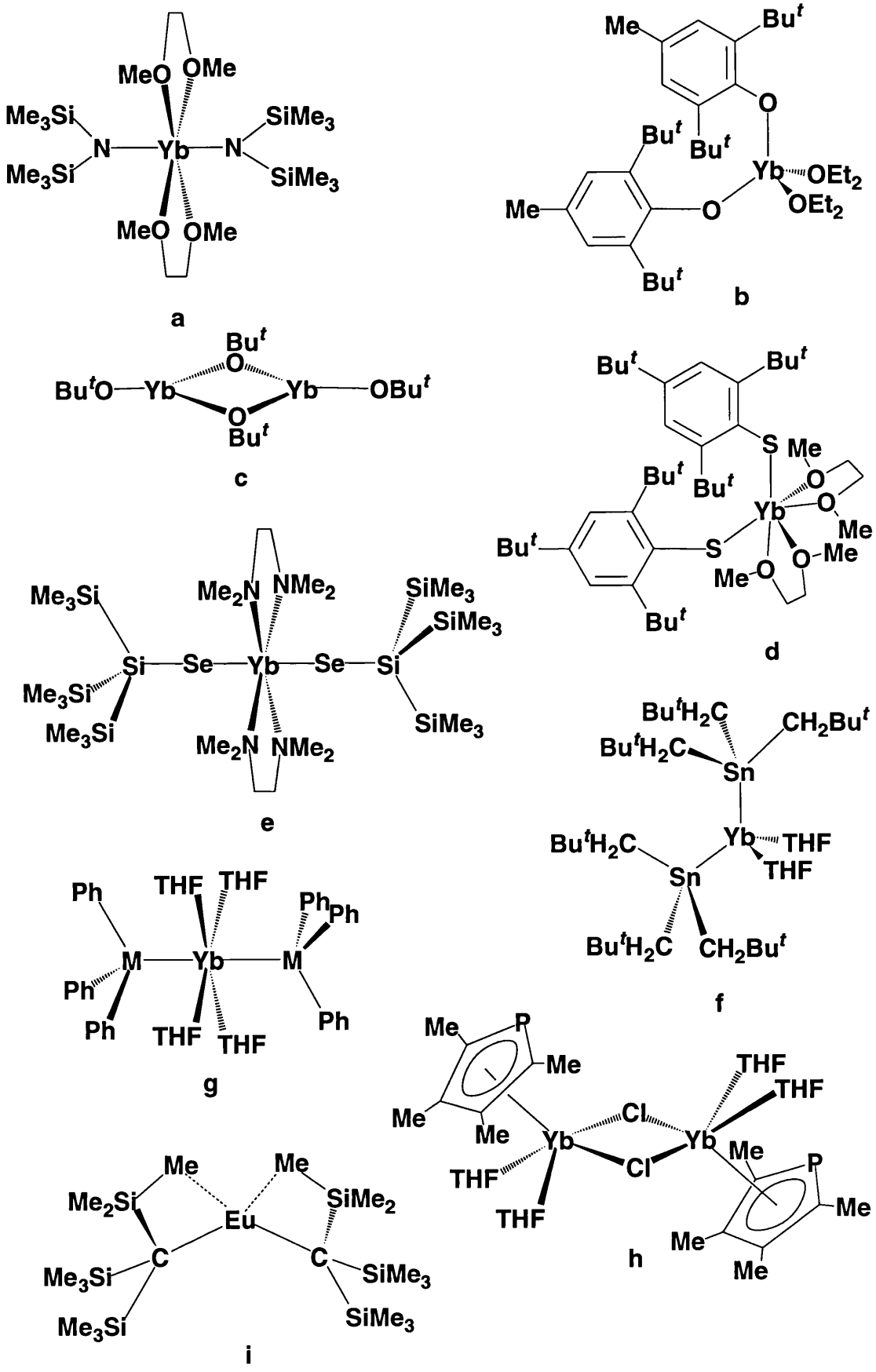

Figure 1.7 The *Poly*-(pyrazolyl)borate Class of Ligands

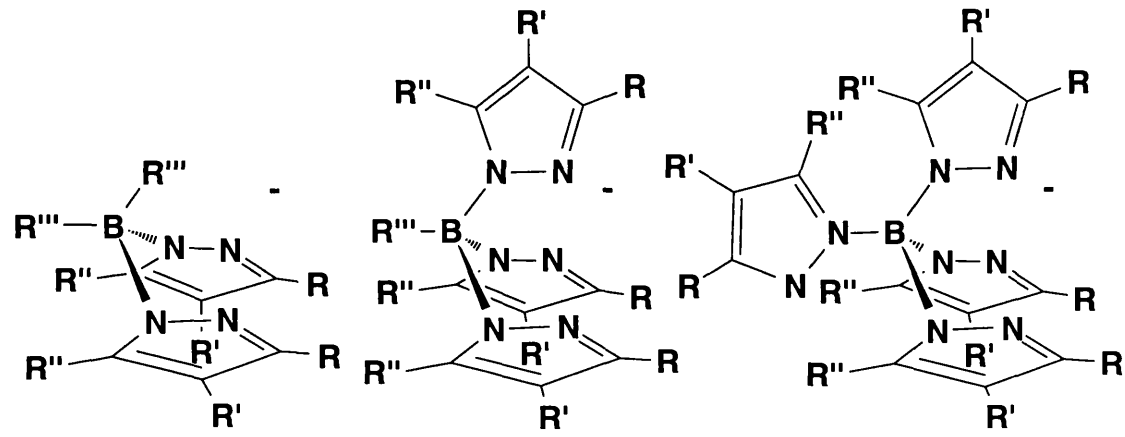

***Bis*-(pyrazolyl)borate** ***Tris*-(pyrazolyl)borate** ***Tetrakis*-(pyrazolyl)borate**

The pyrazolylborates are readily synthesised, usually from KBH_4 or $NaBH_4$ and the corresponding pyrazole in a melt, the degree of substitution being controlled by temperature. Pyrazolylborates in which the substituent(s) on the boron atom (R''') is neither hydrogen nor a pyrazolyl group are generally synthesised by reaction of the substituted borane with the desired pyrazole or pyrazolide anion. 3,5-Disubstituted pyrazoles can be made by condensation of a deprotonated ketone with an ester (to give the β-diketonate), followed by reaction with hydrazine (Equation 1.4). Pyrazole and 3,5-dimethylpyrazole are available commercially. Procedures for the synthesis of 4-substituted pyrazoles are discussed in Chapter 3.

Equation 1.4

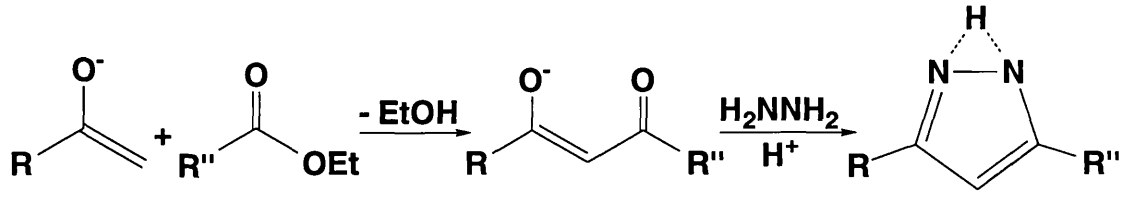

When the pyrazolylborates are synthesised, the B–N bond is usually formed adjacent to the carbon atom bearing the least sterically demanding substituent. Thus, reaction of 3-*tert*-butyl-5-methylpyrazole with KBH_4 leads exclusively to the formation of potassium hydrido-*tris*-(3-*tert*-butyl-5-

methylpyrazol-1-yl)borate, $KTp^{3\text{-}t\text{-}Bu\text{-}5\text{-}Me}$ (Equation 1.5); formation of the *tetrakis* compound in the presence of an excess of pyrazole is prevented by the steric bulk of the 5-Me substituents around the boron atom (Equation 1.6).

Equation 1.5[104]

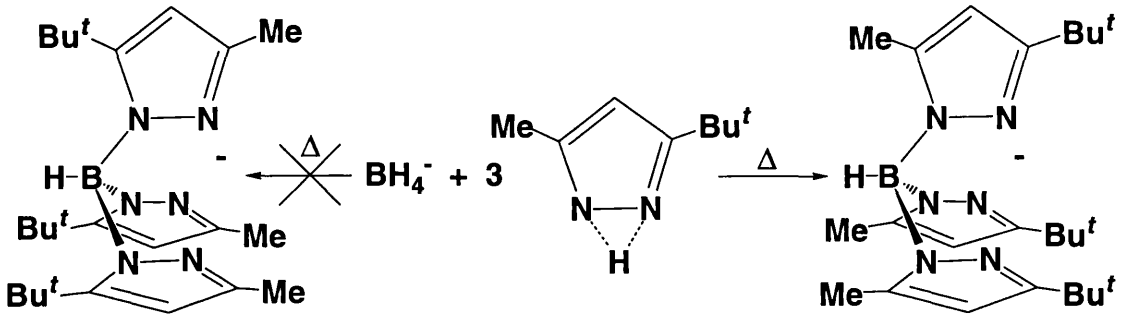

Equation 1.6[104]

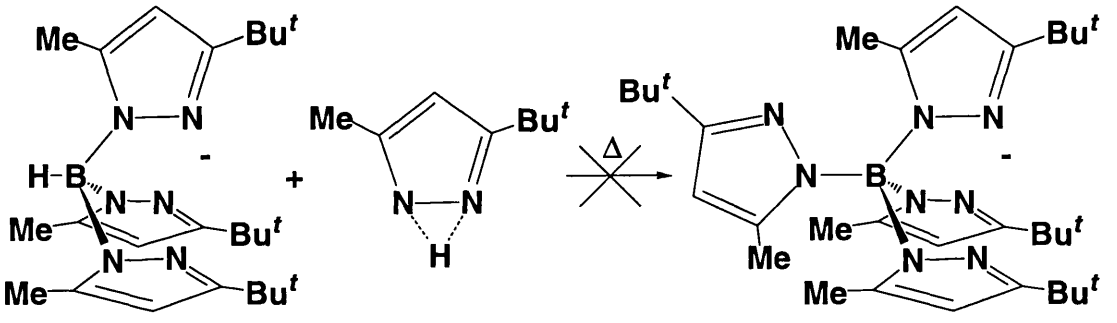

The situation is more complicated when the difference in the size of the 3- and 5-substituents on the pyrazole is less pronounced. Thus, reaction of 3-*iso*-propyl-5-methylpyrazole with KBH_4 leads to the formation of $K^+[HB(3\text{-}Pr^i\text{-}5\text{-}Mepz)_2(3\text{-}Me\text{-}5\text{-}Pr^ipz)]^-$ as well as of $KTp^{3\text{-}i\text{-}Pr\text{-}5\text{-}Me}$ ($K^+[HB(3\text{-}Pr^i\text{-}5\text{-}Mepz)_3]^-$).[105]

When coordinated in an η^3- fashion, the *tris*- and *tetrakis*-(pyrazolyl)borates are often compared with the cyclopentadienyl class of ligands, since they share a uninegative charge, six electron donor properties, a propensity to coordinate in a face capping manner and an ability to complex to a wide range of sizes and types (ionic and covalent) of metal centres. This comparison seems particularly justified in the light of the synthesis of pyrazolylborate analogues of a large number of cyclopentadienyl complexes,

for example, Figure 1.8**a**[106] and **b**,[107,108] **c**[109,110] and **d**,[111] and **e**[112] and **f**.[113] A similar parallel can be drawn between the *bis*-(pyrazolyl)borate and acetylacetonate ligands.

Figure 1.8 *Tris*-(pyrazolyl)borate Analogues (**b**, **d** and **f**) of some Cyclopentadienyl Complexes (**a**, **c** and **e**, respectively)

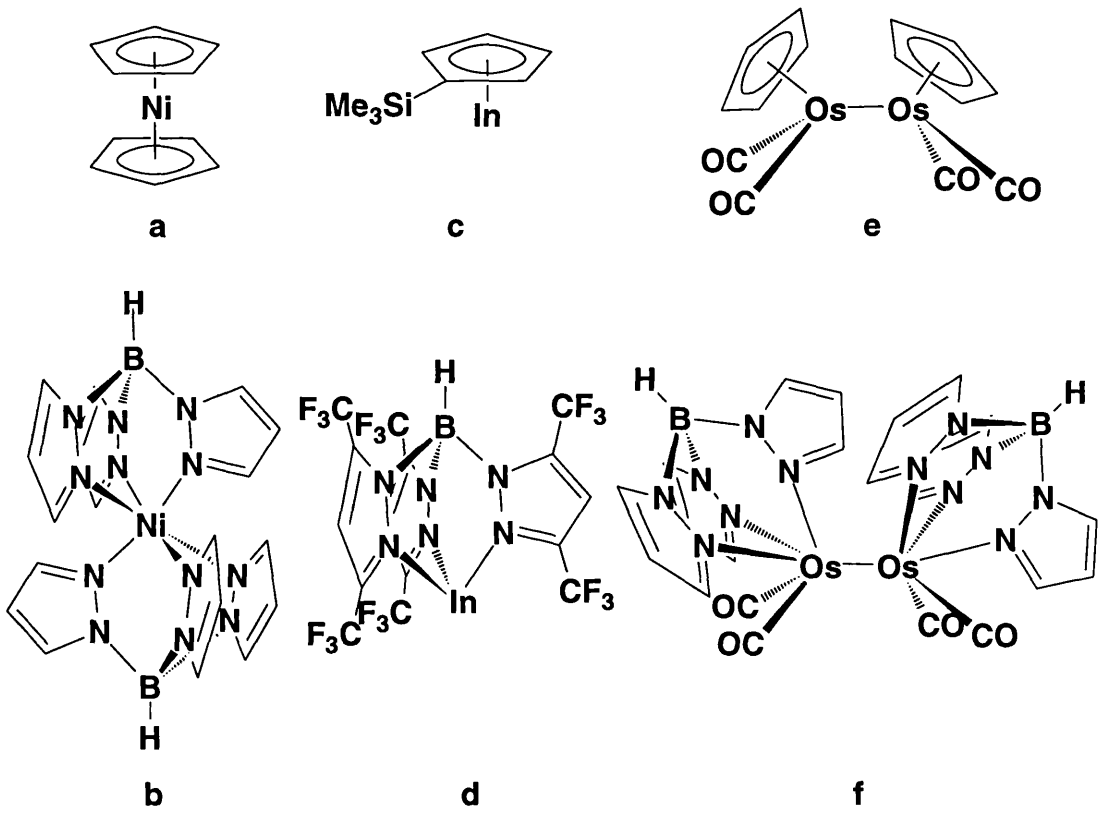

One of the most appealing qualities of the pyrazolylborates is the enormous potential that exists to tailor a ligand with extremely specific properties. This is achieved by the choice of substituents R, R' and R'' on the pyrazolyl ring and of the group R''' bound to boron. Some of the consequences that these different substituents can have on the properties of the ligand are outlined below.

Since B–H bonds are generally subject to ready hydrolysis, the use of R''' groups other than hydrogen can improve the stability of the complexes. Furthermore, if R''' is a group which may be protonated (such as another pyrazolyl ring), compounds which are soluble in acidic media may be synthesised.[108] The use of an alkyl substituent at the 5-position of the

pyrazolyl ring (R'') provides steric protection for the B–H bond (when R''' = H), and tightens the bite angle of the ligand at the metal centre; 5-Me substituted pyrazolyl groups are commonly used for this reason. The nature of the substituent R' will affect the ease with which the individual molecules pack in the solid state. Finally, the steric environment of the complexed metal may be tuned by the choice of the group at the 3-position of the pyrazolyl ring (R). Obviously, all of the substituents have some role in determining the solubility of complexes as well as the electronic (and sometimes chiral) properties of the molecule. Thus, a high degree of flexibility may be achieved by the independent selection of these four substituents. This is in sharp contrast to the situation which exists for the cyclopentadienyls for which there is only one type of substituent that may be altered.

The success of the sterically demanding pentamethylcyclopentadienyl ligand in stabilising lanthanide centres has already been noted, and the question of how the sizes of 3-substituted *tris*-(pyrazolyl)borate and substituted cyclopentadienyl ligands compare must be addressed. The vastly different structures of these two classes of ligand means that a quantitative comparison of their steric bulk is difficult and somewhat meaningless. In particular, the cyclopentadienyls are flat, or cup shaped when substituted, and occupy nominally three coordination sites at the metal, effectively blocking one face. On the other hand, substituents at the 3-position on the pyrazolyl ring of *tris*-(pyrazolyl)borates tend to form a pocket into which the metal fits; again, the ligand occupies three coordination sites at the metal, but this does not necessarily prevent coordination of other groups to the metal in the cleft between the 3-substituents on the pyrazolyl rings, for example, Figure 1.9**a**[114] and **b**.[115]

Furthermore, whilst cyclopentadienyl ligands can bind metal atoms at both faces (an inverse sandwich structure), *tris*-(pyrazolyl)borates have just one 'face' and will normally only complex to a single metal centre; however, note that *tetrakis*-(pyrazolyl)borates frequently bridge metal centres, an example of which is found in the compound $[(\eta^3\text{-allyl})Pd(\mu\text{-}pz_2Bpz_2)Pd(\eta^3\text{-allyl})]^+[PF_6]^-$.[116] This difference between *tris*-(pyrazolyl)borates and cyclopentadienyls is clearly shown by comparison of the extended structures of Figure 1.8**c** and **d** (*vide supra*). Whilst the *tris*-(pyrazolyl)borate complex (**d**) is a genuine monomer,[111] **c** is actually polymeric, consisting of infinite zigzag chains with In–Cp(centroid)–In and Cp(centroid)–In–Cp(centroid) angles of 175.94 and 131.78°, respectively.[110]

Figure 1.9 The Coordination of Ligands in the Cleft Between the 3-Substituents of *Tris*-(pyrazolyl)borates

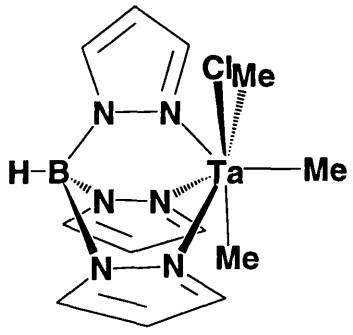

a

B···Ta–C(Me)	B···Ta–Cl
97.2(5)°	106.9(4)°
104.5(5)°	
173.1(5)°	

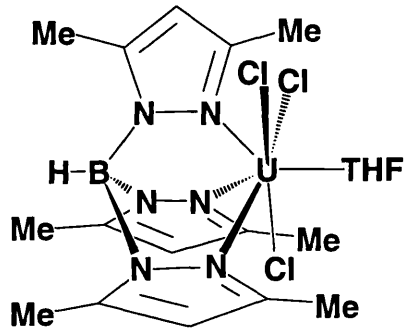

b

B···U–Cl	B···U–O(THF)
101.1(1)°	175.7(2)°
107.4(1)°	
107.7(1)°	

The most commonly invoked measure of ligand bulk is the cone angle, θ; this is defined as the "apex angle of a cone, centred on the metal, just large enough to enclose the Van der Waals radii of the outermost atoms of the ligand" (Figure 1.10).[117] A comparison of the cone angles of common cyclopentadienyl and *tris*-(pyrazolyl)borate ligands is given in Table 1.2.

Figure 1.10 The Measurement of Ligand Cone Angles[117]

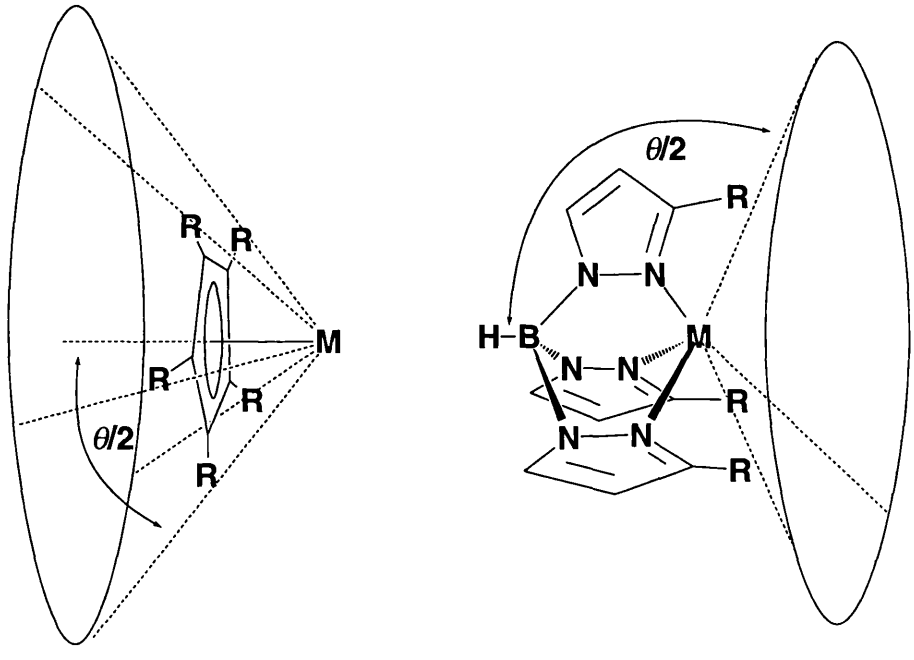

Table 1.2 Cone and Wedge Angles for some Cyclopentadienyl and *Tris*-(pyrazolyl)borate Ligands

Ligand	Cone Angle θ°	Wedge Angle ω°
Cyclopentadienyl (Cp)[118,119]	136 to 150	-
Pentamethylcyclopentadienyl (Cp^*)[119]	*ca* 185	-
Hydrido-*tris*-(pyrazol-1-yl)borate (Tp)[120]	198.5	91
Hydrido-*tris*-(3-phenylpyrazol-1-yl)borate (Tp^{Ph})[121]	235	-
Hydrido-*tris*-(3,5-dimethylpyrazol-1-yl)borate (Tp^{Me_2})[120]	236	75
Hydrido-*tris*-(3-phenyl-5-methylpyrazol-1-yl)borate ($Tp^{3\text{-Ph-5-Me}}$)[120]	250	32
Hydrido-*tris*-(3-*i*-propyl-4-bromopyrazol-1-yl)borate ($Tp^{3\text{-}i\text{-Pr-4-Br}}$)[120]	262	36
Hydrido-*tris*-(2-*H*-benz[g]-4,5-dihydroindazol-2-yl)borate (Tp^{a})[120]†	262	44
Hydrido-*tris*-(3-methyl-2-*H*-benz[g]-4,5-dihydroindazol-2-yl)borate ($Tp^{3\text{-a-5-Me}}$)[120]	263	43.5
Hydrido-*tris*-(3-*tert*-butylpyrazol-1-yl)borate ($Tp^{t\text{-Bu}}$)[120]	265	35

Whilst the concept of cone angles is frequently applied to considerations of ligand bulk, it should be remembered that even within a group of isostructural ligands, this parameter is somewhat unreliable since it is highly sensitive to the ligand-metal bond length. Furthermore, because the values given in Table 1.2 have all been measured in transition element complexes (for which the metal-ligand bond lengths are significantly smaller than for the lanthanides),[15] they should be taken as overestimates for the f elements.

The cone angle of a particular *tris*-(pyrazolyl)borate ligand gives only some insight into its steric properties. The possibility of groups coordinating in the cleft between the 3-substituents on the pyrazolyl rings of these ligands has already been alluded to. A measure of the size of this coordination site, the wedge angle, ω,[120] has been proposed, and values of ω are included in Table

† See Figure 1.11

1.2. The importance of this parameter is demonstrated by the relative stabilities of the complexes [Tp'$_2$M] and [Tp'MX] (Tp' = a *tris*-(pyrazolyl)borate; M = a first row transition metal; X = halide or pseudohalide). For Tp' = Tp the formation of the sandwich complexes [Tp'$_2$M] is strongly favoured. In contrast, for ligands with bulkier substituents such as Pr^i and Bu^t at the 3-position of the pyrazolyl ring, only the tetrahedral complexes [Tp'MX] can be synthesised;[104,122,123] Tp$^{i\text{-Pr}}$ does form a complex of the type [Tp'$_2$M] but this involves rearrangement of the pyrazolylborate ligand - see Equation 1.8. Intermediate behaviour is observed for ligands such as Tp^{Me2}, Tp^{Ph} and Tp$^{3\text{-Ph-5-Me}}$ for which both types of complex can be formed. However, by tethering the phenyl groups in Tp^{Ph} and Tp$^{3\text{-Ph-5-Me}}$ with an alkyl chain, rotation of the phenyl ring is prevented and ligands with much reduced wedge angles are obtained (Tp^a, Figure 1.11, and Tp$^{3\text{-a-5-Me}}$).[120] These show a very strong preference for octahedral coordination with first row transition metals, despite having cone angles which are similar to those of Tp$^{3\text{-}i\text{-Pr-4-Br}}$ and Tp$^{t\text{-Bu}}$.

Figure 1.11 The Structure of Hydrido-*tris*-(2-*H*-benz[g]-4,5-dihydroindazol-2-yl)borate (Tp^a)

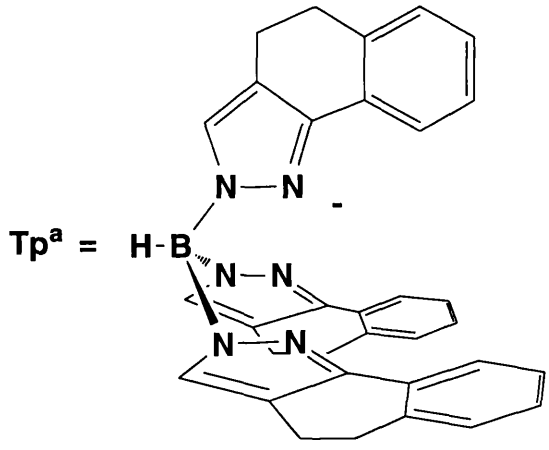

Despite this somewhat complicated picture, it is obvious that the *tris*-(pyrazolyl)borate ligands are significantly more sterically demanding than the cyclopentadienyls. Since a key objective in lanthanide coordination chemistry is to sterically saturate the metal centre (in order to suppress ligand redistribution reactions), the bulky *tris*-(pyrazolyl)borates are expected to be ideal ancillary ligands for these elements. Additional features which make the pyrazolylborates suitable for lanthanide coordination chemistry are that they

bind to the metal through nitrogen donor atoms (which are expected to be compatible with the ionic bonding associated with the lanthanides), they are chelating and will therefore be relatively difficult to displace (an important consideration bearing in mind the general lability of lanthanide systems) and they are fairly resistant to reduction (which will be essential if divalent species are to be synthesised). However, it should be noted that the pyrazolylborates tend to be less robust than the cyclopentadienyls, and there is a number of examples of these ligands undergoing hydrolysis (*eg* Equation 1.7), rearrangement (as in the 1,2 boronic shift in Equation 1.8) and cleavage of the pyrazolyl groups (*eg* Equation 1.9).

Equation 1.7[125]

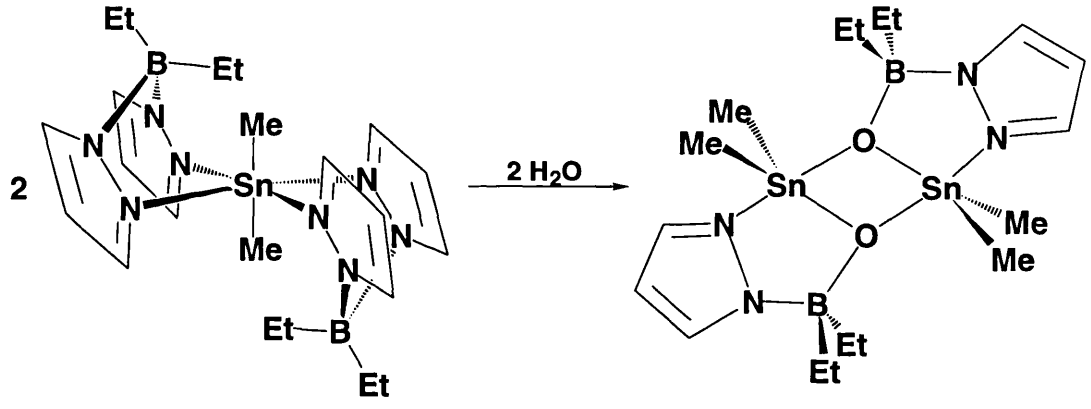

Equation 1.8[123]

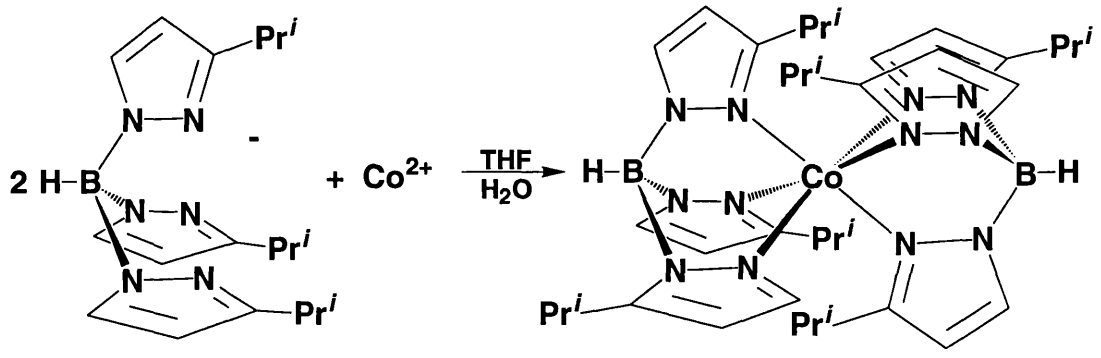

Equation 1.9[126]

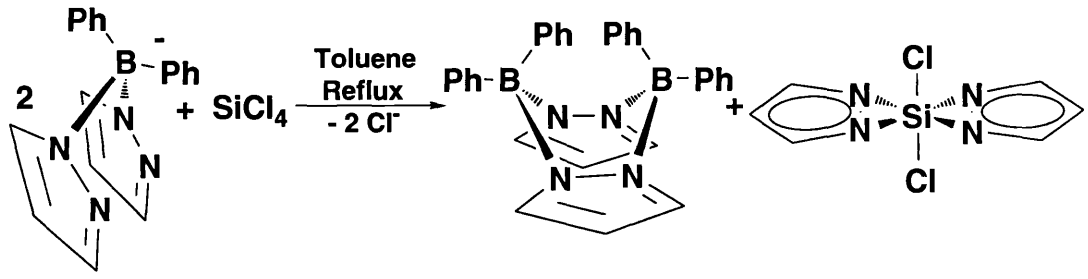

We might also expect these ligands to be incompatible with strongly oxidising species such as Ce^{4+}. However, there has been a report of an Mn^{4+} complex, $[(Tp^{Me2})_2Mn]^{2+}[ClO_4]_2^{2+}$, which was synthesised by the reaction of $[(Tp^{Me2})_2Mn]$ with $NaMnO_4$![124] The compound was found to have an Mn^{4+}/Mn^{3+} redox potential of 1.35 V (relative to the Standard Calomel Electrode); this compares to a couple of only 1.20 V for Ce^{4+}/Ce^{3+}.

Tris-(pyrazolyl)borate Chemistry and the Lanthanides

Pyrazolylborates have been used as ancillary ligands for most metals in the periodic table and several reviews have been published covering the very extensive chemistry that has been developed in this field.[100-102,127,128] Lanthanide pyrazolylborate complexes were first reported by Bagnall and coworkers in 1976[129] and a review of f element pyrazolylborate chemistry[130] has recently been published.

All of the *tris*-(pyrazolyl)borate lanthanide chemistry reported in the literature prior to 1993 utilised the unsubstituted and sterically relatively undemanding ligand Tp. Thus, the compounds $[Tp_3Ln]$ (Ln = La, Ce, Pr, Sm, Gd, Er, Yb and Y) were synthesised in aqueous solution from the corresponding chlorides,[129] and similar routes were used to make the corresponding *tetrakis*-(pyrazolyl)borate analogues $[(pzTp)_3Ln]$.[131] In both cases the Yb complexes are eight coordinate and isostructural (Figure 1.12**a**).[131,132] Interestingly, this structure persists in solution on the NMR time scale (as shown by multinuclear studies);[72] in general, the ionic bonding in lanthanide compounds leads to highly fluxional species in solution. Reaction of lanthanide chlorides with one or two equivalents of KTp or NaTp under a variety of conditions has allowed the isolation of the following complexes: $TpLnCl_2(THF)_{1.5}$ (Ln = Er and

Y),[129,133] Tp_2LnCl (Ln = Sm, Tb, Er and Y),[134-136] $Tp_2LnCl(THF)$ (Ln = Er, Yb, Lu and Y),[129,133,137] $Tp_2LnCl(pzH)$ (Ln = Tb and Y)[135,136] and $Tp_2LnCl(OH_2)$ (Ln = La and Y).[134] However, structural characterisation of these mixed chloride/*tris*-(pyrazolyl)borate compounds is limited to the water adduct (Ln = Y), which contains an eight coordinate metal centre; the coordination geometry of the remaining complexes is not known. Attempts to replace the chloride ligands in these complexes with other monodentate anions (especially alkyls) have invariably resulted in ligand redistribution reactions and the formation of $[Tp_3Ln]$.[130,133] Only the use of bidentate anions such as β-diketonates, oxalates and carboxylates has enabled a number of well characterised complexes of the type Tp_2LnX to be synthesised, for example, Figure 1.12**b**,[135] **c**,[136] **d**,[138,139] **e**[140,141] and **f**.[142] The structures of these complexes were found to vary depending both on the size of the metal and the nature of the X ligand.

In addition, mixed cyclooctatetraenyl/*tris*-(pyrazolyl)borate complexes have been synthesised by reaction of $TpLnCl_2(THF)_{1.5}$ with $K_2(COT)$ at low temperature to give [TpLn(COT)] (Ln = Er, Lu and Y),[133] and more recently by metathesis of $[Y(COT)(\mu\text{-}O_3SCF_3)(THF)]_2$ or $[(COT)LnCl(THF)_n]_2$ with a pyrazolylborate anion to give TpLn(COT) and $Tp^{Me2}Ln(COT)$ (Ln = Y, Ce, Pr, Nd and Sm).[143,144] Crystallographic characterisation showed the complexes to have parallel structures, similar to those observed for the pentamethylcyclopentadienyl analogues.[145,146]

All the structural characterisation obtained for unsubstituted *tris*-(pyrazolyl)borate complexes of the lanthanides indicates fairly normal metal coordination numbers of seven or eight. Most of the compounds were found to be highly fluxional in solution, indicating rapid reorientation of the ligands on the metal. In addition, Jones and coworkers have shown that intermolecular ligand exchange occurs between complexes such as $[Tp_3Yb]$ and $[Tp_2Lu(acac)]$ (acac = acetylacetonate), the mixture coming to equilibrium after a couple minutes (Equation 1.10).[147] Such a mechanism accounts for the problems experienced in synthesising derivatives of the $TpLn^{2+}$ and Tp_2Ln^+ fragments.

Equation 1.10

$$Tp_3Yb + Tp_2Lu(acac) \xrightleftharpoons{CDCl_3} Tp_2Yb(acac) + Tp_3Lu$$

Figure 1.12 Some Hydrido-*tris*-(pyrazol-1-yl)borate Complexes of the Lanthanides

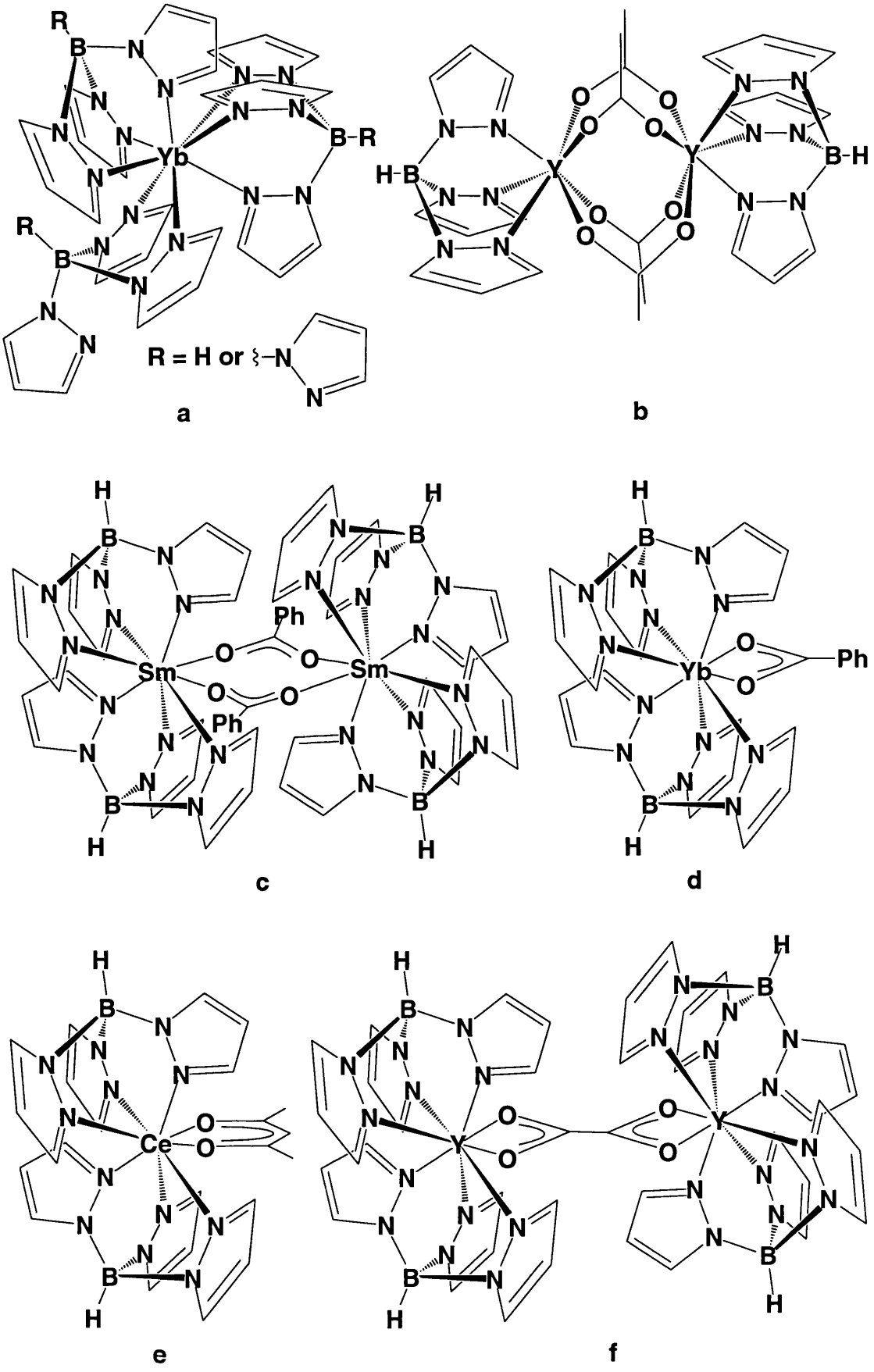

New Lanthanide *Tris*-(pyrazolyl)borate Chemistry

Compounds of the lanthanides have displayed some unique reactivity which has been controlled to a large extent by the choice of ancillary ligands.[24,30,148] Previous studies indicate that the *tris*-(pyrazolyl)borates are suitable ancillary ligands for these elements; however, the ready formation of $[Tp_3Ln]$ as a result of ligand redistribution has been a serious obstacle to further work.[102,130] We hoped that by increasing the steric bulk of the pyrazolylborate ligand through the introduction of substituents at the 3-position of the pyrazolyl ring, trivalent complexes could be synthesised in which ligand redistribution reactions were suppressed. In addition, we planned to extend the pyrazolylborate chemistry of the lanthanides to the divalent state (of which there had been no reports in the literature).

The work presented in this thesis is divided into four chapters. The first of these (Chapter 2) covers the synthesis of trivalent lanthanide complexes of the moderately bulky hydrido-*tris*-(3,5-dimethylpyrazol-1-yl)borate ligand, Tp^{Me_2}, together with some structural and reactivity studies on the new compounds formed. Chapter 3 describes the synthesis and chemistry of divalent lanthanide complexes of Tp^{Me_2} and a closely related derivative. Chapter 4 reports the results of using a much bulkier *tris*-(pyrazolyl)borate group, $Tp^{3\text{-}t\text{-}Bu\text{-}5\text{-}Me}$, as an ancillary ligand for the divalent lanthanides. The experimental details of the work are covered in Chapter 5. This study has resulted in a number of X-ray crystal structure determinations. General comments on the procedures used together with tables of collection data, fractional coordinates and selected bond lengths and bond angles can be found in Appendix 1.

Chapter 2 - Synthesis and Reactivity of Trivalent Lanthanide Complexes of Hydrido-*tris*-(3,5-dimethylpyrazol-1-yl)borate

Introduction

In contrast to previous studies of lanthanide *tris*-(pyrazolyl)borates,[130] which were limited to complexes of the unsubstituted hydrido-*tris*-(pyrazol-1-yl)borate ligand (Tp), in the work presented here we used hydrido-*tris*-(3,5-dimethylpyrazol-1-yl)borate (Tp^{Me2})[149] as an ancillary ligand for these metals. We hoped that the greater steric control offered by Tp^{Me2} would suppress the ligand exchange reactions which had previously restricted the synthesis of well characterised complexes of the type $[Tp_2LnX]$ to systems in which X was a bidentate ligand with oxygen donor atoms.[135,136,138-142] Tp^{Me2} is one of the most widely used pyrazolylborates,[102] a fact not unconnected with the commercial availability of cheap 3,5-dimethylpyrazole. In addition, the presence of 5-Me substituents on the pyrazolyl ring simplifies the preparation of this ligand, since they prevent the formation of the *tetrakis*-compound. Hence, the careful temperature control required for the synthesis of KTp[103] is not so critical for the corresponding Tp^{Me2} salt.

In preliminary studies with this ligand, we focused on its coordination to trivalent lanthanide ions. This was prompted by the redox stability of this oxidation state compared with that of the divalent state of these elements. It also seemed appropriate that initial investigations should address how the previously reported chemistry of the Tp_2Ln^+ fragment was affected by the introduction of 3,5-dimethyl substituents onto the pyrazolyl ring. The lanthanide precursors selected for this work were the anhydrous trifluoromethanesulphonates ($Ln(OTf)_3$; OTf = triflate = O_3SCF_3). These were chosen principally because of their ease of preparation (reaction of the inexpensive lanthanide oxides with aqueous trifluoromethanesulphonic (triflic) acid followed by dehydration under vacuum at 200 °C).[150] This is in contrast to the synthesis of more traditional starting materials such as the anhydrous trichlorides, for which much more rigorous procedures are required in order to prevent hydrolysis which results in the formation LnOCl. In addition, it was hoped that the stability of the free triflate anion, together with its poor ligating properties, would lead to its facile displacement by other groups.[151] Good 'leaving groups' are of particular importance in lanthanide chemistry, for

example, syntheses employing the trichlorides frequently result in the formation of 'ate' complexes in which the unwanted chloride by-product remains coordinated to the lanthanide.[148] Finally, the characteristic IR spectrum of the triflate group provides a simple and convenient means of detecting its presence in reaction products. There have been several reports of the successful use of lanthanide triflates as precursors to cyclopentadienyl complexes,[152-154] and more recently their utility in cyclooctatetraenyl (COT, C_8H_8) lanthanide chemistry has been described.[22,143,155] It is appropriate to note that investigations into the reactivity of some of these COT derivatives have included the successful substitution of a triflate group for a *tris*-(pyrazolyl)borate at an Y centre (Equation 2.1).

Equation 2.1[143]

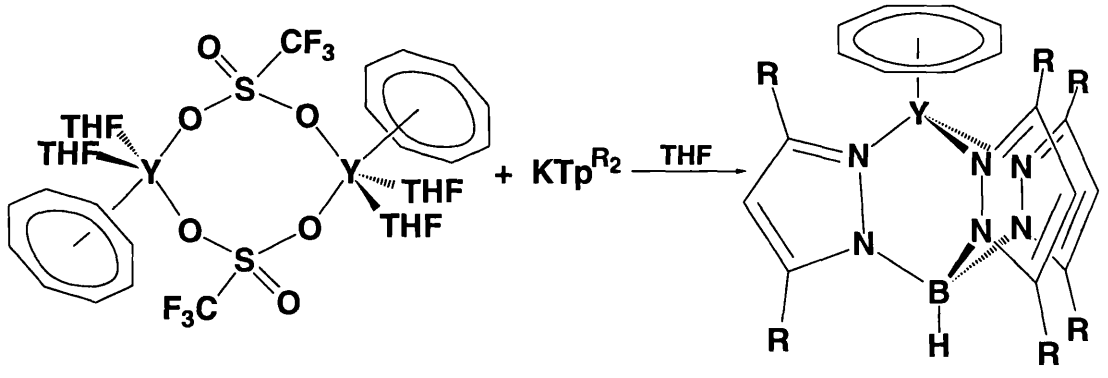

In this chapter, the synthesis, characterisation and reactivity studies of some new trivalent lanthanide complexes of Tp^{Me2} (numbered **2.1** to **2.6**) will be described.

Preparation and Characterisation of *Bis*-(hydrido-*tris*-(3,5-dimethylpyrazol-1-yl)borate) Lanthanide Triflates[1,2]

The metathesis of lanthanide triflates with two equivalents of KTp^{Me2} in THF took one of two courses, depending on the size of the metal (see Figure 2.1). For the larger lanthanides (Ln = La (**2.2**), Nd (**2.3**) and Sm (**2.4**)), a slightly turbid solution was obtained from which, after removal of THF under reduced pressure, the product could be extracted into toluene. Further purification was

achieved by recrystallisation from a concentrated toluene solution, either by cooling or by slow diffusion into 30/40 petrol. In contrast, when Ln was a smaller lanthanide (Y (**2.1**), Dy (**2.5**) and Yb (**2.6**)) the analogous reaction resulted in the formation of a heavy white precipitate. Following the removal of solvent, the solid (which was insoluble in toluene) was extracted with dichloromethane. The crude extract could be crystallised by slow diffusion of 30/40 petrol into the dichloromethane solution. In both cases, after extraction of the product into the appropriate solvent, the residues were confirmed to be $K^+[OTf]^-$ from their IR spectra - the most striking feature being a very strong absorption at *ca* 1275 cm^{-1}. The colours of the lanthanide products were typical of trivalent complexes of these metals: all were white with the exception of the Nd compound (**2.3**) which was pale blue. Elemental analyses confirmed that all the complexes had the composition $(Tp^{Me2})_2LnOTf$.

Figure 2.1 The Preparation of Trivalent Lanthanide Complexes of Tp^{Me2}

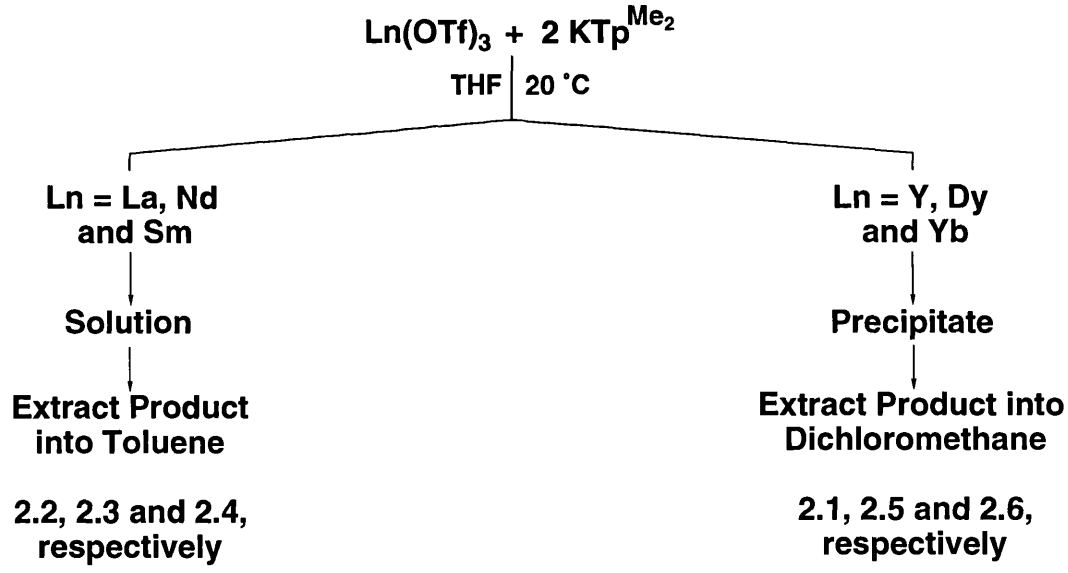

Attempts were also made to synthesise the Pr and Eu complexes. In the case of the former, the failure to isolate a pure product was later found to be due to contamination (*ca* 50 %) of the original Pr_6O_{11} with La_2O_3! The difficulty encountered in synthesising the Eu compound was attributed to the complex having solubility properties which were intermediate between the two extremes outlined above. This considerably complicated the isolation and purification procedures. Both the Pr and Eu complexes, together with those of Ce, Gd and Ho, were later synthesised and isolated by Sung-Ying Liu of our

laboratory.[156] In common with the above trend, the Ce and Pr compounds were found to dissolve readily in non-polar solvents, whilst those of Gd and Ho were insoluble.

The pronounced difference in solubility of the two types of complex isolated, suggested that a significant change in the structure of these products was accompanying the contraction in the ionic radius of the metal. Such behaviour is far from uncommon in lanthanide chemistry, since the negligible covalent contribution to the bonding causes the molecular structure to be determined by a very delicate balance between steric and electrostatic interactions. Indeed, a good example of the effect that the lanthanide contraction can have on structure may be found in previous reports of the pyrazolylborate chemistry of these elements: whilst the complexes $[Tp_2Sm(\mu\text{-}O_2CPh)]_2$[136] and $[Tp_2Yb(\eta^2\text{-}O_2CPh)]$[138,139] both have the same empirical formulae and contain an eight coordinate metal ion, the first is dimeric, whereas the second is monomeric. This can be attributed to the size of the Yb^{3+} ion, which is too small to sustain the steric crowding required for dimer formation. Instead, the carboxylate group chelates to the metal giving a monomer, the much tighter bite angle in this system (O–M–O = 56.5(2)° compared with *ca* 80° for the Sm dimer) relieving the steric oversaturation at the Yb centre. One could envisage a similar dimer to monomer transition for the $(Tp^{Me2})_2LnOTf$ series of compounds. However, in the light of the marked insolubility of the complexes of the smaller lanthanides, it seemed more likely that these species consisted of discrete $[(Tp^{Me2})_2Ln]^+$ cations and triflate anions (Figure 2.2**a**), with the more soluble compounds of the larger metals adopting the molecular structure $[(Tp^{Me2})_2LnOTf]$ (Figure 2.2**b**).

^1H and ^{13}C NMR spectroscopy in $CDCl_3$ confirmed that the pyrazolylborate ligand had remained intact during the reaction. In addition, all of the compounds displayed only one set of pyrazolyl resonances, indicating either that the compounds were highly fluxional at room temperature or that they were of very high symmetry. The pyrazolyl ^1H chemical shifts (δ) for the (diamagnetic) Y^{3+} (**2.1**) and La^{3+} (**2.2**) complexes were virtually identical, consisting of three resonances in a ratio of 3:3:1 at *ca* δ 1.8, 2.4 and 5.8, respectively. Whilst there is no simple way by which to discriminate unambiguously between the 3- and the 5-Me resonances in these two complexes, it has been reported by Reger and coworkers that one of the Me resonances in the crystallographically characterised complex $[Tp^{Me2}In(Bp)Cl]$ (Bp = dihydrido-*bis*-(pyrazol-1-yl)borate) has a rather high field ^1H chemical

shift (Figure 2.3).[157] This was assigned to the Me substituent (a) which points in between the two pyrazolyl rings of the Bp ligand, the shift being understood in terms of the shielding influence of the pyrazolyl ring current.

Figure 2.2 The Proposed Ion Pair (**a**) and Molecular (**b**) Structures of the Complexes $(Tp^{Me2})_2LnOTf$

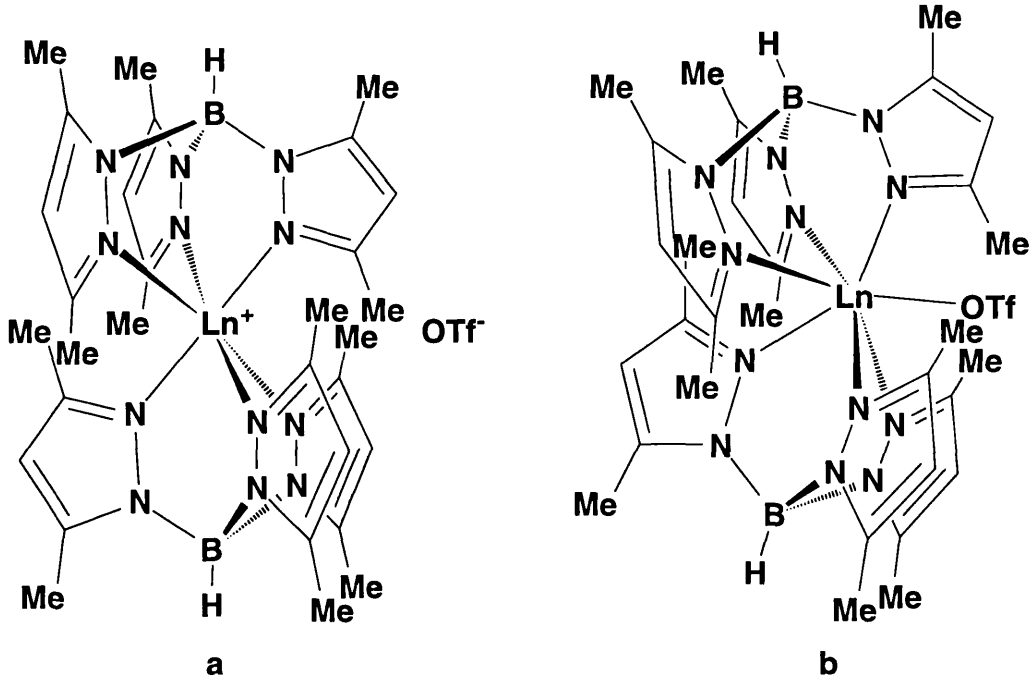

Figure 2.3 The Structure of and Selected ^1H NMR Data for $[Tp^{Me2}In(Bp)Cl]$

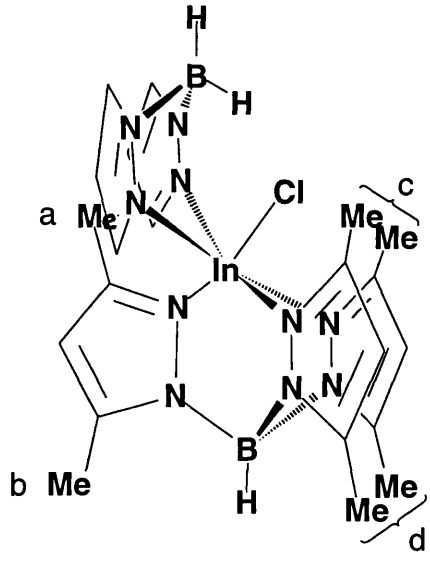

Me Group	^1H Chemical Shift (δ)†
a	0.15 (s, 3H)
b	2.33 (s, 3H)
c, d	2.41, 2.44 (s, 2 × 6H)

† Coupling pattern and relative integration in parentheses

A similarly large effect might be expected for the 3-Me resonances of the $(Tp^{Me2})_2LnOTf$ complexes, due to the interlocking of some or all of these substituents in the static structures shown in Figure 2.2**a** and **b**. Interestingly, this is not observed and the Me resonances in both **2.1** and **2.2** remain relatively unshifted from their positions in KTp^{Me2} (δ 1.99 and 2.30, measured in d_6-acetone). This may be due to the larger size of the Ln^{3+} ions (1.032 and 0.900 Å) compared with In^{3+} (0.800 Å),[15] leading to a much reduced interaction of the Me protons with the field of the pyrazolyl ring electrons. However, it probably also reflects a high degree of lability in these lanthanide complexes, which results in relatively loose coordination of the ligands to the metal in $CDCl_3$ solution. In support of this, a study by Moss & Jones has indicated that intermolecular ligand exchange is quite facile in lanthanide pyrazolylborate systems.[147] However, in the light of Reger's report, the most up field of the two Me singlets in the ^1H NMR spectra of **2.1** and **2.2** is nominally assigned to the 3-Me protons.

The peak in the ^1H NMR spectra of **2.1** and **2.2** corresponding to the *tris*-(pyrazolyl)borate B–H was too broad to be observed at room temperature, presumably due to the quadrupolar effect of the ^{10}B (nuclear spin, I = 3) and ^{11}B (I = 3/2) nuclei. The ^{13}C resonance due to the CF_3 group, which is expected to occur at *ca* δ 120 (*eg* in 4-vinylphenyl triflate),[158] was not observed. This is not uncommon and is a result of both the relatively long relaxation time of the CF_3 carbon nucleus and the lower intensity of the signal as a result of coupling to three fluorine atoms (I = 1/2) to give a quartet.

For the remaining complexes, the pyrazolyl ^1H resonances were shifted from these diamagnetic positions. In all cases, one of the two Me signals was significantly broader and more shifted than the other (exemplified by the spectrum of the Yb complex (**2.6**) shown in Figure 2.4). This broad resonance was assigned to the Me group at the 3-position on the pyrazolyl ring, which is closer to the paramagnetic metal centre and is expected to experience a much greater isotropic shift as a result (Figure 2.5). The spectra of the Dy (**2.4**), Gd and Ho complexes were too broad to be easily interpreted, a fact which is not surprising since the magnetic moments are much larger in the second half of the lanthanide series than in the first (see Chapter 1, p 25). The ^1H chemical shifts (at 20 °C) and assignments for all of these *bis*-(hydrido-*tris*-(3,5-dimethylpyrazol-1-yl)borate)lanthanide triflate complexes are listed in Table 2.1.

Figure 2.4 The ^{1}H NMR Spectrum of $(Tp^{Me2})_2YbOTf$ (**2.6**)

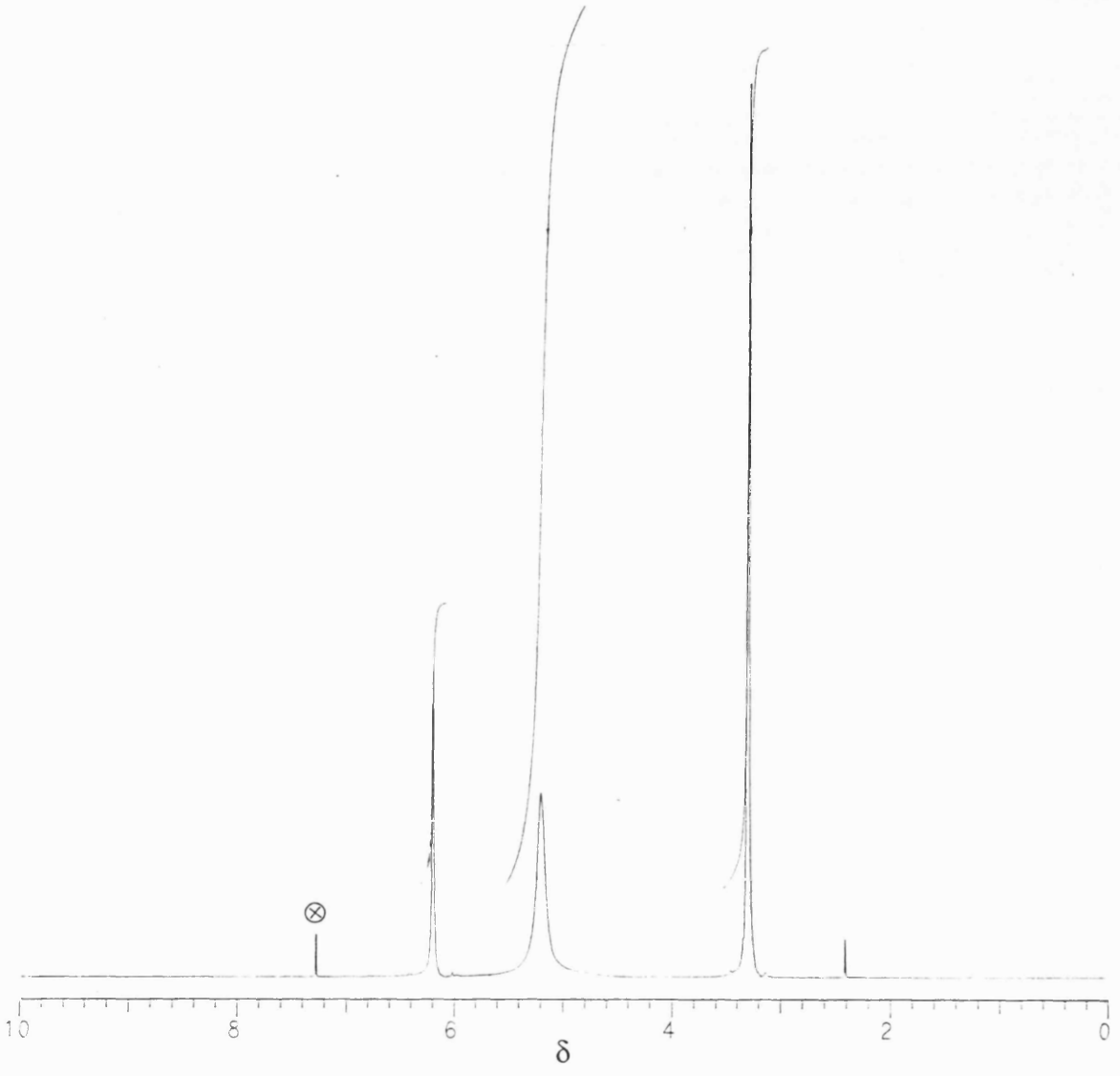

Figure 2.5 The Relative Effect of a Paramagnetic Centre on the NMR Behaviour of the 3- and 5-Substituents in Tp^{Me2}

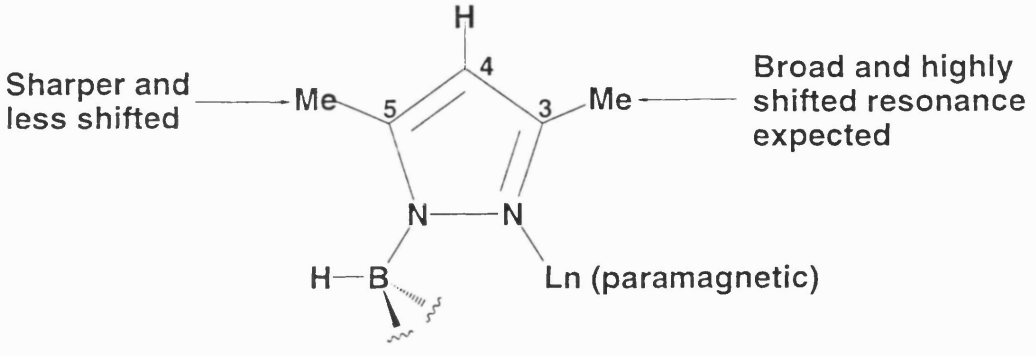

⊗ = $CDCl_3$ resonance

Table 2.1 The Pyrazolyl ^{1}H Chemical Shifts of $(Tp^{Me2})_2LnOTf$†

Lanthanide	δ(3-Me)	δ(5-Me)	δ(4-H)
Y (**2.1**)	1.81	2.47	5.87
La (**2.2**)	1.85	2.41	5.73
Ce§	-14.3	6.0	7.3
Pr§	-12.1	5.4	7.25
Nd (**2.3**)	-9.73	5.16	8.02
Sm (**2.4**)	-1.4	3.3	5.4
Eu§	10.93	-0.14	1.72
Yb (**2.6**)	5.19	3.30	6.19

Plots of reciprocal temperature against ^{1}H chemical shifts of the three pyrazolyl resonances in the Nd complex (**2.3**) were linear (Figure 2.6), consistent with simple Curie-Weiss behaviour and therefore with a monomeric complex whose structure does not change with temperature.[66,74] Similar correlations have been found for the Ce and Eu analogues.[156]

The contact contribution to the isotropic shifts of these ^{1}H resonances may be assumed to be negligible, since bonding is predominantly ionic in lanthanide compounds. The full analysis of the solution NMR spectra of $[(\eta^3\text{-Tp})_2(\eta^2\text{-Tp})Yb]$ in terms of dipolar shifts alone validates this premise for the pyrazolylborate complexes of these metals.[72] The situation is simplified still further if the species being studied has axial symmetry (which in practice means the presence of at least a C_3 symmetry axis). Whilst this clearly does not apply to the static structure proposed for the larger lanthanide complexes (Figure 2.2**b**), the molecular motion of these compounds in solution, which causes the magnetic equivalence of all the pyrazolyl rings, may also confer effective axial symmetry on the system.[159] In this case, the equation for the pseudocontact contribution (Δ_p) to the isotropic shift reduces to:

$$\Delta_p = D'\left(\frac{3\cos^2\theta}{r^3}\right)$$

† In $CDCl_3$. ^{1}H spectra for Ln = Gd, Dy and Ho were too broad to be readable

§ Data provided by Sung-Ying Liu

Figure 2.6 A Plot of Reciprocal Temperature Against ^1H Chemical Shifts for $(Tp^{Me2})_2NdOTf$ (**2.3**)

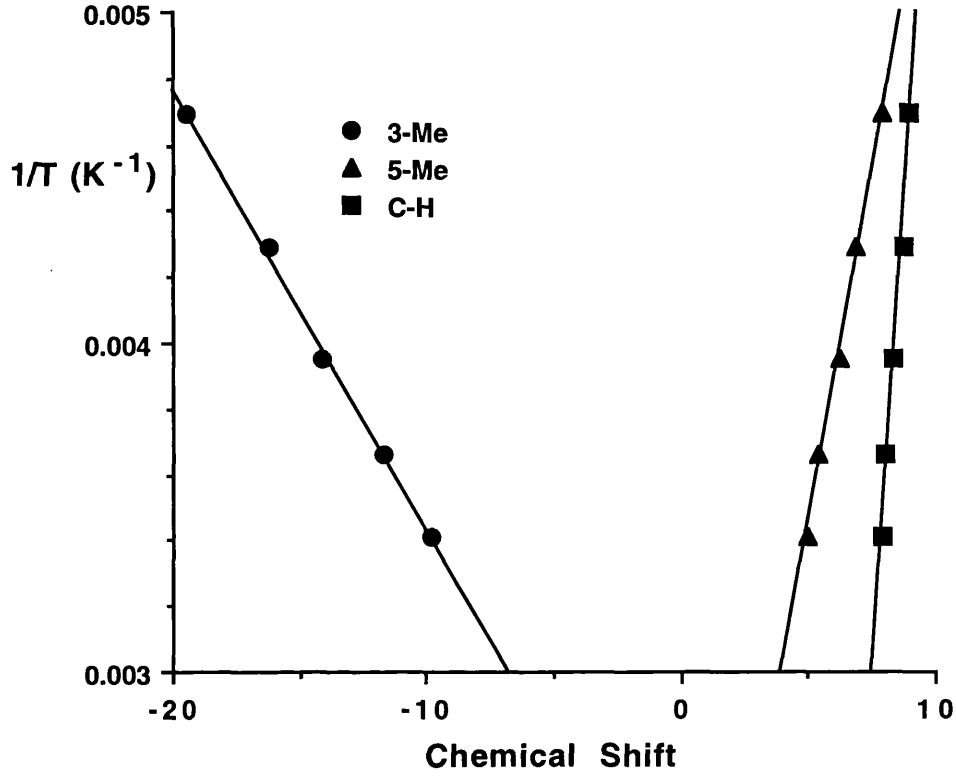

The ratio of the pseudocontact shifts of nuclei *i* and *j* in a single lanthanide complex is therefore independent of the molecular susceptibility anisotropy term *D'*:

$$\frac{\Delta_p^i}{\Delta_p^j} = \frac{r_j^3\left(3\cos^2\theta_i - 1\right)}{r_i^3\left(3\cos^2\theta_j - 1\right)}$$

Hence, this ratio is not affected by the magnetic properties of the metal ion, and should, in theory, be constant for a series of isostructural compounds.[69] The results of this approach applied to the $(Tp^{Me2})_2LnOTf$ series of complexes is shown in Table 2.2.

It is clear that the Ce, Pr and Nd (**2.3**) compounds have ratios which are similar in both sign and magnitude to one another. Furthermore, they are of opposite sign to the ratios calculated for the Yb species (**2.6**). The complexes of Sm (**2.4**) and Eu appear to present an intermediate situation, in that their

Table 2.2 The Ratio of the Isotropic Shifts of the 5-Me and 4-H ^1H Resonances Relative to the 3-Me Peak for $(Tp^{Me2})_2LnOTf$

Lanthanide	Shift (3-Me) / Shift (3-Me)	Shift (5-Me) / Shift (3-Me)	Shift (4-H) / Shift (3-Me)
Ce†	1.00	-0.22	-0.09
Pr†	1.00	-0.22	-0.11
Nd (**2.3**)	1.00	-0.24	-0.19
Sm (**2.4**)	1.00	-0.28	0.13
Eu†	1.00	0.27	-0.45
Yb (**2.6**)	1.00	0.26	0.12

values do not fit with either of these two distinct classes. Attempts to correlate the observed ratios for these two complexes with partial contributions from the two extremes were not successful. Whether this is due to a failure of one or more of the initial assumptions is not clear. In addition, the gross structural change which is proposed might be an oversimplification, and as the change-over from a molecular to an ion pair species approaches, more subtle changes may occur which are not magnetically accounted for in terms of the two extremes.

We obtained additional structural information from a study of the IR spectra of these compounds.[2] In view of our proposed change in structure of $(Tp^{Me2})_2LnOTf$ due to the lanthanide contraction, the vibrational modes of the triflate ligand were of particular interest. *Ab initio* calculations,[160,161] as well as ^{18}O[162] and ^{13}C[161] isotopic labelling studies, have been reported for the uncoordinated triflate anion. Bands due to bending of the CF_3 and SO_3 groups occur mainly below 650 cm^{-1}. For C_{3v} symmetry, two SO_3 stretching frequencies are expected. In $[NBu^n_4]^+[OTf]^-$ these occur at 1032 and 1273 cm^{-1} and are the symmetric and antisymmetric modes, respectively.[162] The latter is the prominent feature in the spectrum of $K^+[OTf]^-$ referred to earlier. Similarly, two absorptions are to be expected for the CF_3 group. In $[NBu^n_4]^+[OTf]^-$ the antisymmetric stretch occurs at 1149 cm^{-1}, whilst the symmetric mode mixes to some degree with the symmetric C–S stretch giving rise to two bands at 752 and 1222 cm^{-1}.[162]

† Calculated from data provided by Sung-Ying Liu

All of these features were found in the IR spectra (run as KBr discs) of the Y (**2.1**), Sm (**2.4**), Dy (**2.5**) and Yb (**2.6**) compounds, as well as in those of Eu, Gd and Ho, confirming that the complexes of the smaller lanthanides contain discrete $[OTf]^-$ anions. In addition to the triflate bands, the IR spectra also contained many absorptions due to vibrations within the pyrazolylborate ligand, including the characteristic B–H stretch which occurs at *ca* 2560 cm^{-1}. The spectra of all of these complexes were completely superimposable. Table A2.1 in Appendix 2 gives a complete list of absorptions for compound **2.5** and also for $[NBu^n_4]^+[OTf]^-$, together with assignments, and calculated wavenumbers for the free triflate anion.

The spectra of the complexes of La (**2.2**) and Nd (**2.3**), together with those of Ce and Pr, bore an obvious resemblance to those of the smaller lanthanides. The positions of the bands due to vibrations within the pyrazolylborate ligand were little affected by the change in ionic radius of the metal. However, several appeared to have split, consistent with these complexes having lower symmetry than the smaller lanthanide analogues. In addition, the positions of many of the bending modes of the triflate group showed little or no change. In contrast, there is a very obvious effect on the SO_3 stretching vibrations upon increasing the size of the lanthanide. Thus, the two bands at 1047 and 1275 cm^{-1} in **2.5** are replaced by three new absorptions at 1013, 1204 and 1331 cm^{-1} in the spectrum of **2.3** (Figure 2.7). The band which remains at *ca* 1045 cm^{-1} in this spectrum is also present in that of KTp^{Me2} and is therefore likely to be due to a vibrational mode of the pyrazolylborate ligand. The splitting of the stretching modes in the SO_3 group is consistent with the reduction in symmetry from C_{3v} to C_s which occurs upon coordination of the triflate group to the metal. The wavenumbers of these new bands are similar to those observed in η^1-coordinated triflate complexes such as $(\mu\text{-H})_2Os_3(CO)_9(\mu,\eta^2\text{-}O_2CCH_3)(\eta^1\text{-OTf})$: 995, 1202 and 1343 cm^{-1}.[163] Similarly, the CF_3 stretching absorptions in **2.3** shift to 783, 1166 and 1234 cm^{-1}. This compares to 1164, 1185 and 1232 cm^{-1} in the Os compound (for which no bands lower than 995 cm^{-1} were reported); a vibration at *ca* 1185 cm^{-1} in **2.3** is impossible to resolve since a rather broad band at approximately this wavenumber is present in the pyrazolylborate ligand itself. Again, the IR spectra for the complexes of these larger lanthanides were superimposable. Table A2.1 in Appendix 2 contains the full listing and assignment of all the bands in compound **2.3** and in $(\mu\text{-H})_2Os_3(CO)_9(\mu,\eta^2\text{-}O_2CCH_3)(\eta^1\text{-OTf})$.

Figure 2.7 A Comparison of the IR Spectra of $(Tp^{Me2})_2LnOTf$ (Ln = Nd (**2.3**) and Dy (**2.5**)) as KBr Discs

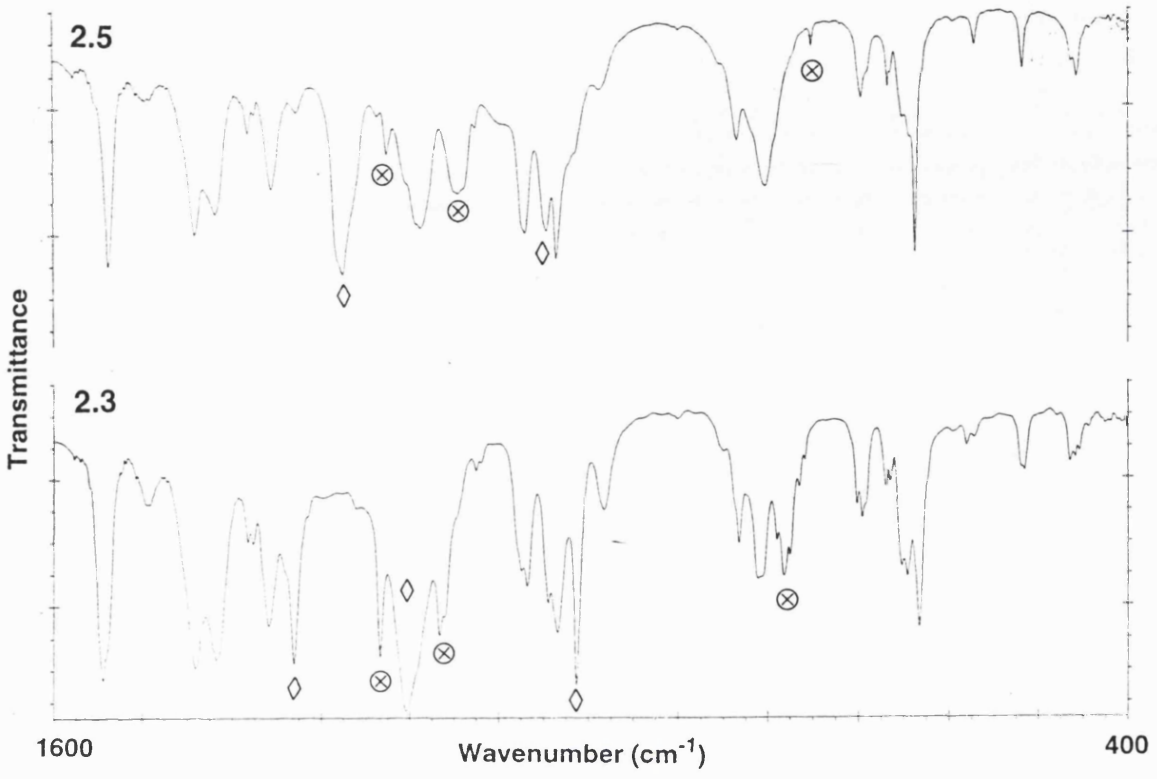

The experimental observations for the Sm complex (**2.4**) are somewhat contradictory: the solubility of the compound in a non-polar solvent (toluene) suggests a molecular species, in contrast to the solid state IR evidence which is consistent with the ionic structure $[(Tp^{Me2})_2Sm]^+[OTf]^-$. In the light of this, it was clearly of interest to determine the IR spectra of the complexes in solution. The solid state IR spectra of **2.1** to **2.6** suggested that the most reliable indicator of an uncoordinated triflate anion was a band at *ca* 1275 cm^{-1}, whilst an absorption at *ca* 1204 cm^{-1} could be taken as good evidence for η^1-coordination of this ligand. $CDCl_3$ was selected as the solvent for this study. This was based on its ability to dissolve both the ionic and molecular complexes, and because it contained no strong absorptions in this critical region of the spectrum.

Whilst the spectra obtained were of somewhat poorer resolution than those from the solid state study, the bands of interest were clearly discernible. The complexes of the lighter lanthanides (La (**2.2**), Ce, Pr and Nd (**2.3**)) all showed a strong absorption in the region 1203 to 1208 cm^{-1}, consistent with

$\otimes = \nu_{CF_3}$; $\Diamond = \nu_{SO_3}$

the solid state IR spectra and indicating an η^1-coordinated triflate group. The spectra obtained for the complexes of smaller metals (Y (**2.1**), Gd, Dy (**2.5**), Ho and Yb (**2.6**)) were also in agreement with the solid state experiments: all exhibited strong bands at *ca* 1264 cm^{-1}, implying an ion pair structure. In contrast to the clear cut situation at either end of the lanthanide series, the solution spectra of the Sm (**2.4**) and Eu compounds indicated that both molecular and ion pair species were present in $CDCl_3$ solution, there being absorptions at *ca* 1208 and 1264 cm^{-1}. Figure 2.8 shows a comparison of the solution IR spectra of the Nd (**2.3**), Sm (**2.4**), Eu and Dy (**2.5**) complexes.

Figure 2.8 A Comparison of the IR Spectra of $(Tp^{Me2})_2LnOTf$ (Ln = Nd (**2.3**), Sm (**2.4**), Eu and Dy (**2.5**)) in $CDCl_3$ Solution

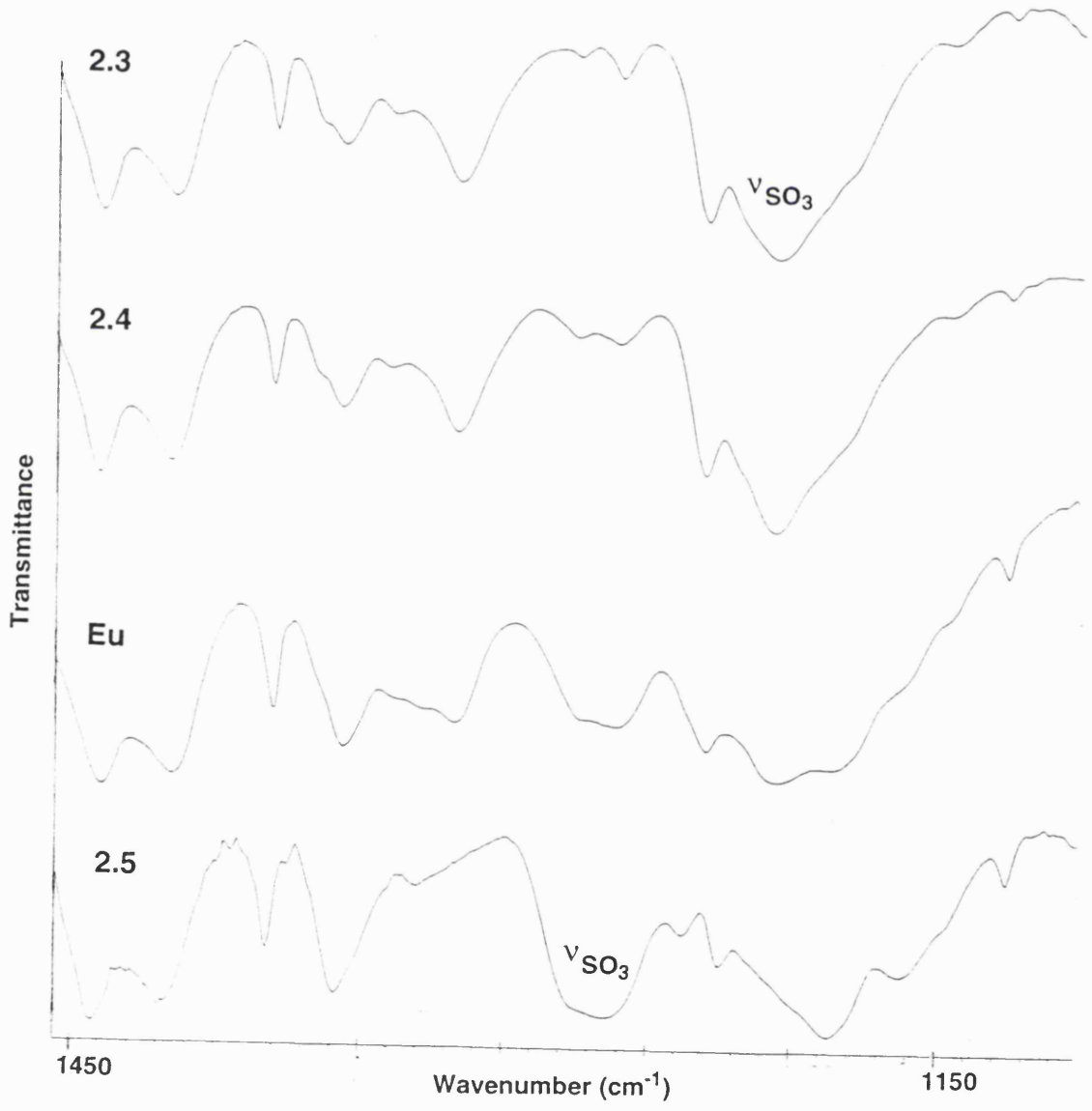

A semi-quantitative estimate of the degree of ionisation in solution was made by comparing the area under the absorption band at 1264 cm^{-1} with that in a normalised spectrum of one of the fully ionised complexes. This approach indicated that *ca* 30 % of the Sm compound (**2.4**) existed in its ionised form in $CDCl_3$, whilst for the Eu complex this figure was *ca* 55 %. Table 2.3 gives a summary of the results of the solid state and solution IR studies of these complexes.

Table 2.3 A Summary of the IR Data for the Complexes $(Tp^{Me2})_2LnOTf$

Lanthanide	KBr Disc ν_{S-O} cm^{-1}	$CDCl_3$ ν_{S-O} cm^{-1}	Implied Structure
La (**2.2**), Ce†, Pr† and Nd (**2.3**)	*ca* 1203	*ca* 1208	Always molecular
Sm (**2.4**)	1273	1208 1263, 1277	Solid: ionic Solution: 70 % molecular, 30 % ionic
Eu†	1274	1207 1263, 1274	Solid: ionic Solution: 45 % molecular, 55 % ionic
Gd†, Dy (**2.5**), Ho†, Yb (**2.6**) and Y (**2.1**)	1276	*ca* 1264	Always ionic

The coexistence of these two structural types in solution is a powerful demonstration of how finely balanced the steric and electrostatic interactions are in lanthanide complexes. Furthermore, the single set of pyrazolyl resonances observed in the NMR spectra of the Sm (**2.4**) and Eu complexes implies that the ion pair and molecular forms are in equilibrium with each other (Equation 2.2) and that the association/dissociation of the triflate ion from the metal is very rapid. In view of this, it is interesting that the Curie-Weiss plot for the Eu complex was linear: as a result of their different structures, the protons in the ion pair and molecular species would not be expected to experience the same isotropic shifts. Hence, we would expect the ^1H chemical shifts to vary depending on the position of this equilibrium and therefore on the temperature of the measurement. That detectable deviation from the

† Data for solid state spectra and samples for solution study from Sung-Ying Liu

Curie-Weiss law is not observed in this case may indicate that this particular equilibrium is rather insensitive to temperature. Alternatively, the chemical shifts may not be altered to a significant degree by the change in structure, although the marked difference in the ratios of the isotropic shifts of the complexes at the extreme ends of the series (*vide supra*), suggests that this is not the case. Finally, it is also interesting to note that none of the NMR spectra showed any significant concentration dependence, which one might expect were such a structural equilibrium operative.

Equation 2.2

$$[(Tp^{Me_2})_2LnOTf] \xrightleftharpoons{CDCl_3} [Tp^{Me_2}{}_2Ln]^+[OTf]^-$$

Ln = Sm and Eu

Attempts to substantiate this proposed structural change further, by vapour pressure osmometry in benzene or dichloromethane solution using the Signer method,[164] were unsuccessful: none of the complexes investigated gave apparent molecular weights which were consistent with either type of structure. It is possible that this was due to ligand redistribution reactions occurring over the long period of time (*ca* 2 weeks) required for the solutions to equilibrate. Solid state confirmation of the two types of structure was obtained from single crystal X-ray diffraction studies of the Nd (**2.3**) and Yb (**2.6**) complexes.[1,2]

Pale blue crystals of $(Tp^{Me2})_2NdOTf$ (**2.3**) were grown by slow cooling of a toluene solution. Details of the data collection may be found in Table A1.1 in Appendix 1, in addition to tables of fractional coordinates, bond lengths and bond angles (Tables A1.2 to A1.4). The complex crystallised in the space group $P2_1/c$, and its molecular structure is shown in Figure 2.9. The two Tp^{Me2} groups are bound to the metal in an η^3-fashion, the inner coordination sphere of the Nd^{3+} ion being best described as a distorted octahedron in which the face defined by N21, N31, and N41 is expanded and capped by the triflate group (Figure 2.10). This coordinates to the metal through a single oxygen atom; thus, the Nd centre is seven coordinate. This is in contrast to previously reported *bis*-(*tris*-(pyrazolyl)borate)lanthanide complexes which all contained eight coordinate metals, and is a reflection of the increased steric bulk of the

3,5-dimethyl substituted ligand and the poor ligating power of the triflate group.

Figure 2.9 The Molecular Structure of $[(Tp^{Me2})_2NdOTf]$ (**2.3**)[2†]

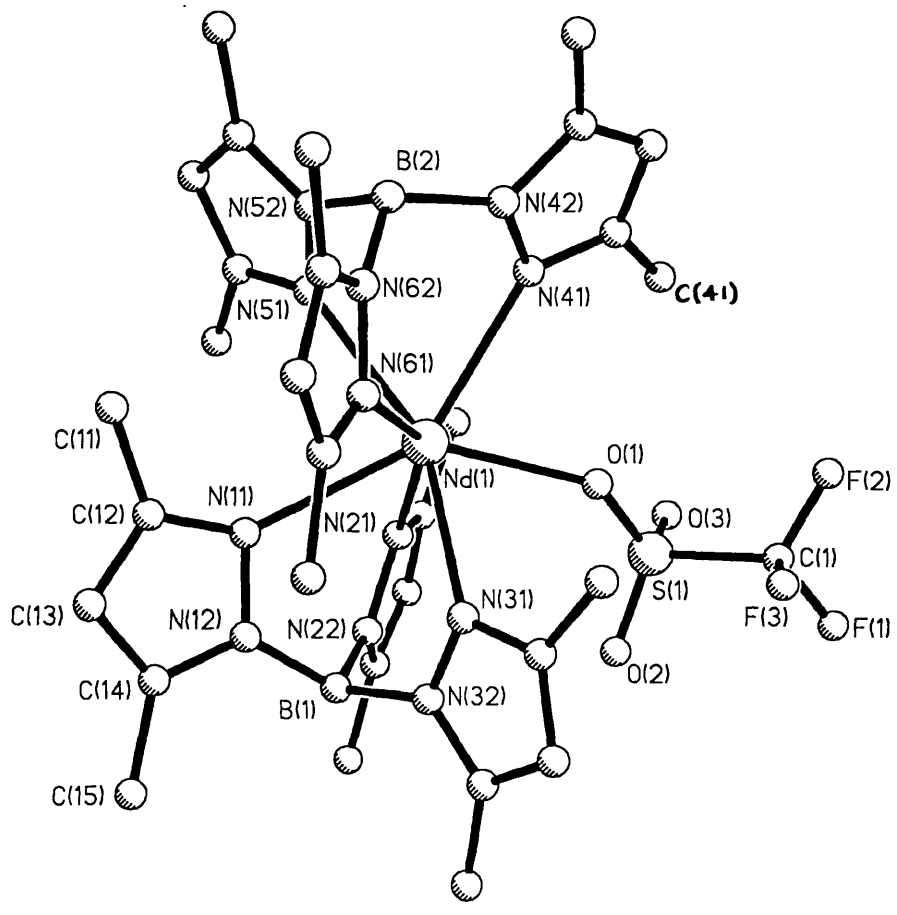

The B(1)···Nd(1)···B(2) angle of *ca* 148° in **2.3** compares with a range of 125° (in $[Tp_2Sm(O_2CPh)]_2$)[136] to 138° (in $[Tp_2Yb(O_2CPh)]$)[138,139] for previously reported complexes containing the Tp_2Ln unit. The smaller degree of bending in the $(Tp^{Me2})_2Nd$ fragment of **2.3** is presumably a consequence both of the more sterically demanding nature of the 3,5-dimethyl substituted ligand and the lower coordination number in this complex. In contrast to the cyclopentadienyl complexes Cp_2LnX, in which the X ligand coordinates approximately symmetrically within the wedge formed by the two carbocyclic rings, the staggered conformation of the pyrazolylborate ligands in **2.3** creates an asymmetric coordination site for the triflate group at the Nd^{3+} ion

† Hydrogen atoms omitted for clarity

Figure 2.10 The Inner Coordination Sphere of $[(Tp^{Me2})_2NdOTf]$ (**2.3**)

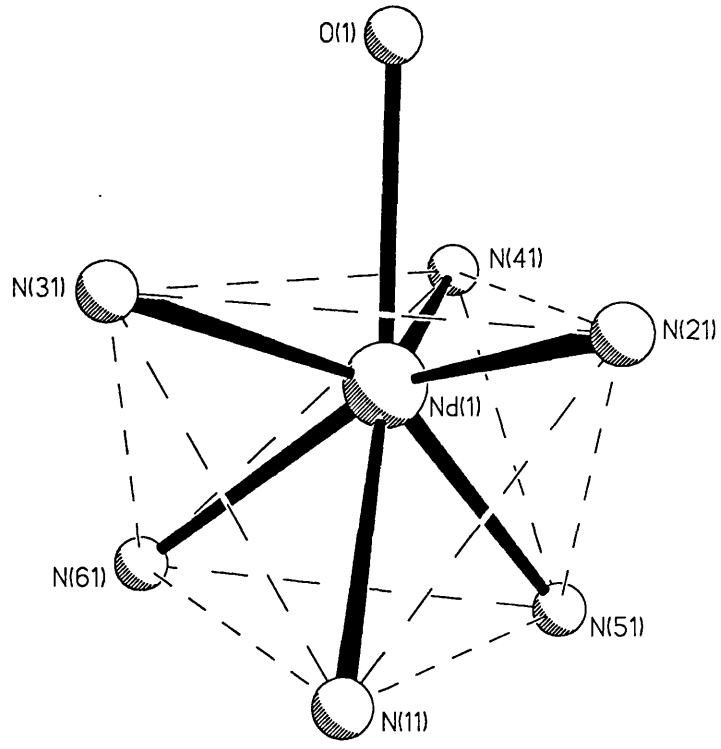

the O(1)–Nd(1)···B(1) and ···B(2) angles being 92 and 117°, respectively. The Nd(1)–O(1)–S(1) angle at first sight seems remarkably large at 141.4(3)°. However, the combination of the steric repulsion of the C(41) Me group on O(1), and the disinclination of the remainder of the triflate group to sink too deeply into the wedge formed by the pyrazolyl rings of the other Tp^{Me2} ligand accounts for this. Even larger M–O–S angles have been reported in other η^1-coordinated triflate complexes such as $[Pd\{Et_2N(CH_2)_2C(O)\}(NHEt_2)(\eta^1\text{-OTf})]$ (150.5(4)°)[165] and $[Cp_2Zr(\eta^1\text{-OTf})_2(THF)]$ (155.2(5)°).[166] The Nd(1)–O(1) distance of 2.421(5) Å is significantly shorter than the range reported in the dimeric cyclooctatetraenyl complex $[(COT)Nd(THF)_2(\mu\text{-}\eta^1\text{-}\eta^1\text{-OTf})]_2$ (2.468(3) to 2.515(3) Å)[155] - a reflection of the decreased bond order associated with a bridging compared with a non-bridging triflate. The only structurally characterised lanthanide complex containing a non-bridging triflate group, $[Lu(\eta^5\text{-Cp})(THF)_3(\eta^1\text{-OTf})_2]$,[152] has a much shorter Ln–O bond length (2.237(4) Å), consistent with the relative sizes of the Nd^{3+} and Lu^{3+} ions. With the exception of complex **2.3**,[2] no reports of Nd *tris*-(pyrazolyl)borate structures exist in the current literature. However, the range of Nd–N bond lengths in this complex - 2.485(5) to 2.598(5) Å - may be compared with those in $[Tp_2Ce(acac)]$ (acac = acetylacetonate) - 2.583(3) to 2.664(3) Å - the increased lengths in the Ce^{3+} compound being a consequence of the larger

ionic radius and coordination number of this metal ion. The only reported crystallographically characterised seven coordinate lanthanide pyrazolylborate complex, $[TpY(\mu\text{-}O_2CMe)_2]_2$,[135] has an average metal-nitrogen bond length which is significantly shorter than that observed in **2.3** (2.474(6) compared with 2.543(6) Å), as expected for the smaller Y^{3+} ion. The Tp^{Me2} ligands in **2.3** are unremarkable, the boron atom being tetrahedrally coordinated with an average B–N–N angle of 120° within experimental error. Thus, no distortion of the ligand seems to occur in order to accommodate the large metal ion.

Crystals of $(Tp^{Me2})_2YbOTf$ (**2.6**) were grown by slow diffusion of 30/40 petrol into a dichloromethane solution of the complex. Details of the data collection and tables of fractional coordinates, bond lengths and bond angles can be found in Appendix 1 (Tables A1.1 and A1.5 to A1.7). The complex crystallised in the space group *C*2/*m*, and the structure confirmed that the Yb^{3+} ion was only six coordinate, the 3-Me substituents on the pyrazolyl ring interlocking and preventing coordination of the triflate group. The molecular structure of the $[(Tp^{Me2})_2Yb]^+$ cation in **2.6** is shown in Figure 2.11.

Figure 2.11 The Molecular Structure of the Cation in $[(Tp^{Me2})_2Yb]^+[OTf]^-$ (**2.6**)[1,2†]

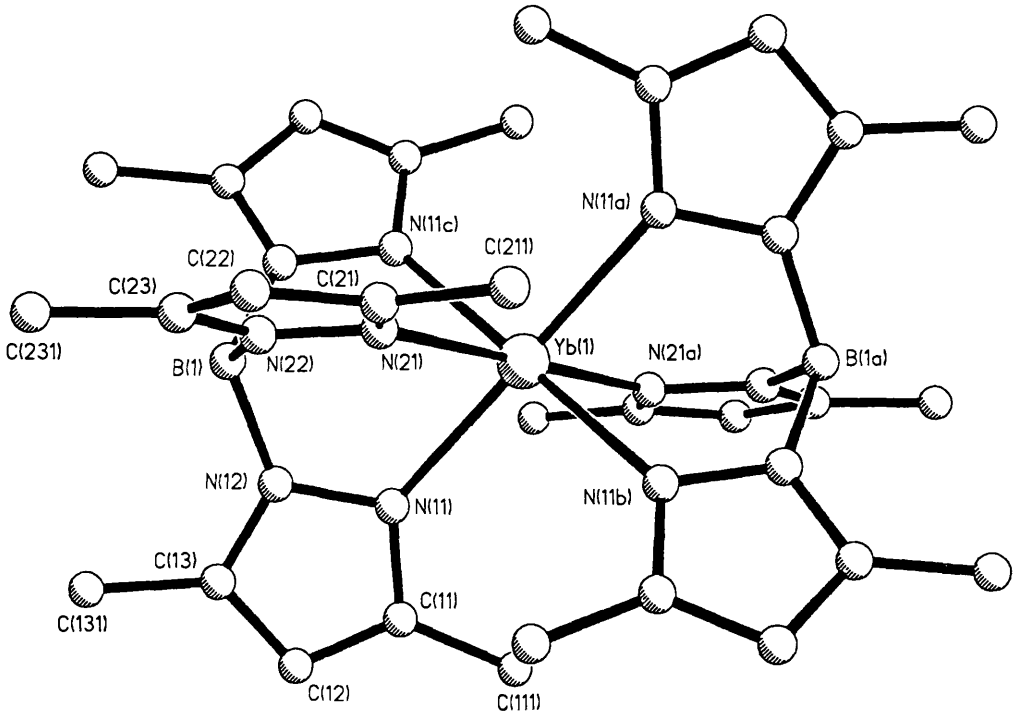

† Hydrogen atoms omitted for clarity

The metal centre lies on a crystallographic C_2 axis and a mirror plane which includes one of the crystallographically unique pyrazolyl rings (numbered 2 in the molecular structure). The triflate anion also lies across the mirror plane; disorder in this group was modelled by refining 50 % occupancy of CF_3 and SO_3 groups in each of the two sites. The two independent Yb(1)–N(11) and Yb(1)–N(21) distances are 2.304(5) and 2.347(6) Å, respectively. These seem remarkably short compared with those observed in **2.3** and in previously reported Yb^{3+} complexes containing η^3-coordinated *tris*-(pyrazolyl)borate groups, for example, [(η^3-Tp)$_2$(η^2-Tp)Yb] (2.401(8) to 2.601(6) Å)[131] and [(η^3-Tp)$_2$Yb(η^2-O_2CPh)] (2.363(6) to 2.481(6) Å)[138,139]. However, in view of the much reduced coordination number in **2.6**, and the ability of the two staggered pyrazolylborate ligands to slot together giving an extremely compact structure, this observation is not surprising. Two analogous structurally characterised Sm^{3+} complexes, [(Tp^{Me2})$_2$Sm]$^+$[BPh_4]$^-$ and [(Tp^{Me2})$_2$Sm]$^+$$I^-$, are known, and these also have short Ln–N bond lengths (of *ca* 2.44 and 2.447(7) Å, respectively).[130,167-169]

Reactivity of *Bis*-(hydrido-*tris*-(3,5-dimethylpyrazol-1-yl)borate) Lanthanide Triflates

Attempts were made to investigate the substitution chemistry of these complexes. For this purpose, the diamagnetic compounds [(Tp^{Me2})$_2$Y]$^+$[OTf]$^-$ (**2.1**) and [(Tp^{Me2})$_2$LaOTf] (**2.2**) were selected in order to simplify product identification by NMR spectroscopy. The remarkable reactivity of the complexes [Cp^*_2Ln(μ-Me)Ln(η^1-Me)Cp^*_2] (Ln = Yb and Lu), shown by Watson to be capable of activating C–H bonds in substrates as inert as methane,[79] made the preparation of alkyl species a particularly attractive goal. Therefore, initial investigations focused on the use of Grignard reagents to substitute the triflate group in these complexes.

The principal reactions which we attempted are outlined in Equations 2.3, 2.4 and 2.5. The metathesis reactions for **2.2** were carried out at room temperature. In contrast, the insolubility of **2.1** in THF meant that no reaction occurred with Bu^{t}MgBr under these conditions. However, heating the mixture to 120 °C caused the precipitate of [(Tp^{Me2})$_2$Y]$^+$[OTf]$^-$ to disappear over a period of *ca* 2 hr. In all cases the toluene soluble part of the reaction mixture was then analysed by ^{1}H NMR spectroscopy. The products **A**, **B**, **C**, **D** and **E** were the main species formed, and their ^{1}H chemical shifts are given in Table

2.4. The ratios of these products were not reproducible and have not been indicated in the following equations.

Equation 2.3

$$[(Tp^{Me_2})_2LaOTf] + Bu^tMgBr \xrightarrow{THF} A + B$$

Equation 2.4

$$[(Tp^{Me_2})_2LaOTf] + EtMgBr \xrightarrow{THF} A + C \xrightarrow[C_6D_6,\ 24\ hrs]{110\ ^\circ C} A + D$$

Equation 2.5

$$[(Tp^{Me_2})_2Y]^+[OTf]^- + Bu^tMgBr \xrightarrow[120\ ^\circ C]{THF} A + B \begin{cases} \xrightarrow[C_6D_6,\ 6\ hrs]{120\ ^\circ C} A + B + D \\ \xrightarrow[12\ hrs]{\Delta,\ vacuum} A + E \end{cases}$$

Table 2.4 The ^1H Chemicals Shifts of Products **A**, **B**, **C**, **D** and **E**†

A	B	C	D	E
2.05 (s, 9H)	2.11 (s, 9H)	2.11 (s, 9H)	1.65 (s, 9H)	2.19 (s, 9H)
2.30 (s, 9H)	2.22 (s, 9H)	2.20 (s, 9H)	2.29 (s, 9H)	2.51 (s, 9H)
5.45 (s, 3H)	5.43 (s, 3H)	5.46 (s, 3H)	5.66 (s, 3H)	5.56 (s, 3H)
	1.77 (s, 9H)	0.57 (q, 2H)		
		2.14 (t, 3H)		

The most revealing aspect of the NMR data is that the Bu^t group in **B** and the Et group in **C** both integrate in a ratio of 1:1 with the Tp^{Me2} ligands in these species. This is not what would be expected if the desired products, $(Tp^{Me2})_2LnR$, had been formed. One possible explanation for this ratio is that these two ligands are complexed to a divalent metal centre - *ie* that **B** and **C**

† Coupling pattern and relative integration in parentheses

are the Mg complexes [$Tp^{Me2}MgBu^t$] and [$Tp^{Me2}MgEt$], respectively. These compounds have been reported by Parkin and coworkers[170] and their ^1H chemical shifts were found to correspond exactly with those of **B** and **C**. It was also reported that heating a solution of the pure alkyl complexes [$Tp^{Me2}MgR$], causes ligand exchange to occur and an equilibrium mixture to be formed (Equation 2.6).[171]

Equation 2.6

$$2\,[Tp^{Me_2}MgR] \rightleftharpoons^{\Delta} [Tp^{Me_2}{}_2Mg] + [MgR_2]$$

A further comparison of ^1H NMR data confirmed that species **D** was [$(Tp^{Me2})_2Mg$]. The formation of small quantities of [$(Tp^{Me2})_2Mg$], which always accompanied the initial reaction of **2.1** with Bu^tMgBr, is not surprising in view of the high temperature required for the reaction. In contrast, heating a solid sample containing **B**, [$Tp^{Me2}MgBu^t$], led to its conversion to a different product (**E**). This might be the unreported hydride derivative $Tp^{Me2}MgH$, formed by the β-elimination of 2-methylpropene from the Bu^t complex. No attempt was made to identify the resonance due to the putative hydride ligand in the ^1H NMR spectrum.

In a straightforward ligand exchange reaction between **2.1** or **2.2** and RMgBr giving [$Tp^{Me2}MgR$], the other product would be [$Tp^{Me2}Ln(OTf)Br$] (Equation 2.7). This species may be responsible for the final set of pyrazolyl peaks observed in the above reactions. However, it is notable that both the Y and La reactions appear to give rise to the same product (**A**). Assuming that the ^1H resonances of [$Tp^{Me2}Y(OTf)Br$] and [$Tp^{Me2}La(OTf)Br$] are not precisely the same, then it is possible that **A** is the compound [$Tp^{Me2}MgBr$], formed by a second ligand exchange reaction (Equation 2.8). Since [$Tp^{Me2}MgBr$] has not been prepared, it was not possible to confirm this hypothesis. However, Parkin has suggested that a compound of this type is liable to undergo ligand redistribution (to give [$(Tp^{Me2})_2Mg$] and $MgBr_2$), and is therefore unlikely to have been formed in the above reactions.[172]

Equation 2.7

$$[(Tp^{Me_2})_2LnOTf] + RMgBr \xrightarrow{THF} [Tp^{Me_2}MgR] + [Tp^{Me_2}Ln(OTf)Br]$$

Equation 2.8

$$[(Tp^{Me_2})_2LnOTf] + RMgBr \xrightarrow{THF} [Tp^{Me_2}MgBr] + [Tp^{Me_2}Ln(OTf)R]$$

The reaction of **2.1** with (allyl)MgCl was also attempted. This resulted in a large number of products, none of which could be identified. In view of the obvious lability of the $(Tp^{Me_2})_2Ln^+$ fragment in the presence of Mg^{2+} ions, the use of Grignard reagents to prepare alkyl derivatives was not pursued further. Attempts to substitute the triflate group in **2.1** and **2.2** using Bu^tLi, MeLi and KBH_4 also resulted in the formation of many species; no tractable product could be isolated from the reaction mixtures. In the case of Bu^tLi, the reactions resulted in a dark orange solution which may indicate that the Tp^{Me_2} ligand itself was being attacked.

A number of substitution reactions have subsequently been successfully carried out on these complexes by Sung-Ying Liu of our laboratory.[156] Derivatives prepared include aryloxides, aryl chalcogenolates, pyrazolides, β-diketonates, borohydrides (using $NaBH_4$), thiocyanates and tetraphenylborates. In addition, it has been shown crystallographically that there is sufficient room at the metal centre in the La compound to accommodate an acetonitrile molecule within the inner coordination sphere - $[(Tp^{Me_2})_2LaOTf(N{\equiv}CMe)]$ - and also that the triflate group can be displaced altogether in the Nd complex by two acetonitrile molecules - $[(Tp^{Me_2})_2Nd(N{\equiv}CMe)_2]^+[OTf]^-$.[156] The successful derivatisation of this series of compounds indicates that the $(Tp^{Me_2})_2Ln^+$ moiety is significantly less prone to ligand redistribution reactions than the previously reported Tp analogues.[130,133] Certainly, these complexes show no tendency to form $(Tp^{Me_2})_3Ln$ when substitution reactions are carried out. Indeed, it has been shown by Liu that attempts to synthesise $(Tp^{Me_2})_3Ln$ result in B–N bond cleavage and the formation of the $[(Tp^{Me_2})_2Ln(pz^{Me_2})]$ in high yields (Equation 2.9).

Equation 2.9[156]

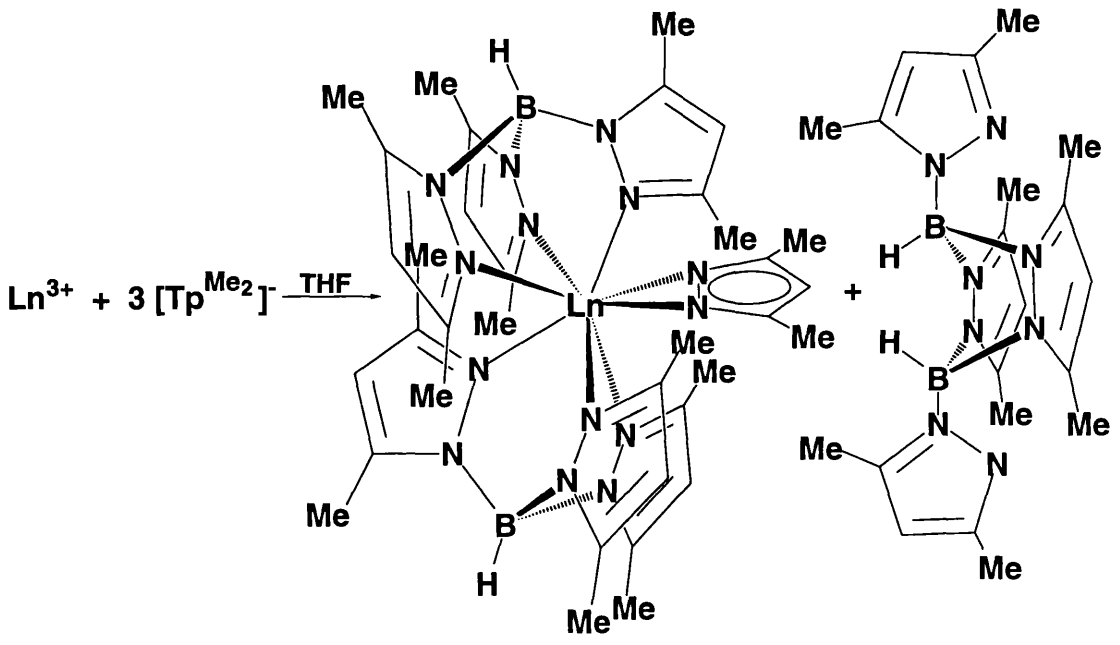

Conclusion

The utility of the substituted *tris*-(pyrazolyl)borate Tp^{Me2} as an ancillary ligand for the trivalent lanthanide ions has been demonstrated in this chapter. Complexes with the composition $(Tp^{Me2})_2LnOTf$ (Ln = Y (**2.1**), La (**2.2**), Nd (**2.3**), Sm (**2.4**), Dy (**2.5**) and Yb (**2.6**)) have been synthesised.[1,2] A variety of techniques have been used to show that for the larger lanthanides, the triflate group coordinates to the metal to give $[(Tp^{Me2})_2LnOTf]$ (**2.2** and **2.3**), whilst for the smaller members of the series, ion pair complexes of the type $[(Tp^{Me2})_2Ln]^+[OTf]^-$ (**2.1**, **2.5** and **2.6**) are formed. For lanthanides of intermediate ionic radius, there are good indications from solution IR studies that these two forms coexist in $CDCl_3$ (**2.4**).[2] Initial attempts to derivatise these complexes were not successful; however, subsequent work by another member of the group has been more fruitful in this respect. The reduction of some of these trivalent complexes to divalent species is reported in Chapter 3.

Chapter 3 - Synthesis and Reactivity of Divalent Lanthanide Complexes with 3-Methyl Substituted *Tris*-(pyrazolyl)borates

Introduction

The work described in Chapter 2 of this thesis was motivated, in part, by the desire to synthesise trivalent lanthanide complexes of Tp^{Me2} which could be used as precursors to divalent compounds. In particular, it was hoped that complexes of the type $(Tp^{Me2})_2LnOTf$ could be reduced to the 'sandwich' molecules $[(Tp^{Me2})_2Ln]$. In the light of the spectacularly rich chemistry of the decamethyllanthanocenes (especially $[Cp^*_2Sm]$),[24,148] it was hoped that a similarly unique and rich reactivity would be found for the Tp^{Me2} analogues. It has already been noted in Chapter 1 that the majority of the lanthanides are extremely unstable in the divalent oxidation state; for this reason, the work presented here was restricted to the divalent species formed upon reduction of $(Tp^{Me2})_2LnOTf$ for Ln = Sm, Eu and Yb.

When our work began in 1993, there had been no reports in the literature of divalent lanthanide complexes of the pyrazolylborates. However, in May of that year, a review of *poly*-(pyrazolyl)borate chemistry[102] referred to the unpublished syntheses by Takats and coworkers of Yb^{2+} and Sm^{2+} sandwich complexes of Tp^{Ph}, Tp^{Tn} (Tn = thienyl) and Tp.† It was claimed that the structures of $[(Tp^{Ph})_2Yb]$ and $[Tp_2Sm]$ had been determined and found to be octahedral, and that oxidation of $[Tp_2Sm]$ with azobenzene (PhNNPh) and Tl^+ gave $[Tp_2Sm(\eta^2\text{-PhNNPh})]$ and $[Tp_2Sm]^+$, respectively. In this chapter, we report our independent syntheses and reactivity studies of *poly*-(pyrazolyl)borate sandwich complexes of divalent lanthanides; new compounds are numbered **3.1** to **3.21**.

Preparation and Characterisation of Divalent *Bis*-(hydrido-*tris*-(3,5-dimethylpyrazol-1-yl)borate) Lanthanide Complexes

The reduction of solutions/suspensions of $[(Tp^{Me2})_2Sm]^+[OTf]^-$ (**2.4**) and $[(Tp^{Me2})_2Yb]^+[OTf]^-$ (**2.6**) in THF with an excess of Na amalgam immediately

† There appeared to be some confusion as to whether this last ligand was Tp or Tp^{Me2}

gave rise to purple and pink solutions, respectively, from which solids of the same colours rapidly precipitated. The freshly prepared products were slightly soluble in the reaction solvent, but were virtually insoluble once dried. The isolated precipitates were moderately oxygen sensitive and their IR spectra showed bands characteristic of both an uncoordinated triflate anion and the hydrido-*tris*-(3,5-dimethylpyrazol-1-yl)borate group, consistent with the reaction shown in Equation 3.1. Since the complex $[(Tp^{Me2})_2Eu]^+[OTf]^-$ had not been purified successfully at this time, the corresponding Eu product was synthesised by first mixing two equivalents of KTp^{Me2} with $Eu(OTf)_3$ in THF, and then reducing with Na amalgam *in situ* (Equation 3.2). This procedure resulted in the formation of a bright orange product with solubility properties similar to those described for the Sm and Yb analogues.

Equation 3.1

$$[(Tp^{Me2})_2Ln]^+[OTf]^- + Na/Hg \xrightarrow{THF} (Tp^{Me2})_2Ln + Na^+[OTf]^- + Hg$$

Ln = Sm and Yb

Equation 3.2

$$Eu(OTf)_3 + 2\,KTp^{Me2} \xrightarrow{THF} + Na/Hg \xrightarrow{THF} (Tp^{Me2})_2Eu + 3\,Na/K^+[OTf]^- + Hg$$

Attempts to synthesise the complexes $(Tp^{Me2})_2Ln$ (Ln = Sm and Yb) by metathesis of SmI_2 or YbI_2 with two equivalents of KTp^{Me2} gave the same insoluble compounds (Equation 3.3), this time mixed with KI. The solid state ^{13}C cross-polarised magic angle spinning (CP MAS) NMR spectrum of the Yb product from this reaction (Figure 3.1) consisted of unshifted resonances with narrow line widths, implying that a diamagnetic Yb^{2+} ($[Xe]4f^{14}$) species had been formed. In addition, the single set of pyrazolyl peaks observed in this spectrum indicated that the product was probably highly symmetric. Thus, the spectroscopic evidence was consistent with this Yb species being $[(Tp^{Me2})_2Yb]$. However, such a molecular structure appeared to be at odds with the almost total insolubility of these products in THF, and further characterisation was hampered by their contamination with alkali metal by-products. Attempts to isolate the lanthanide containing species by continuous

extraction into refluxing THF failed, and whilst the coloured products were found to dissolve in chlorinated solvents (CH_2Cl_2 and $CHCl_3$), these solutions rapidly decolourised, presumably due to chloride abstraction from the solvent by the divalent metals.

Equation 3.3

$$LnI_2 + 2\,KTp^{Me_2} \xrightarrow{THF} (Tp^{Me_2})_2Ln + 2\,KI$$

Ln = Sm and Yb

Figure 3.1 The ^{13}C CP MAS NMR Spectrum of the Crude Product from the Reaction of YbI_2 with Two Equivalents of KTp^{Me_2}

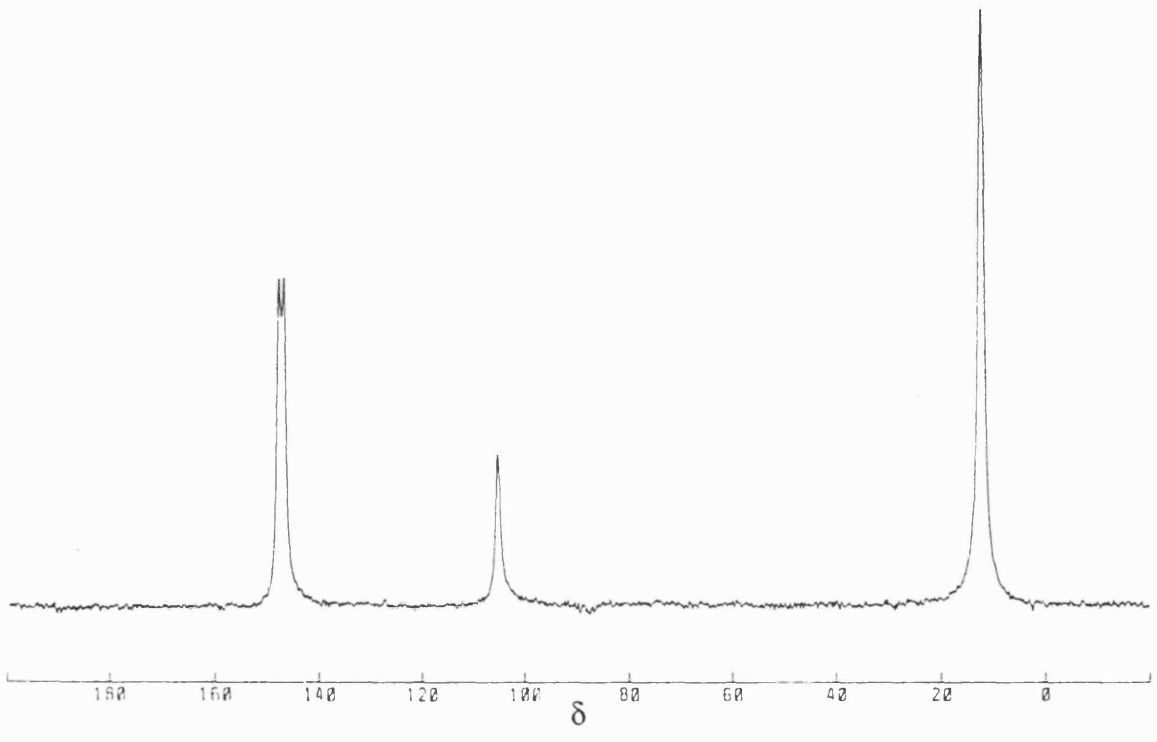

Although the marked insolubility of these complexes made it unlikely that they would be very volatile, purification by vacuum sublimation appeared to be the only route that remained unexplored; however, before we were able to investigate this possibility, a joint communication by the groups of Jones and Evans was published, in which the preparation of $Tp_2Ln(THF)_n$ and $(Tp^{Me_2})_2Ln$ (Ln = Sm, Eu and Yb) was described.[173] The complexes $(Tp^{Me_2})_2Ln$ had been synthesised by metathesis of the relevant lanthanide

diiodide with KTp^{Me2} and purified by vacuum sublimation at 10^{-6} torr and 200 °C. No reactivity of the Tp^{Me2} complexes was described, and the authors had been unable to obtain any structural information for these compounds.

In the light of this report, we confirmed that the products from the Yb (**3.3**) and Eu (**3.2**) reactions could be purified by vacuum sublimation (10^{-2} torr, 300 °C) to give analytically pure complexes of composition $(Tp^{Me2})_2Ln$. However, in the case of the Sm complex (**3.1**), this method resulted in significant decomposition, the purple sublimate being contaminated with a large amount of unidentified white material. Similar problems, albeit to a far lesser degree, were encountered in the sublimation of **3.3**. This decomposition was probably caused by the rather high temperature which was necessary for volatilisation in this poorer vacuum. In contrast, it was found that a sample of **3.2**, sealed in a glass tube at 10^{-2} torr, could be heated to a temperature in excess of 350 °C (such that an orange vapour was clearly visible) with no apparent sign of decomposition. Thus, the instability of these complexes at elevated temperatures parallels the reducing ability of the metal.

In response to the problems encountered in preparing pure samples of the Sm (**3.1**) and Yb (**3.3**) complexes, an improved synthetic strategy was sought. The reaction of $LiTp^{Me2}(THF)_n$ (prepared from LiI and KTp^{Me2}) with $SmI_2(THF)_n$ in THF gave the desired product (uncontaminated with LiI, which is soluble in the reaction solvent). However, significant quantities of a soluble Sm species also appeared to be formed, since the THF remained a green/blue colour even in the presence of an excess of $LiTp^{Me2}(THF)_n$. The use of $NaTp^{Me2}$ was more successful, and seemed to cause complete precipitation of $(Tp^{Me2})_2Ln$ (Ln = Sm and Yb). After decanting the reaction solvent and washing the precipitate with several portions of THF, iodide free† products were obtained in high yield (80 to 93 %).

In view of the remarkable insolubility of these complexes in most solvents, it was of interest to determine the nature of their structure in the solid state. By subliming $(Tp^{Me2})_2Yb$ (**3.3**) under dynamic vacuum in a temperature gradient, it was eventually possible to isolate crystals suitable for an X-ray crystallographic study.[1] Crystals of $(Tp^{Me2})_2Eu$ (**3.2**) were also grown, by slow sublimation under vacuum in a sealed tube. Details of the data collections, and tables of fractional coordinates, bond lengths and bond angles are given in Appendix 1 (Tables A1.1 and A1.8 to A1.13). The structures of **3.2** and **3.3**

† Shown by dissolving in concentrated nitric acid, diluting, and testing with $AgNO_3$ solution

proved that these species were molecular - each metal lying in a six coordinate environment best described as trigonally distorted octahedral. A ball and stick diagram of **3.2** is shown in Figure 3.2 and a space filling diagram of **3.3** is given in Figure 3.3. Both complexes are isomorphous, crystallising in the space group $R\bar{3}$; hence, these molecules have S_6 symmetry, consistent with the single pyrazolyl environment which was observed in the solid state NMR spectrum of **3.3**. In contrast to the decamethyllanthanocenes, $[Cp^*_2Ln]$, which have bent geometries,[48-51] the pair of Tp^{Me2} ligands in these complexes are crystallographically parallel. This is, presumably, a consequence of the much larger size of the hydrido-*tris*-(3,5-dimethylpyrazol-1-yl)borate ligand over Cp^*. The 3-Me groups in the structures of $[(Tp^{Me2})_2Ln]$ interlock and prevent the coordination of solvent molecules to the metal centre. This is again in contrast to the Cp^* analogues for which numerous solvates have been isolated and characterised.[174-179] The structure of $(Tp^{Me2})_2Sm$ (**3.1**) was subsequently reported by Takats, and is isomorphous with **3.2** and **3.3**.[180]

In addition to these lanthanide complexes, the structures of the related Ca,[181] Ba,[182,183] Pb[184] and Cd[185] compounds have been reported. These complexes also crystallise in the space group $R\bar{3}$ and key structural parameters for this series of molecules are compared in Table 3.1.

Figure 3.2 The Molecular Structure of $[(Tp^{Me2})_2Eu]$ (**3.2**)†

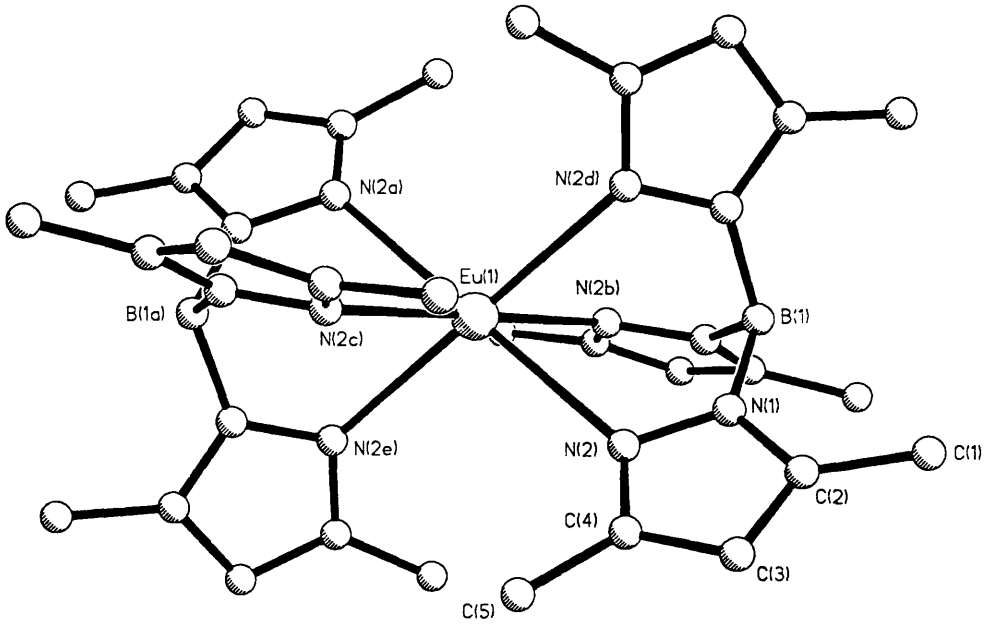

† Hydrogen atoms omitted for clarity

Figure 3.3 A Space Filling Diagram of $[(Tp^{Me2})_2Yb]$ (**3.3**)[1†]

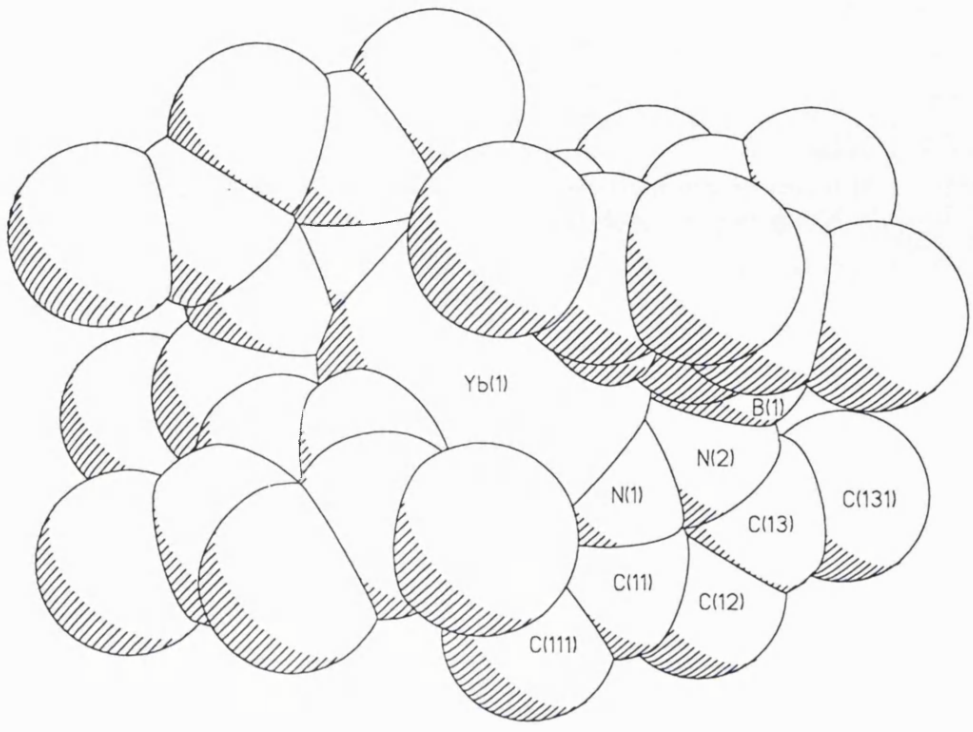

Table 3.1 Some Structural Parameters of the Isomorphous Complexes $[(Tp^{Me2})_2M]$[§]

M	Cd[185]	Ca[181]	Yb (**3.3**)	Eu (**3.2**)	Pb[184]	Sm[180] (**3.1**)	Ba[182,183]
Ionic Radius[15]	0.95	1.00	1.02	1.17	1.19	1.22	1.35
M–N(2)	2.348(5)	2.454(2)	2.480(4)	2.598(3)	2.610(5)	2.617(4)	2.754(3)
M···B	3.33	3.44	3.47	3.59	3.62	3.63	3.81
N(2)–M–N(2b)	82.7(1)	79.98(6)	79.3(1)	76.3(1)	75.2(1)	75.5(1)	71.48(5)
N(1)–B–N(1b)	110.6(4)	110.7(1)	110.6(4)	111.2(2)	110.6(4)	110.9(4)	111.2
N(2)···N(2b)	3.10	3.15	3.17	3.21	3.19	3.20	3.22

† Hydrogen atoms omitted for clarity

§ Numbering scheme for pyrazolyl rings is as shown in the structure of **3.2** (Figure 3.2)

The first point to note about these complexes is that despite the increase in ionic radii of the metals across Table 3.1, the geometry of the pyrazolylborate at the boron atom does not alter significantly - the N(1)–B–N(1b) bond angle remaining approximately tetrahedral. This rather rigid geometry is probably enforced to some degree by the 5-Me substituents in Tp^{Me2}. For example, a comparison of the two unsubstituted *tris*-(pyrazolyl)borate complexes Tp_2Fe[186] and Tp_2Ca[187] (for which the ionic radii of the metals differ by 0.45 Å),[15] reveals that the average N–B–N angle (107.6(5) and 110.3(4)°, respectively) does alter significantly upon increasing the size of the metal. Table 3.1 shows that there is a good correlation between the observed M–N(2) bond lengths in the $[(Tp^{Me2})_2M]$ compounds and literature values of the ionic radii for the (six coordinate) M^{2+} ions. The increasing size of the metal as one moves across the table is accommodated by the $[(Tp^{Me2})_2M]$ system in two ways. Firstly, by a slippage of the pair of pyrazolylborate ligands back along the S_6 axis (revealed by an increase in the M···B separation), and secondly, by subtle changes in the geometry of the Tp^{Me2} ligand itself. These are fairly insignificant in themselves (a slight lengthening of the B–N(1) bonds and a steady increase in the N(2)–N(1)–B angles), but taken together they amount to a definite opening up of the pyrazolylborate 'bite' angle (shown by an increase in N(2)···N(2b) distance). The overall effect of this is that, in general, the smaller the size of the metal ion, the further into the pocket of the Tp^{Me2} ligand it moves. This is seen clearly as a steady decrease in N(2)–M–N(2b) bond angles with increasing ionic radius.

Deviations from this general behaviour may be expected for the complexes of Sm^{2+} (**3.1**) and Pb^{2+}, since the distribution of valence electron charge on the metal is potentially non-uniform - the ions having electronic configurations of $[Xe]4f^6$ and $[Xe]4f^{14}5d^{10}6s/p^2$†, respectively - which may result in a Jahn-Teller type distortion of the ligands.[188]

There are no short range intermolecular contacts in the solid state structures of any of these complexes; hence, the reason for the insolubility of the lanthanide compounds is unclear. However, the most likely explanation lies in the very compact nature of these molecules (Figure 3.3), which enables them to pack together extremely efficiently in the solid state and leads to a relatively high lattice energy. In addition, it is also apparent from the space filling diagram of **3.2** that the structure presents little in the way of accessible

† The lone pair in $[(Tp^{Me2})_2Pb]$ is stereochemically inactive in the sense that the molecule has high (S_6) symmetry, although whether it is localised in an s or a p orbital is not known

diagram of **3.2** that the structure presents little in the way of accessible lipophilic groups with which solvent molecules could interact. It is interesting to note that the non-lanthanide complexes all had sufficient solubility in aromatic solvents to allow crystals to be grown from their solutions.[181-185] No reason for this increased solubility when the metal is not a lanthanide is apparent from the crystallographic data.

The pair of complexes $[(Tp^{Me2})_2Yb]$ (**3.3**) and $[(Tp^{Me2})_2Yb]^+[OTf]^-$ (**2.6**) serves as an example of a lanthanide ion which has the same coordination environment in two different oxidation states.[1] This situation is quite unusual, since the requirement to sterically saturate the metal centre in lanthanide chemistry usually results in a change in coordination number as the ionic radius of the metal is altered. Hence, it is interesting to compare the structural changes which occur at the metal ion as a result of the reduction shown in Equation 3.1. In common with the divalent compounds discussed above, the geometry at the boron atom is not significantly affected by the change in metal radius. Rather, the increase in size of the Yb ion is accommodated by a lengthening of the Yb···B separation from 3.35 to 3.47 Å, and by an opening up of the pyrazolylborate ligand bite, the average intraligand metal bonded N···N distance in **2.6** being 3.04 Å. The two independent Yb–N bond lengths in **2.6** are 2.304(5) and 2.347(6) Å, compared with 2.480(4) Å in **3.3**, and thus represent an average increase of 0.16 Å in the radius of the Yb ion upon reduction. This is in good agreement with the difference between these two oxidation states of *ca* 0.15 Å reported by Shannon.[15] The two independent N–Yb–N angles for **2.6** are 82.8(2) and 79.9(3)°, consistent with the metal ion lying deeper within the pocket of the pyrazolylborate ligand than in its divalent analogue. Two crystallographically characterised trivalent analogues of the Sm complex (**3.1**) are also known: $[(Tp^{Me2})_2Sm]^+[I]^-$ and $[(Tp^{Me2})_2Sm]^+[BPh_4]^-$.[130,167-169] Similar structural modifications accompany the change in oxidation state of the metal between these complexes and **3.1**, for example, the average metal-nitrogen bond lengths in these trivalent compounds are 2.447(7) and 2.44 Å, respectively, representing an average increase of 0.17 Å upon oxidation of $[(Tp^{Me2})_2Sm]$. The only other reports of isoleptic redox related lanthanide ions are the pair of complexes $[Cp^*_2Sm(THF)_2]$[177] and $[Cp^*_2Sm(THF)_2]^+[BPh_4]^-$[189] (for which the changes in the Sm–C and Sm–O bond lengths are 0.17 and 0.18 Å, respectively), and the mixed valence complex $[Cp^*_2Yb–F–YbCp^*_2]$[190] (in which the difference between the divalent and trivalent Yb–F and average Yb–C distances are 0.11 and 0.233 Å, respectively).

Preparation of Other Divalent *Bis*-(*poly*-(pyrazolyl)borate) Lanthanide Complexes

In view of the surprising insolubility of complexes **3.1**, **3.2** and **3.3**, we decided to ascertain whether this property could be altered by modification of the pyrazolylborate ligand. Since the 3- and 5-Me substituents on the pyrazolyl ring are critical for determining the steric and chemical properties of the ligand, the effect of introducing alkyl substituents at the 4-position was investigated. General synthetic routes to 4-substituted pyrazoles have not been widely reported. The pyrazole required for the ligand $Tp^{3\text{-}i\text{-}Pr\text{-}4\text{-}Br}$ was synthesised by direct treatment of 3-*iso*-propylpyrazole with bromine.[123] However, for the introduction of an alkyl group at this position, it seemed more appropriate to use a β-diketone as the starting material - in this instance the cheap and readily available acetylacetone (acacH). Alkylation of acacH at the desired position has been reported, by conversion to the Tl salt[191] followed by reaction with the appropriate alkyl iodide, the driving force for the reaction being provided by the formation of highly insoluble thallium iodide.[192] Thus, reaction of thallium acetylacetonate with ethyl iodide gave 3-ethyl-acetylacetone; this was not isolated but was converted directly to the pyrazole by treatment with aqueous hydrazine *in situ*.(Equation 3.4). However, in view of the toxicity of Tl salts, it was desirable to devise a less hazardous route to this pyrazole. Unfortunately, we found that simply heating Na(acac) with neat EtI, or with a mixture of THF and EtI, did not result in any reaction. However, the addition of some hexamethylphosphoramide (HMPA; unfortunately carcinogenic) to the reaction mixture did result in the formation of the desired product (Equation 3.5). The fact that HMPA is only required in one of the reaction steps (compared with Tl salts which are involved in three of the steps in the other route) together with the improved yield of pyrazole, makes this second synthesis superior.† The crude 3,5-dimethyl-4-ethylpyrazole is purified by distillation under reduced pressure, and can be synthesised on a relatively large scale (*ca* 60 g). Reaction with KBH_4 in the usual manner gave $KTp^{Me_2\text{-}4\text{-}Et}$.

The reaction of two equivalents of $KTp^{Me_2\text{-}4\text{-}Et}$ with the diiodides of Sm or Yb gave purple complexes which were soluble in THF, ether and aromatic

† The synthesis of 3-benzylacetylacetone by reaction of $PhCH_2Br$ with acacH and potassium carbonate in acetone has been made[193] and if generally applicable, may provide an even better route to 3-substituted β-diketones

Equation 3.4

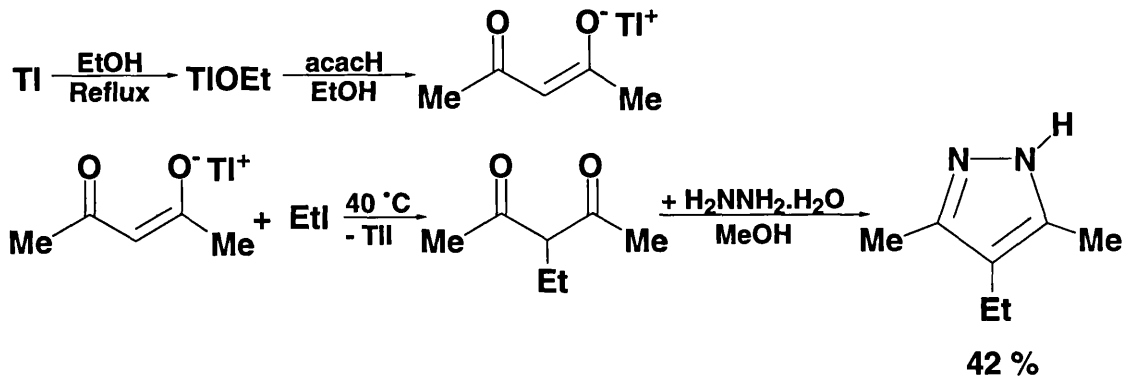

Equation 3.5

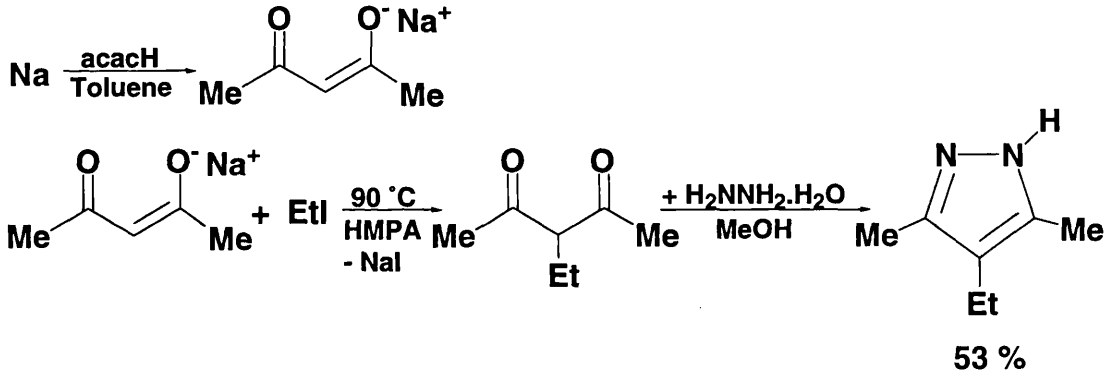

solvents, but not in 30/40 petrol. They were purified by recrystallisation from THF or ether to give products which had elemental analyses consistent with the formulae $[(Tp^{Me2\text{-}4\text{-}Et})_2Sm]$ (**3.4**) and $[(Tp^{Me2\text{-}4\text{-}Et})_2Yb]$ (**3.6**). The corresponding Eu complex (**3.5**) was synthesised from $Eu(OTf)_3$ by metathesis with two equivalents of $KTp^{Me2\text{-}4\text{-}Et}$ followed by reduction with Na amalgam. This compound was orange and was purified by vacuum sublimation. Complexes **3.4**, **3.5** and **3.6** were significantly more air sensitive than their Tp^{Me2} analogues. The solution NMR spectra of **3.6** were consistent with a diamagnetic Yb^{2+} compound in which high symmetry or fluxionality caused equivalence of all the pyrazolyl rings. Thus, the ^1H NMR spectrum consisted of one triplet (δ 1.02), two singlets (δ 2.05, 2.26) and one quartet (δ 2.31), in the ratio 3:3:3:2, the chemical shifts of these peaks being essentially unshifted from those observed in the spectrum of the potassium salt of $Tp^{Me2\text{-}4\text{-}Et}$. In common with the diamagnetic complexes $[(Tp^{Me2})_2Y]^+[OTf]^-$ (**2.1**) and $[(Tp^{Me2})_2LaOTf]$ (**2.2**), it was not possible to distinguish between the 3- and the 5-Me resonances in the ^1H and ^{13}C spectra of **3.6**. However,

unambiguous assignment of most of the peaks in the ^{13}C spectrum was possible by a combination of coupling pattern analysis, comparison of chemical shifts with those observed in the ^{13}C spectra of **2.1** and **2.2**, and ^{1}H-^{13}C correlation spectroscopy. The ^{11}B (I = 3/2) spectrum of **3.6** consisted of a single resonance at δ -8.2; this was rather broad due to the very rapid relaxation which is characteristic of a quadrupolar nucleus in a non-cubic environment. The corresponding resonances in the solution NMR spectra of the Sm compound (**3.4**) were shifted from their positions in **3.6**, consistent with the paramagnetism of the Sm^{2+} ion. The ^{1}H NMR spectrum of **3.4** is shown in Figure 3.4. In common with the spectra observed for the paramagnetic trivalent complexes **2.3** to **2.6**, one of the two Me singlets in this spectrum is considerably more shifted (δ 17.76) and broadened ($w_{1/2}$ = 16 Hz) than the other, and is assigned to the substituent at the 3-position on the pyrazolyl ring; shifting and broadening of the 3-Me resonance was also observed in the ^{13}C NMR spectrum. However, all of the peaks in this spectrum were sufficiently well resolved for the coupling patterns to be discerned, and assignment of most of the resonances was possible by methods analogous to those used for complex **3.6**. The broad singlet observed in the ^{11}B spectrum of the Yb complex is also significantly shifted (to δ -49.0) in the spectrum of **3.4**. No readable NMR spectra were obtained for the Eu compound (**3.5**), presumably due to the large magnetic moment of the Eu^{2+} ion (calculated effective magnetic moment, μ_{eff} = 7.94 BM).

Figure 3.4 The ^{1}H NMR Spectrum of $[(Tp^{Me_2\text{-}4\text{-}Et})_2Sm]$ (**3.4**)

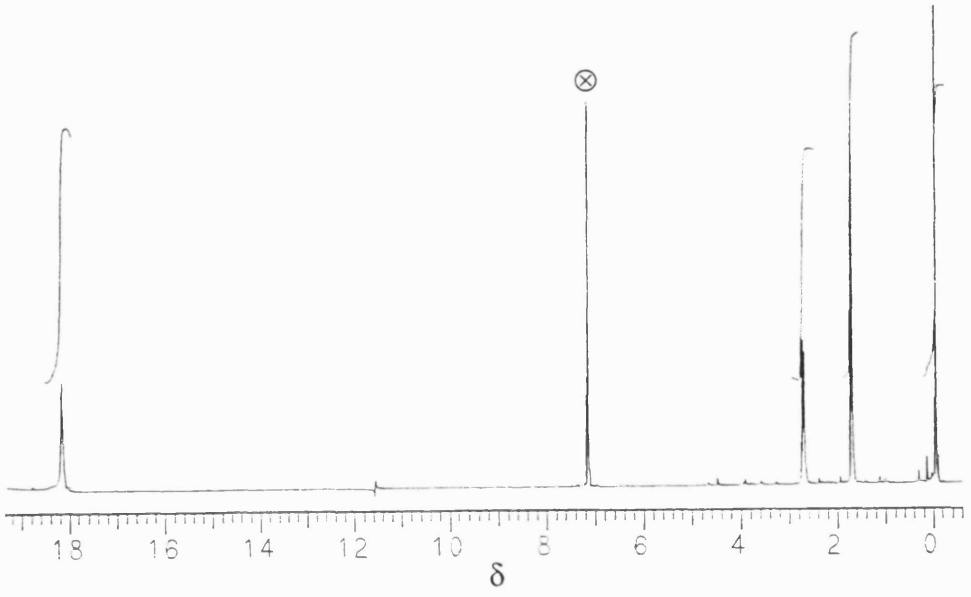

⊗ = d_6-benzene resonance

The UV/vis spectra (in THF solution) of complexes **3.4**, **3.5** and **3.6** are very similar to those observed for their Tp^{Me2} analogues (Table 3.2). Unfortunately, attempts to grow crystals of sufficient quality for an X-ray crystal structure determination of one of these complexes were not successful. However, the spectroscopic data obtained for these compounds supports a six coordinate structure analogous to that of the Tp^{Me2} derivatives, as shown in Figure 3.5.

Table 3.2 A Comparison of the UV/vis Spectra of $[(Tp^{Me2})_2Ln]$ and $[(Tp^{Me2-4-Et})_2Ln]$ for Ln = Sm (**3.1** and **3.4**), Eu (**3.2** and **3.5**) and Yb (**3.3** and **3.6**) in THF

Lanthanide	Samarium		Europium		Ytterbium	
Compound	3.1	3.4	3.2	3.5	3.3	3.6
Absorption Maxima (nm)	398 514 765	399 519 767	410 440	413 (sh)† 457	340 530	369 533

Figure 3.5 The Proposed Structure of the Complexes $[(Tp^{Me2-4-Et})_2Ln]$ (**3.4**, **3.5** and **3.6**)

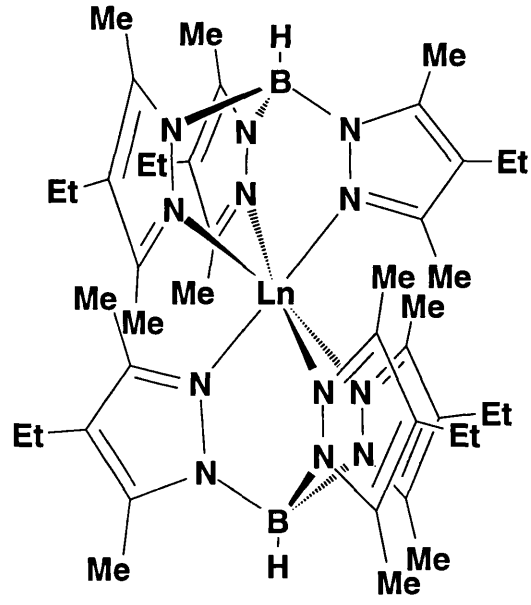

Ln = Sm (3.4), Eu (3.5) and Yb (3.6)

† sh = shoulder

Attempts were made to synthesise sandwich complexes using the substituted pyrazolylborate ligand hydrido-*tris*-(3-(2'-pyridyl)pyrazol-1-yl)borate ($Tp^{pyridyl}$).† This is capable of coordinating to a metal through the nitrogens of both the pyridyl and the pyrazolyl rings, and is therefore potentially an η^6-ligand.[194] The reaction of two equivalents of $KTp^{pyridyl}$ with YbI_2 gave a red/purple solution. The isolated solid was soluble in toluene, and could be recrystallised from this solvent to give a black/purple crystalline material. The ^1H NMR spectrum and elemental analysis of the complex were broadly consistent with a complex of formula $(Tp^{pyridyl})_2Yb$, although the product was clearly not pure. The corresponding reaction for Sm gave a brown solution which was extremely prone to decomposition and was not characterised. The synthesis of an Sm^{3+} complex of this ligand, $[(Tp^{pyridyl})_2Sm]^+[BPh_4]^-$, has since been reported, in which the metal ion is 12 coordinate.[195] We also attempted to prepare a Yb^{2+} sandwich complex of the pyrazolylborate analogue hydrido-*tris*-(benzotriazol-1-yl)borate, but again the product was prone to decomposition and was not characterised.

Magnetic and Electronic Properties of Divalent *Bis*-(hydrido-*tris*-(3,5-dimethylpyrazol-1-yl)borate) and *Bis*-(hydrido-*tris*-(3,5-dimethyl-4-ethylpyrazol-1-yl)borate) Lanthanide Complexes

The magnetic and electronic properties of some of the divalent sandwich complexes $[(Tp^{Me_2})_2Ln]$ and $[(Tp^{Me_2\text{-}4\text{-}Et})_2Ln]$ have been studied in collaboration with Dr Norman Edelstein.

The temperature dependent magnetic susceptibilities of the paramagnetic complexes $[(Tp^{Me_2})_2Sm]$ (**3.1**) and $[(Tp^{Me_2})_2Eu]$ (**3.2**) have been measured and the results are summarised in Table 3.3. The data generally agree with the Curie-Weiss relationship, which predicts a linear correlation of susceptibility (χ) with temperature (see Chapter 1, p 25). Although the ground state for Sm^{2+} is diamagnetic ($^7F_0$), paramagnetic excited terms are significantly populated at all but very low temperatures. Thus, the effective magnetic moment observed for **3.1** between 100 and 300 K is considerably higher than zero. For the Eu^{2+} ion, the ground term is $^8S_{7/2}$ and the first excited state is more than 10000 cm^{-1} higher in energy.[196] The effective magnetic moment (μ_{eff}) expected for complexes of Eu^{2+} is therefore 7.93 BM. The observed moment for compound **3.2** is somewhat higher than this

† A sample of $KTp^{pyridyl}$ was donated by Dr Mike Ward of the University of Bristol

theoretical value and displays some unexpected (albeit slight) temperature and field dependence. Such behaviour could be explained by some degree of magnetic ordering, although it is not possible to draw any firm conclusions from the data obtained thus far.

Table 3.3 The Results of Magnetic Susceptibility Measurements on $[(Tp^{Me2})_2Sm]$ (**3.1**) and $[(Tp^{Me2})_2Eu]$ (**3.2**)

Compound	**3.1**	**3.2**
***C* (emu K/mol)**	2.56	8.46
Θ (K)	-225	-2.3
μ_{eff} (BM)	4.52	8.22
Temperature Range (K)	100 to 300	5 to 300
Magnetic Field (T)	0.5 and 4.0	0.1 and 0.5

The magnetic susceptibilities of $[(Tp^{Me2\text{-}4\text{-}Et})_2Sm]$ (**3.4**) and $[(Tp^{Me2\text{-}4\text{-}Et})_2Eu]$ (**3.5**) have also been studied, although no data are available at present. In addition, the electron paramagnetic resonance (EPR) spectra of **3.2** and **3.5** have been measured as dilute (1 %) solid solutions in the corresponding Ba complexes; $[(Tp^{Me2})_2Ba]$ was prepared as reported in the literature,[182,183] whilst $[(Tp^{Me2\text{-}4\text{-}Et})_2Ba]$ (**3.7**) was synthesised in a similar fashion. Dilution was achieved by sublimation of a finely ground mixture of the Eu and Ba complexes. Once again, no results are currently available from these experiments.

The low temperature fluorescence (10 K) and absorption (4 K) spectra of $[(Tp^{Me2})_2Eu]$ (**3.2**) have also been investigated. The absorption spectrum consisted of a broad band (f $\rightarrow$ d) at *ca* 17700 cm^{-1} (560 nm), whilst in fluorescence this maximum was shifted to *ca* 16600 cm^{-1} (600 nm). In both spectra, vibrational fine structure was clearly discernible, with the fluorescence spectrum exhibiting a particularly long series of progressions. These have been correlated with absorptions observed in the resonance Raman spectrum of $[(Tp^{Me2})_2Ba]$.

Photoelectron Spectroscopic Studies of Divalent *Bis*-(hydrido-*tris*-(3,5-dimethylpyrazol-1-yl)borate) and *Bis*-(hydrido-*tris*-(3,5-dimethyl-4-ethylpyrazol-1-yl)borate) Lanthanide Complexes[197]

In collaboration with Dr Jennifer Green, Kathryn Longley and Richard Parkin, the photoelectron (PE) spectroscopy of complexes **3.1** to **3.6** was studied.

In this technique, relatively low energy (UV) radiation from an He discharge lamp is used to ionise the valence electrons of a compound in the vapour phase.[198] The Einstein equation states that, to a first approximation, the sum of the ionisation energy and the kinetic energy of the electron is equal to the energy of the incident photon. For a 'closed shell' molecule, this ionisation energy can be equated with the negative of the energy of the molecular orbital (MO) from which the ionisation occurred (Koopmans' theorem).[199] This is an oversimplification, ignoring as it does effects such as electron correlation and charge relaxation (which can lead to a reordering of the MOs in the ion). When ionisation of an 'open shell' molecule occurs, a number of ionic states (with different energies) can result from ionisation from a single MO. In addition, spin-orbit coupling (particularly important for the heavier elements) can increase still further the number of possible energy levels which the ionised molecule can adopt. The theoretical states which arise from the ionisation of a given $4f^n$ configuration, together with their relative intensities, have been studied by Cox.[200] Figure 3.6 shows the results of this work as they pertain to the ionisation of Sm^{2+} ($[Xe]4f^6$), Eu^{2+} ($[Xe]4f^7$) and Yb^{2+} ($[Xe]4f^{14}$).

Figure 3.6 Theoretical Intensity Profiles and Final States[200] for the Ionisation of Sm^{2+}, Eu^{2+} and Yb^{2+}

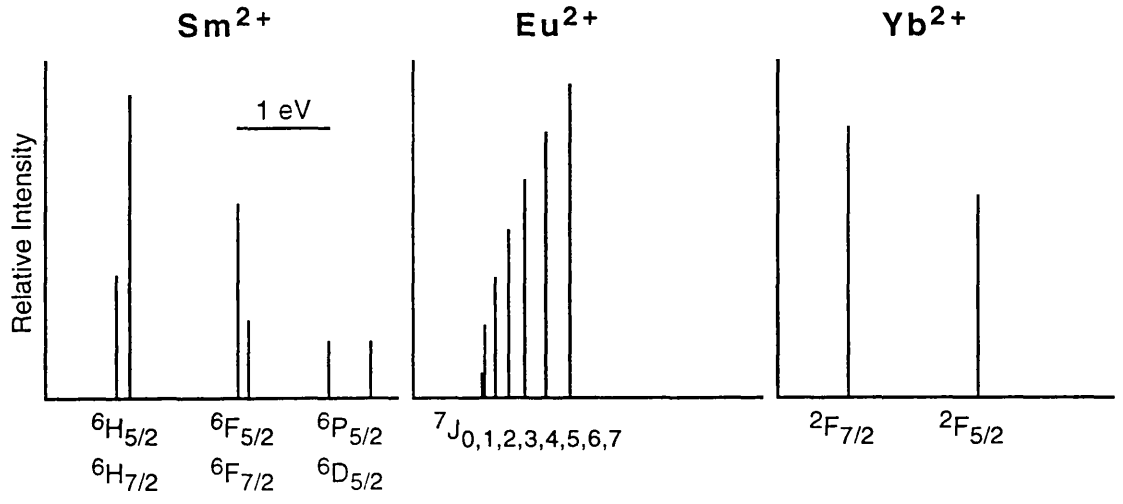

Thus, the assignment of bands in PE spectra is far from straightforward. However, clues are available from studying a series of related complexes, from any structure (*eg* vibrational) which is observed in the bands, and from the changes which occur in the relative intensities of the bands upon altering the energy of the ionising photons. This last technique is particularly useful in identifying ionisations from principally metal derived orbitals, since the intensity of these bands typically increases relative to ligand ionisations at higher photon energies.[198,201] The PE spectra presented here have been measured using two photon energies, HeIα (21.22 eV) and HeIIα (40.81 eV), with ionisations from lanthanide based orbitals expected to be more prominent in the latter. Thus, in conjunction with computational methods, PE spectroscopy can be used to probe the electronic structure of not only simple molecules, but also of large organometallic systems. In this latter category, it is pertinent to note the work of Green & Rösch on the electronic structure of the decamethyllanthanocenes,[35,36] as well as studies on trivalent complexes of the lanthanides.[38,39,43] There has also been a PE spectroscopic study of the first row transition metal pyrazolylborate compounds [Tp_2M].[202]

In addition to the lanthanide complexes, the Group 2 analogues [$(Tp^{Me2})_2M$] (M = Ca, Sr and Ba) were also studied.[181,183†] For these compounds, the PE spectra consist of three types of ionisation, and these are indicated in the HeIα and HeIIα spectra of [$(Tp^{Me2})_2Ba$] shown in Figure 3.7. Band **1** (8.30 eV) is invariant with a change in the metal within Group 2 and is assigned to ionisations from the π-orbitals of the pyrazolyl ring. On the other hand, band **2** shifts from 10.28 eV in [$(Tp^{Me2})_2Ca$] to 10.06 eV in [$(Tp^{Me2})_2Ba$]. This is consistent with an ionisation from the σ-donor orbital on nitrogen, which is stabilised to some degree by the smaller (more polarising) cations at the beginning of Group 2. A similar trend is noted in the e_1 ionisations of the analogous decamethylmetallocenes of these elements.[203] Finally, the broad envelope **3** is due mainly to ionisations from the σ-framework of the hydrido-*tris*-(3,5-dimethylpyrazol-1-yl)borate ligand.

The spectra obtained for the lanthanide complexes **3.1** to **3.3** also exhibited these three features which, as detailed above, are attributable principally to ligand based ionisations. In addition, the HeIα spectrum of [$(Tp^{Me2})_2Eu$] (**3.2**) showed a weak band (**0**) at 6.46 eV, which was of significantly greater relative intensity in the HeIIα spectrum (Figure 3.8). The slightly asymmetrical

† Samples provided by Professor Ernesto Carmona and coworkers

Figure 3.7 The PE Spectra of $[(Tp^{Me2})_2Ba]$

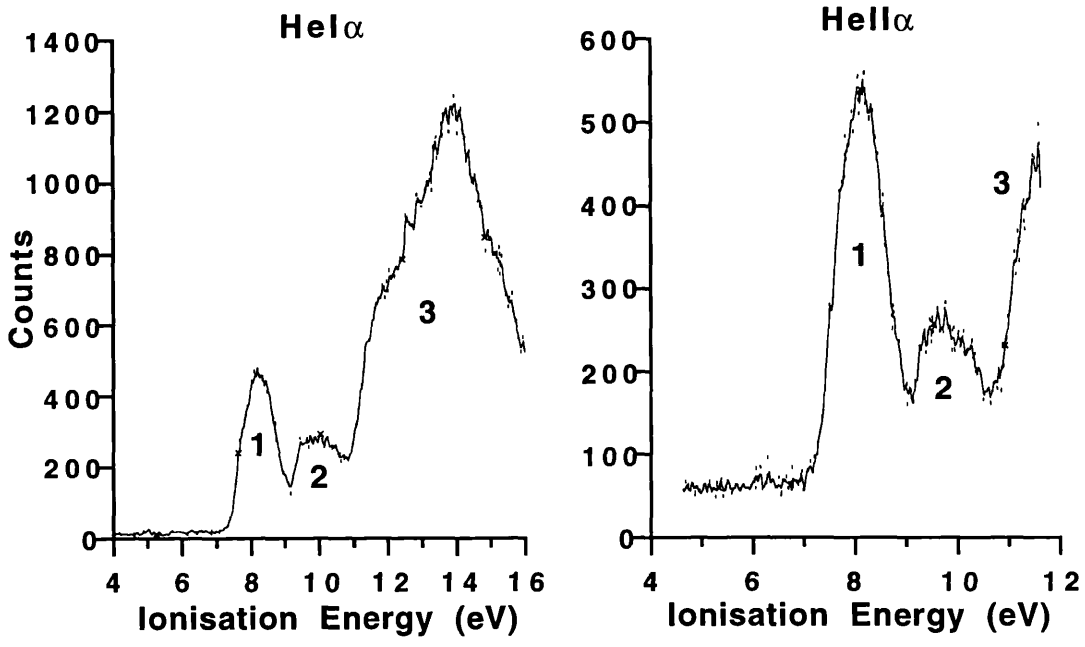

appearance of this band is consistent with it being composed of the overlapping spin-orbit components of the ^7F state (see Figure 3.6). In addition, the ionisation energy which is indicated by this band (6.46 eV) is in close agreement with that of 6.3 eV observed in $[Cp^*_2Eu]$.[35,36]

The corresponding spectrum of $[(Tp^{Me2})_2Yb]$ (**3.3**) was found to have two bands at low binding energy (labelled **0a** and **0b**), which increased markedly in relative intensity on moving from HeIα to HeIIα radiation (Figure 3.9). The separation of bands **0a** and **0b** (*ca* 1.2 eV) is in good agreement with that predicted by the relative energies of the two spin-orbit states, $^2F_{7/2}$ and $^2F_{5/2}$, of the Yb^{3+} ion.[200] Furthermore, the relative intensities of these bands (8:6.3) is also consistent with the degeneracies of these states (8 and 6, respectively). However, whilst the corresponding bands in the spectrum of $[Cp^*_2Yb]$ are also separated by *ca* 1.2 eV, their positions are markedly different from those observed in **3.3**, being *ca* 1.1 eV higher in energy.[35,36] Considering that the bonding in lanthanide complexes is almost totally ionic, this apparent shift is completely unexpected, and no satisfactory explanation for it exists at the moment.

The PE spectra of $[(Tp^{Me2})_2Sm]$ (**3.1**) showed no evidence of f electron ionisations in the low binding energy region. This is not surprising, since the

Figure 3.8 The PE Spectra of $[(Tp^{Me2})_2Eu]$ (**3.2**)

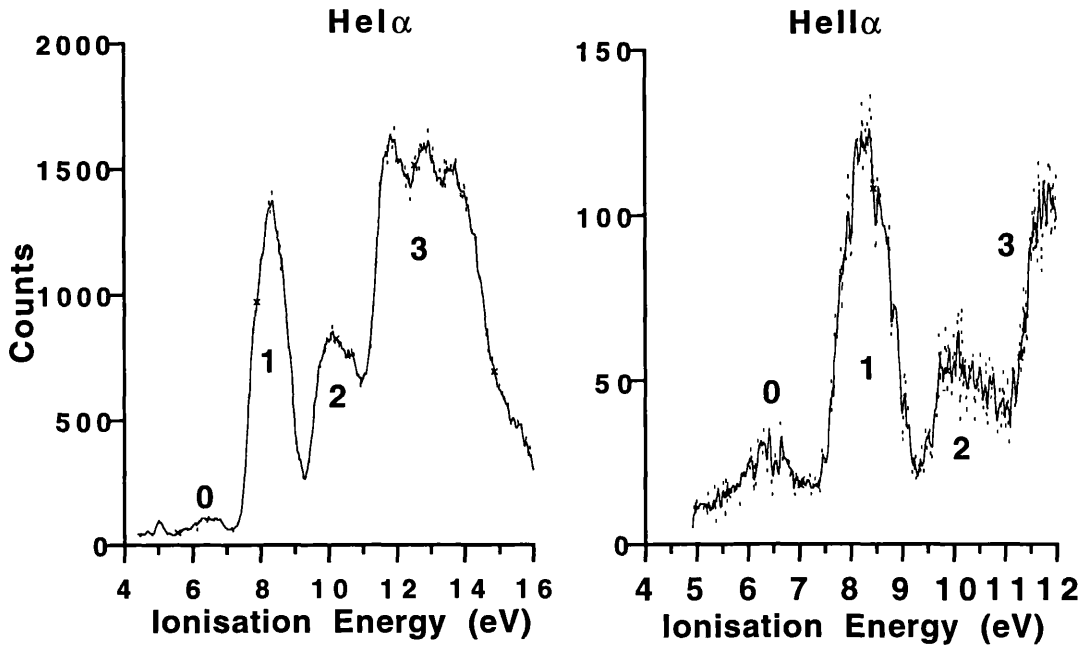

Figure 3.9 The PE Spectra of $[(Tp^{Me2})_2Yb]$ (**3.3**)

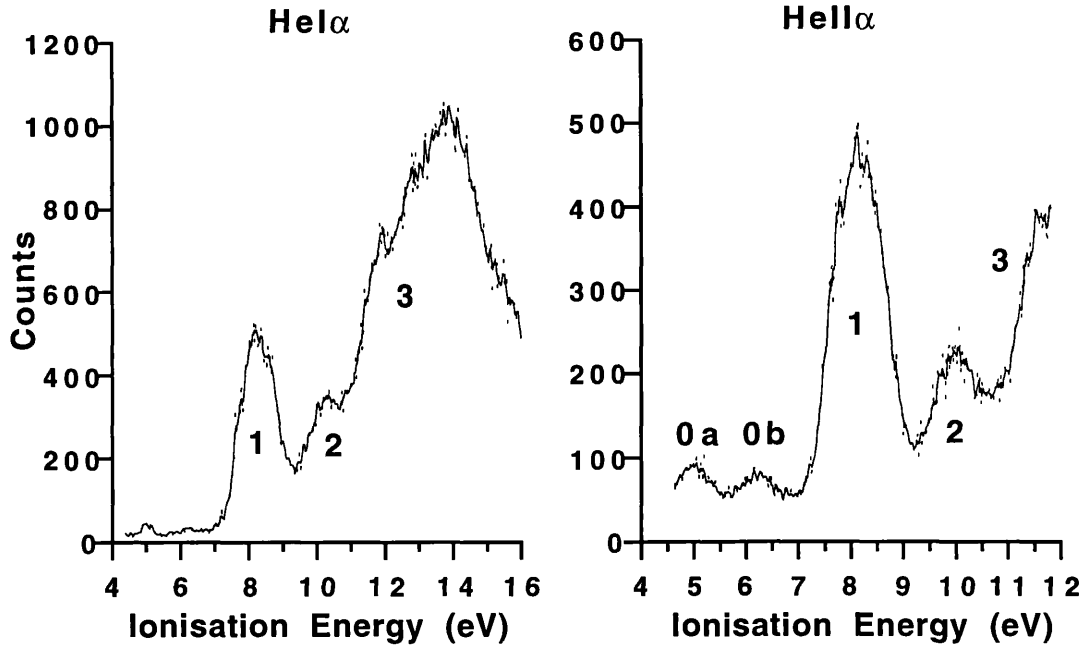

working pressure of the PE spectrometer in the region of the lamp (the heat of which sublimes the sample) is probably higher by a factor of ten than in the laboratory sublimation of **3.1** for which extensive decomposition was observed (*vide supra*). Thus, no useful information was obtained from the

spectrum of this complex. The PE spectra of **3.4**, **3.5** and **3.6** were also studied. No f electron ionisations were observed for these complexes, again possibly on account of significant decomposition during sublimation.

Reactivity of Divalent *Bis*-(hydrido-*tris*-(3,5-dimethylpyrazol-1-yl)borate) and *Bis*-(hydrido-*tris*-(3,5-dimethyl-4-ethylpyrazol-1-yl)borate) Lanthanide Complexes

The complexes **3.1** to **3.6** did not display any apparent tendency to form simple adducts with a variety of Lewis bases, and in general, no reactivity was observed with unsaturated organic molecules. Hence, they were isolated from THF as the unsolvated species, and they did not react with pyridine, diethyl ether, carbon monoxide, *tert*-butylisonitrile, ethylene, or alkynes such as phenylacetylene and but-2-yne. A similar lack of reactivity has been observed by other workers in their investigations of the chemistry of $[(Tp^{Me2})_2Ln]$[167,173,180] and is presumably related, in part at least, to the interlocked 3-Me groups which hinder the coordination of even small molecules to the metal centre. Analogous complexes of the unsubstituted *tris*-(pyrazolyl)borate have also been reported.[132,173] Consistent with the smaller size of this ancillary ligand, these were isolated as the THF adducts $Tp_2Ln(THF)_2$ (Ln = Sm, Eu, Yb), but were also rather unreactive towards poor Lewis bases such as alkenes.[173] This is in contrast to the extremely rich reactivity observed in this respect for the decamethyllanthanocenes.[24,87,148,204-206]

Greater reactivity of **3.1** to **3.6** was observed with more reducible substrates. Thus, the complexes were found to react readily with one equivalent of the electron deficient molecules tetracyanoquinodimethane (TCNQ) and tetracyanoethylene (TCNE) - see Equation 3.6 and Tables 3.4 and 3.5. The reactions of the Sm (**3.1** and **3.4**) and Eu (**3.2**) complexes with TCNQ produced considerable quantities of THF insoluble material, whilst the analogous reactions of the Yb complexes (**3.3** and **3.6**) did not; products from all the TCNE reactions were found to be reasonably soluble in warm THF. All of the products isolated from these reactions contained variable amounts of THF, and as a result, elemental analyses were generally poor.

Equation 3.6

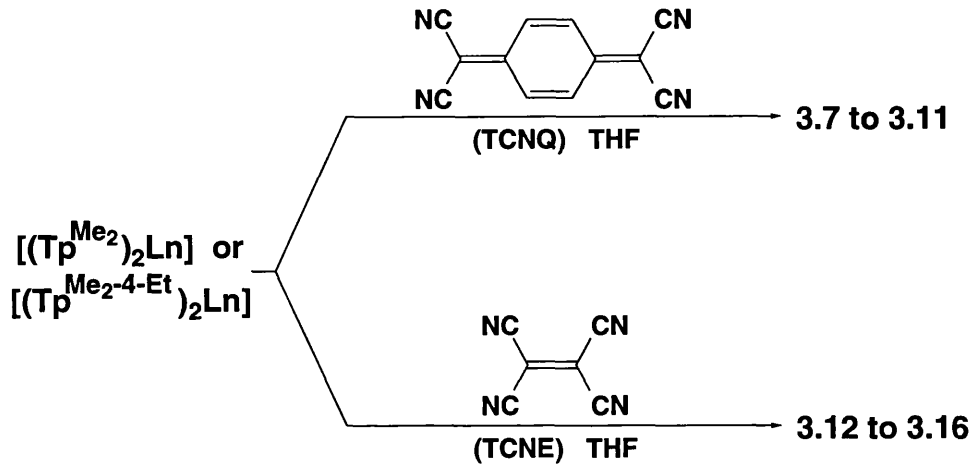

Table 3.4 The Reactions of $[(Tp^{Me_2})_2Ln]$ and $[(Tp^{Me_2\text{-}4\text{-}Et})_2Ln]$ with TCNQ

a THF Soluble Products

Lanthanide Complex	Number	Colour	$\nu_{C\equiv N}$ (cm^{-1})†
$[(Tp^{Me_2})_2Sm]$	**3.8a**	Dark green	2118 (br), 2182, 2196
$[(Tp^{Me_2})_2Eu]$	**3.9a**	Dark green	2119, 2139, 2183, 2199
$[(Tp^{Me_2})_2Yb]$	**3.10**	Green	2152, 2181
$[(Tp^{Me_2\text{-}4\text{-}Et})_2Sm]$	**3.11a**	Dark green	2117 (br), 2184, 2196 (sh)
$[(Tp^{Me_2\text{-}4\text{-}Et})_2Yb]$	**3.12**	Green	2154, 2180

b THF Insoluble Products

Lanthanide Complex	Number	Colour	$\nu_{C\equiv N}$ (cm^{-1})
$[(Tp^{Me_2})_2Sm]$	**3.8b**	Pale green	2133, 2149, 2186, 2200
$[(Tp^{Me_2})_2Eu]$	**3.9b**	Pale brown	2132, 2155, 2186 ,2203
$[(Tp^{Me_2\text{-}4\text{-}Et})_2Sm]$	**3.11b**	Pale green	2130 (sh), 2139, 2155, 2186, 2200 (sh)

† br = broad; sh = shoulder

Table 3.5 The Reactions of $[(Tp^{Me2})_2Ln]$ and $[(Tp^{Me2\text{-}4\text{-}Et})_2Ln]$ with TCNE

Lanthanide Complex	Number	Colour	$\nu_{C\equiv N}$ (cm^{-1})
$[(Tp^{Me2})_2Sm]$	**3.13**	Red/brown	2155, 2197
$[(Tp^{Me2})_2Eu]$	**3.14**	Red/brown	2155, 2197
$[(Tp^{Me2})_2Yb]$	**3.15**	Yellow/orange	2148, 2187
$[(Tp^{Me2\text{-}4\text{-}Et})_2Sm]$	**3.16**	Red/brown	2153, 2162, 2198, 2203
$[(Tp^{Me2\text{-}4\text{-}Et})_2Yb]$	**3.17**	Yellow/orange	2144, 2183

IR spectroscopy provided some information on the possible structures of these products. All contained bands due to the pyrazolylborate ligand, including the characteristic B–H stretch which occurred between 2528 and 2569 cm^{-1}. The C≡N stretching frequencies for both TCNE and TCNQ are highly sensitive to the degree of negative charge which the molecules carry, since the highest occupied molecular orbital (HOMO) in the uncharged species is an antibonding π-orbital (b_{3g}) whose occupation results in a decrease in C≡N bond order.[207,208] Typical absorption frequencies ($\nu_{C\equiv N}$) for the free monoanions of these molecules are 2153 and 2179 cm^{-1} for $[TCNQ]^-$ and 2144 and 2183 cm^{-1} in $[TCNE]^-$.[209,210] These values are similar to those observed for the Yb compounds **3.10**, **3.12**, **3.15** and **3.17**; thus, it appears that with this small lanthanide, complexes of the type $[(Tp^{Me2})_2Yb]^+[X]^-$ and $[(Tp^{Me2\text{-}4\text{-}Et})_2Yb]^+[X]^-$ (X = TCNE or TCNQ) are formed.

In the case of the reaction between TCNE and **3.3**, the yellow/orange toluene solution obtained from the reaction, produced large yellow/orange crystals upon cooling. These desolvated very rapidly upon removal from the solvent, and elemental analysis suggested that the resulting compound had the composition $(Tp^{Me2})_2$YbTCNE.THF. We were unable to transfer the crystals into Lindemann capillaries without serious desolvation; however, in collaboration with Dr Mark Elsegood of the University of Newcastle, the crystal structure of this complex was obtained at low temperature using the oil drop method.[211] This confirmed that the structure of **3.15** consists of discrete cations and anions, having the molecular formula $[(Tp^{Me2})_2Yb]^+[TCNE]^-.(THF)_6$. Details of the data collection and tables of fractional coordinates, bond lengths and bond angles are given in Appendix 1 (Tables A1.1 and A1.14 to A1.16); the structure of **3.5** is shown in Figure 3.10.

Figure 3.10 The Molecular structure of $[(Tp^{Me2})_2Yb]^+[TCNE]^-.(THF)_6$ **(3.15)**†

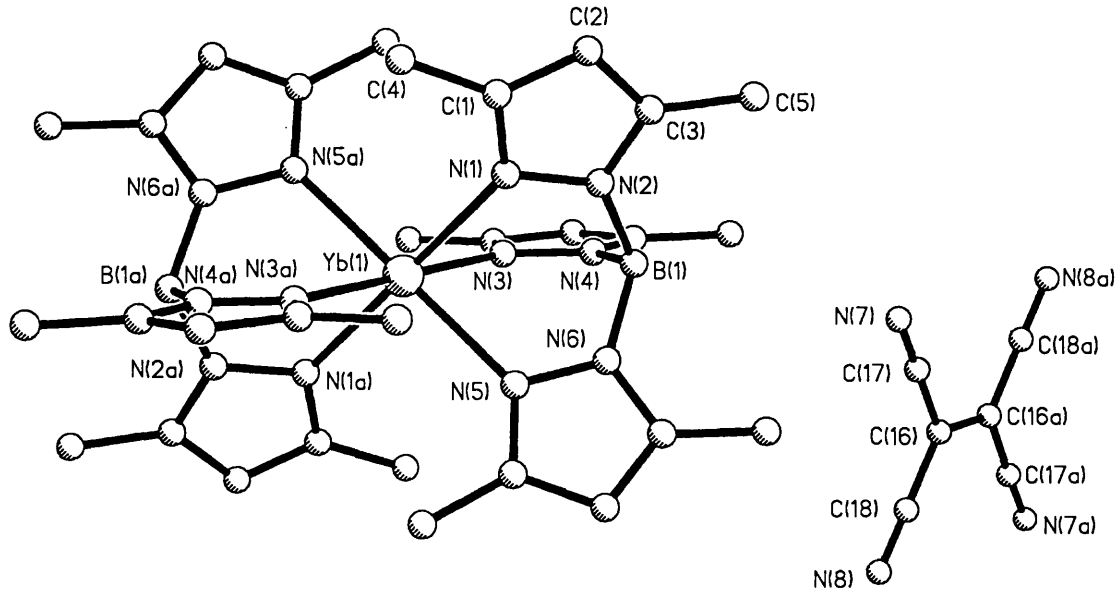

The Yb^{3+} ion in the cation of **3.15** is approximately octahedrally coordinated, and has structural parameters which are very close to those found in the isoleptic cation of $[(Tp^{Me2})_2Yb]^+[OTf]^-$ (**2.6**). Thus, the Yb···B separation and average Yb–N distances in **3.15** are 3.37 and 2.336(4) Å, and the average intraligand N–Yb–N angle is 81.77(9)°, compared with corresponding values of 3.35 and 2.318(5) Å and 81.8(2)° in **2.6**. The bond distances in the TCNE molecule are very similar to those reported for other charge transfer complexes containing $[TCNE]^-$, such as $[Cp^*_2Fe]^+[TCNE]^-$.[210] Thus, the anion is planar with average C≡N and C–CN bond lengths of 1.133(7) and 1.427(7) Å, respectively, and a C(16)–C(16a) distance of 1.398(11) Å. The corresponding lengths in the Fe complex above are 1.140(4), 1.417(2) and 1.392(9) Å, respectively. A comparison of the structural features of the anion in **3.15** with those observed in neutral TCNE[212] shows that upon reduction by a single electron, the central C–C bond length increases by *ca* 0.04 Å, the C≡N decreases very slightly (by *ca* 0.03 Å) and the C–CN bond length remains approximately unchanged. It is interesting to note that despite the decrease in the C≡N bond length upon reduction from TCNE to $[TCNE]^-$, $\nu_{C\equiv N}$ also decreases (from 2228 and 2260 cm^{-1} in TCNE[213] to 2148 and 2187 cm^{-1} in **3.15**). A similar result is obtained for $[Cp^*_2Fe]^+[TCNE]^-$[210] and for other compounds containing polycyano anions[214], and may be related to the

† Hydrogen atoms and THF molecules omitted for clarity

difficulty in determining short C–N distances accurately in X-ray structures. A detailed experimental and theoretical analysis of the structural and spectroscopic (both vibrational and electronic) changes which accompany the one and two electron reductions of TCNE has been reported.[215]

No significant interionic interactions are observed in the solid state structure of **3.15**. For example, the closest Yb···TCNE, Yb···Yb and TCNE···TCNE contacts are 7.49, 8.62 and 10.64 Å, respectively. A structure of this type is not expected to give rise to unusual magnetic or electronic properties, for which close interactions are a prerequisite, such as those which have been reported for other charge transfer TCNE and TCNQ salts.[216] The uncertain stoichiometry and hence uncertain structure of **3.15**, caused by its ready desolvation, means that a study of its magnetic properties is intrinsically complicated and has not been attempted. However, simple paramagnetic behaviour may be anticipated. It is pertinent to note that there has been a recent report of a transition metal *tris*-(pyrazolyl)borate TCNQ complex, $[(Tp^{Me2})_2Fe]^+[TCNQ]^-$, in which there were no short range interactions in the solid state structure.[217] A study of the magnetic properties of this compound showed that, consistent with this structure, it behaved as a simple paramagnet. This arrangement of non-interacting cations and anions was attributed to the absence of available π-electron density on the Tp^{Me2} ligand, in which respect it differs markedly from Cp^*.[217]

In contrast to the reasonably straightforward situation for the Yb complexes, the nature of the products obtained from the reactions of the Sm (**3.1** and **3.4**) and Eu (**3.2**) compounds with TCNQ and TCNE is less clear. Many of the IR spectra of these products displayed more than two peaks in the C≡N stretching region and the bands were generally rather broad. This may indicate some type of interaction in the solid state, or simply that more than one product had been formed. The isolation of two types of complex from the TCNQ reactions was an additional complication; furthermore, it was noted that the THF insoluble species (**3.8b**, **3.9b** and **3.11b**) darkened substantially (becoming dark green) when scraped from the wall of the Schlenk or when ground with KBr for IR spectroscopy. Whether this was due to a change in particle size, or was caused by some structural modification is not known. It is well established that TCNQ and TCNE are able to coordinate to metal complexes in a variety of modes, and that this affects the number and positions of the C≡N stretching vibrations in the ligand.[216] Hence, it is possible that the larger size of the Sm^{3+} and Eu^{3+} ions (relative to Yb^{3+})

allows the TCNQ or TCNE anions to coordinate to the metal centre. In an attempt to investigate this possibility, the fast atom bombardment (FAB) mass spectra of the complexes were measured. However, in common with the Yb compounds **3.10**, **3.12** and **3.15**, for which an ion pair structure is proven, the Sm and Eu products showed only parent ion peaks and fragmentation patterns consistent with the cations $[(Tp^{Me2})_2Ln]^+$ or $[(Tp^{Me2\text{-}4\text{-}Et})_2Ln]^+$. Whether this is a true reflection of the lanthanide species present in these products, or was due to facile cleavage of the putative TCNQ/TCNE–lanthanide bond or decomposition in the *m*-nitrobenzyl alcohol matrix used for the experiment, is impossible to say. Since no firm conclusions could be drawn as to the structures of these products on the basis of the IR data alone, and since even their stoichiometry was uncertain, further investigation was abandoned.

During one attempt to grow crystals of **3.16** by slow evaporation of a THF solution in a glove box, hydrolysis occurred and a new complex, **3.18**, was formed. The IR spectrum of this compound showed that it no longer contained any TCNE, there being no bands in the $\nu_{C\equiv N}$ stretching region of the spectrum. In addition, there were two distinct types of B–H stretching absorptions: one split pair at 2541 and 2523 cm^{-1} (in the region characteristic of Tp^{Me2}) and one at 2393 cm^{-1}. In order to determine the molecular structure of **3.18**, an X-ray crystallographic study was carried out in collaboration with Dr Mark Elsegood. Details of the data collection and tables of fractional coordinates, bond lengths and bond angles are given in Appendix 1 (Tables A1.1 and A1.17 to A1.19). The structure of **3.18** is shown in Figure 3.11.

The structural determination confirmed that **3.18** contains two types of boron ligand, one being Tp^{Me2} itself, and the other the hydrolysis product of Tp^{Me2}: $\{(pz^{Me2})_2B(H)O\}^{2-}$. The oxygen of the latter ligand bridges the two Sm centres of the dimeric structure, the two halves of which are related by an inversion centre. In addition to half of the Sm dimer, the asymmetric unit also contained one molecule of THF. The ligand $\{(pz^{Me2})_2B(H)O\}^{2-}$ has been previously reported in a U complex formed by unintentional hydrolysis of $(Bp^{Me2})_2UCl_2$ (Equation 3.7; Bp^{Me2} = dihydrido-*bis*-(3,5-dimethylpyrazol-1-yl)borate).

Figure 3.11 The Molecular Structure of $[(Tp^{Me2})Sm\{(pz^{Me2})_2B(H)O\}]_2 \cdot (THF)_2$ **(3.18)**†

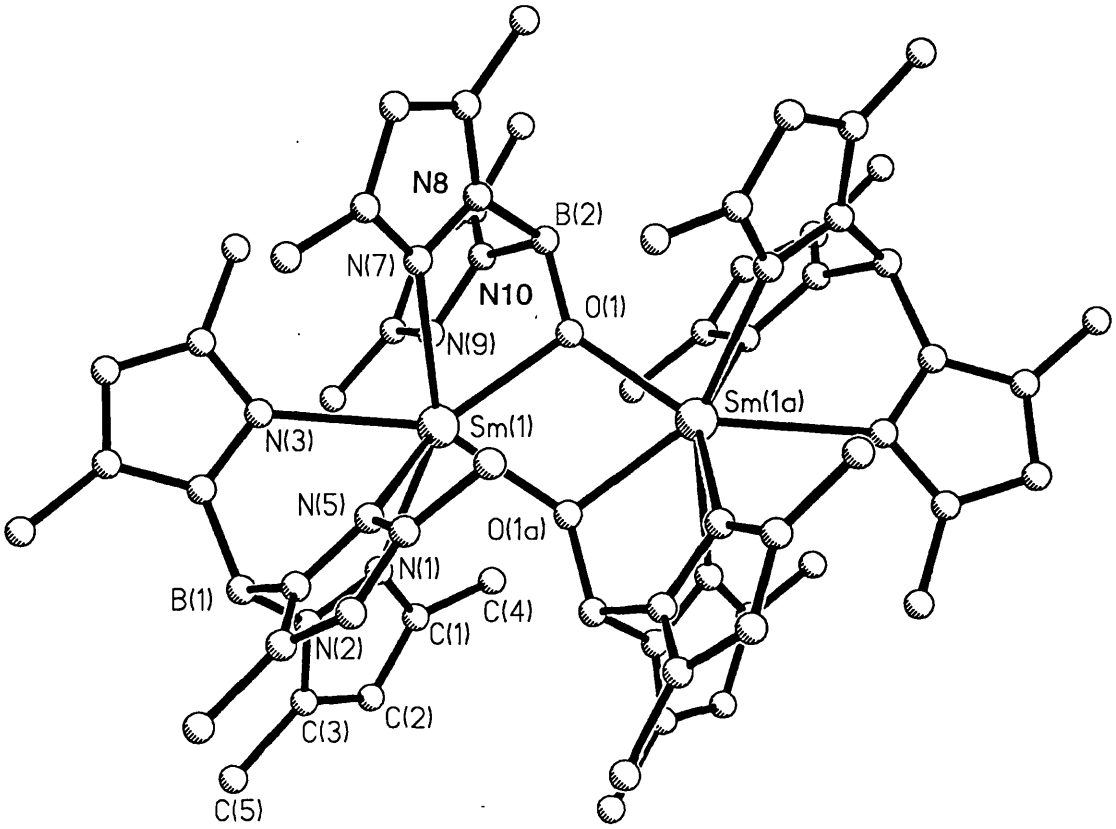

Equation 3.7[218]

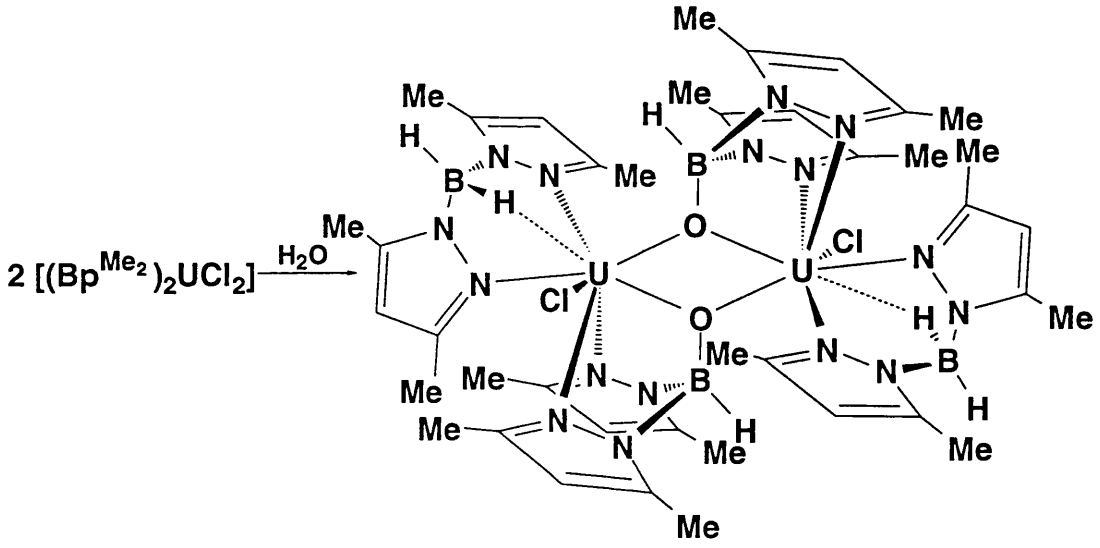

† Hydrogen atoms and THF molecules omitted for clarity

The coordination geometry around the Sm^{3+} ions in **3.18** can be described as capped trigonal prismatic, with the two triangular faces being defined by O(1), N(7) and N(9), and O(1a), N(1) and N(5); N(3) caps the rectangular face N(1), N(5), N(7) and N(9). The Sm(1)–N bond length of this capping nitrogen is significantly longer at 2.611(3) Å than the other distances, which lie in the range 2.515(3) to 2.530(3) Å. The average Sm(1)–N distance in this complex is 2.540(3) Å, similar to that observed in the seven coordinate Sm^{3+} complex $[(Tp^{Me2})_2SmCl]$ (2.564(16) Å).[156,219] The oxygen bridges in **3.18** lie slightly asymmetrically, with the Sm(1)–O(1) and Sm(1a)–O(1) distances being 2.319(2) and 2.240(2) Å, respectively. These bond lengths are significantly longer than the Sm–O distance observed in the seven coordinate complex $[(Tp^{Me2})_2Sm(4\text{-}tert\text{-butylphenoxide})]$ of 2.159(2) Å[156,220], and may be the result of the constrained geometry of the $\{(pz^{Me2})_2B(H)O\}$ ligand around the boron atom (which is tetrahedral to within 4°). Hence, a compromise between the Sm–O bond length and the strain in the Sm(1)–N(7)–N(8) and Sm(1)–N(9)–N(10) angles has to be sought. As it is, these angles are remarkably acute (being 111.3(2) and 110.0(2)°, respectively), compared to those observed in the $Tp^{Me2}Sm$ fragment in **3.18** (for which the range is 119.0(2) to 122.4(2)°). Similar structural features are observed in the coordination mode of $\{(pz^{Me2})_2B(H)O\}^{2-}$ to U in $[Bp^{Me2}UCl\{(pz^{Me2})_2B(H)O\}]_2$ (Equation 3.7). Furthermore, the U–O bond lengths (2.312(5) and 2.204(5) Å) and the average U–N distance (2.523(7) Å) are comparable with those noted above. This is consistent with the similar ionic radii reported for seven coordinate Sm^{3+} and eight coordinate U^{4+}.[15] The O(1)–Sm(1)–O(1a) angle in **3.18** (70.67(9)°) is somewhat larger than the corresponding angle in the U complex (66.5(2)°), a fact that is probably related to the smaller coordination number in the former compound. In both complexes the M_2O_2 unit is planar, and this causes the Sm(1)–O(1)–Sm(1a) angle to be smaller (109.33(9)°) than the corresponding angle observed in $[Bp^{Me2}UCl\{(pz^{Me2})_2B(H)O\}]_2$ (113.4(2)°); the Sm(1)···Sm(1a) distance is therefore significantly shorter than the U···U separation (3.7197(4) and 3.777 Å, respectively). The La analogue (cocrystallised with two molecules of toluene) of **3.18** has also been synthesised (by accidental hydrolysis of $[(Tp^{Me2})_2La(pz^{Me2})]$) and structurally characterised.[156,220] Taking into account the larger size of the La^{3+} ion over Sm^{3+}, the molecular parameters of this compound are extremely similar to those observed in **3.18**.

Whilst the reaction shown in Equation 3.7 involves the hydrolysis of a B–H bond in Bp^{Me2} to give the new ligand $\{(pz^{Me2})_2B(H)O\}^{2-}$, the reaction which

gave rise to this same ligand in **3.18**, and in the La analogue, involved B–N(pyrazolyl) cleavage. There is a precedent for such a reaction in pyrazolylborate chemistry, for example, in the hydrolysis of $[(Et_2B(pz)_2)_2SnMe_2]$ to $[Et_2B(\mu\text{-}pz)(\mu\text{-}O)SnMe_2]_2$ (see Equation 1.7).[125] It is probable that the B–H bond is preferentially cleaved in the hydrolysis of $(Bp^{Me2})_2UCl_2$ because of the agostic interaction with the metal in this complex. This may cause the B–H bond to be intrinsically weak and hence more susceptible to nucleophilic attack by water in an S_N2 type manner than the B–N(pyrazolyl) bond. An analogous attack on a coordinated Tp^{Me2} ligand can only lead to B–N cleavage (Figure 3.12). On the other hand, the mechanism may involve precoordination of water to the metal centre (indeed, it is to be expected that nucleophilic attack will be less favoured at the more highly substituted boron atom in Tp^{Me2} than it is in Bp^{Me2}). This would also explain why B–N bond cleavage appears to be favoured in the hydrolysis of **3.16**, since the Tp^{Me2} ligand only coordinates to the metal through pyrazolyl nitrogens, whilst for Bp^{Me2}, hydrolysis of the weak B–H bond is once again favoured. It is worth noting that the free *poly*-(pyrazolyl)borate anions (as in the alkali metal complexes) are generally very stable to hydrolysis, and can even be protonated by weak acids.[99] Thus, they only become susceptible to attack once they are coordinated to metal ions.

Figure 3.12 Nucleophilic S_N2 Attack by Water on Bp^{Me2} and Tp^{Me2}

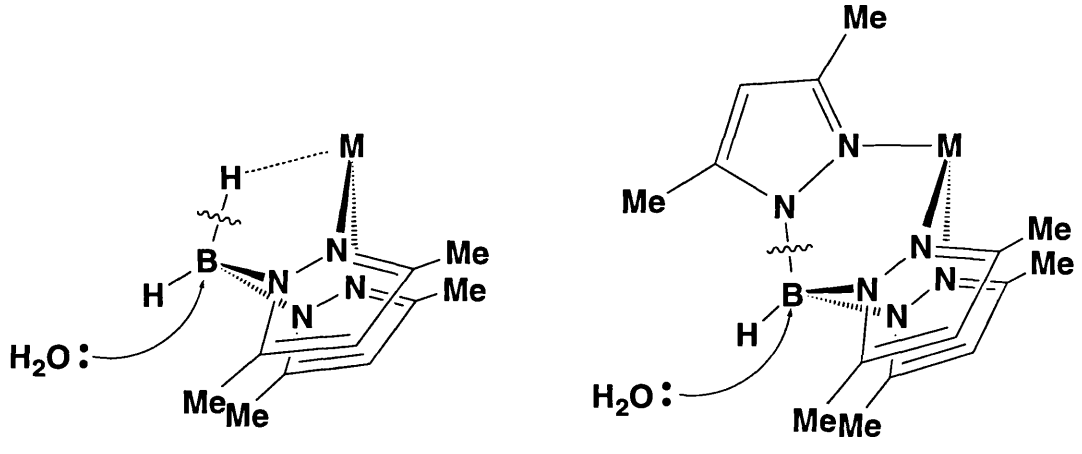

As part of their investigation into the chemistry of $[(Tp^{Me2})_2Sm]$ (**3.1**), Takats & Zhang noted that this compound reacted with NO.[167,168] Unfortunately, they were not able to characterise the product(s) formed, but encouraged us to probe the analogous reaction with our more soluble complexes (**3.4** to **3.6**). It

was hoped that the such a reaction would yield a product in which the NO molecule was bonded to the lanthanide in a side-on fashion, a coordination mode which has not been previously observed for this ligand. The possibility of isolating such a product was given added credence by the synthesis and unambiguous characterisation by Takats & Zhang of the complex $[(Tp^{Me2})_2Sm(\eta^2\text{-}O_2]$,[221] in which the very unusual side-on interaction of the O_2^- ligand was attributed to the "protective cradle" which the 3-Me substituents provide (Figure 3.13).

Figure 3.13 The Molecular Structure of $[(Tp^{Me2})_2Sm(\eta^2\text{-}O_2]$[221]†

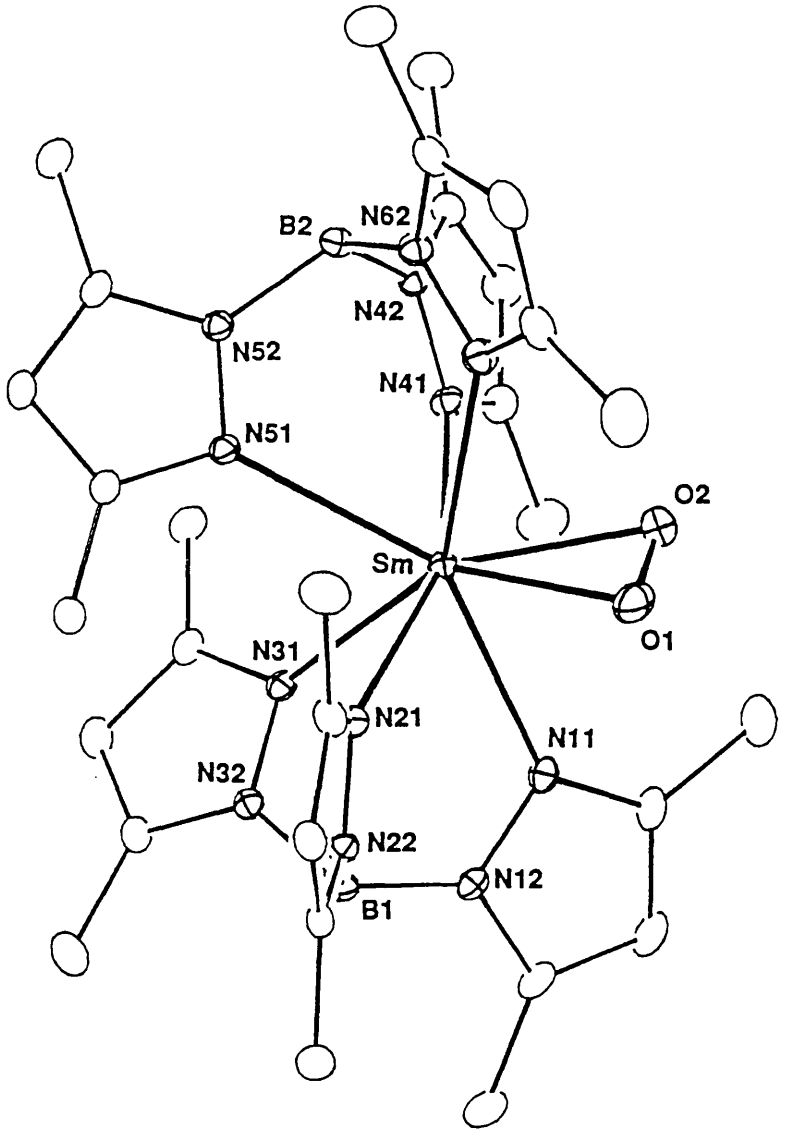

† Hydrogen atoms omitted for clarity

A Schlenk tube containing a solution/suspension of **3.4** in 30/40 petrol was filled with NO to a pressure of 760 torr (1 atmosphere) and the contents stirred at low temperature (-78 °C). As the flask was allowed to warm to room temperature, the purple starting material gradually disappeared, leaving a yellow solution. A white solid could be isolated by removal of the solvent under reduced pressure, and was recystallised from diethyl ether to give a white microcrystalline product (**3.19**). The ^{1}H and ^{13}C NMR spectra of this complex displayed resonances attributable to a single pyrazolyl environment in $Tp^{Me_2\text{-}4\text{-}Et}$. In addition, these resonances were fairly sharp and were only slightly shifted from their corresponding positions in the diamagnetic complexes **3.6** and **3.7**. Similarly, the ^{11}B NMR spectrum consisted of a single resonance at δ -9.3 (*cf.* δ *ca* -8.2 in **3.6** and **3.7**). Such observations are consistent with **3.19** being a complex of Sm^{3+} (for which the relatively small magnetic moment, normally 1.4 to 1.7 BM,[5] leads to much smaller paramagnetic NMR shifts than are generally observed for Sm^{2+}). The IR spectrum of this material showed typical bands corresponding to the $Tp^{Me_2\text{-}4\text{-}Et}$ ligand, including the characteristic B–H stretch which occurred at 2522 cm^{-1}. The fingerprint region of the spectrum was strikingly similar to that observed for **3.4**, except that many of the bands appeared to have split somewhat, consistent with **3.19** being a complex of lower symmetry than **3.4** in the solid state. In addition, there were two new bands at 1200 (strong) and 1297 (weak) cm^{-1}. The stretching frequencies and relative intensities of these bands are similar to absorptions observed in complexes containing chelated nitrito ligands, for example: $[Ni(TMEDA)(\eta^2\text{-}O_2N)_2]$ ($\nu_{N\text{-}O(s)}$ 1200 cm^{-1}; $\nu_{N\text{-}O(as)}$ 1289 cm^{-1}; TMEDA = $Me_2N(CH_2)_2NMe_2$), $[Ni(quinoline)_2(\eta^2\text{-}O_2N)_2]$ ($\nu_{N\text{-}O(s)}$ 1193, 1203 cm^{-1}; $\nu_{N\text{-}O(as)}$ 1289, 1299 cm^{-1}) and $[Co(OPPh_3)_2(\eta^2\text{-}O_2N)]$ ($\nu_{N\text{-}O(s)}$ 1176, 1199 cm^{-1}; $\nu_{N\text{-}O(as)}$ 1266 cm^{-1}).[222†]

Thus, it appeared that the reaction of NO with **3.4** had resulted in the formation of an NO_2^- complex. Elemental analysis indicated that the likely composition of the compound was $(Tp^{Me_2\text{-}4\text{-}Et})_2Sm(NO_2)$. This was confirmed by an X-ray diffraction study on a single crystal of **3.19** grown by slow evaporation of a toluene solution of the complex. Details of the data collection and tables of fractional coordinates, bond lengths and bond angles are given in Appendix 1 (Tables A1.1 and A1.20 to A1.22). The structure of **3.19** is shown in Figure 3.14.

† s = symmetric; as = antisymmetric

Figure 3.14 The Molecular Structure of $[(Tp^{Me2\text{-}4\text{-}Et})_2Sm(\eta^2\text{-}O_2N)]$ (**3.19**)†

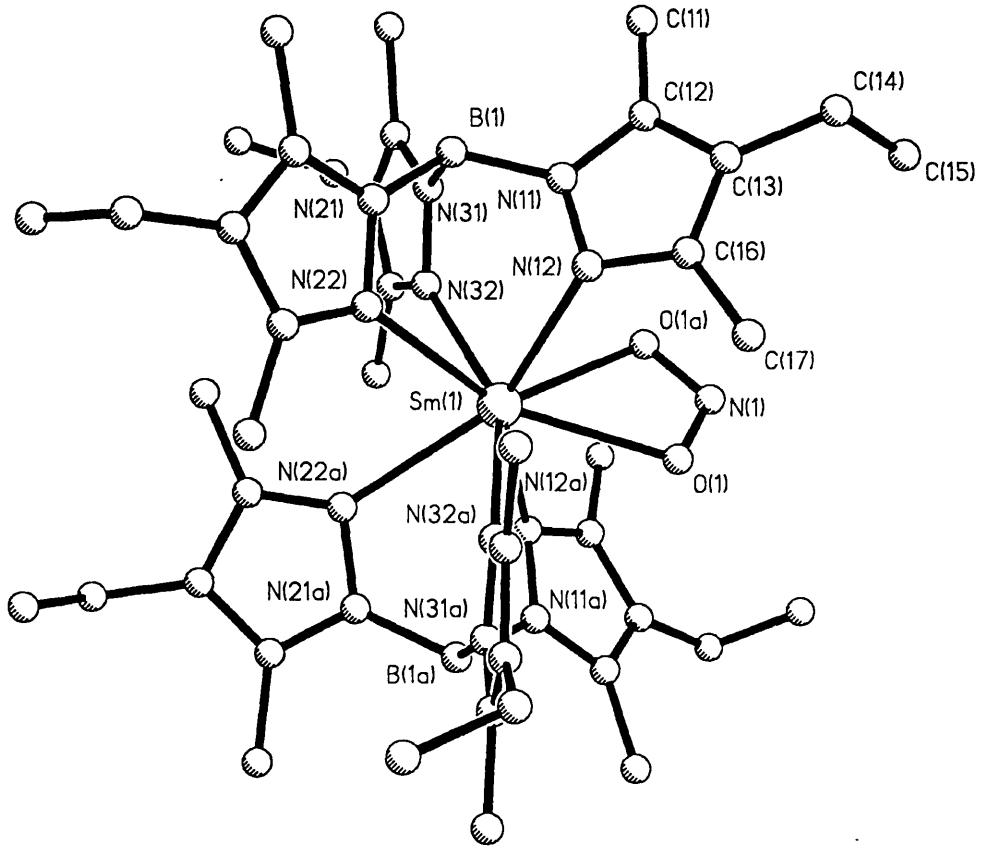

The NO_2^- group in **3.19** is coordinated to Sm^{3+} through both oxygen atoms - the chelate being symmetrical by virtue of the crystallographic C_2 symmetry of the molecule. The frequency difference between the symmetric and antisymmetric absorptions in the IR spectra of nitrito complexes has been shown to be a good indication of the difference in the M–O bond lengths of the chelate.[223] Thus, in compounds containing symmetrically bound η^2-nitrito groups (*eg* $[Zn(en)_2(\eta^2\text{-}O_2N)]^+[ClO_4]^-$; en = ethylenediamine) this difference is *ca* 70 cm^{-1}, whilst for η^1-coordinated complexes (*eg* $[Ni(dmen)(\eta^1\text{-}ONO)]$; DMEN = *N,N*-dimethylethylenediamine) it is as large as 260 cm^{-1}.[223] The separation of the symmetric and antisymmetric bands in the IR spectrum of **3.19** is *ca* 100 cm^{-1}, consistent with the observed symmetrical coordination mode of NO_2^- in this complex. The two $Tp^{Me2\text{-}4\text{-}Et}$ ligands coordinate to the Sm^{3+} ion in **3.19** in an η^3-fashion, hence, the metal centre is eight coordinate, with a geometry that is best described as distorted pentagonal bipyramidal. Thus, the equatorial sites are occupied by N(12), N(22), N(12a), N(22a) and the N(1) atom of the nitrito group, whilst the axial atoms are N(32)

† Hydrogen atoms omitted for clarity

and N(32a). This type of geometry is observed in the related eight coordinate Sm^{3+} complexes $[(Tp^{Me2})_2Sm(\eta^2\text{-}O_2)]$[221] and $[(Tp^{Me2})_2Sm(\eta^2\text{-}PhNNPh)]$[180]. The Sm(1)–N(32) and –N(32a) bond lengths in **3.19** are significantly shorter at 2.494(6) Å than the other Sm(1)–N distances (which average 2.559(4) Å), reflecting the lower congestion of the axial sites in this complex. A similar observation was made in the case of the Sm–N bond lengths in $[(Tp^{Me2})_2Sm(\eta^2\text{-}O_2)]$.[221] The coordination site for the NO_2^- ligand is created in **3.19** by bending back of the $Tp^{Me2\text{-}4\text{-}Et}$ ligands on the Sm^{3+} ion, the B···Sm···B angle being 159°. This is larger than the corresponding angle of 148° observed in the seven coordinate complex $[(Tp^{Me2})_2Nd(\eta^1\text{-}OTf)]$ (**2.3**), and may be a result of the greater steric crowding at the metal centre in **3.19** as a result of the smaller ionic radius of Sm^{3+}. In addition, pyrazolyl rings 1 and 1a are twisted about their B–N bonds in **3.19** such that their planes are at an angle of *ca* 56° to the Sm(1)···B(1) and Sm(1)···B(1a) vectors, respectively. This compares with twist angles of only *ca* 1° and 7° for rings 2(a) and 3(a). The coordination site which is so created for the nitrito group at the Sm centre is such that the plane of the NO_2^- ligand lies at an angle of *ca* 45° relative to the plane defined by Sm(1), B(1) and B(1a). In this position, it fits snugly between the 3-Me substituents C(17) and C(17a) (the C(17)···O(1) distance being 3.06 Å) and is protected from above and below by 4-Et substituents (Figure 3.15). This highly controlled coordination environment is in stark contrast to that of the cyclopentadienyl complex $[Cp_2Yb(\eta^2\text{-}O_2N)(THF)]$[224] for which the three oxygens of the NO_2^- and THF groups lie approximately in an equatorial plane with respect to the canted Cp rings.

The O···O separation of 2.10 Å in the nitrito group of **3.19** is larger than that observed in $[Cp_2Yb(\eta^2\text{-}O_2N)(THF)]$, consistent with the smaller size of the Yb^{3+} ion with respect to Sm^{3+}. In addition, the N–O bond length in **3.19** (1.264(7) Å) is comparable with that observed in $NaNO_2$ (1.240(3) Å)[225], but is significantly longer than those observed in $[Cp_2Yb(\eta^2\text{-}O_2N)(THF)]$, for which the average is 1.102(14) Å. The shortness of the N–O bonds in the Yb complex, which is reflected in the IR spectrum of this compound in which the NO_2^- bands occur at 1226 and 1307 cm^{-1}, was attributed to the partial transfer of π-antibonding electron density to the metal.[224] However, given the absence of covalent interactions in trivalent lanthanide bonds, significant electron transfer seems unlikely, although the more polarising nature of the Yb^{3+}cation over Sm^{3+} (and Na^+) may result in a substantial weakening of this antibonding interaction. As a consequence of the longer N–O bond length in

Figure 3.15 A Space Filling Model of $[(Tp^{Me_2\text{-}4\text{-}Et})_2Sm(\eta^2\text{-}O_2N)]$ (**3.19**)†

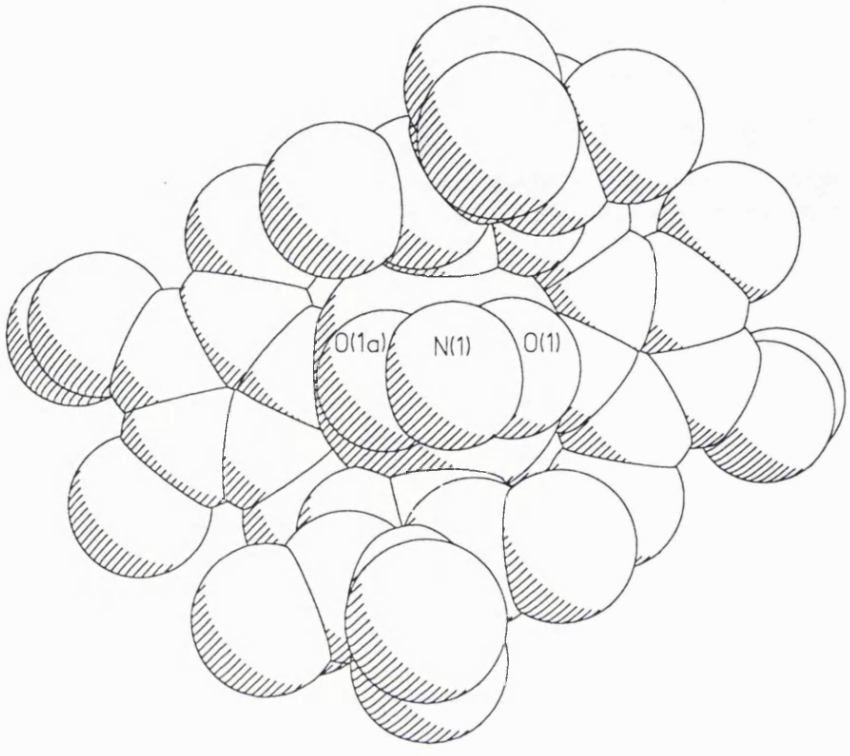

3.19, the O(1)–N(1)–O(1a) angle (112.4(7)°) is much smaller than that observed in $[Cp_2Yb(\eta^2\text{-}O_2N)(THF)]$ (127.0(1)°). The Sm–O distance in **3.19** is 2.487(4) Å compared with 2.389(9) Å in $[Cp_2Yb(\eta^2\text{-}O_2N)(THF)]$. This difference is slightly larger than would be predicted on the basis of the relative ionic radii of eight coordinate Sm^{3+} and nine coordinate Yb^{3+}, which are reported to differ in size by only *ca* 0.04 Å,[15] and may reflect the sterically demanding nature of the $Tp^{Me_2\text{-}4\text{-}Et}$ ligand.

The reaction of NO with **3.5** and **3.6** was also studied; in both cases the crude products were analysed by IR spectroscopy only. For the reaction with **3.5**, the IR spectrum of the product formed (**3.20**; $\nu_{N\text{-}O(s)}$ 1202 cm^{-1}; $\nu_{N\text{-}O(as)}$ 1298 cm^{-1}) was virtually identical to that of **3.19**, consistent with the similar sizes of Sm^{3+} and Eu^{3+}. In contrast to the IR spectra of **3.19** and **3.20**, the spectrum of the corresponding Yb product (**3.21**) did not show obvious splitting of the pyrazolylborate bands, implying that this species may have relatively high symmetry in the solid state. In addition, **3.21** is significantly less soluble than its Sm and Eu analogues: for example, when synthesised, it precipitates from 30/40 petrol rather than remaining in solution as is observed for **3.19** and

† Hydrogen atoms omitted for clarity

3.20. This is consistent with the formation of an ion pair complex containing the $[(Tp^{Me_2\text{-}4\text{-}Et})_2Yb]^+$ cation (similar to that observed in complexes **2.6** and **3.15**). However, the bands due to the nitrito group in this complex are still of approximately the same frequency as in **3.19** and **3.20**, occurring at 1210 and 1303 cm^{-1}. Since the vibrational spectrum of the 'free' nitrite anion has not been reported - the spectrum of $NaNO_2$ has been measured ($\nu_{N\text{-}O(s)}$ 1261 cm^{-1}; $\nu_{N\text{-}O(as)}$ 1328 cm^{-1})[226], but there is significant interaction between the cation and anion in the solid state[225] - it is not possible to say whether these bands are consistent with the presence of uncoordinated NO_2^-.

The mechanism by which the NO_2^- moiety in these complexes is formed is not known. However, it is not believed to be formed directly by the reduction of nitrogen dioxide (which is frequently a significant contaminant of commercially purchased NO), since the same products are obtained when the NO is purified by passing it through a cold trap at -78 °C. Due to the practical difficulties involved in adding exactly one equivalent of NO to the divalent complexes $[(Tp^{Me_2\text{-}4\text{-}Et})_2Ln]$, an alternative experiment was carried out in which the reaction between **3.6** and an excess of NO was allowed to proceed in THF at -78 °C for 30 min, such that it was still incomplete (shown by the presence of significant quantities of purple $[(Tp^{Me_2\text{-}4\text{-}Et})_2Yb]$). After this time, the solution was completely degassed before being allowed to warm to room temperature as the solvent was removed. The IR spectrum of this product was no different from that obtained previously. In the light of this observation, it appears that the putative NO^- complex (for which no evidence has been obtained) is rapidly attacked by more NO to ultimately give NO_2^-. Tolman and coworkers have reported that the isolable copper complexes $[Tp^{R_2}Cu(NO)]$ (R = Me or Ph) react with excess NO to give $[Tp^{R_2}Cu(\eta^2\text{-}O_2N)]$; almost quantitative formation of N_2O was observed and labelling studies indicated that disproportionation of NO (rather than reaction of a contaminant such as NO_2) was probably responsible for the formation of the nitrito complex.[227]

The formation of complexes **3.19** to **3.21** is in contrast to the equivalent reaction of $[Cp^*_2Sm]$ with NO, when the only identifiable product is the oxo-bridged dimer $[(Cp^*_2Sm)_2(\mu\text{-}O)]$.[228] This serves as yet another example of the degree to which lanthanide chemistry is controlled by the steric properties of the ancillary ligands.

Following the reaction reported by Takats & Zhang between azobenzene and $[(Tp^{Me_2})_2Sm]$ (**3.1**; Equation 3.8),[180] the analogous reaction of PhNNPh with

3.4 was carried out in an NMR tube to give the green complex **3.22**. The ^1H chemical shifts of this compound were virtually identical to those reported by Takats for $[(Tp^{Me2})_2Sm(\eta^2\text{-PhNNPh})]$ (excepting the signals arising from the 4-C substituent on the pyrazolyl ring) indicating that the two complexes have the same eight coordinate structure in which the crystallographic pseudo-C_2 symmetry is retained in solution (Figure 3.16). Whilst for the Tp^{Me2} and $Tp^{Me2\text{-}4\text{-}Et}$ systems only one product is isolated, independent of the stoichiometry of the reagents, the species obtained with $[Cp^*_2Sm]$ does depend on the proportions used, giving either $[Cp^*_2Sm(THF)(\eta^2\text{-PhNNPh})]$ or $[(Cp^*_2Sm)_2(\mu\text{-}\eta^1,\eta^1\text{-PhNNPh})]$.[229] The inability of the *tris*-(pyrazolyl)borate complexes to form an analogous azobenzene bridged dimer is presumably related to the excessive interligand steric interactions which would be present in such a complex.

Equation 3.8[180]

$$[(Tp^{Me2})_2Sm] + PhNNPh \xrightarrow{Toluene} [(Tp^{Me2})_2Sm(\eta^2\text{-PhNNPh})]$$

Figure 3.16 The ^1H NMR Data for $(Tp^{Me2\text{-}4\text{-}Et})_2Sm(PhNNPh)$ (**3.22**) and $[(Tp^{Me2})_2Sm(\eta^2\text{-PhNNPh})]$,† and the Proposed Structure of **3.22**

Assignment	3.22	Tp^{Me2} Complex[180]
Ph	72.2	73.19
Tp^{Me2} Me	25.94	23.21
Tp^{Me2} B–H	5.2	5.40
Tp^{Me2} Me	4.78	4.55
Tp^{Me2} Me	2.76	2.75
Tp^{Me2} Me	2.36	2.40
Tp^{Me2} Me	2.34	2.20
Tp^{Me2} Me	-3.96	-4.55
Ph	-168.1	-170.30
Ph	-187.9	-189.55

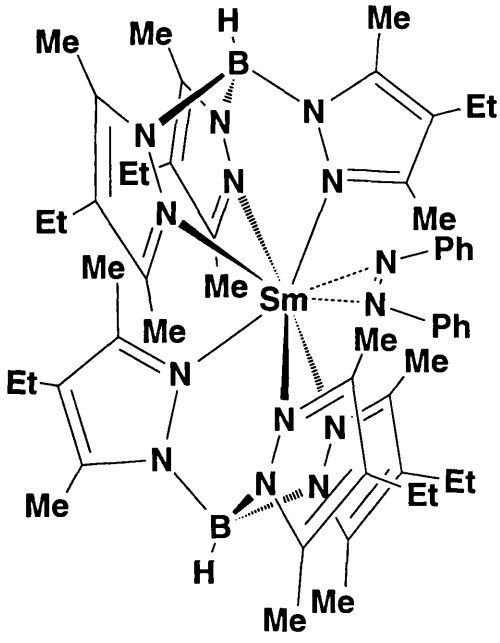

3.22

† Resonances due to the 4-substituents on the pyrazolyl ring are not included

In addition to the reactivity presented here, the chemistry of complexes **3.1** to **3.3** has been actively investigated by other members of our group, and by the research groups of Takats and Marques. In common with the work outlined above, the chemistry is currently restricted to reactions in which the divalent metals are formally oxidised to the trivalent state. For example, the reactions of **3.1** with $TlBPh_4$, iodine, alkyl halides and diaryldichalcogenolides have been studied (Equations 3.9 to 3.12).

Equation 3.9[167,168]

$$[(Tp^{Me_2})_2Sm] + Tl^+[BPh_4]^- \longrightarrow [(Tp^{Me_2})_2Sm]^+[BPh_4]^- + Tl$$

Equation 3.10[130,169]

$$2\,[(Tp^{Me_2})_2Sm] + I_2 \longrightarrow 2\,[(Tp^{Me_2})_2Sm]^+I^-$$

Equation 3.11[156,219†]

$$[(Tp^{Me_2})_2Sm] + EtBr \longrightarrow \{(Tp^{Me_2})_2SmBr\} + C_4H_{10}$$

Equation 3.12[230]

$$2\,[(Tp^{Me_2\text{-}4\text{-}Et})_2Sm] + PhTe\text{-}TePh \longrightarrow 2\,[(Tp^{Me_2\text{-}4\text{-}Et})_2Sm(TePh)]$$

In addition, the reaction of **3.1** to **3.6** with transition metal carbonyls containing metal–metal bonds is currently being studied.[230,231] For example, the reaction of **3.1** with $[(MeC_5H_4)Mo(CO)_3]_2$ in toluene gives the seven coordinate complex $[(Tp^{Me_2})_2Sm(\eta^1\text{-}OCMo(CO)_2(MeC_5H_4)]$ which was characterised by X-ray crystallography.[231] Finally, in the light of the failure to observe any reactivity of $[(Tp^{Me_2})_2Ln]$ with simple alkynes (*vide supra*), Takats & Zhang§ found that a reaction does occur between **3.1** and the highly

† The structure of the bromide complex is not known at this time

§ Following a suggestion from Sella

electron deficient molecule hexafluorobut-2-yne. However, the product isolated was not a simple adduct, but rather the seven coordinate fluoride complex, [$(Tp^{Me2})_2$SmF], which was characterised crystallographically.[167] The activation of C–F bonds in unsaturated fluorocarbons (*e g* hexafluorobenzene and 1,1-difluoroethene) by Cp^*_2Yb has been reported by Andersen.[190]

Attempted Synthesis of Divalent Hydrido-*tris*-(3,5-dimethyl-4-ethylpyrazol-1-yl)borate Lanthanide Iodide Complexes

The synthesis and derivatisation of divalent 'half sandwich' complexes of the type [$ALnXL_n$] (A = ancillary ligand; X = anionic ligand; L = Lewis base) is an area which is relatively unexplored in divalent lanthanide chemistry (see Chapter 4). This is principally because the ancillary ligands used (such as the substituted cyclopentadienyls) are generally unable to sterically saturate the metal centre sufficiently to prevent undesirable ligand redistribution reactions. In the light of the large steric bulk of the Tp^{Me2} and $Tp^{Me2\text{-}4\text{-}Et}$ ligands, it was hoped that they would allow the isolation of more stable half sandwich complexes. Takats & Zhang had already found that, by reaction of one equivalent of KTp^{Me2} with YbI_2, the orange complex [(Tp^{Me2})YbI$(THF)_2$] could be isolated.[167,168] An X-ray crystal diffraction study of this compound revealed that the molecule was monomeric with a half sandwich structure. However, this complex was rather unstable, readily undergoing ligand redistribution to give [$(Tp^{Me2})_2$Yb] (**3.3**). Furthermore, the Sm analogue could not be isolated, a fact that was attributed by these workers to the inability of this combination of ligands to sterically saturate the larger Sm^{2+} cation.[168] Reasoning that the extreme insolubility of the [$(Tp^{Me2})_2$Ln] class of compounds might act as a driving force for such a ligand redistribution reaction, we attempted to synthesise the analogous half sandwich complexes of the $Tp^{Me2\text{-}4\text{-}Et}$ ligand. The reactions were generally carried out at low temperature (-78 °C), with the ligand being added slowly to a solution of LnI_2 in THF (Ln = Sm and Yb), such that an excess of $Tp^{Me2\text{-}4\text{-}Et}$ was never present. This procedure gave a purple/red solution/suspension for Ln = Yb, and rather more promisingly, a dark green solution/suspension for Ln = Sm. However, upon concentrating these solutions and then cooling slowly, a mixture of purple and black (Sm) or purple and yellow (Yb) powders was precipitated, indicating that ligand redistribution had occurred (Equation 3.13).

Equation 3.13

$$KTp^{Me_2\text{-}4\text{-}Et} + LnI_2 \xrightarrow[-KI]{THF} `(Tp^{Me_2\text{-}4\text{-}Et})LnI(THF)_n' \xrightarrow{-20\ ^\circ C} [(Tp^{Me_2\text{-}4\text{-}Et})_2Ln]\downarrow + LnI_2(THF)_m\downarrow$$

Ln = Sm, Yb

Comparison of the UV/vis spectra of the THF solutions of these products with those of LnI_2, the sandwich complexes **3.4** and **3.6**, and the half sandwich complexes $[(Tp^{3\text{-}t\text{-}Bu\text{-}5\text{-}Me})LnI(THF)_n]$ (Ln = Sm (**4.1**) and Yb (**4.2**); introduced in Chapter 4), suggests that they are mixtures of $LnI_2(THF)_n$, $[(Tp^{Me_2\text{-}4\text{-}Et})LnI(THF)_n]$ and $[(Tp^{Me_2\text{-}4\text{-}Et})_2Ln]$ (Table 3.6).

Table 3.6 A Comparison of the UV/vis Spectra of $(Tp^{Me_2\text{-}4\text{-}Et})LnI(THF)_n$ with those of LnI_2, $[(Tp^{Me_2\text{-}4\text{-}Et})_2Ln]$ (**3.4** and **3.6**) and $[(Tp^{3\text{-}t\text{-}Bu\text{-}5\text{-}Me})LnI(THF)_n]$ (**4.1** and **4.2**)

Absorption Maxima in THF (nm)							
Samarium				Ytterbium			
$KTp^{Me_2\text{-}4\text{-}Et}$ + SmI_2	SmI_2	**3.4**	**4.1**	$KTp^{Me_2\text{-}4\text{-}Et}$ + YbI_2	YbI_2	**3.6**	**4.2**
380		399	409	350		369	
425	424						
560	559	519	563	400	408		
619	618			437			420
†		767		537		533	

Conclusion

In this chapter, the syntheses of the sandwich complexes $[(Tp^{Me_2})_2Ln]$ (Ln = Sm (**3.1**), Eu (**3.2**) and Yb (**3.3**)) and $[(Tp^{Me_2\text{-}4\text{-}Et})_2Ln]$ (Ln = Sm (**3.4**), Eu (**3.5**) and Yb (**3.6**)) have been described; the synthesis of the Ba complex $[(Tp^{Me_2\text{-}4\text{-}Et})_2Ba]$ (**3.7**) was also reported. Complexes **3.2** and **3.3** have been characterised by X-ray crystallography and their structures compared with those of a number of isomorphous compounds; the Yb centre in **3.3** is also

† Whilst no maximum was evident in the spectrum at *ca* 770 nm, significant absorption (in the form of a long tail on the band at 619 nm) is observed in this region

isoleptic with that in the trivalent complex $[(Tp^{Me2})_2Yb]^+[OTf]^-$ (**2.6**).[1] The magnetic properties of some of these divalent complexes have been studied, and their electronic and PE spectra measured. The latter technique revealed likely f electron ionisations from compounds **3.2** and **3.3**, and these were compared with those observed in Cp^*_2Eu and Cp^*_2Yb. Initial reactivity studies of **3.1** to **3.6** showed that they were significantly less reactive than the decamethyllanthanocenes; this was attributed to the interlocked 3-Me groups in these structures, which prevent the coordination of further ligands to the metal centre. However, by the selection of more reactive substrates, a number of new complexes has been successfully synthesised. Thus, **3.1** to **3.4** and **3.6** are readily oxidised by TCNQ and TCNE. The Yb complexes formed (**3.10**, **3.12**, **3.15** and **3.17**) were shown to be simple charge transfer salts by IR spectroscopy, and by the X-ray crystal structure determination of $[(Tp^{Me2})_2Yb]^+[TCNE]^-.(THF)_6$ (**3.15**). The complexes formed for Sm and Eu (**3.8**, **3.9**, **3.11**, **3.13**, **3.14** and **3.16**) were not fully characterised, although IR spectroscopy suggests that some interaction between the polycyano anion and the metal centre may exist. During one attempt to grow crystals of **3.16**, the hydrolysis product $[(Tp^{Me2})Sm\{(pz^{Me2})_2B(H)(\mu\text{-}O)\}]_2.THF$ (**3.18**) was isolated and characterised crystallographically. The reaction of **3.4**, **3.5** and **3.6** with NO gave the nitrito complexes $(Tp^{Me2\text{-}4\text{-}Et})_2Ln(NO_2)$ (**3.19**, **3.20** and **3.21**). The structure of the Sm compound (**3.19**) was determined by X-ray crystallography and the metal found to be eight coordinate, with the NO_2^- group chelating symmetrically, consistent with the IR spectrum of the compound. The reaction of **3.4** with azobenzene was investigated by NMR spectroscopy, and the product shown to be $[(Tp^{Me2\text{-}4\text{-}Et})_2Sm(\eta^2\text{-}PhNNPh)]$ by comparison of its chemical shifts with those of the previously reported Tp^{Me2} analogue. The chemistry of **3.1** to **3.3** is currently under further investigation by our group and others. The current interest in this area of lanthanide chemistry is a testament to the unique properties which the *tris*-(pyrazolyl)borate ligands are able to confer on these elements.

Attempts to synthesise stable half sandwich complexes of the type $[(Tp^{Me2\text{-}4\text{-}Et})LnI(THF)_n]$ (Ln = Sm and Yb) were unsuccessful, and evidence was obtained for these species being in equilibrium with $[(Tp^{Me2\text{-}4\text{-}Et})_2Ln]$ and $LnI_2(THF)_n$ in THF solution. The instability of these half sandwich complexes was attributed to the inability of this combination of ligands to sterically saturate the metal centre to a sufficient degree. The use of a more sterically demanding pyrazolylborate to isolate stable species of this type is addressed in Chapter 4.

Chapter 4 - Synthesis and Reactivity of Divalent Lanthanide Complexes of Hydrido-*tris*-(3-*tert*-butyl-5-methylpyrazol-1-yl)borate

Introduction

The chemistry of the decamethyllanthanocenes, $[Cp^*_2Ln]$, is remarkable,[24,148] and preliminary studies described in Chapter 3 indicate that their *tris*-(pyrazolyl)borate analogues $[(Tp^{Me2})_2Ln]$ and $[(Tp^{Me2\text{-}4\text{-}Et})_2Ln]$ (**3.1** to **3.6**) are somewhat less reactive. However, the scope for extending the chemistry of such divalent 'sandwich' complexes is limited by the presence of two ancillary ligands and hence the availability of only neutral binding sites at the metal. An investigation of the behaviour of more reactive ligands at a divalent lanthanide centre, in which steric control is provided by a single ancillary ligand, is desirable. It has been found that 'half sandwich' complexes of this type, $[ALnXL_n]$ (A = ancillary ligand; X = anionic ligand; L = Lewis base), are not readily formed when A is a cyclopentadienyl group. Thus, the only structurally characterised examples, $[Cp^*Sm(\mu\text{-}I)(THF)_2]_2$[177] and the phospholyl analogue $[(Me_4C_4P)YbCl(THF)_2]_2$ (see Chapter 1, Figure 1.6**h**),[97] are dimeric and prone to ligand redistribution. The complexes $CpYbClL_n$ and Cp^*YbClL_n (L = THF, n = 2; L = DME, n=1) have also been synthesised and monomeric structures proposed on the basis of their mass spectra, although no crystallographic characterisation or reactivity of these molecules has been reported.[232] Other types of sterically demanding ligand have been used as alternatives to the cyclopentadienyls, but again the compounds are invariably dimeric: $[(SiMe_3)_3CYb(\mu\text{-}I)(OEt_2)]_2$,[98] $[(SiMe_3)_2NSm(\mu\text{-}I)(\eta^2\text{-}DME)(THF)_2]_2$[233] and $[YbI(\mu\text{-}OCPh_3)(\eta^2\text{-}DME)]_2$.[234] Only by the use of two bulky anions are well characterised monomeric half sandwich complexes obtained, as in the case of $[Cp^*Yb(Sn(CH_2Bu^t)_3)(THF)_2]$.[95]

As discussed in Chapter 1, the substituted *tris*-pyrazolylborates are potentially much more sterically demanding than the cyclopentadienyls, and may therefore be suitable ancillary ligands for the formation of stable half sandwich complexes of divalent lanthanides. The synthesis and structural characterisation of $[Tp^{Me2}YbI(THF)_2]$ by Takats and coworkers was alluded to in the previous chapter; however, they found that this molecule was extremely prone to ligand redistribution (readily precipitating $[(Tp^{Me2})_2Yb]$ (**3.3**)) and no derivatisation was possible. Furthermore, in our studies using the related

ligand $Tp^{Me_2\text{-}4\text{-}Et}$ (see Chapter 3, p 104), we were unable to isolate stable half sandwich complexes due to the facile formation of $[(Tp^{Me_2\text{-}4\text{-}Et})_2Ln]$. This was attributed to the inability of a single 3-Me substituted pyrazolylborate ligand to sterically saturate the large Ln^{2+} ions. However, the size of these ligands can be readily increased, by placing more sterically demanding groups at the 3-position on the pyrazolyl ring, as reported by Trofimenko *et al* in 1987 with the introduction of Tp^{Ph} and $Tp^{t\text{-}Bu}$.[122]

In the work described in this chapter, we have utilised the bulky hydrido-*tris*-(3-*tert*-butyl-5-methylpyrazol-1-yl)borate ligand ($Tp^{3\text{-}t\text{-}Bu\text{-}5\text{-}Me}$)[104] to isolate the first stable half sandwich derivatives of the lanthanide diiodides.† The synthesis, structural characterisation and chemistry of these unique synthetic precursors is discussed; new compounds are numbered **4.1** to **4.14**.

Preparation of Divalent Lanthanide Complexes of *Tris*-(3-*tert*-butyl-5-methylpyrazol-1-yl)borate[3]

The reaction of one equivalent of $KTp^{3\text{-}t\text{-}Bu\text{-}5\text{-}Me}$ with $LnI_2(THF)_n$ (Ln = Sm and Yb) in THF gave dichroic green/red and yellow solutions, respectively. Both the Sm (**4.1**) and Yb (**4.2**) complexes were found to dissolve readily, not only in THF but also in aromatic and ethereal solvents, although their solubility in 30/40 petrol was poor. Recrystallisation of both complexes was achieved by cooling a concentrated diethyl ether solution to -20 °C, and gave large black blocks in the case of **4.1**, and smaller, bright yellow crystals of **4.2** (Figure 4.1). The compounds were extremely air and moisture sensitive, both in solution and in the solid state.

The ^1H NMR spectrum of **4.2** (in C_6D_6 at 20 °C) displayed three resonances at δ 1.47, 2.16 and 5.65 in the ratio 9:3:1, consistent with a diamagnetic compound of the $Tp^{3\text{-}t\text{-}Bu\text{-}5\text{-}Me}$ ligand. This single pyrazolyl environment (which was also observed in the ^{13}C spectrum of this compound) indicated a high degree of symmetry or fluxionality in the molecule. The low temperature ^1H NMR spectrum (in d_8-toluene) was also studied, and the same set of resonances was found to persist, even at -100 °C. In addition to the pyrazolyl peaks, two multiplets were observed in the ^1H NMR spectrum (at δ 1.06

† $Tp^{3\text{-}t\text{-}Bu\text{-}5\text{-}Me}$ was used in preference to $Tp^{3\text{-}t\text{-}Bu}$ since synthesis of the former was more reproducible in our hands

Figure 4.1 The Preparation of Sm (**4.1**) and Yb (**4.2**) Complexes of $Tp^{3\text{-}t\text{-}Bu\text{-}5\text{-}Me}$

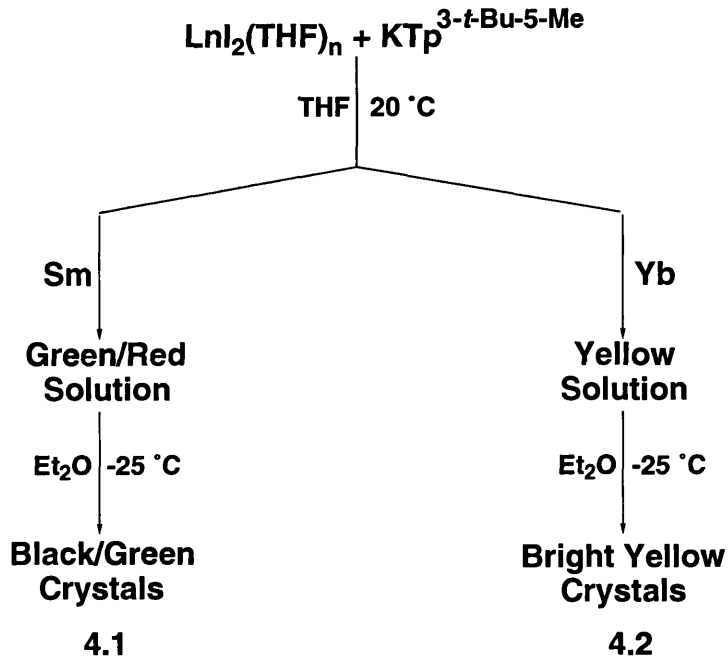

and 3.21). These were shown to be due to THF, rather than diethyl ether, from the pair of triplets observed in the $^{13}C\{^1H\}$ NMR spectrum of **4.2**. The fact that THF from the original synthesis was present in this compound and had not been displaced by diethyl ether during recrystallisation, indicated that it was probably coordinated quite strongly to the Yb^{2+} ion. Integration of the peaks in the ^1H NMR spectrum showed that there was one molecule of THF for each $Tp^{3\text{-}t\text{-}Bu\text{-}5\text{-}Me}$ ligand. In contrast to the solution NMR experiments, the Bu^t and Me resonances in the solid state ^{13}C CP MAS spectrum of **4.2** were both split into three peaks, showing that the pyrazolyl rings in the coordinated $Tp^{3\text{-}t\text{-}Bu\text{-}5\text{-}Me}$ ligand are inequivalent in the static structure.

In common with those of **4.2**, the solution NMR spectra of **4.1** showed that the pyrazolyl rings in the $Tp^{3\text{-}t\text{-}Bu\text{-}5\text{-}Me}$ ligand were equivalent at room temperature. All of the resonances were shifted from their diamagnetic positions and were broadened somewhat compared with those of **4.2**, on account of the paramagnetism of the Sm^{2+} ion ($[Xe]4f^6$). The ^1H NMR spectrum of **4.1** is shown in Figure 4.2. The most shifted and broadened pyrazolyl resonance is the singlet due to the 3-Bu^t group (δ 4.74, $w_{1/2}$ = 13 Hz at 90 mM), consistent with this substituent being closest to the paramagnetic metal ion. In addition to the pyrazolylborate ligand resonances, the spectrum

revealed that there were two molecules of THF for every $Tp^{3\text{-}t\text{-}Bu\text{-}5\text{-}Me}$ group; these appeared to be interacting strongly with the Sm^{2+} ion since their peaks were broad ($w_{1/2}$ = *ca* 13 Hz) and shifted (δ -0.64 and -0.74). The spectrum was found to be concentration dependent (particularly with regard to the positions of these two peaks), suggesting that substantial dissociation of the THF molecule(s) might occur in solution. In addition, the presence of half a molecule of diethyl ether per $Tp^{3\text{-}t\text{-}Bu\text{-}5\text{-}Me}$ ligand was noted from the ^1H NMR spectrum; interestingly, its resonances were extremely sharp, indicating that if partial dissociation of THF from the Sm^{2+} centre does occur in solution, then it is not replaced by diethyl ether.

Elemental analyses of these complexes were consistent with the compositions $Tp^{3\text{-}t\text{-}Bu\text{-}5\text{-}Me}SmI(THF)_2.(Et_2O)_{0.5}$ (**4.1**) and $Tp^{3\text{-}t\text{-}Bu\text{-}5\text{-}Me}YbI(THF)$ (**4.2**).

Figure 4.2 The ^1H NMR Spectrum of $[Tp^{3\text{-}t\text{-}Bu\text{-}5\text{-}Me}SmI(THF)_2].(Et_2O)_{0.5}$ (**4.1**) (90 mM in C_6D_6)

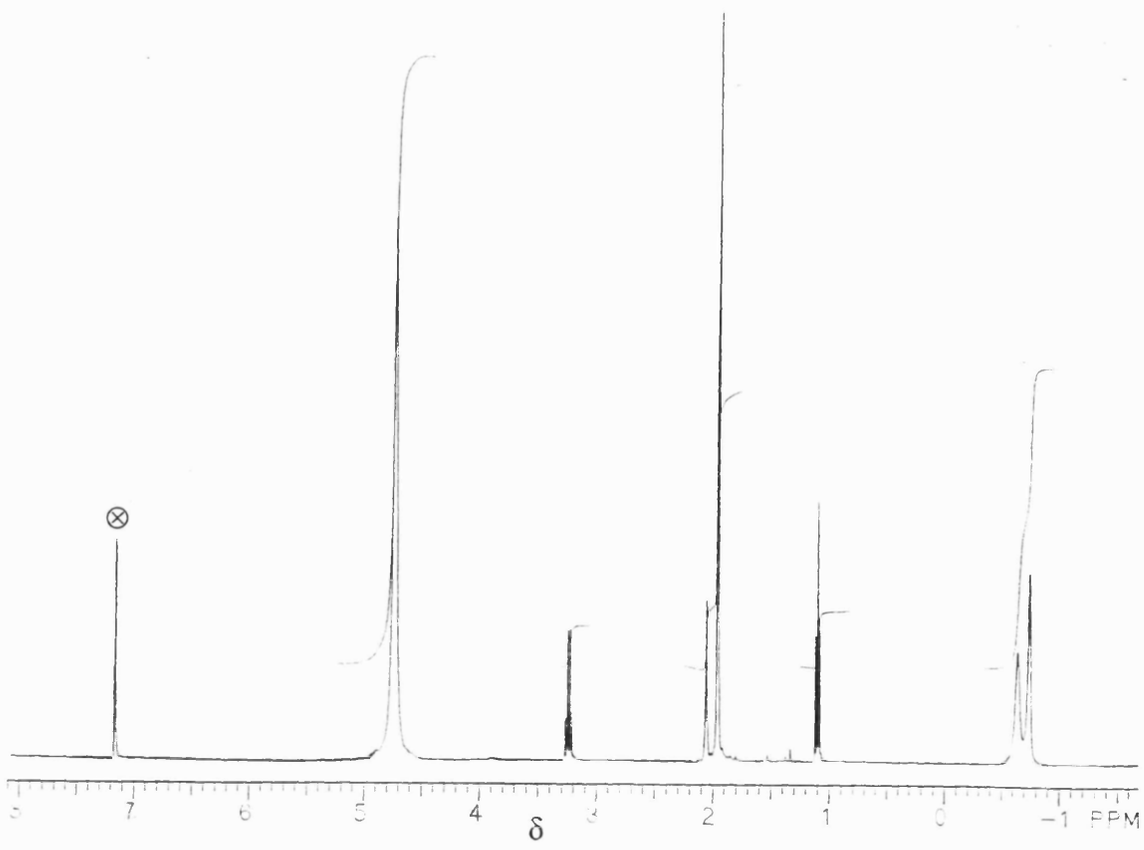

⊗ = d_6-benzene resonance

The IR spectrum of the Yb complex (**4.2**) exhibited characteristic absorptions for the $Tp^{3\text{-}t\text{-}Bu\text{-}5\text{-}Me}$ ligand, most notably, a single B–H stretching mode at 2554 cm^{-1}. Intriguingly, the corresponding spectrum for **4.1** revealed two B–H stretching vibrations of approximately equal intensity, at 2546 and 2516 cm^{-1}. This result was reproducible and may be due to rapid decomposition of the compound whilst recording the spectrum.

Slow cooling of diethyl ether solutions of **4.1** and **4.2** enabled good quality crystals to be grown, and an X-ray diffraction study of the complexes was undertaken to determine their molecular geometries. Details of the data collections and tables of fractional coordinates, bond lengths and bond angles are given in Appendix 1 (Tables A1.1 and A1.23 to A1.28). The molecular structures of **4.1** and **4.2**† are shown in Figures 4.3 and 4.4.

Figure 4.3 The Molecular Structure of $[Tp^{3\text{-}t\text{-}Bu\text{-}5\text{-}Me}SmI(THF)_2].(Et_2O)_{0.5}$ (**4.1**)§

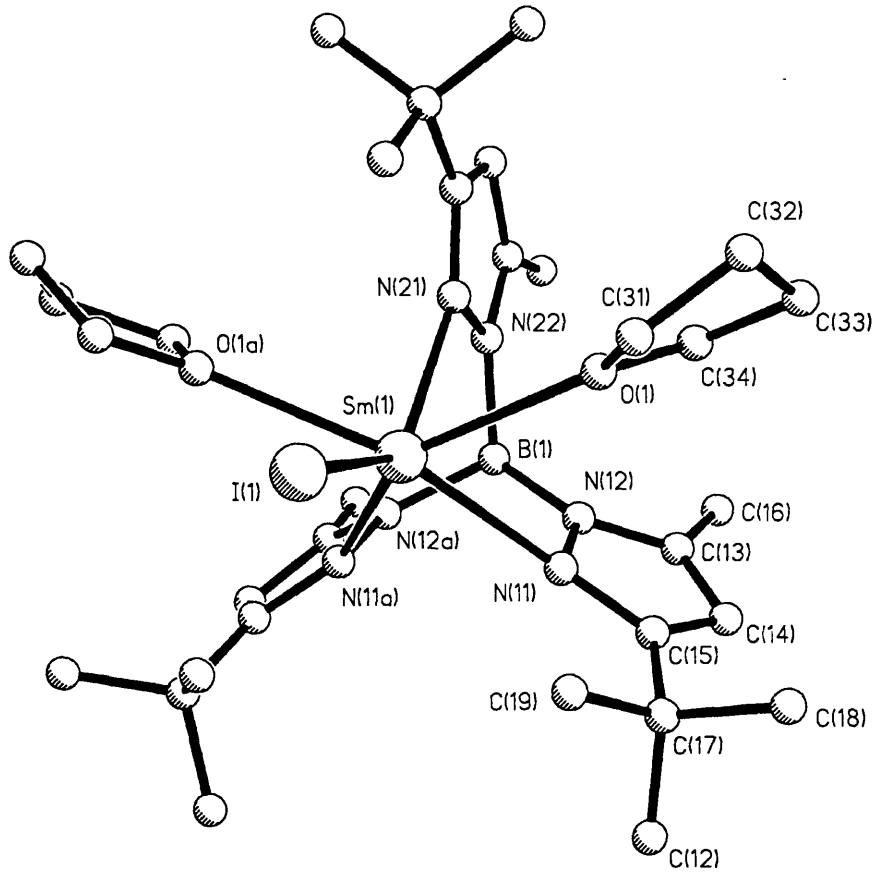

† Complexes **4.1** and **4.2** have also been synthesised by Takats and coworkers, who independently determined the structure of **4.2**[235]

§ Hydrogen atoms and diethyl ether molecule omitted for clarity

Figure 4.4 The Molecular Structure of [$Tp^{3\text{-}t\text{-}Bu\text{-}5\text{-}Me}$YbI(THF)] (**4.2**)[3†]

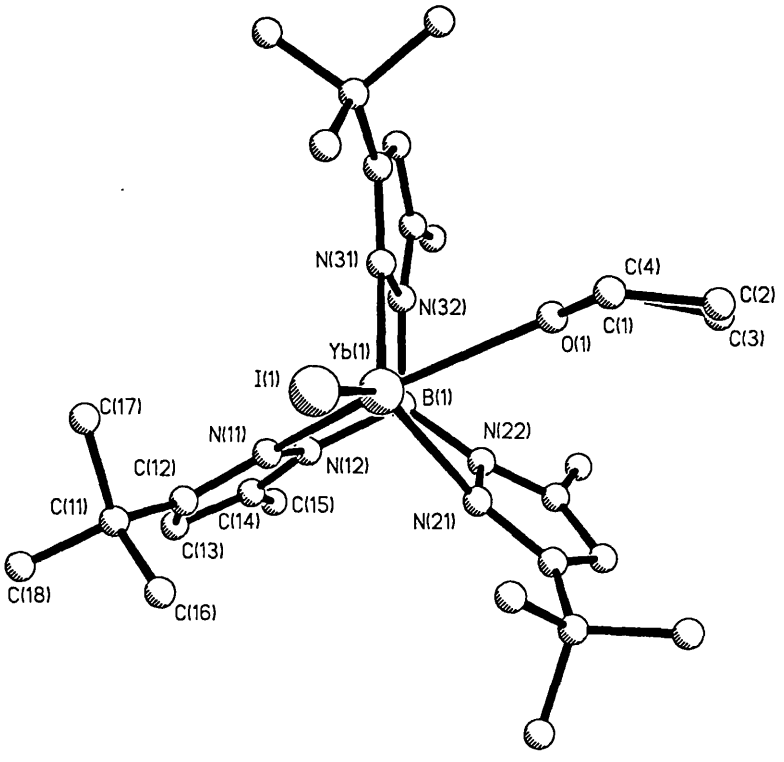

Complexes **4.1** and **4.2** have coordination numbers of six and five, respectively. Whilst these are quite low for divalent lanthanide compounds (eight being considered 'normal'),[236] they are unusually high for complexes containing the $Tp^{3\text{-}t\text{-}Bu\text{-}5\text{-}Me}$ ligand, for which four coordinate tetrahedral geometries are most common.[102,127] However, the monomeric structures of **4.1** and **4.2** are a testament to the steric control which can be achieved at a metal centre by the use of a bulky pyrazolylborate ligand such as $Tp^{3\text{-}t\text{-}Bu\text{-}5\text{-}Me}$.

Compound **4.1** crystallised in the space group *C2/m*; thus, half of the molecule is unique, with the two halves being related by a mirror plane which includes Sm(1), B(1), I(1) and pyrazolyl ring 2. The geometry around the metal centre may be described as distorted 'bicapped trigonal pyramidal' (Figure 4.5).

It is striking that the B(1)···Sm(1)–I(1) vector in this structure is virtually linear (at 177°) and hence, at first sight, coordination of the two THF molecules appears to result in only minimal disruption to the idealised trigonal pyramidal

† Hydrogen atoms omitted for clarity

Figure 4.5 The Inner Coordination Sphere of $[Tp^{3\text{-}t\text{-}Bu\text{-}5\text{-}Me}SmI(THF)_2].(Et_2O)_{0.5}$ (**4.1**)

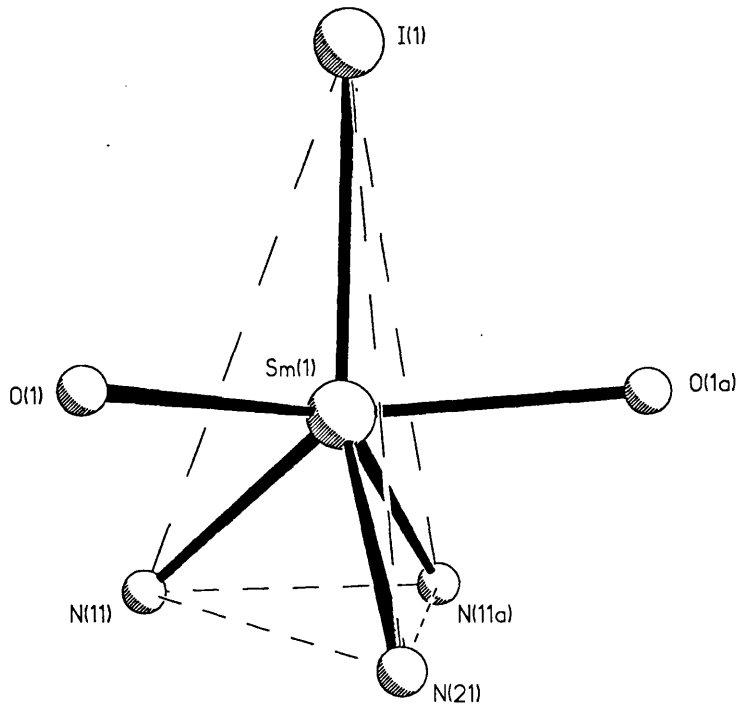

structure one might expect for the solvent free species. The THF groups lie within the cleft of the Bu^t substituents on the $Tp^{3\text{-}t\text{-}Bu\text{-}5\text{-}Me}$ ligand, the O(1)–Sm(1)···B(1) angle being 97° (*cf.* the cone angle in $Tp^{t\text{-}Bu}$ of 265°; see Chapter 1, p 39).[120] Whilst the range of N–B(1)–N angles (111.9(5) to 112.4(6)°) is small, and shows that coordination of the THF molecules causes little distortion to the structure of the ligand around the boron atom, the N–Sm(1)–N angles are affected significantly by the presence of THF. Thus, the N(21)–Sm(1)–N(11) and N(21)–Sm(1)–N(11a) angles (83.9(2)°) are much greater than the N(11)–Sm(1)–N(11a) angle (65.5(2)°). Since pyrazolyl ring 2 lies on the mirror plane in the structure of **4.1**, it is necessarily planar with B(1) and Sm(1). On the other hand, rings 1 and 1a are twisted such that the dihedral angle between B(1)–N(12)–N(11) and N(12)–N(11)–Sm(1) is *ca* 31°. This twisting results in a shortening of the B···Sm separation, which is only 3.52 Å - considerably shorter than the 3.63 Å observed in the six coordinate complex $[(Tp^{Me2})_2Sm]$ (**3.1**).[180] In contrast, the two independent Sm–N bond lengths in **4.1** (2.632(5) and 2.647(6) Å) are similar to those observed in **3.1** (2.617(4) Å). The Sm(1)–I(1) bond length in **4.1** is 3.191(1) Å and is comparable with the terminal Sm–I bonds in the six coordinate divalent complexes $[SmI_2(3,5\text{-dimethylpyridine})_4]$ (3.221(1) Å; see Appendix 3) and $[SmI(\mu\text{-}I)(N\text{-MeIm})_3]_2$ (3.237(1) Å; *N*-MeIm = *N*-methylimidazole),[237] but much shorter than that

observed in $[SmI_2(HMPA)_4]$ (3.390(2) Å; HMPA = hexamethylphosphoramide).[238] The Sm(1)–O(1) bond length in **4.1** (2.652(5) Å) is longer than might be anticipated for a six coordinate Sm^{2+} complex. Thus, it is similar to that found in the formally eight coordinate compound $[Cp^*_2Sm(THF)_2]$ (2.64(2) Å),[177] and somewhat larger than the O(THF)–Sm lengths in the seven coordinate complexes $SmI_2(THF)(DME)_2$ and $SmI_2(THF)_3(DME)$ (which are between 2.530(5) and 2.581(4) Å);[239] it is also longer than that observed in the six coordinate dimeric species $[Sm(N(SiMe_3)_2)(\mu\text{-}I)(\eta^2\text{-}DME)(THF)_2]_2$ (2.592(6) Å).[233] This probably reflects a considerable degree of steric congestion at the THF coordination sites, due to the bulky Bu^t substituents in $Tp^{3\text{-}t\text{-}Bu\text{-}5\text{-}Me}$. The wedge angle ($\omega$; see Chapter 1, p 40) of the related ligand $Tp^{t\text{-}Bu}$ is reported to be only 35°[120] and hence, the long Sm(1)–O(1) bond length is not surprising.

In contrast to the structure of **4.1**, **4.2** crystallised in the space group $P2_1/n$, with only one molecule of THF within the first coordination sphere of Yb^{2+}.[3] Hence, the metal centre is five coordinate, consistent with the small ionic radius of Yb^{2+} relative to Sm^{2+}. The coordination geometry around the metal centre is best described as distorted trigonal bipyramidal (TBP), the axial sites being occupied by O(1) and N(11) and the O(1)–Yb(1)–N(11) angle being 146.6(2)° (Figure 4.6). As in **4.1**, the B(1)···Yb(1)–I(1) vector is almost linear in **4.2** at 170°.

Figure 4.6 The Inner Coordination Sphere of $[Tp^{3\text{-}t\text{-}Bu\text{-}5\text{-}Me}YbI(THF)]$ (**4.2**)

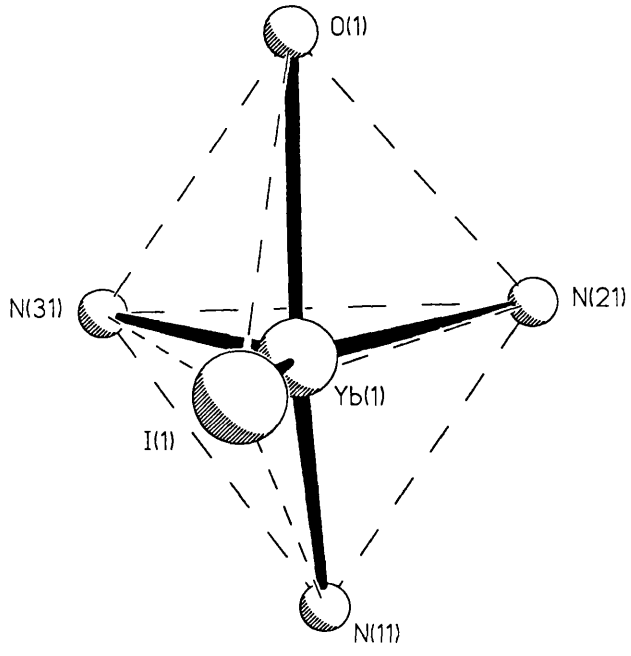

The Yb(1)–N(11) distance in **4.2** is 2.499(7) Å, compared with only 2.434(8) and 2.442(8) Å for Yb(1)–N(21) and Yb(1)–N(31), respectively. This may be related to the strong σ-donor properties of the THF molecule, which is coordinated opposite N(11). The average Yb(1)–N distance in **4.2** (2.458(8) Å) is similar to that observed in $[(Tp^{Me2})_2Yb]$ (**3.3**) (2.480(4) Å); hence, the lower coordination number in the former complex does not appear to be reflected in a significant overall shortening of the Yb–N bond lengths. The Yb(1)–O(1) distance (2.469(7) Å) is similar to the corresponding bond lengths found in $Cp^*_2Yb(NH_3)(THF)$ (2.46(3) Å)[176] and $Cp^*_2Yb(THF)$ (2.412(5) Å),[174] although these have higher formal Yb^{2+} coordination numbers than **4.2**.

The N–B(1)–N angles in **4.2** are tetrahedral (109.6(8) to 112.3(7)°), whereas the N–Yb(1)–N angles are affected significantly by the presence of the THF molecule at the inner coordination sphere, as is the case for **4.1**. Thus, the pair of pyrazolyl rings which flank the THF ligand are pushed outwards, the N(31)–Yb(1)–N(21) angle being 91.8(3)°, compared with *ca* 75° for N(11)–Yb(1)–N(21) and N(11)–Yb(1)–N(31). All of the pyrazolyl rings are significantly twisted, the dihedral angles between the B(1)–N–N and Sm(1)–N–N planes being *ca* 8, 34 and 14° for rings 1, 2 and 3, respectively. The B(1)···Yb(1) separation in **4.2** (3.40 Å) is somewhat shorter than that of 3.47 Å observed in $[(Tp^{Me2})_2Yb]$ (**3.3**); whether this is related to the twisting of the pyrazolyl rings or to the lower coordination number in **4.2** is not clear. The B···Yb–O angle of 98° is similar to that observed in **4.1** (97°); thus, the THF is coordinated within the 'cone' of the pyrazolylborate ligand. The Yb(1)–I(1) distance in **4.2** (3.065(1) Å) is similar to Yb–I bond lengths in other Yb^{2+} complexes containing terminally bonded iodide ligands, for example, five coordinate $[YbI(\mu\text{-}OCPh_3)(\eta^2\text{-}DME)]_2$ (3.090(2) Å)[234] and six coordinate $[YbI_2(THF)_4]$ (3.103(1) Å).[240]

It has already been noted that in the solution NMR spectra of complexes **4.1** and **4.2**, the pyrazolyl rings are equivalent. It is interesting to speculate as to the mechanism by which this equivalence is achieved. Since the THF molecule in **4.2** appears to be coordinated strongly to the Yb^{2+} ion (*vide infra*), a simple dissociative mechanism (by which the THF is lost and then recoordinates in between another pair of pyrazolyl rings) might not be feasible. The coordination geometry at the Yb centre in **4.2** was described above as being distorted TBP, and interchange of the axial and equatorial sites in such structures by Berry pseudorotation is well known.[241] As shown in Figure 4.7, this involves the formation of a square pyramidal (SP) intermediate

(**b**); whilst initially, N(11) is trans to O(1) (**a**), after two pseudorotations, the trans atom becomes N(21) (**d**).

Figure 4.7 The Interconversion of Trigonal Bipyramidal Structures of [$Tp^{3\text{-}t\text{-}Bu\text{-}5\text{-}Me}$YbI(THF)] (**4.2**) via a Square Pyramidal Intermediate (Berry Pseudorotation)[241]

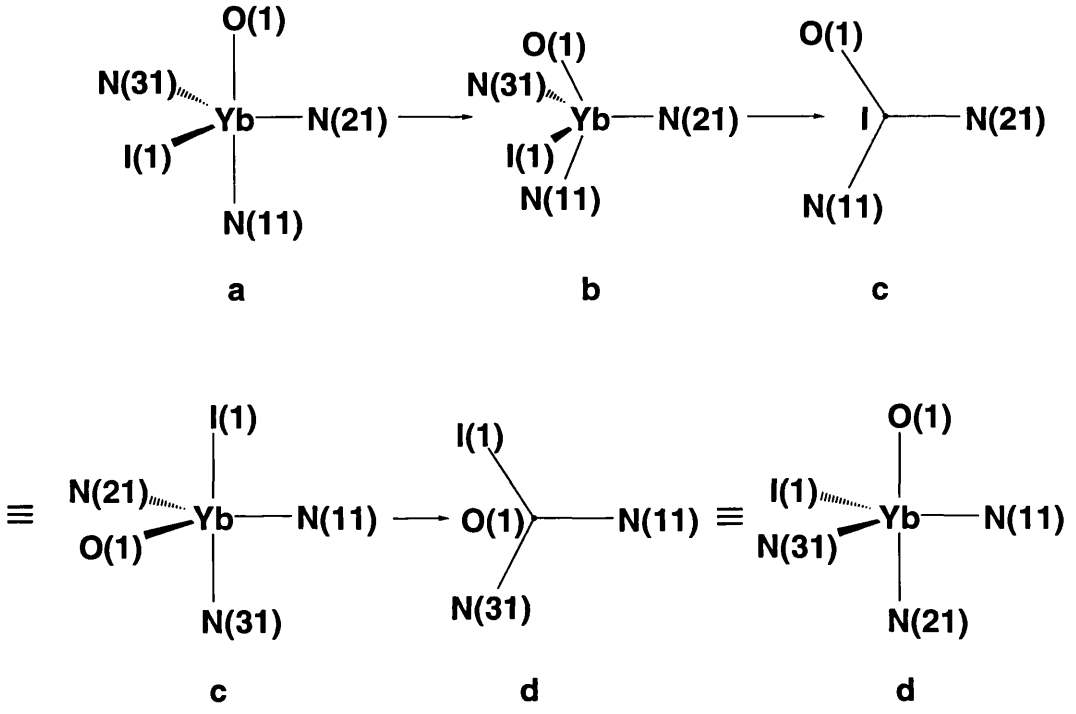

Whilst this is a possible mechanism, the constraints of the tripodal $Tp^{3\text{-}t\text{-}Bu\text{-}5\text{-}Me}$ ligand in **4.2** may make the Berry pseudorotation a very high energy process. In addition, it should be noted that in order to scramble the nitrogen atoms of the pyrazolylborate ligand, the iodide ion is required to occupy an axial (more sterically demanding) site in the intermediate TBP structure (**c**). In practice, this involves sliding the iodide ligand between the Bu^t substituents of two of the pyrazolyl rings. It is interesting that Carmona and coworkers have isolated and characterised crystallographically a half sandwich complex of Ba, [(Tp^{Me2})BaI(HMPA)$_2$], in which the iodide ligand is coordinated in such a manner (B···Ba–I angle = 89°).[183] However, the wedge angle in Tp^{Me2} (ω = 75°) is much larger than in a 3-Bu^t substituted ligand (*ca* 35°)[120] and hence, the intermediate TBP structure (**c**) is likely to be of very high energy.

Two other mechanisms are possible. The first is a simple 'trigonal twist' of the $Tp^{3\text{-}t\text{-}Bu\text{-}5\text{-}Me}$ ligand about the B···Yb vector. This mechanism was reported to be the most probable source of the fluxionality in the complexes $[(pzTp)ZrCl_2OBu^t]$ and $[(Bu^nTp)ZrCl_2OBu^t]$.[242] However, since the THF molecule in **4.2** is coordinated between the Bu^t substituents on the pyrazolylborate ligand, such a twist would fail to cause equivalence of the pyrazolyl rings without the THF first moving out of the 'cone' of the $Tp^{3\text{-}t\text{-}Bu\text{-}5\text{-}Me}$ ligand. The second mechanism involves the dissociation of one of the pyrazolyl rings of the $Tp^{3\text{-}t\text{-}Bu\text{-}5\text{-}Me}$ ligand from the lanthanide, to give a four coordinate intermediate. The necessary rearrangement of this structure prior to recoordination of the pendant ring is expected to be a fairly low energy process. Given the precedent for η^2-coordination of *tris*- and *tetrakis*-pyrazolylborate ligands to lanthanide ions,[72,131,132,243] such a mechanism appears to be the most likely of the four proposed.

For the six coordinate complex $[Tp^{3\text{-}t\text{-}Bu\text{-}5\text{-}Me}\ SmI(THF)_2]$ (**4.1**) there is good evidence (from the concentration dependence of the ^1H NMR spectrum) that the THF groups are labile in solution. However, whether such a dissociation is responsible for the exchange of the pyrazolyl rings in **4.1** is not known.

Complexes **4.1** and **4.2** are potential starting materials for a range of new species. We have investigated three areas of their reactivity: desolvation, reaction with Lewis bases, and reaction with anionic ligands.

Desolvation of Divalent Lanthanide Complexes of *Tris*-(3-*tert*-butyl-5-methylpyrazol-1-yl)borate

We found that $[Tp^{3\text{-}t\text{-}Bu\text{-}5\text{-}Me}SmI(THF)_2].(Et_2O)_{0.5}$ (**4.1**) could be readily desolvated, consistent with the observed lability of the THF groups in the solution NMR spectra of this compound (*vide supra*). Whilst this was not possible at room temperature, heating the finely ground solid under vacuum to *ca* 80° C led to the formation of $Tp^{3\text{-}t\text{-}Bu\text{-}5\text{-}Me}SmI$ (**4.3**). This was characterised by elemental analysis and IR and NMR spectroscopies. In common with that of **4.1**, two B–H bands were observed in the IR spectrum of **4.3** (at 2548 and 2523 cm^{-1}), possibly due to decomposition of the sample whilst acquiring the spectrum. The ^1H NMR spectrum of **4.3** was significantly different from that of **4.1**, with all of the pyrazolyl resonances shifting substantially upon loss of THF. Such a change is consistent with a rearrangement of the inner

coordination sphere of the Sm^{2+} ion.[69] In addition, a plot of reciprocal temperature against the ^1H chemical shifts of **4.3** was found to be linear (Figure 4.8); thus, the compound displays simple Curie-Weiss behaviour.[66,74] Finally, it was noted that the solution NMR spectra of **4.3** were not significantly concentration dependent. Unfortunately, it was not possible to grow crystals of sufficient quality to carry out an X-ray crystallographic determination of the structure of this complex; however, the NMR spectroscopic evidence outlined above is consistent with the monomeric compound [$Tp^{3\text{-}t\text{-}Bu\text{-}5\text{-}Me}$SmI].

Figure 4.8 A Plot of Reciprocal Temperature Against ^1H Chemical Shift for [$Tp^{3\text{-}t\text{-}Bu\text{-}5\text{-}Me}$SmI] (**4.3**)

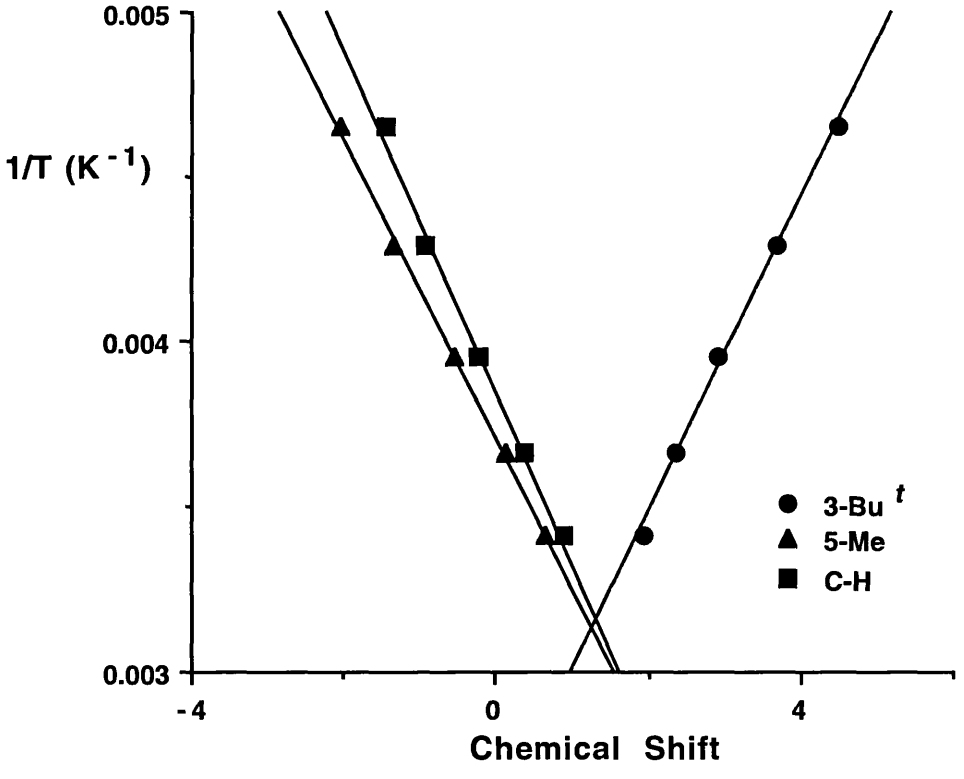

In comparison to **4.1**, [$Tp^{3\text{-}t\text{-}Bu\text{-}5\text{-}Me}$YbI(THF)] (**4.2**) was more resistant to desolvation. Only under quite extreme conditions was this achieved (180 °C, 10^{-2} torr) to give a pale yellow toluene soluble product (**4.4**). The ^1H NMR spectrum of this compound showed just three peaks (indicating that the THF had been lost), which integrated in the ratio 9:3:1. The chemical shifts of these resonances were consistent with this being a diamagnetic complex of $Tp^{3\text{-}t\text{-}Bu\text{-}5\text{-}Me}$. However, the peaks were somewhat broader ($w_{1/2}$ = 10 to 20

Hz) than is usually observed in such complexes, and may indicate partial decomposition of the sample to a paramagnetic Yb^{3+} species; elemental analysis of the crude product was also rather poor. Unfortunately, attempts to grow crystals of the complex or to purify it further were unsuccessful.

It is interesting to speculate as to why **4.2** is less prone to desolvation than **4.1**. Due to the larger size of Sm over Yb (when both are in the same oxidation state), steric saturation of the latter frequently requires a greater number of ligands at the inner coordination sphere.[236] Thus, it might be anticipated that desolvation of the Sm^{2+} complex (**4.1**) to give a four coordinate species would be more difficult. On the other hand, the higher charge/radius ratio of Yb^{2+} over Sm^{2+} will probably lead to the Ln–O(THF) bond being stronger in **4.2**. A similar effect has been observed in some cyclopentadienyl chemistry of these divalent ions. Thus, whilst $[Cp^*_2Sm(THF)_2]$ is readily converted to $[Cp^*_2Sm]$ upon gentle heating under vacuum,[48] $[Cp^*_2Yb(THF)_2]$ only loses one molecule of THF under similar conditions, and decomposes upon further heating.[174,244]

Reaction of Divalent Lanthanide Complexes of *Tris*-(3-*tert*-butyl-5-methylpyrazol-1-yl)borate with Lewis Bases

It was found that the coordinated THF in **4.1** was readily displaced by pyridines.[3] Thus, reaction of a solution of **4.1** in toluene with excess pyridine (py) or 3,5-dimethylpyridine (3,5-Me_2py), resulted in a colour change from dark green/red to dark green. The products could be crystallised by slow diffusion of 30/40 petrol into these solutions, to give the analytically pure complexes $[Tp^{3\text{-}t\text{-Bu-5-Me}}SmI(py)_2]$ (**4.5**) and $[Tp^{3\text{-}t\text{-Bu-5-Me}}SmI(3,5\text{-}Me_2py)_2]$ (**4.6**). The 4-*tert*-butylpyridine (4-Bu^{t}py) analogue was much more soluble than **4.5** and **4.6** and was prepared by the reaction of a suspension of **4.1** in 30/40 petrol with 4-Bu^{t}py, the dark green solution slowly depositing black crystals of $[Tp^{3\text{-}t\text{-Bu-5-Me}}SmI(4\text{-}Bu^tpy)_2]$ (**4.7**) on standing. The multinuclear (^1H, ^{13}C and ^{11}B) NMR spectra of these complexes were structurally informative. Compounds **4.5**, **4.6** and **4.7** all showed paramagnetically shifted and broadened pyrazolyl and pyridine resonances in the ^1H and ^{13}C spectra. In each of these complexes, the pyrazolyl rings were equivalent on the NMR time scale at room temperature, as in the case of **4.1**. Similarly, only a single set of peaks was observed for the pyridine ligands in each compound. It was also noted that the chemical shifts in the NMR spectra of

4.5, 4.6 and 4.7 were somewhat concentration dependent, consistent with their being partially dissociated in solution. However, this concentration dependence did not obscure the obvious similarities in the NMR spectra of these complexes, which also bore a striking resemblance to those of **4.1**. Table 4.1 shows the ^{1}H NMR shifts observed for [Tp$^{3\text{-}t\text{-Bu-5-Me}}$SmI(3,5-Me$_2$py)$_2$] (**4.6**) at two different concentrations, and compares them with those of **4.1**.

Table 4.1 The ^{1}H Chemical Shifts for [Tp$^{3\text{-}t\text{-Bu-5-Me}}$SmI(3,5-Me$_2$py)$_2$] (**4.6**; 2 mM and 20 mM) and [Tp$^{3\text{-}t\text{-Bu-5-Me}}$SmI(THF)$_2$].(Et$_2$O)$_{0.5}$ (**4.1**; 90 mM) in C_6D_6 at 20 °C

Assignment	4.6 (2 mM)	4.6 (20 mM)	4.1 (90 mM)
2-H py	-1.7	-3.4	-
THF	-	-	-0.74
THF	-	-	-0.64
Me py	-0.03	-0.38	-
Me pz	1.81	2.28	1.96
C–H pz	2.32	2.38	2.06
4-H py	4.33	3.77	-
Bu^t pz	5.37	5.23	4.74

The similarities in the ^{1}H and ^{13}C NMR spectra of this series of compounds enabled their complete assignment, and indicate that the complexes are probably isostructural.[69] In the light of the X-ray crystal structure of **4.1**, we therefore suggest that the pyridine molecules in **4.5**, **4.6** and **4.7** coordinate to the Sm^{2+} ion in the cleft between adjacent pairs of 3-Bu^t substituents on the Tp$^{3\text{-}t\text{-Bu-5-Me}}$ ligand (Equation 4.1).

Substitution of the single THF ligand in [Tp$^{3\text{-}t\text{-Bu-5-Me}}$YbI(THF)] (**4.2**) was also possible with pyridines, although in the case of this smaller metal, the stoichiometry of the product varied depending upon the size of the Lewis base. Thus, with an excess of py and 3,5-Me$_2$py, the products [Tp$^{3\text{-}t\text{-Bu-5-Me}}$YbI(py)$_2$] (**4.8**) and [Tp$^{3\text{-}t\text{-Bu-5-Me}}$YbI(3,5-Me$_2$py)$_2$] (**4.9a**) were obtained, whilst the corresponding reaction with 4-Bu^{t}py gave only a 1:1

Equation 4.1

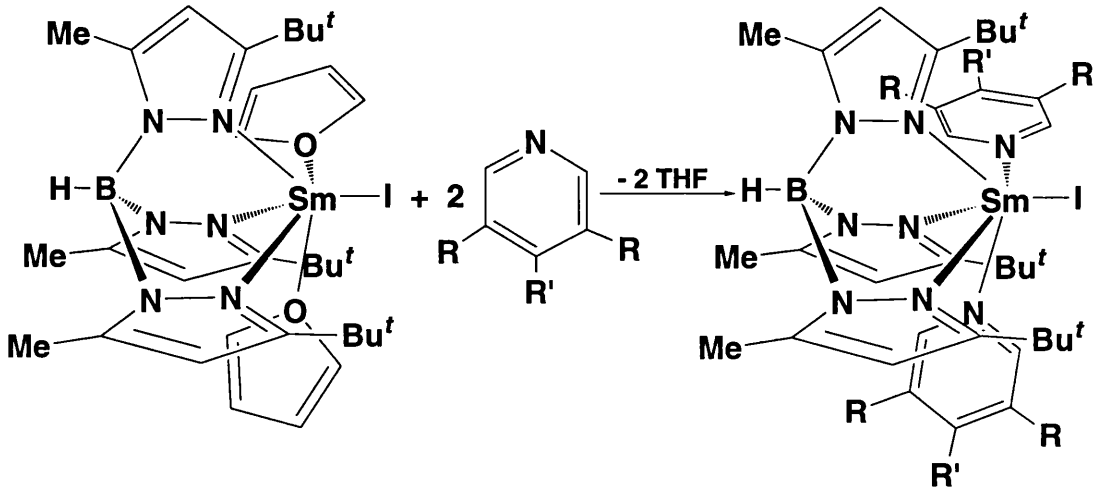

4.1

4.5 - R = H, R' = H
4.6 - R = Me, R' = H
4.7 - R = H, R' = Bu^t

complex, [Tp$^{3\text{-}t\text{-Bu-5-Me}}$YbI(4-Bu^{t}py)] (**4.10**). By the addition of a single equivalent of 3,5-Me$_2$py to **4.2** in diethyl ether, it was also possible to isolate a compound of stoichiometry [Tp$^{3\text{-}t\text{-Bu-5-Me}}$YbI(3,5-Me$_2$py)] (**4.9b**).

All of these complexes were fluxional at room temperature, exhibiting only single sets of pyrazolyl and pyridine resonances in the ^{1}H and ^{13}C spectra. In contrast to the situation for the Sm^{2+} complexes, the diamagnetism of Yb^{2+} meant that the chemical shifts of these compounds were structurally uninformative. Since the stoichiometry of **4.8** and **4.9a** suggested that the Yb^{2+} centre in these products might be six coordinate (compared with only five in **4.2**), it was of interest to investigate their structures further. Crystals of **4.9a** suitable for X-ray crystallography were grown from 30/40 petrol.[3] Details of the data collection and tables of fractional coordinates, bond lengths and bond angles are given in Appendix 1 (Tables A1.1 and A1.29 to A1.31). The molecular structure of **4.9a** is shown in Figure 4.9, and confirms that the Yb^{2+} ion is six coordinate.

The general structural features of **4.9a** are very much in line with those observed in **4.1** and **4.2**. Thus, the two pyridine molecules are coordinated in the clefts formed by adjacent pairs of Bu^t-pyrazolyl substituents, the geometry at the Yb^{2+} ion being best described as bicapped trigonal prismatic (Figure 4.10).

Figure 4.9 The Molecular Structure of [$Tp^{3\text{-}t\text{-}Bu\text{-}5\text{-}Me}YbI(Me_2py)_2$] (**4.9a**)[3†]

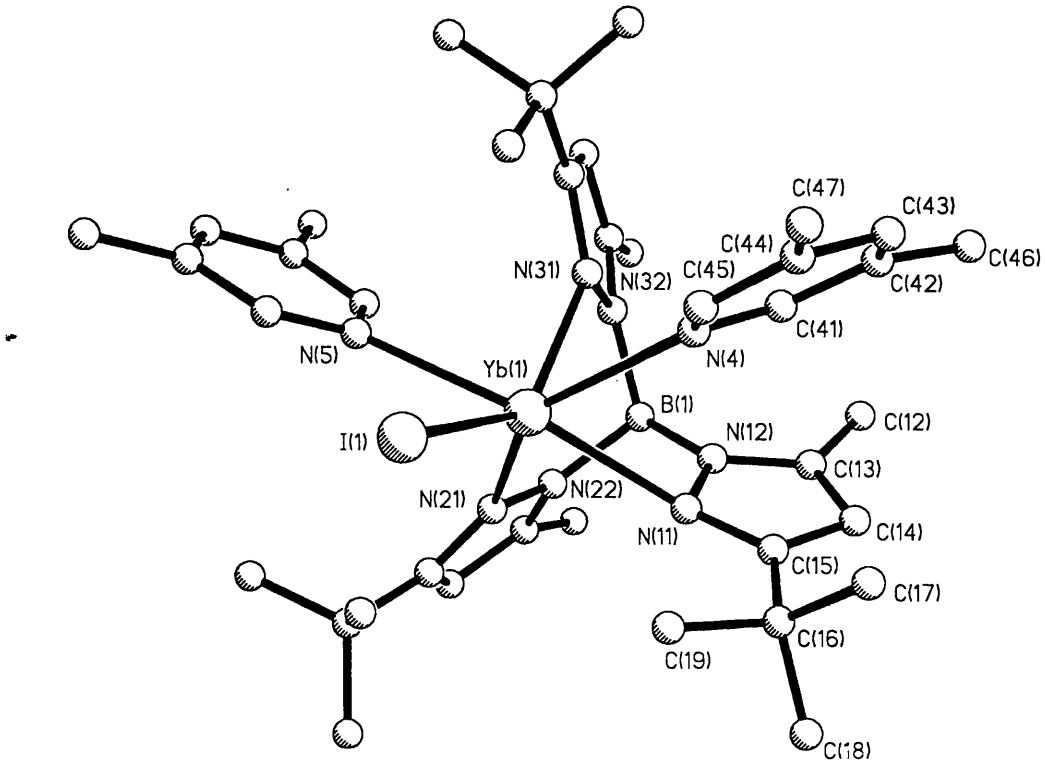

Figure 4.10 The Inner Coordination Sphere of [$Tp^{3\text{-}t\text{-}Bu\text{-}5\text{-}Me}YbI(Me_2py)_2$] (**4.9a**)

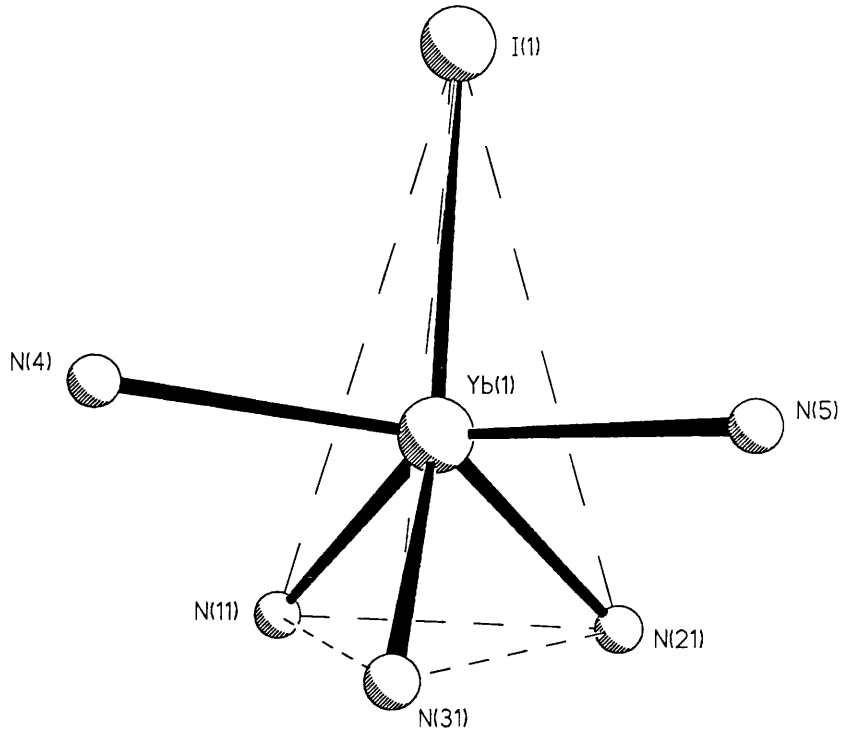

† Hydrogen atoms omitted for clarity

The Me_2py ligands in **4.9a** both lie within the cone angle of the pyrazolylborate ligand, with B(1)···Yb(1)–N(4) and B(1)···Yb(1)–N(5) angles of 98 and 95°, respectively. As was remarked upon in the case of **4.1** and **4.2**, such coordination seems, at first sight, to result in little disruption of the arrangement of the two anionic ligands in this structure, since the I–Yb···B vector is almost linear at 174°. However, on closer examination it is obvious that twisting of pyrazolyl rings about their B–N bonds is required in order to accommodate the two 3,5-Me_2py ligands at the Yb^{2+} centre. Thus, the average dihedral angles between the B(1)–N–N and N–N–Yb(1) planes are 7, 39 and 22 ° for rings 1,2 and 3, respectively, and lead to a short B···Yb separation of 3.39 Å (similar to that observed in the five coordinate structure of **4.2**). In contrast, the average Yb(1)–N bond length in **4.9a** is some 0.05 Å greater than in **4.2**, consistent with the increase in coordination number at the metal. A similar lengthening of the Yb(1)–I(1) bond is observed (from 3.065(1) Å in **4.2** to 3.123(1) Å in **4.9a**).

The Yb(1)–N(4) and Yb(1)–N(5) distances in **4.9b** are 2.727(7) and 2.684(5) Å, respectively. These are significantly longer than those observed in other six coordinate structures such as $[Yb(SPh)_2(py)_4]$ (2.529(7) and 2.565(7) Å),[245] $[Yb(SePh)_2(py)_4]$ (2.502(4) and 2.563(5) Å)[245] and $[YbI_2(Me_2py)_4]$ (2.583(4) Å; see Appendix 3). This effect is presumed to have its origins in the rather small wedge angle of the $Tp^{3\text{-}t\text{-}Bu\text{-}5\text{-}Me}$ ligand; similarly long Ln–O(THF) bond lengths were noted in **4.1** and **4.2** (*vide supra*).

The ability of 3,5-Me_2py (and presumably of py itself) to give complexes with coordination numbers of six, is in contrast to the five coordinate structure of **4.2**, and may be related to the greater Lewis basicity of the pyridines compared with THF. In addition, the planarity of the aromatic pyridine ring may also make these ligands less sterically demanding than the aliphatic (and hence more 3-dimensional) THF molecule.

Having failed to 'freeze' out the fluxionality in the ^1H NMR spectrum of **4.2** in solution, it was of interest to investigate the behaviour of $[Tp^{3\text{-}t\text{-}Bu\text{-}5\text{-}Me}YbI(3,5\text{-}Me_2py)]$ (**4.9b**) in this respect. Since the basicity of 3,5-Me_2py is greater than that of THF, it is expected to coordinate to the Yb^{2+} ion more strongly than the latter; therefore the rate of any dissociation dependent fluxionality should be slower in **4.9b** than in **4.2**. In addition, the presence of the 3,5-Me_2 substituents on the pyridine ring may also provide an additional steric barrier to an intramolecular rearrangement of the coordination sphere.

Upon cooling a sample of **4.9b** in d_8-toluene, the ^{1}H NMR resonances due to the 3-Bu^t, 5-Me and C–H substituents of the Tp$^{3\text{-}t\text{-Bu-5-Me}}$ ligand were seen to broaden and eventually give rise to three new pairs of resonances, each pair showing a 2:1 integration (coalescence temperatures, T_c, of *ca* 193, 193 and 188 K, respectively). Similarly, the 3,5-Me_2 and the 2,6-H_2 singlets of the pyridine ligand each gave rise to two new peaks at low temperature (T_c = *ca* 188 and 203 K, respectively).

It is possible that a single process causes the equivalence of the two sets of 3,5-Me_2py and pyrazolyl resonances at room temperature. As discussed earlier, this may involve dissociation of the Lewis base followed by its recoordination between a different pair of pyrazolyl rings. Alternatively, an intramolecular process (involving pseudorotation, a trigonal twist or the dissociation of one of the pyrazolyl groups from the metal) could account for both types of ligand being fluxional. However, the 3,5-Me_2py group may also be able to rotate independently within the cleft of the Tp$^{3\text{-}t\text{-Bu-5-Me}}$ ligand. It was hoped that activation parameters for the fluxional process(es) in **4.1b** could be obtained from the variable temperature NMR spectra of this compound, which would allow us to learn more about its underlying mechanism. Activation barriers were obtained from analysis of the exchange broadening of the peaks at temperatures higher than T_c, and from the values of T_c themselves.[246] The results and discussion of this analysis may be found in Appendix 4.

Unfortunately, it was not possible to determine whether the fluxionality of the pyrazolyl rings and pyridine substituents was due to a concerted process. However, we were able to obtain an estimate of the free energy of activation ($\Delta G^{\ddagger}$) for the rearrangement of the Yb^{2+} coordination sphere in **4.9b** of 40±1 kJ mol^{-1} at 293 K. This compares with a range of 40 to 54 kJ mol^{-1}† for actinide (An) complexes of the type Tp_2AnX_2 (X = a bulky aryloxide, alkoxide or alkyl sulphide) for which trigonal twist mechanisms have been proposed.[247-250]

It was also found that the THF molecule in [Tp$^{3\text{-}t\text{-Bu-5-Me}}$YbI(THF)] (**4.2**) could be displaced by *tert*-butylisonitrile (CNBu^t).[3] Thus, reaction of a solution/slurry of **4.2** in diethyl ether with CNBu^t gave an immediate colour change from yellow to orange. Slow diffusion of 30/40 petrol into this solution produced red/orange crystals of the new complex **4.11** in *ca* 55 % yield. The ^{1}H, ^{13}C

† Calculated from T_c measurements

and ^{11}B NMR spectra of **4.11** indicated that it was diamagnetic, and that the ratio of $Tp^{3\text{-}t\text{-}Bu\text{-}5\text{-}Me}$ to $CNBu^t$ ligands was 1:1. The IR spectrum of the compound showed bands which were characteristic of the $Tp^{3\text{-}t\text{-}Bu\text{-}5\text{-}Me}$ ligand, including the diagnostic B–H stretch which occurred at 2556 cm^{-1}. In addition, there were two bands in the $\nu_{C\equiv N}$ stretching region of the spectrum. The weaker of these, at 2133 cm^{-1}, corresponded to free $CNBu^t$[251] which was presumably produced as a result of partial decomposition of the sample. The second occurred at 2172 cm^{-1}, and was due to a coordinated $CNBu^t$ ligand. This binds to metal centres by donation from the C–N σ^*-orbital on carbon. This σ-donation is very strong, in contrast to that for carbon monoxide (with which isonitriles are isoelectronic), whilst the π-acceptor behaviour of isonitriles tends to be much weaker than that of CO. Hence, whilst coordination of CO to a d block element invariably results in a reduction in the C–O bond order, for isonitriles, the C–N stretching frequency can move either up or down upon complexation.[252] Since the 4f electrons in divalent lanthanide ions have a very small radial extension, the observed increase in C≡N stretching frequency of the $CNBu^t$ ligand upon coordination to Yb^{2+} is entirely expected. Similar absorption frequencies to that observed in **4.11** have been noted in the trivalent lanthanide complexes $[Cp^*_2Sm(CNC_6H_{11})(\mu\text{-}CN)]_3$ and $[Cp^*_2Sm(CNBu^t)(\mu\text{-}CN)]_3$ (2180 cm^{-1}),[253] and in $[\{Cp^*_2Sm(CNBu^t)\}_2(\mu\text{-}O)]$ (2170 cm^{-1}).[254] Somewhat larger increases in $\nu_{C\equiv N}$ (to *ca* 2205 cm^{-1}) have been reported in the compounds $[Cp_3Ln(CNC_6H_{11})]$ (Ln = Y, Pr, Nd, Tb, Ho and Yb).[255,256]

As far as we are aware, **4.11** is the first example of an isonitrile coordinated to a divalent lanthanide centre[3] - reaction of CNR (R = C_6H_{11} or Bu^t) with $[Cp^*_2Sm]$ having given the trivalent complexes $[Cp^*_2Sm(CNR)(\mu\text{-}CN)]_3$.[253] As such, it was of interest to determine the molecular geometry of the complex. Crystals grown as above were suitable for X-ray diffraction analysis, and the details of the data collection together with tables of fractional coordinates, bond lengths and bond angles are given in Appendix 1 (Tables A1.1 and A1.32 to A1.34). The complex crystallised in the space group $P2_1/n$; the molecular geometry is shown in Figure 4.11.

The general structural features of **4.11** are broadly similar to those described for the other half sandwich molecules **4.1**, **4.2** and **4.9a**. As for **4.2**, the coordination environment of the metal may be described as distorted TBP, with the axial sites being occupied by C(1) and N(21). The Yb(1)–I(1) and

Figure 4.11 The Molecular Structure of [$Tp^{3\text{-}t\text{-}Bu\text{-}5\text{-}Me}$YbI(CNBu^t)] (**4.11**)†

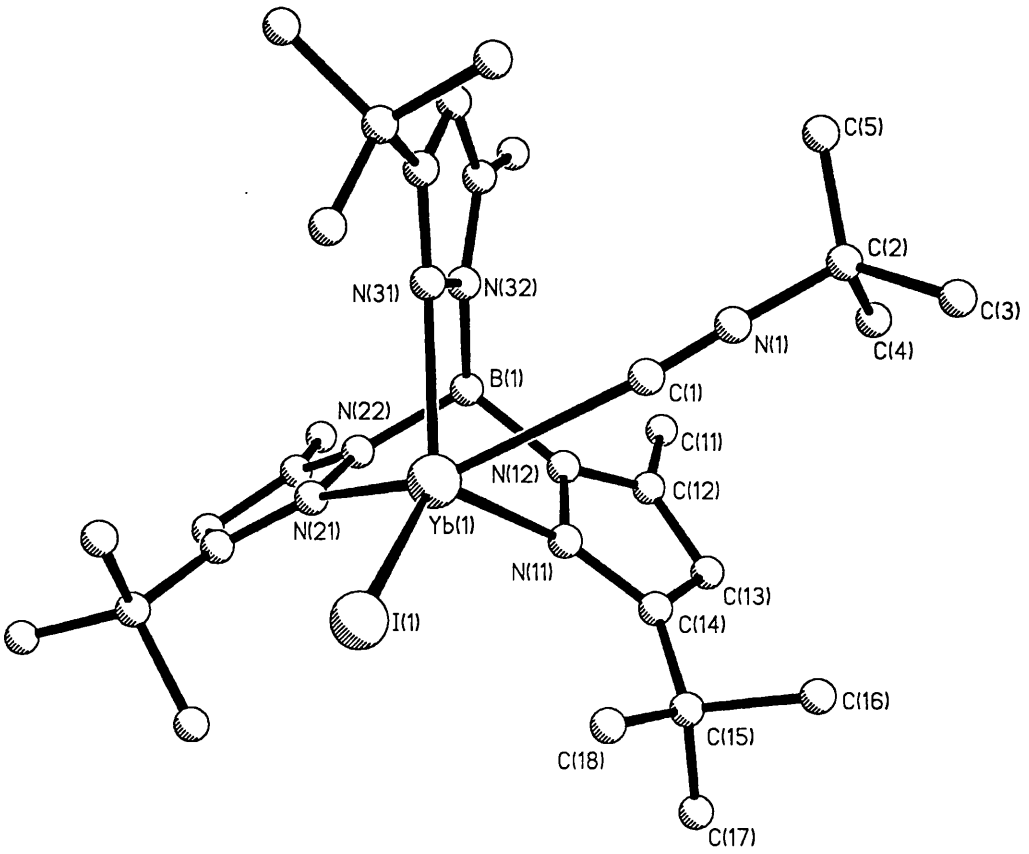

average Yb(1)–N distances in **4.11** (3.051(1) and 2.439(6) Å, respectively) are similar to those in **4.2** (3.065 and 2.458 Å) as is the (near linear) I–Yb···B angle of 168° (*cf.*170° in **4.2**). The pyrazolyl rings (1 and 3) which flank the coordinated CNBu^t ligand are forced apart, the N(11)–Yb(1)–N(31) angle being 91.7(2)° compared with N(11)–Yb(1)–N(21) and N(21)–Yb(1)–N(31) angles of 77.6(2)° and 76.4(2)°, respectively. This distortion leads to a considerable twisting of the pyrazolyl rings in **4.11**, with the average dihedral angle between B(1)–N–N and N–N–Yb(1) being 15°. The C(1)–Yb(1)···B(1) angle in **4.11** (90°) is somewhat smaller than the corresponding angles for the coordination of THF or 3,5-Me_2py in **4.1**, **4.2** and **4.9a** (in the range 95 to 98°). In addition, the isonitrile ligand is not coordinated in a linear fashion to the metal centre, the Yb(1)–C(1)–N(1) angle being 157.9(7)° (Figure 4.12).

This bent coordination geometry in **4.11** is in contrast to the near linear Ln–C–N angles in previously reported isonitrile complexes of the lanthanides:

† Hydrogen atoms omitted for clarity

Figure 4.12 The Molecular Structure of [$Tp^{3\text{-}t\text{-}Bu\text{-}5\text{-}Me}YbI(CNBu^t)$] (**4.11**) Showing the Bent Coordination Mode of the $CNBu^t$ Ligand†

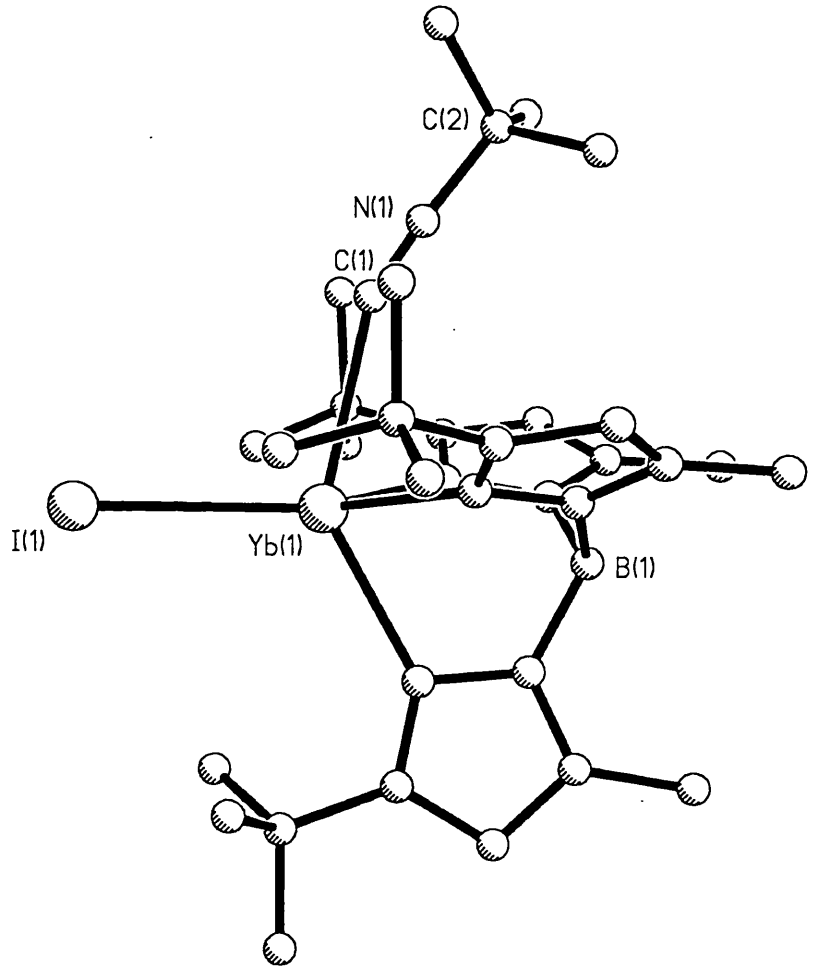

$[Cp^*_2Sm(CNC_6H_{11})(\mu\text{-}CN)]_3$ (172.3(16) to 173.7°)[253] and $[Cp_3Pr(CNC_6H_{11})]$ (174.1(11)°).[257] This bending may reflect some steric interaction of N(1) with the Bu^t substituents of the pyrazolyl ring. The Yb(1)–C(1) distance in **4.11** is 2.670(9) Å, similar to the distances observed in the Sm^{3+} complexes $[Cp^*_2Sm(CNC_6H_{11})(\mu\text{-}CN)]_3$ (2.58(2) Å)[253] and $[\{Cp^*_2Sm(CNBu^t)\}_2(\mu\text{-}O)]$ (2.62(1) and 2.66(1) Å).[254] This is somewhat surprising - Shannon predicts that five coordinate Yb^{2+} should be significantly smaller than eight or nine coordinate Sm^{3+}[15] - and may reflect reduced σ-donation from the $CNBu^t$ ligand due to its bent coordination mode in **4.11**. We would expect a reduction in σ-donation to be manifest in a relatively long C–N bond in the isonitrile ligand of **4.11**; however, no significant difference between the C–N bond length in this complex and those in $[Cp^*_2Sm(CNC_6H_{11})(\mu\text{-}CN)]_3$[253] and

† Hydrogen atoms omitted for clarity

$[\{Cp^*_2Sm(CNBu^t)\}_2(\mu\text{-}O)]$[254] was apparent, possibly due to the difficulty in accurately determining short C–N separations.[210,214] In addition, no pattern was evident in the IR stretching frequencies of the C≡N bonds in these isonitrile complexes.

The reaction of $[Tp^{3\text{-}t\text{-}Bu\text{-}5\text{-}Me}SmI(THF)_2].(Et_2O)_{0.5}$ (**4.1**) with $CNBu^t$ on a preparative scale did not give an isonitrile adduct: the THF free complex $[Tp^{3\text{-}t\text{-}Bu\text{-}5\text{-}Me}SmI]$ (**4.3**) being recovered instead. This was attributed to the facile loss of the isonitrile ligand from the adduct upon standing. However, the complex was prepared on an NMR scale by reaction of **4.3** with $CNBu^t$ - the formation of the adduct being recognised by the dramatic shift in the pyrazolyl peaks in the ^1H NMR spectrum to positions similar to those observed in **4.1**, **4.5**, **4.6** and **4.7**. The signal due to the Bu^t resonance of the isonitrile ligand in this complex appeared to overlap with that of free $CNBu^t$ and hence, the precise composition of the product, $[Tp^{3\text{-}t\text{-}Bu\text{-}5\text{-}Me}SmI(CNBu^t)_n]$ (**4.12**), is not known. Both **4.1** and **4.2** failed to react with xylylisonitrile (2,6-dimethylphenylisonitrile), possibly due to the steric effect of the 2,6-dimethyl substituents on this ligand.

Reactivity of Divalent Lanthanide Complexes of *Tris*-(3-*tert*-butyl-5-methylpyrazol-1-yl)borate with Anionic Reagents

The most commonly used reagents for metathesis reactions in organometallic chemistry are the readily prepared Grignard reagents or commercially available Li compounds. In view of the observed lability of the pyrazolylborate ligand in $[(Tp^{Me2})_2Y]^+[OTf]^-$ (**2.1**) and $[(Tp^{Me2})_2LaOTf]$ (**2.2**) in the presence of Mg^{2+} ions, and of the isolation by Parkin and coworkers of a large number of complexes of the type $Tp^{t\text{-}Bu}MgR$,[170,258] the reactivity of Grignard reagents was not investigated.† The reaction of LiPh, LiMe or $LiAlH_4$ with **4.1** and **4.2** gave mixtures of products from which no single tractable compound could be isolated. The corresponding reaction with $Li^+[CH(SiMe_3)_2]^-$ gave a product upon recrystallisation from 30/40 petrol which displayed a single set of diamagnetic $Tp^{3\text{-}t\text{-}Bu\text{-}5\text{-}Me}$ resonances in the ^1H NMR spectrum. However, no resonances due to a $CH(SiMe_3)$ group were observed, and no evidence of a hydride complex could be found; the identity of this product is unknown. In the hope that the metathesis of Yb–Cl bonds would be more successful, we

† The reaction of Grignard reagents with **4.1** and **4.2** was investigated by Takats & Zhang, who confirmed that the $Tp^{3\text{-}t\text{-}Bu\text{-}5\text{-}Me}$ ligand transferred to the Mg^{2+} ion

attempted to prepare [$Tp^{3\text{-}t\text{-}Bu\text{-}5\text{-}Me}$YbCl(THF)$_n$]. No reaction between $YbCl_2$ and $KTp^{3\text{-}t\text{-}Bu\text{-}5\text{-}Me}$ occurred in THF at room temperature; heating the mixture gave an orange solution from which a petrol soluble product was isolated. ^1H NMR of this material showed it to consist mainly of the complex [($Tp^{3\text{-}t\text{-}Bu\text{-}5\text{-}Me}$)$_2$Yb] which has been reported by Takats *et al* (Figure 4.13).[243] We also obtained this product (or its Sm analogue) upon reaction of **4.2** (or **4.1**) with KCH_2Ph.

Figure 4.13 The Structure of [($Tp^{3\text{-}t\text{-}Bu\text{-}5\text{-}Me}$)$_2$Ln][243]

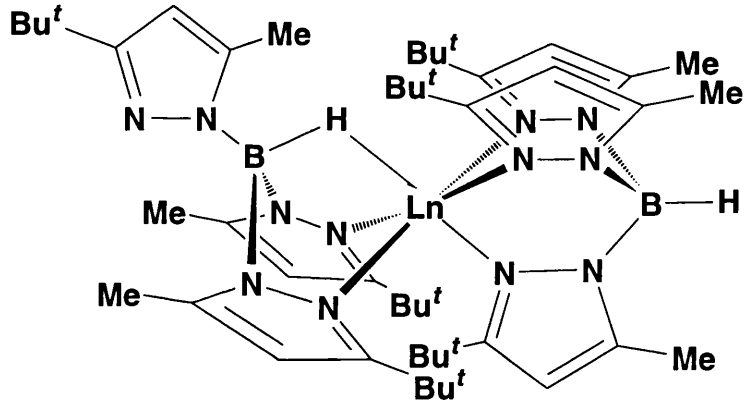

Ln = Sm and Yb

Metathesis reactions with KBH_4 appeared to fail due to the insolubility of this reagent in THF. However, the more soluble $NaBH_4$ did react with **4.2** to give a yellow product (**4.13**) which was freely soluble in 30/40 petrol. This gave rise to two distinct types of B–H stretch in the IR spectrum: one sharp band at 2557 cm^{-1} due to the $Tp^{3\text{-}t\text{-}Bu\text{-}5\text{-}Me}$ ligand, and a number of much broader bands between 2464 and 2170 cm^{-1} corresponding to a BH_4^- ion. The $^{11}B\{^1H\}$ NMR spectrum of **4.13** showed two resonances at δ -8.3 and -30.4, the latter being a quintet (coupling constant, J = 80 Hz) due to the BH_4 ligand; ^1H and ^{13}C NMR showed there to be one THF ligand for each $Tp^{3\text{-}t\text{-}Bu\text{-}5\text{-}Me}$ in **4.13**. Crystals of the complex were grown from 30/40 petrol, and an X-ray data set was collected. This confirmed that the molecular formula of **4.13** was [$Tp^{3\text{-}t\text{-}Bu\text{-}5\text{-}Me}$Yb($BH_4$)(THF)], and showed it to be structurally analogous to **4.2**; the reaction which had occurred is shown in Equation 4.2. Unfortunately, the data were of insufficient quality for any of the atoms in the structure to be refined anisotropically.

Equation 4.2

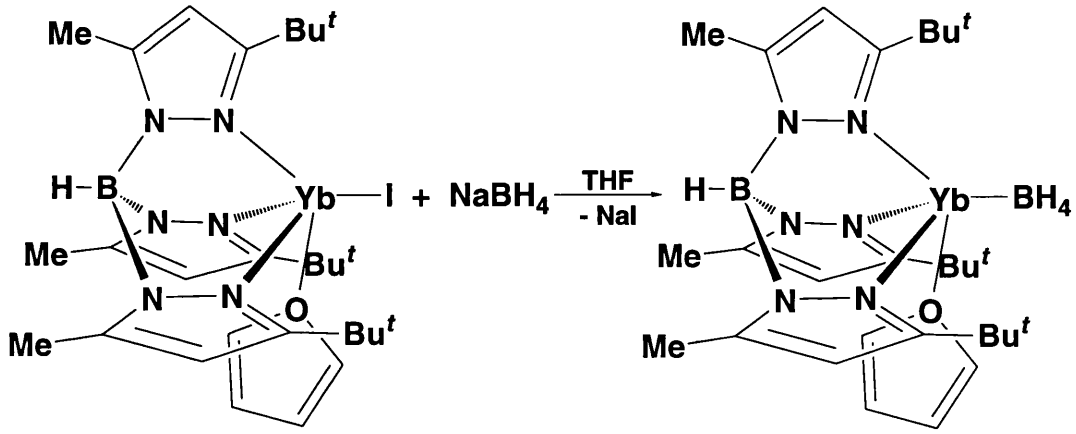

4.2 **4.13**

In collaboration with Professor Josef Takats and coworkers, we have studied the ^{171}Yb NMR spectroscopy of **4.13**. Intriguingly, whilst no resonance was observed at room temperature, two peaks were seen in the spectrum at -80 °C; the ^{11}B spectrum remained unchanged. At present, we have no explanation for this behaviour and we have not been able to determine the coordination mode of the BH_4 ligand in **4.13**.

Heating a sample of [Tp$^{3\text{-}t\text{-Bu-5-Me}}$Yb($BH_4$)(THF)] (**4.13**) in C_6D_6, and monitoring the reaction by ^{1}H NMR spectroscopy, revealed that two major new species were formed (Figure 4.14). However, it was not possible to identify a hydride resonance in this spectrum, and attempts to purify the reaction products on a preparative scale failed. The thermal decomposition of **4.13** was studied by Professor Josef Takats and colleagues whilst observing the ^{171}Yb NMR spectrum, and four new peaks were identified. Once again, no evidence for the formation of a hydride complex was obtained. Attempts to remove 'BH_3' from **4.13** by chemical means - with Lewis bases such as PMe_3 and 3,5-Me_2py - were unsuccessful. In the case of 3,5-Me_2py, a new compound, identified by NMR and IR spectroscopies as [Tp$^{3\text{-}t\text{-Bu-5-Me}}$Yb($BH_4$)(3,5$Me_2$py)$_n$] (**4.14**; n ≈ 1.5 by integration of the ^{1}H NMR spectrum), was isolated. However, attempts to determine the X-ray crystal structure of this complex at low temperature (in collaboration with Professor Josef Takats) were thwarted by poor crystal quality. In addition, it was suspected that the crystal contained a significant amount of the unreacted iodide compound **4.2**.

Figure 4.14 The ^{1}H NMR Spectra of [Tp$^{3\text{-}t\text{-Bu-5-Me}}$YbBH$_4$(THF)] (**4.13**) and the Product Mixture after Heating **4.13** at 110 °C for 2 hr in C_6D_6

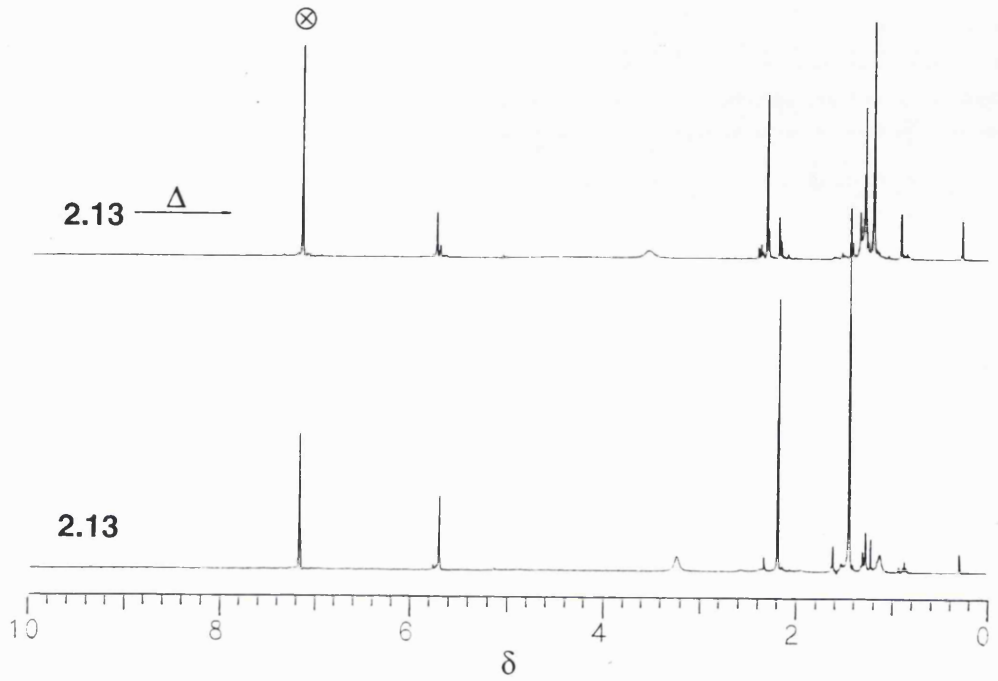

During our investigation of the chemistry of **4.1** and **4.2**, we became aware of the work of Takats and coworkers in this area.[167,168,235,243] They had independently synthesised **4.1** and **4.2** and found that reaction with Grignard and Li reagents did not give clean metathesis products. In contrast, they reported that reaction with K compounds allowed substitution of the iodide ligand in these complexes (Equations 4.3 to 4.5).†

These workers have determined a number of crystal structures, including those of [Tp$^{3\text{-}t\text{-Bu-5-Me}}$YbN(SiMe$_3$)$_2$] and [Tp$^{3\text{-}t\text{-Bu-5-Me}}$YbCH(SiMe$_3$)$_2$] in which significant agostic interactions were identified.[235] The amide and alkyl complexes were found to react with molecules containing acidic protons (*eg* with phenylacetylene, [Tp$^{3\text{-}t\text{-Bu-5-Me}}$YbN(SiMe$_3$)$_2$] gives [Tp$^{3\text{-}t\text{-Bu-5-Me}}$Yb(C≡CPh)]).[168,235] The alkyl complexes formed in Equation 4.4 also react with hydrogen, although the nature of the products formed is unknown and they do not appear to the same as those obtained upon heating [Tp$^{3\text{-}t\text{-Bu-5-Me}}$YbBH$_4$(THF)] (**4.13**). Neither of the alkyl complexes were found to polymerise alkenes.

⊗ = d_6-benzene resonance

† The sensitivity of syntheses of lanthanide complexes to the precise nature of the reagents and solvents is well documented[24,89,148]

Equation 4.3[235]

$$[Tp^{3\text{-}Bu^t\text{-}5\text{-}Me}YbI(THF)] + K^+[N(SiMe_3)_2]^- \xrightarrow[-50\ ^\circ C]{Toluene} [Tp^{3\text{-}Bu^t\text{-}5\text{-}Me}YbN(SiMe_3)_2]$$

Equation 4.4[235]

$$[Tp^{3\text{-}Bu^t\text{-}5\text{-}Me}YbI(THF)] + K^+R^- \xrightarrow[-50\ ^\circ C]{Et_2O} [Tp^{3\text{-}Bu^t\text{-}5\text{-}Me}YbR(Et_2O)_n]$$

$R = CH(SiMe_3)_2$, n = 1
$R = CH_2SiMe_3$, n = 0

Equation 4.5[235]

$$[Tp^{3\text{-}Bu^t\text{-}5\text{-}Me}YbI(THF)] + K^+[HBEt_3]^- \xrightarrow[-40\ ^\circ C]{Toluene} [Tp^{3\text{-}Bu^t\text{-}5\text{-}Me}Yb(\mu\text{-}H\text{-}BEt_3)(THF)]$$

Conclusion

In this chapter we have demonstrated that a considerable degree of steric control can be achieved at a divalent lanthanide centre by the use of a bulky pyrazolylborate ligand. The preparation and crystallographic characterisation of the first stable half sandwich derivatives of the lanthanide diiodides - the monomeric complexes $[Tp^{3\text{-}t\text{-}Bu\text{-}5\text{-}Me}SmI(THF)_2].(Et_2O)_{0.5}$ (**4.1**) and $[Tp^{3\text{-}t\text{-}Bu\text{-}5\text{-}Me}YbI(THF)]$ (**4.2**) - have been described and their reactivity investigated.[3]

Heating **4.1** under vacuum gave THF free $[Tp^{3\text{-}t\text{-}Bu\text{-}5\text{-}Me}SmI]$ (**4.3**); **4.2** was more resistant to desolvation, and the product formed by heating under vacuum (**4.4**) has not been unambiguously confirmed to be $[Tp^{3\text{-}t\text{-}Bu\text{-}5\text{-}Me}YbI]$. Reaction of **4.1** with pyridines gave complexes of composition $[Tp^{3\text{-}t\text{-}Bu\text{-}5\text{-}Me}SmIL_2]$ (L = py (**4.5**), 3,5-Me_2py (**4.6**) and 4-Bu^{t}py (**4.7**)); these compounds are believed to have structures analogous to that of **4.1** on the basis of their NMR spectra. The products obtained from the corresponding reactions of pyridines with **4.2** were found to be dependent on the stoichiometry of the reagents and the steric bulk of the pyridine used: $[Tp^{3\text{-}t\text{-}Bu\text{-}5\text{-}Me}YbIL_n]$ (L = py and n = 2 (**4.8**); L = 3,5-Me_2py and n = 2 (**4.9a**); L = 3,5-Me_2py and n = 1 (**4.9b**); L = 4-Bu^{t}py and n = 1 (**4.10**)); the structure of

4.9a was determined by X-ray crystallography.[3] The isonitrile complexes [$Tp^{3\text{-}t\text{-}Bu\text{-}5\text{-}Me}$LnI($CNBu^t$)$_n$] (Ln = Yb and n = 1 (**4.11**); Ln = Sm and n = undetermined (**4.12**)) were synthesised, and the X-ray crystal structure of **4.11** found to be isostructural with **4.2**; this is thought to be the first structurally characterised example of an isonitrile ligand coordinated to a divalent lanthanide ion.

The reaction of **4.1** and **4.2** with Li reagents did not lead to clean metathesis of the Yb–I bond. The borohydride complex [$Tp^{3\text{-}t\text{-}Bu\text{-}5\text{-}Me}$Yb($BH_4$)(THF)] (**4.13**) was synthesised by reaction of **4.2** with $NaBH_4$; a poor quality X-ray diffraction data set for this compound revealed that its molecular structure is analogous to that of **4.2**. Upon heating **4.13**, at least two new species were formed, as seen by ^{1}H NMR spectroscopy; however, the use of multinuclear (including ^{171}Yb) NMR studies failed to establish the nature of these products. No reaction was found to occur between the BH_4^- ligand in **4.13** and pyridines or PMe_3. In one reaction, the 3,5-Me_2py adduct [$Tp^{3\text{-}t\text{-}Bu\text{-}5\text{-}Me}$Yb($BH_4$)(3,5-$Me_2$py)] (**4.14**) was isolated. The successful substitution of the iodide ligand in **4.1** and **4.2** for a number of more reactive groups has been accomplished by Takats & Zhang using K reagents.[235]

In all of the crystallographically characterised complexes of the type [$Tp^{3\text{-}t\text{-}Bu\text{-}5\text{-}Me}LnXL_n$], the B···Yb–X arrangement is approximately linear, with L coordinating to the lanthanide in the cleft between the Bu^t substituents of the pyrazolyl ring such that the B···Yb–L angle is *ca* 90°. It is tempting to speculate that this highly controlled environment will result in novel and unique reactivity.

Chapter 5 - Experimental Details

General Procedures

Unless otherwise stated, all reactions and manipulations were carried out under an atmosphere of dry nitrogen using standard Schlenk line techniques or in a Braun Lab Star 50 or a Vacuum Atmospheres HE-493 glove box.[259] All air sensitive compounds and the reagents required for their synthesis were stored in a glove box. Sublimations were generally carried out in horizontal tubes of diameter *ca* 8 to 35 mm, with a tube furnace serving as the heat source. On account of their toxicity, all manipulations involving thallium compounds or hexamethylphosphoramide (HMPA) were carried out in a fume cupboard with secondary containment precautions. Molecular sieves were predried in an oven at 150 °C for several days, and activated prior to use by heating to *ca* 200 °C under vacuum.

Purification of Reagents

"Oxygen free nitrogen" (BOC, 99.998 %) was further dried and deoxygenated by passage through columns containing 5 Å molecular sieves and MnO prior to use on the Schlenk line.[260] Nitrogen used for the glove boxes was not prepurified, but an atmosphere thoroughly freed from oxygen and moisture was achieved by continuous circulation through R311 catalyst and 5 Å molecular sieves, and was regularly monitored by the use of a toluene solution of $(Cp_2TiCl_2)_2Zn$ (which remains green in the absence of these contaminants).

Reaction solvents were predried over Na wire (or 3 Å molecular sieves in the case of dichloromethane), prior to drying by refluxing over and distillation from the appropriate drying agent as follows: 1:3 alloy of Na and K (for diethyl ether and 30/40 petrol); K metal (for tetrahydrofuran (THF)), Na metal (for toluene) and CaH_2 (for dichloromethane). Solvents used for the preparation of pyrazoles and pyrazolylborate ligands were not dried or otherwise purified; HMPA, methanol and ethanol (95 %) were similarly used as received.

Sm and Yb metals were purchased from Aldrich as ingots (99.9 %), and the oxides of La, Nd, Sm, Dy, Yb and Y (99.9 %) were purchased from Berkshire Ores or Aldrich; all were used as received.

NH_4I was heated at 120 °C for *ca* 2 hr under vacuum, washed with 100 ml ether and dried under dynamic vacuum. NH_4Cl and BaI_2 were dried under vacuum (overnight at *ca* 150 °C) prior to use. Diiodoethane was freed from iodine by dissolving in diethyl ether, and washing with aqueous $Na_2S_2O_3$ and then with water. The solution was then dried over anhydrous $MgSO_4$ and the solvent removed on a rotavap, to give a white crystalline solid which was thoroughly dried overnight under dynamic vacuum. Pyridine (py), 3,5-dimethylpyridine (3,5-Me_2py), 4-*tert*-butylpyridine (4-Bu^tpy) and tetramethylethylenediamine (TMEDA) were dried by refluxing over CaH_2 for several days under vacuum, before being distilled under reduced pressure. NO was either used directly from a lecture bottle (BDH, 99.6 %) or synthesised by the reaction of nitric acid (*ca* 8 M) with Cu metal. NO prepared in this manner was freed from water and NO_2 by passage through a cold trap at -78 °C and the gas itself was condensed in a liquid nitrogen trap until it was required. NH_3 gas was not predried. Bu^nLi was purchased as a 2.5 M solution in hexanes from Aldrich, and used as received. KH (80 % suspension in mineral oil, Aldrich) was washed with several portions of 40/60 petrol, dried under vacuum and stored in a glove box. NaH (60 % suspension in mineral oil, Aldrich) was not washed prior to use. Na and K metals were usually cleaned by removing the oxidised surface with a knife in a glove box. Hg was not treated prior to use and Na amalgam was prepared, as required, in a glove box. Excess pyrazoles recovered from pyrazolylborate syntheses by sublimation were reused in subsequent preparations.

The following reagents were purchased from various suppliers and were used without further purification: acetylacetone (acacH), allyl chloride, azobenzene, bromoform, Bu^tBr, *tert*-butylisonitrile, 3,5-dimethylpyrazole (3,5-Me_2pz), ethyl acetate, ethyl iodide, hydrazine hydrate, hydrazinium sulphate, Mg metal, $MgSO_4$ (anhydrous), $Mo(CO)_6$, pinacolone, KBH_4, $NaBH_4$, tetracyanoethylene (TCNE), tetracyanoquinodimethane (TCNQ), Tl metal, trimethylchlorosilane, trichloromethylsilane, trifluoromethanesulphonic (triflic) acid (HOTf) and 2,6-dimethylphenylisonitrile.

All NMR solvents were purchased from Aldrich. d_6-Benzene and d_8-toluene were dried over a 1:3 alloy of Na and K and then either filtered through glass

wool or vacuum transferred to a clean, dry ampoule and stored in a glove box. d-Chloroform was dried and stored over activated 3 Å molecular sieves in a glove box. d_6-Acetone and D_2O were used as received.

Instrumentation

NMR spectra were run on Varian XL200 (^1H) and Varian VXR400 (^1H, ^{13}C and ^{11}B) spectrometers. Air sensitive samples were prepared in a glove box in tubes which were fitted with a Young's valve or which were subsequently sealed under vacuum with a glass blowing torch. Spectra were referenced to peaks produced by residual non-deuterated molecules present in the solvent, except for ^{11}B spectra which were referenced externally to $BF_3.OEt_2$. Solid state cross-polarised magic angle spinning (CP MAS) ^{13}C NMR spectra were run on a Bruker MSL 300 spectrometer by Dr Patrick Barrie and Mr David Butler. IR spectra were obtained by use of a Nicolet 205 FT IR spectrometer. UV/vis spectra were run on a Shimadzu UV-160A spectrometer. Mass spectra were run on a VG Analytical ZAB2F spectrometer by Ms Margaret Mruzek; the *m*-nitrobenzyl alcohol matrix was not purified before use.

All analyses were performed by Mr Alan Stones or Mrs Jill Maxwell of Christopher Ingold Laboratories Analytical Services. Moderately air sensitive samples were sealed in Pyrex tubes and then weighed rapidly in air or under an atmosphere of argon. The analysis of more reactive compounds was achieved by sealing the sample directly inside a preweighed aluminium analysis boat in a glove box, reweighing to determine the mass of the sample and analysing as normal.

X-ray crystallographic data were collected on a Nicolet R3mV four circle diffractometer using Mo-Kα radiation (λ = 0.71073 Å). Solution and refinement of the data were carried out using the SHELXTL PLUS suite of programs[261] on a MicroVAX II computer. The structures of compounds **3.15** and **3.18** were determined by Dr Mark Elsegood of the University of Newcastle X-ray crystallographic service using a Siemens SMART CCD diffractometer fitted with an area detector. More specific details of the X-ray crystallographic studies may be found in Appendix 1. Powder diffraction patterns were measured on a Siemens D5000 diffractometer.

Photoelectron (PE) spectra were recorded on a PES Laboratories 0078 spectrometer by Dr Jennifer Green, Ms Kathryn Longley and Mr Richard Parkin of the University of Oxford. Samples were transported in sealed Pyrex tubes under nitrogen. These were broken open and loaded into the machine in air, with exposure times of *ca* 20 to 30 s. Magnetic and luminescence measurements were carried out by the group of Professor Norman Edelstein.

Preparation of Lanthanide Trifluoromethanesulphonates ($Ln(OTf)_3$)[150]

Triflic acid (99 %) was carefully diluted with water to *ca* 30 %. The aqueous triflic acid (10 to 20 ml) was heated in a round bottomed flask and the lanthanide oxide added in small portions until no more would dissolve and the solution was neutral to pH paper. The solution was then filtered into a Schlenk tube and the water removed under reduced pressure. The solid obtained was dehydrated by heating under vacuum (200 °C, 10^{-2} torr) for 16 hr to give the anhydrous lanthanide trifluoromethanesulphonate (triflate), $Ln(OTf)_3$, in essentially quantitative yield.

Preparation of Samarium Dilodide[262]

In a typical preparation a piece of Sm metal (9.65 g, 0.0642 mol) and diiodoethane (11.50 g, 0.0408 mol) were placed in a Schlenk flask, THF (300 ml) added and the mixture stirred. The yellow solution which initially formed, slowly turned blue with a yellow precipitate of SmI_3. After several weeks the yellow precipitate had completely disappeared and the blue (red by transmitted light) solution was filtered, the THF removed under reduced pressure and the grey/black solid dried under dynamic vacuum to give 21.2 g of $SmI_2(THF)_{1.83}$ (0.0395 mol, 97 %).

UV/vis (THF): 424 nm (ε = 400); 559 nm (ε = 500); 618 nm (ε = 500). Analysis (%) calculated for $C_{7.32}H_{14.64}O_{1.83}I_2Sm$: C, 16.40; H, 2.75; N, 0.00. Found: C, 16.80; H, 2.68; N, 0.00.

Preparation of Ytterbium Diiodide[263]

A piece of Yb metal (5.55 g, 0.0321 mol) was placed in a three necked round bottomed flask containing a glass stir bar and fitted with a take-off adaptor and a cardice condenser. The flask was evacuated, cooled to -78 °C and liquid NH_3 (150 ml) condensed on to the metal. A blue solution was immediately formed and the contents of the flask were stirred for *ca* 30 min to allow the Yb metal to dissolve. NH_4I (8.85 g, 0.0611 mol) was then added in five portions under a counter flow of nitrogen, causing the formation of a yellow/orange precipitate of $YbI_2(NH_3)_n$. Following addition of the final portion, the contents of the flask (a blue solution with an orange/yellow precipitate) were stirred at -78 °C for 1 hr before the ammonia was allowed to warm to reflux and boil off. The solid obtained was freed from solvated NH_3 by heating under dynamic vacuum overnight (200 °C, 10^{-2} torr) to leave YbI_2 (containing *ca* 10 mol % of Yb metal) as a yellow, free flowing powder. Yield: 12.90 g (97 %).

UV/vis (THF): 408 nm (ε = 150). Analysis (%) calculated for $YbI_{1.8}$: C, 0.00; H, 0.00; N, 0.00; I, 56.90. Found: C, 0.00; H, 0.32; N, 0.15; I, 53.01.

Preparation of Ytterbium Dichloride

Yb metal (4.59 g, 0.0265 mol) was dissolved in liquid NH_3 (150 ml) in a procedure analogous to that in the preparation of YbI_2. NH_4Cl (2.69 g, 0.0503 mol) was added in several portions upon which an orange precipitate formed. The mixture was refluxed for 1 hr, after which the NH_3 was allowed to boil off. The residue was dried under dynamic vacuum overnight (200 °C, 10^{-2} torr) to give $YbCl_2$ as a grey powder.

Powder diffraction (film): 2θ = 22.75, 25.49, 26.44, 27.01, 32.59, 37.23, 37.52, 38.18, 39.89, 41.21, 43.39, 44.62, 45.38, 49.55°.

Preparation of Potassium Hydrido-*tris*-(3,5-dimethylpyrazol-1-yl)borate (KTp^{Me_2})[149]

A mixture of KBH_4 (6.0 g, 0.111 mol) and 3,5-dimethylpyrazole (64.0 g, 0.666 mol) was heated in a round bottomed flask fitted with an air condenser and a nitrogen bubbler. The temperature (measured by means of a thermometer

situated within the apparatus) was steadily increased to 230 °C until a clear melt was obtained and hydrogen evolution had ceased. Heating was stopped, and the melt allowed to cool to 200 °C before being poured carefully into 200 ml of stirred 40/60 petrol in air. Following removal of the solvent on a rotary evaporator, the excess pyrazole was separated from the product by vacuum sublimation (100 to 130 °C, 10^{-1} torr) to leave 31.0 g (0.092 mmol, 83 %) of potassium hydrido-*tris*-(3,5-dimethylpyrazol-1-yl)borate (KTp^{Me_2}) as a white powder.

IR (KBr): 2453 cm^{-1} (B–H). ^1H NMR (d_6-acetone): δ 5.52 (s, 3H, C–H); 2.16, 1.99 (s, 2 × 9H, 3- and 5-Me). Analysis (%) calculated for $C_{15}H_{22}N_6BK$: C, 53.57; H, 6.59; N, 24.99. Found: C, 53.39; H, 6.71; N, 24.93.

Preparation of Sodium Hydrido-*tris*-(3,5-dimethylpyrazol-1-yl)borate ($NaTp^{Me_2}$)[149]

A mixture of $NaBH_4$ (1.64 g, 0.043 mol) and 3,5-dimethylpyrazole (25.0 g, 0.260 mol) was heated in a three necked round bottomed flask in a procedure analogous to that for the K salt. After the reaction was complete, the contents of the flask were allowed to cool to 200 °C before being poured carefully into 100 ml of stirred 40/60 petrol in air. Following removal of the solvent under reduced pressure, the excess pyrazole was separated from the product by vacuum sublimation (100 to 130 °C, 10^{-1} torr) to leave 11 g (0.034 mmol, 80 %) of sodium hydrido-*tris*-(3,5-dimethylpyrazol-1-yl)borate as a white powder.

IR (KBr): 2453 cm^{-1} (B–H). ^1H NMR (d_6-acetone): δ 5.52 (s, 3H, C–H); 2.15, 2.01 (s, 2 × 9H, 3- and 5-Me). Analysis (%) calculated for $C_{15}H_{22}N_6BNa$: C, 56.26; H, 6.93; N, 26.25. Found: C, 54.77; H, 6.89; N, 25.82.

Preparation of Thallium Ethoxide[191]

Tl metal (25.0 g, 0.122 mol) was continuously extracted with refluxing ethanol (*ca* 100 ml) in the presence of oxygen. After *ca* 1.5 days the metal had dissolved to give a solution of thallium ethoxide in ethanol (which deposited an oil upon cooling). The volume of the mixture was reduced by *ca* 50 ml under reduced pressure and this was then used directly for the synthesis of thallium acetylacetonate.

Preparation of 3,5-Dimethyl-4-ethylpyrazole (Method A)[192]

Addition of acetylacetone (12.2g, 0.123 mol) to the solution of thallium ethoxide (0.122 mol) in ethanol (*vide supra*), followed by cooling to -10 °C, gave thallium acetylacetonate as a white crystalline powder. The solid was isolated, dried under dynamic vacuum, placed in an ampoule with ethyl iodide (74 g, 0.474 mol) and the mixture heated under partial vacuum for 12 hr at *ca* 40 °C until the white precipitate of thallium acetylacetonate had been replaced by yellow thallium iodide. The mixture was then filtered in air and the residue extracted with dichloromethane (2 × 50 ml). The solvent (and excess ethyl iodide) were removed from the combined extracts on a rotary evaporator and methanol (50 ml) was added to the residue. Hydrazine hydrate (6.1 g, 0.122 mol) was then added drop-wise to the stirred mixture resulting in an exothermic reaction. Once cool, dichloromethane (50 ml) and water (50 ml) were added and the organic layer separated. The aqueous layer was extracted with a further 25 ml of dichloromethane and the combined extracts washed with water (25 ml). After drying over $MgSO_4$, distillation (104 to 116 °C, 6 torr) in a short path distillation apparatus gave 3,5-dimethyl-4-ethylpyrazole (3,5-Me_2-4-EtpzH) as a yellow oil which slowly crystallised at room temperature. Yield: 6.4 g (0.052 mol, 42 %).

Preparation of 3,5-Dimethyl-4-ethylpyrazole (Method B)

Acetylacetone (110 g, 1.10 mol) was added drop-wise to a suspension of Na sand (23.0 g, 1.00 mol) in toluene (1000 ml) over a period of 30 min. Following addition, the mixture was refluxed for 30 min until all the Na had dissolved. After cooling, the white solid was filtered in air on a frit, washed with 40/60 petrol (2 × 100 ml) and dried under dynamic vacuum. The sodium acetylacetonate was then mixed with ethyl iodide (530 g, 3.40 mol) and HMPA (60 ml) in a pressure vessel and maintained at 90 °C for 3 days, after which time the solution had turned dark red/brown and a pale yellow precipitate had formed. Water (600 ml) and toluene (750 ml) were added to the mixture and the coloured toluene layer separated. This was washed with water (2 × 250 ml) to remove HMPA. The toluene was then removed on a rotary evaporator, the residue dissolved in methanol (500 ml) and hydrazine hydrate (50.1 g, 1.00 mol) added to the stirred solution. A mildly exothermic reaction occurred, after which the methanol was removed under reduced pressure, the resulting oil dissolved in toluene (250 ml) and the solution washed with water (2 × 100

ml). Removal of solvent and distillation as in Method A yielded 3,5-Me_2-4-EtpzH as a yellow crystalline solid. Yield: 66 g (0.53 mol, 53 %).

^{1}H NMR ($CDCl_3$): δ 2.22 (q, 2H, CH_2 4-Et); 2.04 (s, 6H, Me); 0.91 (t, 3H, Me 4-Et). Analysis (%) calculated for $C_7H_{12}N_2$: C, 67.70; H, 9.74; N, 22.56. Found: C, 67.05; H, 9.99; N, 21.89.

Preparation of Potassium Hydrido-*tris*-(3,5-dimethyl-4-ethylpyrazol-1-yl)borate ($KTp^{Me_2\text{-}4\text{-}Et}$)

3,5-Me_2-4-EtpzH (20.0 g, 0.161 mol) and KBH_4 (1.44 g, 0.0267 mol) were placed in a round bottomed flask fitted with an air condenser and a nitrogen bubbler. The temperature (monitored by means of a thermometer situated within the apparatus) was steadily increased to 175 °C and maintained at this temperature overnight, after which time hydrogen evolution had ceased. Most of the excess pyrazole was then distilled out of the mixture by attaching a distillation head directly to the round bottomed flask. Final traces of pyrazole were removed by sublimation onto a nitrogen cooled probe under vacuum, to leave 9.0 g of $KTp^{Me_2\text{-}4\text{-}Et}$ (0.021 mol, 79 %).

IR (KBr): 2440 cm^{-1} (B–H). ^{1}H NMR (d_6-acetone): δ 2.25 (q, 6H, CH_2 4-Et); 2.13, 1.97 (s, 2 × 9H, 3- and 5-Me); 0.94 (t, 9H, Me 4-Et). Analysis (%) calculated for $C_{21}H_{34}N_6BK$: C, 60.00; H, 8.15; N, 19.99. Found: C, 58.20; H, 8.04; N, 19.30.

Preparation of 3-*tert*-Butyl-5-methylpyrazole[104,264]

A three necked round bottomed flask (5000 ml) fitted with an overhead stirrer, an efficient condenser and a nitrogen bubbler, was charged with ethyl acetate (176 g, 2.0 mol), NaH (80 g of 60 % NaH in mineral oil, 2.0 mol) and 2500 ml of diethyl ether. A solution of pinacolone (100 g, 1.0 mol) in diethyl ether (500 ml) was then added drop-wise to the stirred mixture. Slight warming was necessary to initiate the reaction (as seen by the evolution of hydrogen) after which the heat generated kept the mixture at reflux. Stirring was continued for 12 hr (with additional ether being added when necessary to keep the mixture fluid) until hydrogen evolution had almost ceased and the colour of the contents of the flask had become off-white. The mixture was then refluxed

gently for 2 hr, allowed to cool, and water (1000 ml) carefully added in air. The aqueous layer was separated and the ether extracted with a further 500 ml of water. The combined aqueous extracts were then added to a stirred solution of hydrazinium sulphate ($H_2NNH_2.H_2SO_4$; 130 g, 1.0 mol) in water (2500 ml) and stirring was continued for 30 min. The pyrazole, which had separated out as a brown oil was extracted into dichloromethane (3 × 250 ml), this solvent removed from the combined extracts on a rotary evaporator, and the crude product purified by sublimation (150 to 160 °C, 5×10^{-2} torr) to give pale yellow crystalline 3-*tert*-butyl-5-methylpyrazole (3-Bu^t-5-MepzH). Yield: 78 g (0.56 mol, 56 %).

^{1}H NMR ($CDCl_3$): δ 5.86 (s, 3H, C–H); 2.25 (s, 9H, Me); 1.29 (s, 27H, CMe_3). Analysis (%) calculated for $C_8H_{14}N_2$: C, 69.52; H, 10.21; N, 20.27. Found: C, 69.60; H, 10.38; N, 20.35.

Preparation of Potassium Hydrido-*tris*-(3-*tert*-butyl-5-methylpyrazol-1-yl)borate (KTp$^{3\text{-}t\text{-Bu-5-Me}}$)[104]

A mixture of KBH_4 (2.03 g, 0.0377 mol) and 3-Bu^t-5-MepzH (31.25 g, 0.226 mol) was heated in a round bottomed flask fitted with an air condenser and a nitrogen bubbler. The temperature (monitored by means of a thermometer situated inside the apparatus) was steadily increased to 210 °C until a clear melt was obtained and hydrogen evolution had ceased. Heating was stopped, and the melt allowed to cool to 180 °C before being poured carefully into 200 ml of stirred 40/60 petrol in air. Following removal of the solvent on a rotary evaporator, excess pyrazole was removed from the product by vacuum sublimation (150 to 180 °C, 5×10^{-2} torr). The product could be sublimed at higher temperatures, although this crude material was found to be adequate for all the reactions carried out. Yield: 14.0 g (0.0302 mol, 80 %) of potassium hydrido-*tris*-(3-*tert*-butyl-5-methylpyrazol-1-yl)borate (KTp$^{3\text{-}t\text{-Bu-5-Me}}$) as a white solid.

IR (KBr): 2500 cm^{-1} (B–H). ^{1}H NMR (d_6-acetone): δ 5.68 (s, 3H, C–H); 2.08 (s, 9H, Me); 1.16 (s, 27H, CMe_3). Analysis (%) calculated for $C_{24}H_{40}N_6BK$: C, 62.32; H, 8.72; N, 18.17. Found: C, 60.84; H, 8.56; N, 17.37 (crude material) and C, 62.23; H, 8.76; N, 18.20 (sublimed material).

Preparation of Grignard Reagents

The Grignard reagents EtMgBr, Bu^{t}MgBr and (allyl)MgCl were all prepared from Mg metal and the corresponding alkyl halide. In a typical reaction, Mg turnings (1.0 g, 0.041 mol) were stirred for 2 hr under nitrogen to activate the metal. THF (50 ml) was added to the Mg and the mixture stirred as a solution of *tert*-butyl bromide (2.82 g, 2.4 ml, 0.021 mol) in THF (50 ml) was added drop-wise. It was necessary to reflux the mixture momentarily to initiate the reaction (the ethyl bromide and allyl chloride began to react immediately and needed slight cooling) which then proceeded smoothly over *ca* 30 min as the rest of the *tert*-butyl bromide was added. The mixture was allowed to cool and settle somewhat before being filtered to give a clear, pale yellow solution of Bu^{t}MgBr. The concentration of the Grignard reagent was determined by titration with a solution of methanol in toluene (0.025 M) using phenanthroline as an indicator, and found to be 0.14 M.

Preparation of Potassium Benzyl

KOBu^t (1.89 g, 0.0168 mol) was stirred in toluene (*ca* 40 ml) and a 2.5 M solution of Bu^{n}Li in hexanes (6.5 ml, 0.0163 mol) added drop-wise by syringe. A red/orange precipitate was immediately formed and the mixture was stirred for a further hour. Following filtration, the precipitate was washed with toluene (2 × 40 ml) and 30/40 petrol (1 × 20 ml) and dried under dynamic vacuum to give 1.8 g (0.0138 mol, 85 %) of KCH_2Ph as a red/orange powder.

Preparation of *Bis*-(trimethylsilyl)methylbromide[265]

$CHBr_3$ (40 ml, 116 g, 0.46 mol) and chlorotrimethylsilane (145 ml, 124 g, 1.14 mol) were dissolved in THF (800 ml). The solution was degassed, cooled to -78 °C and a 2.5 M solution of Bu^{n}Li in hexanes (384 ml, 0.96 mol) added drop-wise over a period of 6 hr. After the mixture had been allowed to warm slowly to room temperature, it was filtered through a frit (in air) and the solvent removed on a rotary evaporator. The yellow oil obtained was then distilled under reduced pressure (67 to 74 °C, 10 torr) to obtain pure $(SiMe_3)_2CHBr$ (32.3 g, 0.135 mol, 29 %).

^{1}H NMR ($CDCl_3$): δ 2.30 (s, 1H, CH); 0.17 (s, 18H, Me).

Preparation of *Bis*-(trimethylsilyl)methyl Lithium[265]

A solution of $(SiMe_3)_2CHBr$ (10.4 g, 0.0435 mol) in diethyl ether (150 ml) was cooled to -78 °C and a 2.5 M solution of Bu^nLi in hexanes (17.5 ml, 0.0438 mol) added drop-wise over a period of *ca* 20 min. The mixture was stirred at -78 °C for 1.5 hr before the solvent was removed under reduced pressure, the temperature of the mixture being maintained between -25 and -20 °C during this process to avoid the formation of LiBr. The crude product was then purified by sublimation (140 °C, 10^{-2} torr) to give pure $(SiMe_3)_2CHLi$ (4.9 g, 0.0295 mol, 68 %) as a pyrophoric white crystalline solid.

^1H NMR (C_6D_6): δ 0.16 (s, 18H, Me); -2.57 (s, 1H, CH).

Preparation of *Bis*-(trimethylsilyl)methyl Potassium[266,267]

A suspension of $(SiMe_3)_2CHLi$ (1.25 g, 7.51 mmol) was stirred in 30/40 petrol and $KOBu^t$ (0.77 g, 6.86 mmol) added in several portions over a period of *ca* 30 min. After the addition was complete, the mixture was allowed to stir for 4.5 days at room temperature during which time a fine white precipitate formed. The precipitate was then allowed to settle and the colourless 30/40 petrol solution was decanted. The residue was dried under dynamic vacuum and then extracted into diethyl ether (50 ml). Following filtration, the ether was removed under reduced pressure and the resultant white solid washed with 30/40 petrol (2 × 15 ml) and dried under dynamic vacuum at *ca* 50 °C for 2 hr to give $(SiMe_3)_2CHK$ as a white powder (0.5 g, 2.52 mmol, 37 %).

Preparation of $[(Tp^{Me2})_2LnOTf]$ (Ln = La (2.2), Nd (2.3) and Sm (2.4))

In a typical preparation, KTp^{Me2} (3.90 g, 11.6 mmol) and $La(OTf)_3$ (3.40 g, 5.80 mmol) were stirred in THF (100 ml) at room temperature for 12 hr. The solvent was removed under reduced pressure and the resultant solid extracted into toluene (2 × 100 ml) leaving a residue which was shown by IR spectroscopy to consist mainly of KOTf. The combined toluene extracts were concentrated under reduced pressure to *ca* 30 ml. Cooling the toluene solution overnight to -25 °C gave 3.58 g (4.06 mmol, 70 %) of $[(Tp^{Me2})_2LaOTf]$ as analytically pure colourless crystals.

$[(Tp^{Me2})_2LaOTf]$ (**2.2**)
White; yield: 70 %.
IR (KBr): 2558 cm^{-1} (B–H); 1203 cm^{-1} (S–O). IR ($CDCl_3$): 1203 cm^{-1} (S–O). ^1H NMR ($CDCl_3$): δ 5.73 (s, 6H, C–H pz); 2.41, 1.85 (s, 2 × 18H, 3- and 5-Me). ^{13}C NMR ($CDCl_3$): δ 150.2, 145.7 (s, 3- and 5-C pz); 106.3 (d, C–H pz); 13.5, 12.9 (q, 3- and 5-Me). Analysis (%) calculated for $LaC_{31}H_{44}N_{12}B_2F_3O_3S$: C, 42.20; H, 5.03; N, 19.05; S, 3.63. Found: C, 42.22; H, 4.99; N, 18.91; S, 3.68.

$[(Tp^{Me2})_2NdOTf]$ (**2.3**)
Pale Blue; yield: 56 %.
IR (KBr): 2565 cm^{-1} (B–H); 1204 cm^{-1} (S–O). IR ($CDCl_3$): 1206 cm^{-1} (S–O). ^1H NMR ($CDCl_3$): δ 8.02 (s, $w_{1/2}$ = 9.7, 6H, C–H pz); 5.16 (s, $w_{1/2}$ = 8.6 Hz, 18H, 5-Me); -9.73 (s, 27.2 Hz, 18H, 3-Me). ^{13}C NMR ($CDCl_3$): δ 169.1, 159.7 (s, 3- and 5-C pz); 133.3 (d, C–H pz); 18.8, -1.3 (q, 3- and 5-Me). Analysis (%) calculated for $NdC_{31}H_{44}N_{12}B_2F_3O_3S$: C, 41.94; H, 5.00; N, 18.93. Found: C, 42.04; H, 4.95; N, 18.94.

$[(Tp^{Me2})_2SmOTf]$ (**2.4**)
White; yield: 55 %.
IR (KBr): 2560 cm^{-1} (B–H); 1273 cm^{-1} (S–O). IR ($CDCl_3$): 1208, 1263, 1277 cm^{-1} (S–O). ^1H NMR ($CDCl_3$): δ 5.4 (s, 6H, C–H pz); 3.3 (s, 18H, 5-Me); -1.4 (s, 18H, 3-Me). ^{13}C NMR ($CDCl_3$): δ 147.4, 146.7 (s, 3- and 5-C pz); 104.4 (d, C–H pz); 14.5, 9.8 (q, 3- and 5-Me). Analysis (%) calculated for $SmC_{31}H_{44}N_{12}B_2F_3O_3S$: C, 41.66; H, 4.96; N, 18.80. Found: C, 41.19; H, 4.76; N, 18.62.

Preparation of $[(Tp^{Me2})_2Ln]^+[OTf]^-$ (Ln = Y (2.1), Dy (2.5) and Yb (2.6))

In a typical preparation, a mixture of $Y(OTf)_3$ (3.00 g, 5.60 mmol) and KTp^{Me2} (3.75 g, 11.2 mmol) was stirred in THF (100 ml) for 12 hr during which time a heavy white precipitate formed. The solvent was removed under reduced pressure and the solid residue washed with toluene (2 x 20 ml). Extraction with dichloromethane (2 x 50 ml) followed by removal of this solvent under reduced pressure from the filtered extracts yielded 3.60 g (4.33 mmol, 77 %) of $[(Tp^{Me2})_2Y]^+[OTf]^-$ as a white solid.

$[(Tp^{Me2})_2Y]^+[OTf]^-$ (**2.1**)
White; yield: 77 %.
IR (KBr): 2566 cm^{-1} (B–H); 1276 cm^{-1} (S–O). IR ($CDCl_3$): 1264 cm^{-1} (S–O). ^1H NMR ($CDCl_3$): δ 5.87 (s, 6H, C–H pz); 2.47, 1.81 (s, 2 × 18H, 3- and 5-Me). ^{13}C NMR ($CDCl_3$): δ 150.4, 148.4 (s, 3- and 5-C pz); 106.7 (d, C–H pz); 13.3, 12.6 (q, 3- and 5-Me). Analysis (%) calculated for $YC_{31}H_{44}N_{12}B_2F_3O_3S$: C, 44.73; H, 5.33; N, 20.19. Found: C, 44.63; H, 5.17; N, 19.93.

$[(Tp^{Me2})_2Dy]^+[OTf]^-$ (**2.5**)
White; yield: 65 %.
IR (KBr): 2566 cm^{-1} (B–H); 1276 cm^{-1} (S–O). IR ($CDCl_3$): 1264 cm^{-1} (S–O). Analysis (%) calculated for $DyC_{31}H_{44}N_{12}B_2F_3O_3S$: C, 41.10; H, 4.90; N, 18.55. Found: C, 40.44; H, 4.77; N, 17.89.

$[(Tp^{Me2})_2Yb]^+[OTf]^-$ (**2.6**)
White; yield: 82 %.
IR (KBr): 2567 cm^{-1} (B–H); 1276 cm^{-1} (S–O). IR ($CDCl_3$): 1263 cm^{-1} (S–O). ^1H NMR ($CDCl_3$): δ 6.19 (s, 6H, C–H pz); 5.19 (s, $w_{1/2}$ = 27 Hz, 18H, 3-Me), 3.30 (s, 18H, 5-Me). ^{13}C NMR ($CDCl_3$): δ 167.2, 158.8 (s, 3- and 5-C pz); 111.3 (d, C–H pz); 17.9, 11.9 (q, 3- and 5-Me). Analysis (%) calculated for $YbC_{31}H_{44}N_{12}B_2F_3O_3S$: C, 40.63; H, 4.84; N, 18.34. Found: C, 40.76; H, 4.78; N, 18.28.

Preparation of $[(Tp^{Me2})_2Sm]$ (3.1)

$SmI_2(THF)_{1.65}$ (2.00 g, 3.82 mmol) and $NaTp^{Me2}$ (2.69 g, 8.40 mmol) were placed in a Schlenk flask. THF (100 ml) was added with stirring and the mixture immediately turned from blue to purple. Stirring was continued for 1 hr before the mixture was allowed to settle overnight. The purple supernatant was decanted and the solid residue washed with further THF (2 × 50 ml). The solid was dried under dynamic vacuum at 80 °C to give $[(Tp^{Me2})_2Sm]$ as a purple powder (2.27 g, 3.05 mmol, 80 %). The product was shown to be free of iodide by dissolving a small portion in concentrated HNO_3, diluting with water and testing with $AgNO_3$ solution; no yellow precipitate of AgI was observed.

IR (KBr): 2529 cm^{-1} (B–H). UV/vis (THF): 398 nm; 514 nm; 765 nm. Analysis (%) calculated for $C_{30}H_{44}N_{12}B_2Sm$: C, 48.38; H, 5.95; N, 22.57. Found: C, 45.39; H, 5.59; N, 21.18.

Preparation of $[(Tp^{Me2})_2Eu]$ (3.2)

$Eu(OTf)_3$ (0.500 g, 0.834 mmol) and KTp^{Me2} (0.560 g, 1.665 mmol) were combined in a Schlenk flask. THF (50 ml) was added and the mixture stirred for 10 min to give a pale yellow turbid solution. Following addition of Na amalgam (0.10 g, 4.3 mmol Na in *ca* 10 ml Hg) the solution gradually became orange and a bright orange solid precipitated. After stirring the mixture overnight, the orange THF slurry was decanted off the amalgam with a cannula. The solid was allowed to settle, the supernatant was decanted and the solid residue washed with further THF (25 ml). The resulting solid was dried under vacuum, and purified by sublimation at 250 to 275 °C (5×10^{-2} torr). Yield: 0.410 g (0.549 mmol, 66 %).

IR (KBr): 2528 cm^{-1}. UV/vis (KBr): 413 nm; 670 nm. Analysis (%) calculated for $C_{30}H_{44}N_{12}B_2Eu$: C, 48.28; H, 5.94; N, 22.52. Found: C, 48.40; H, 5.74; N, 22.99.

Preparation of $[(Tp^{Me2})_2Yb]$ (3.3)

YbI_2 (2.00 g, 4.48 mmol) and $NaTp^{Me2}$ (3.30 g, 10.31 mmol) were placed in a Schlenk flask. THF (125 ml) was added with stirring. The mixture immediately turned from yellow to red/pink. Stirring was continued for 30 min after which the mixture was heated in an oil bath to 80 °C for 2 hr. The mixture was then allowed to stand until the product had settled. The pink supernatant solution was decanted and the solid washed with THF (2×75 ml). The product was dried under dynamic vacuum at 80 °C to give a red/pink powder, which was shown to be free of iodide. Yield: 3.20 g (4.17 mmol, 93 %).

IR (KBr): 2527 cm^{-1} (B–H). Solid state CP MAS ^{13}C NMR: δ 147.7, 146.8 (3- and 5-C); 105.2 (C–H); 12.6 (3- and 5-Me). UV/vis (THF): 340 nm; 530 nm. Analysis (%) calculated for $C_{30}H_{44}N_{12}B_2Yb$: C, 46.95; H, 5.78; N, 21.90. Found: C, 45.88; H, 5.54; N, 21.53. Found (sublimed material): C, 46.61; H, 5.59; N, 21.64.

Preparation of $[(Tp^{Me2})_2Ba]$[182,183]

BaI_2 (1.00 g, 2.56 mmol) and KTp^{Me2} (1.72 g, 5.11 mmol) were mixed in a Schlenk tube and THF (150 ml) was added. The mixture was stirred overnight to give a colourless solution and a heavy white precipitate. The solution was filtered in air and THF removed from the filtrate on a rotary evaporator. The resultant white powder was washed with water (2 × 50 ml), ethanol (2 × 25 ml) and diethyl ether (2 × 25 ml). This crude product was purified by sublimation under dynamic vacuum (250 °C, 10^{-2} torr) to give $[(Tp^{Me2})_2Ba]$ as colourless crystals (1.26 g, 1.72 mmol, 67 %).

IR (KBr): 2526cm^{-1} (B–H). Analysis (%) calculated for $C_{30}H_{44}N_{12}B_2Ba$: C, 49.24; H, 6.06; N, 22.97. Found: C, 49.57; H, 5.99; N, 23.37.

Preparation of $[(Tp^{Me2\text{-}4\text{-}Et})_2Sm]$ (3.4)

$SmI_2(THF)_{1.65}$ (0.600 g, 1.147 mmol) was dissolved in THF (50 ml), cooled to -78 °C, and a solution of $KTp^{Me2\text{-}4\text{-}Et}$ (0.965 g, 2.295 mmol) in THF (50 ml) added over a period of 10 min, with stirring. The resultant green solution was then allowed to warm slowly to room temperature, during which time it became purple. Stirring was continued for 2 hr. The solution was then filtered and the residue extracted with 3 × 20 ml THF until it was virtually colourless. The volume of the combined filtrates was reduced to 40 ml, while keeping the solution above *ca* 50 °C to prevent the product from crystallising. Slow cooling to -25 °C gave a purple microcrystalline product which was dried under vacuum at 80 °C. Yield: 0.670 g (0.734 mmol, 64 %).

IR (KBr): 2527 cm^{-1} (B–H). ^{1}H NMR (C_6D_6, 10 mM): δ 17.76 (s, $w_{1/2}$ = 16 Hz, 18H, 3-Me); 2.70 (q, 12H, CH_2 4-Et); 1.69 (t, 18H, Me 4-Et); -0.06 (s, 18H, 5-Me). ^{13}C NMR (C_6D_6): δ 209.7, 123.4, 69.4 (s, 3-, 4- and 5-C pz); 94.1 (q, $w_{1/2}$ = 42 Hz, 3-Me); 18.8 (t, CH_2 4-Et); 16.5 (q, Me 4-Et); -0.9 (q, 5-Me). ^{11}B (C_6D_6): δ -49.0. UV/vis (THF): 399 nm (ε = 200); 519 nm (ε = 800); 767 nm (ε = 800). Analysis (%) calculated for $C_{42}H_{68}N_{12}B_2Sm$: C, 55.25; H, 7.51; N, 18.41. Found: C, 54.81; H, 7.63; N, 18.43.

Preparation of $[(Tp^{Me_2\text{-}4\text{-}Et})_2Eu]$ (3.5)

$Eu(OTf)_3$ (0.557 g, 0.930 mmol) and $KTp^{Me_2\text{-}4\text{-}Et}$ (0.782 g, 1.860 mmol) were combined in a Schlenk flask. THF (50 ml) was added and the mixture stirred for 30 min to give a pale yellow solution and a fine precipitate. Na amalgam (0.080 g, 3.5 mmol Na in *ca* 10 ml Hg) was added, and the solution gradually became orange with an orange precipitate. After stirring overnight, the reaction mixture was decanted off the amalgam and the solvent removed under reduced pressure. The residue was extracted three times with diethyl ether (1 × 50 ml, 2 × 25 ml). Removal of solvent yielded a bright orange solid which was purified by sublimation at 250 °C (10^{-2} torr). Yield: 0.460 g (0.503 mmol, 54 %).

IR (KBr): 2522 cm^{-1} (B–H). UV/vis (THF): 413 nm (sh, ε = 600); 457 nm (ε = 800). Analysis (%) calculated for $C_{42}H_{68}N_{12}B_2Eu$: C, 55.15; H, 7.49; N, 18.38. Found: C, 55.26; H, 7.49; N, 18.65.

Preparation of $[(Tp^{Me_2\text{-}4\text{-}Et})_2Yb]$ (3.6)

YbI_2 (0.607 g, 1.36 mmol) and $KTp^{Me_2\text{-}4\text{-}Et}$ (1.171 g, 2.79 mmol) were mixed in a Schlenk and cooled to -78 °C. THF (60 ml) was added and the resultant purple mixture stirred at -78 °C for 10 min before being allowed to warm to room temperature to give a purple solution and precipitate. Warming in water to 50 °C caused the purple solid to dissolve. The solution was filtered and the volume of THF reduced to 40 ml under reduced pressure. Cooling to -25 °C resulted in the formation of a purple microcrystalline solid which was dried under dynamic vacuum at 80 °C. Yield: 0.882 g (0.943 mmol, 69 %).

IR (KBr): 2522 cm^{-1} (B–H). ^1H NMR (C_6D_6): δ 5.1 (br, 2H, B–H); 2.31 (q, 12H, CH_2 4-Et); 2.26, 2.05 (s, 2 × 18H, 3- and 5-Me); 1.02 (t, 18H, Me 4-Et). ^{13}C NMR (C_6D_6): δ 146.4, 141.3 (s, 3- and 5-C pz); 117.0 (s, 4-C pz); 17.1 (t, CH_2 4-Et) 15.9 (q, Me 4-Et); 11.55, 11.46 (q, 3- and 5-Me). ^{11}B (C_6D_6): δ -8.2. UV/vis (THF): 369 nm (ε = 500); 533 nm (ε = 1400). Analysis (%) calculated for $C_{42}H_{68}N_{12}B_2Yb$: C, 53.91; H, 7.32; N, 17.96. Found: C, 53.11; H, 7.18; N, 18.17.

Preparation of $[(Tp^{Me2\text{-}4\text{-}Et})_2Ba]$ (3.7)

BaI_2 (0.180 g, 0.460 mmol) and $KTp^{Me2\text{-}4\text{-}Et}$ (0.388 g, 0.923 mmol) were placed in a Schlenk flask and THF (40 ml) was added. The mixture was stirred for 3 hr to give a colourless solution and a heavy white precipitate. The solution was filtered and THF removed under reduced pressure to give a white powder. The product was purified by sublimation under dynamic vacuum (260 °C, 10^{-2} torr) to give $[(Tp^{Me2\text{-}4\text{-}Et})_2Ba]$ as a white crystalline solid (0.190 g, 0.211 mmol, 46 %).

IR (KBr): 2505 cm^{-1} (B–H). ^1H NMR ($CDCl_3$): δ 4.95 (br,2H, B–H); 2.33, 2.02 (s, 2 × 18H, 3- and 5-Me); 2.31 (q, 12H, CH_2 4-Et); 1.02 (t, 18H, Me 4-Et). ^{13}C NMR ($CDCl_3$): δ 145.1, 141.4 (s, 3- and 5-C pz); 116.7 (s, 4-C pz); 16.7 (t, CH_2 4-Et) 15.5 (q, Me 4-Et); 11.6, 11.4 (q, 3- and 5-Me). ^{11}B (C_6D_6): δ -8.3. Analysis (%) calculated for $C_{42}H_{68}N_{12}B_2Ba$: C, 56.05; H, 7.62; N, 18.67. Found: C, 56.22; H, 7.67; N, 18.71.

Reaction of $[(Tp^{Me2})_2Sm]$ with Tetracyanoquinodimethane (TCNQ) (3.8)

$[(Tp^{Me2})_2Sm]$ (0.181 g, 0.243 mmol) and TCNQ (0.050 g, 0.245 mmol) were placed in a Schlenk flask. THF (*ca* 40 ml) was added at -78 °C and the mixture allowed to warm to room temperature overnight, with stirring, to give a dark green solution and a pale green precipitate. Following filtration, the residue was dried under dynamic vacuum to give a pale green solid (**3.8a**; 0.150 g); removal of THF from the filtrate under reduced pressure yielded a dark green solid (**3.8b**; 0.025 g). It was noted that the colour of the solid darkened substantially upon scraping the pale green solid from the walls of the Schlenk tube.

Soluble (**3.8a**)
IR (KBr): 2555, 2528 cm^{-1} (B–H); 2196 (sh), 2182, 2118 (br) cm^{-1} (C≡N). Mass spectrum (FAB^+, *m*-nitrobenzyl alcohol): m/z 746 ($[(Tp^{Me2})_2Sm]^+$); 544 ($[(Tp^{Me2})Sm(3,5\text{-}Me_2pz)]^+$); 342 ($[(3,5\text{-}Me_2pz)_2Sm]^+$).

Residue (**3.8b**)
IR (KBr): 2556, 2528 cm^{-1} (B–H); 2200, 2186, 2149, 2133 cm^{-1} (C≡N). Mass spectrum (FAB^+, *m*-nitrobenzyl alcohol): m/z 746 ($[(Tp^{Me2})_2Sm]^+$); 544 ($[(Tp^{Me2})Sm(3,5\text{-}Me_2pz)]^+$); 342 ($[(3,5\text{-}Me_2pz)_2Sm]^+$); 247 ($[Sm(3,5\text{-}Me_2pz)]^+$).

Reaction of $[(Tp^{Me2})_2Eu]$ with TCNQ (3.9)

$[(Tp^{Me2})_2Eu]$ (0.143 g, 0.192 mmol) and TCNQ (0.039 g, 0.191 mmol) were placed in a Schlenk flask. THF (*ca* 30 ml) was added at -78 °C, and the mixture was allowed to warm to room temperature overnight, with stirring, to give a dark green solution and a pale brown precipitate. Following filtration, the residue was dried under dynamic vacuum to give a pale brown solid (**3.9a**; 0.100 g); removal of THF from the filtrate under reduced pressure yielded a dark green solid (**3.9b**; 0.040 g). It was noted that upon scraping the pale brown solid from the walls of the Schlenk tube, there was a tendency for it to change to a dark green colour.

Soluble (**3.9a**)
IR (KBr): 2555, 2528 cm^{-1} (B–H); 2199, 2183, 2139 (sh), 2119 cm^{-1} (C≡N). Mass spectrum (FAB^+, *m*-nitrobenzyl alcohol): m/z 747 ($[(Tp^{Me2})_2Eu]^+$); 545 ($[(Tp^{Me2})Eu(3,5\text{-}Me_2pz)]^+$); 458 ($[(Tp^{Me2})Eu]^+$); 248 ($[Eu(3,5\text{-}Me_2pz)]^+$).

Residue (**3.9b**)
IR (KBr): 2555, 2528 cm^{-1} (B–H); 2203, 2186, 2155, 2132 (sh) cm^{-1} (C≡N). Mass spectrum (FAB^+, *m*-nitrobenzyl alcohol): m/z 747 ($[(Tp^{Me2})_2Eu]^+$); 545 ($[(Tp^{Me2})Eu(3,5\text{-}Me_2pz)]^+$); 458 ($[(Tp^{Me2})Eu]^+$); 248 ($[Eu(3,5\text{-}Me_2pz)]^+$).

Preparation of $[(Tp^{Me2})_2Yb]^+[TCNQ]^-.(THF)_n$ (3.10)

$[(Tp^{Me2})_2Yb]$ (0.211 g, 0.275 mmol) and TCNQ (0.056 g, 0.274 mmol) were placed in a Schlenk flask, THF (*ca* 40 ml) was added and the mixture stirred for *ca* 1 hr. The pink/red $[(Tp^{Me2})_2Yb]$ dissolved rapidly to give a dark green solution and a dark green solid. The reaction solvent was removed under reduced pressure and the residue extracted into acetonitrile. Cooling to -25 °C gave a green microcrystalline product (0.130 g).

IR (KBr): 2566 cm^{-1} (B–H); 2181, 2152 cm^{-1} (C≡N). Mass spectrum (FAB^+, *m*-nitrobenzyl alcohol): m/z 768 ($[(Tp^{Me2})_2Yb]^+$); 566 ($[(Tp^{Me2})Yb(3,5\text{-}Me_2pz)]^+$); 364 ($[(3,5\text{-}Me_2pz)_2Yb]^+$); 269 ($[(3,5\text{-}Me_2pz)Yb]^+$). UV/vis (THF): 422 nm; 749 nm; 767 nm; 850 nm. Analysis (%) calculated for $C_{44}H_{52}N_{16}B_2O_{0.5}Yb$ ($(Tp^{Me2})_2$YbTCNQ.0.5THF): C, 52.45; H, 5.20; N, 22.24. Found: C, 52.67; H, 4.99; N, 22.13.

Reaction of $[(Tp^{Me2\text{-}4\text{-}Et})_2Sm]$ with TCNQ (3.11)

$[(Tp^{Me2\text{-}4\text{-}Et})_2Sm]$ (0.147 g, 0.161 mmol) and TCNQ (0.033 g, 0.162 mmol) were placed in a Schlenk flask and THF (50 ml) added with stirring. A dark green solution and precipitate were formed. Filtration followed by removal of the reaction solvent under reduced pressure gave a dark green solid (**3.11a**; 0.075 g); the residue from the filtration was dried under dynamic vacuum (**3.11b**; 0.055 g).

Soluble (**3.11a**)
IR (KBr): 2555, 2529 cm^{-1} (B–H); 2196 (sh), 2184, 2117 (br) cm^{-1} (C≡N).

Residue (**3.11b**)
IR (KBr): 2556, 2530 cm^{-1} (B–H); 2186, 2139 (br) cm^{-1} (C≡N).

Preparation of $[(Tp^{Me2\text{-}4\text{-}Et})_2Yb]^+[TCNQ]^-.(THF)_n$ (3.12)

$[(Tp^{Me2\text{-}4\text{-}Et})_2Yb]$ (0.088 g, 0.094 mmol) and TCNQ (0.020 g, 0.098 mmol) were placed in a Schlenk flask and THF (*ca* 20 ml) added at -78 °C with stirring. The colour of the solution changed rapidly from purple to green. The contents of the flask were allowed to warm slowly to room temperature and stirred overnight. The resultant green precipitate was dissolved by warming the mixture to *ca* 50 °C, and filtered to give a clear green solution. This was cooled to -25 °C to give a bright green microcrystalline solid (0.040 g).

IR (KBr): 2560 cm^{-1} (B–H); 2180, 2154, (2132) cm^{-1} (C≡N). Mass spectrum (FAB^+, *m*-nitrobenzyl alcohol): m/z 935 ($[(Tp^{Me2\text{-}4\text{-}Et})_2Yb]^+$); 678 ($[(Tp^{Me2\text{-}4\text{-}Et})Yb(3,5\text{-}Me_2\text{-}4\text{-}Etpz)]^+$); 420 ($[(3,5\text{-}Me_2\text{-}4\text{-}Etpz)_2Yb]^+$); 297 ($[(3,5\text{-}Me_2\text{-}4\text{-}Etpz)Yb]^+$).

Reaction of $[(Tp^{Me2})_2Sm]$ with Tetracyanoethylene (TCNE) (3.13)

$[(Tp^{Me2})_2Sm]$ (0.194 g, 0.260 mmol) and TCNE (0.033 g, 0.258 mmol) were mixed in a Schlenk flask and THF (20 ml) was added with stirring. The purple solid dissolved rapidly and an orange solution was formed from which a red/brown solid slowly precipitated. The solution was filtered and the residue extracted with THF (2 × 10 ml). The volume of the filtrate was reduced to *ca* 30 ml under reduced pressure and the solution cooled to -25 °C to give a red/brown microcrystalline solid (0.060 g). Further concentration of the solution followed by cooling gave an additional 0.015 g of product which appeared slightly contaminated with a yellow material.

IR (KBr): 2554 cm^{-1} (B–H); 2197, 2155 cm^{-1} (C≡N). Mass spectrum (FAB^+, *m*-nitrobenzyl alcohol): m/z 746 ($[(Tp^{Me2})_2Sm]^+$); 544 ($[(Tp^{Me2})Sm(3,5\text{-}Me_2pz)]^+$); 342 ($[(3,5\text{-}Me_2pz)_2Sm]^+$). Analysis (%) calculated for $SmC_{40}H_{52}N_{16}B_2O$ ($(Tp^{Me2})_2$SmTCNE.THF): C, 50.84; H, 5.55; N, 23.72. Found: C, 50.89; H, 5.56; N, 23.72.

Reaction of $[(Tp^{Me2})_2Eu]$ with TCNE (3.14)

$[(Tp^{Me2})_2Eu]$ (0.150 g, 0.201 mmol) and TCNE (0.033 g, 0.203 mmol) were mixed in a Schlenk flask and THF (20 ml) added with stirring. The orange starting material dissolved rapidly and an orange/brown solution was formed from which red/brown solid slowly precipitated. The solution was filtered and the residue extracted with THF (2 × 10 ml). The volume of the filtrate was reduced to *ca* 20 ml under reduced pressure and the solution cooled to -25 °C to give a red/brown microcrystalline solid (0.040 g).

IR (KBr): 2554 cm^{-1} (B–H); 2197, 2155 cm^{-1} (C≡N). Mass spectrum (FAB^+, *m*-nitrobenzyl alcohol): m/z 747 ($[(Tp^{Me2})_2Eu]^+$); 545 ($[(Tp^{Me2})Eu(3,5\text{-}Me_2pz)]^+$); 458 ($[(Tp^{Me2})Eu]^+$); 248 ($[Eu(3,5\text{-}Me_2pz)]^+$). Analysis (%) calculated for $EuC_{40}H_{52}N_{16}B_2O$ ($(Tp^{Me2})_2$EuTCNE.THF): C, 50.76; H, 5.54; N, 23.68. Found: C, 50.24; H, 5.30; N, 23.59.

Preparation of $[(Tp^{Me2})_2Yb]^+[TCNE]^-.(THF)_6$ (3.15)

$[(Tp^{Me2})_2Yb]$ (0.196 g, 0.255 mmol) and TCNE (0.033 g, 0.257 mmol) were placed in a Schlenk flask and THF (50 ml) was added. The red/pink starting material dissolved rapidly to give a yellow/orange solution and a small amount of orange precipitate. The solution was filtered, the volume reduced to *ca* 15 ml and the solution warmed slightly to dissolve any solid. Slow cooling to -25 °C gave yellow/orange crystals (0.150 g, 0.167 mmol, 66 %) which desolvated rapidly upon removing the solvent.

IR (KBr): 2560 cm^{-1} (B–H); 2187, 2148 cm^{-1} (C≡N). Mass spectrum (FAB^+, *m*-nitrobenzyl alcohol): m/z 768 ($[(Tp^{Me2})_2Yb]^+$); 566 ($[(Tp^{Me2})Yb(3,5\text{-}Me_2pz)]^+$); 364 ($[(3,5\text{-}Me_2pz)_2Yb]^+$); 269 ($[(3,5\text{-}Me_2pz)Yb]^+$). UV/vis (THF): 428 nm. Analysis (%) calculated for $C_{40}H_{52}N_{16}B_2OYb$ ($(Tp^{Me2})_2YbTCNE.THF$): C, 49.65; H, 5.42; N, 23.16. Found: C, 48.66; H, 5.21; N, 22.96.

Reaction of $[(Tp^{Me2\text{-}4\text{-}Et})_2Sm]$ with TCNE (3.16)

$[(Tp^{Me2\text{-}4\text{-}Et})_2Sm]$ (0.133 g, 0.146 mmol) and TCNE (0.019 g, 0.148 mmol) were placed in a Schlenk flask and THF (*ca* 30 ml) added at -78 °C with stirring. The resultant yellow/brown solution was warmed to *ca* 50 °C. Filtration followed by cooling to -25 °C gave a red/brown microcrystalline solid (0.080 g).

IR (KBr): 2566 cm^{-1} (B–H); 2203, 2198, 2162 (sh), 2153 cm^{-1} (C≡N). Mass spectrum (FAB^+, *m*-nitrobenzyl alcohol): m/z 915 ($[(Tp^{Me2\text{-}4\text{-}Et})_2Sm]^+$).

Preparation of $[(Tp^{Me2\text{-}4\text{-}Et})_2Yb]^+[TCNE]^-.(THF)_n$ (3.17)

$[(Tp^{Me2\text{-}4\text{-}Et})_2Yb]$ (0.150 g, 0.160 mmol) and TCNE (0.033 g, 0.164 mmol) were placed in a Schlenk flask, THF (*ca* 30 ml) added at -78 °C and the mixture stirred overnight whilst warming slowly to room temperature. The resultant yellow/orange solution was filtered and the volume of THF reduced to *ca* 10 ml under reduced pressure. Cooling to -25 °C gave an orange crystalline powder (0.090 g). Further concentration to 5 ml gave a second crop of product (0.025 g).

IR (KBr): 2569 cm^{-1} (B–H); 2183, 2144 cm^{-1} (C≡N).

Preparation of $[(Tp^{Me2\text{-}4\text{-}Et})_2Sm(\eta^2\text{-}O_2N)]$ (3.19)

$[(Tp^{Me2\text{-}4\text{-}Et})_2Sm]$ (0.135 g, 0.148 mmol) was placed in a Schlenk flask. 30/40 petrol (20 ml) was added and the solvent frozen in liquid nitrogen. The flask was evacuated and the mixture stirred at -78 °C before being filled with NO to a pressure of 760 torr (1 atmosphere). As the mixture was warmed to room temperature, the purple solid/solution disappeared and a yellow solid was formed. Solvent was removed under reduced pressure and the solid became white. The crude product was extracted into diethyl ether (50 ml), the solution filtered and the volume of the filtrate reduced to 25 ml. Cooling to -25 °C gave a white microcrystalline solid (*ca* 0.050 g, 0.052 mmol, 35 %).

IR (KBr): 2522 cm^{-1} (B–H); 1297 cm^{-1} (w, N–O antisymmetric); 1200 cm^{-1} (s, N–O symmetric). ^1H NMR (C_6D_6): δ 4.70 (br s, 2H, B–H); 2.20 (q, 12H, CH_2 4-Et); 2.16, 1.07 (s, 2 × 18H, Me); 1.03 (t, 18H, Me 4-Et). ^{13}C NMR (C_6D_6): δ 148.1, 141.5, 117.5 (s, 3-, 4- and 5-C pz); 16.9 (t, CH_2 4-Et); 15.5 (q, Me 4-Et); 12.1, 11.5 (q, 3- and 5-Me); ^{11}B (C_6D_6): δ -9.3. Analysis (%) calculated for $C_{42}H_{68}N_{13}B_2O_2Sm$: C, 52.60; H, 7.15; N, 18.99. Found: C, 53.32; H, 7.15; N, 18.68.

Preparation of $[(Tp^{Me2\text{-}4\text{-}Et})_2Eu(\eta^2\text{-}O_2N)]$ (3.20)

The preparation was carried out in an analogous fashion to that of the Sm complex. No attempt was made to purify the crude product.

IR (KBr): 2522 cm^{-1} (B–H); 1298 cm^{-1} (w, N–O antisymmetric); 1202 cm^{-1} (s, N–O symmetric).

Preparation of $(Tp^{Me2\text{-}4\text{-}Et})_2YbNO_2$ (3.21)

The preparation was carried out in an analogous fashion to that of the Sm complex. No attempt was made to purify the crude product.

IR (KBr): 2522 cm^{-1} (B–H); 1303 cm^{-1} (w, N–O antisymmetric); 1210 cm^{-1} (s, N–O symmetric).

Preparation of $[(Tp^{Me_2\text{-}4\text{-}Et})_2Sm(\eta^2\text{-}PhNNPh)]$ (3.22)

Azobenzene (2 mg, 0.01 mmol) was added to a purple solution of $[(Tp^{Me_2\text{-}4\text{-}Et})_2Sm]$ (8 mg, 0.009 mmol) in C_6D_6 (*ca* 0.9 ml). The solution immediately changed colour to dark green, and the new product was characterised as being $[(Tp^{Me_2\text{-}4\text{-}Et})_2Sm(\eta^2\text{-}PhNNPh)]$ from its ^1H NMR spectrum.

^1H NMR (C_6D_6): δ 72.2 (s, 4H, Ph); 23.21 (s, 6H, Me); 5.40 (s, 2H, B–H); 4.55 (s, 6H, Me); 2.75 (s, 6H, Me); 2.40 (s, 6H, Me); 2.20 (s, 6H, Me); -4.55 (s, 6H, Me); -170.30 (s, 4H, Ph); -189.55 (s, 4H, Ph).

Attempted Preparation of $[Tp^{Me_2\text{-}4\text{-}Et}SmI(THF)_n]$

$SmI_2(THF)_{1.65}$ (0.650 g, 1.242 mmol) was dissolved in THF (50 ml), cooled to -78 °C, and a solution of $KTp^{Me_2\text{-}4\text{-}Et}$ (0.490 g, 1.165 mmol) in THF (50 ml) added over a period of *ca* 10 min, with stirring. The resultant green solution was allowed to warm slowly to room temperature and stirring continued for a further 2 hr. The solution was then filtered and the residue extracted with THF (3 × 20 ml). Attempts to grow crystals of the green compound by cooling this solution were unsuccessful, a mixture of $[(Tp^{Me_2\text{-}4\text{-}Et})_2Sm]$ and $SmI_2(THF)_n$ being precipitated.

UV/vis (THF): 380 nm; 425 nm; 560 nm; 619 nm.

Attempted Preparation of $[Tp^{Me_2\text{-}4\text{-}Et}YbI(THF)_n]$

$KTp^{Me_2\text{-}4\text{-}Et}$ (0.200 g, 0.476 mmol) and YbI_2 (0.205 g, 0.460 mmol) were placed in a Schlenk and cooled to -78 °C. THF (*ca* 30 ml) was added, the mixture stirred for 5 min and then allowed to warm to room temperature, giving a red solution. Stirring was continued overnight, after which the reaction solvent was removed under reduced pressure to leave a red residue. Cooling

a diethyl ether solution of the product gave a mixture of purple and yellow solids.

UV/vis (THF): 350 nm; 400 nm; 437 nm; 537 nm. IR (KBr): 2520 cm^{-1} (B–H). ^1H NMR (C_6D_6): δ 3.60 (br, THF); 2.31 (q, 12H, CH_2 4-Et); 2.26, 2.04 (s, 2 × 18H, 3- and 5-Me); 1.43 (br, THF); 1.01 (t, 18H, Me 4-Et).

Preparation of $[Tp^{3\text{-}t\text{-}Bu\text{-}5\text{-}Me}SmI(THF)_2].(Et_2O)_{0.5}$ (4.1)

$SmI_2(THF)_{1.65}$ (2.00 g, 3.82 mmol) and $KTp^{3\text{-}t\text{-}Bu\text{-}5\text{-}Me}$ (1.77 g, 3.83 mmol) were mixed in a Schlenk flask, cooled to -78 °C and 100 ml THF was added. The mixture was stirred for 12 hr, whilst warming to room temperature, and then allowed to settle. The green (red by transmitted light) solution was filtered and the residue extracted with THF (2 × 25 ml). Solvent was removed from the combined extracts under reduced pressure and the resultant green solid was extracted into diethyl ether (50 ml followed by 2 × 25 ml). Following filtration, the volume of the solution was reduced to *ca* 75 ml under reduced pressure. Cooling to *ca* 5 °C gave 1.94 g (2.26 mmol) of $[Tp^{3\text{-}t\text{-}Bu\text{-}5\text{-}Me}SmI(THF)_2].(Et_2O)_{0.5}$ as black crystals. Further concentration of the supernatant to 10 ml followed by cooling gave another 0.23 g of crystals (0.27 mmol). Total yield: 65 %.

IR (KBr): 2546, 2516 cm^{-1} (B–H). ^1H NMR (C_6D_6, 90 mM): δ 4.74 (s, $w_{1/2}$ = 13 Hz, 27H, CMe_3); 3.25 (q, 2H, CH_2 Et_2O); 2.06 (s, 3H, C–H pz); 1.96 (s, 9H, Me pz); 1.10 (t, 3H, Me Et_2O); -0.64 (s, $w_{1/2}$ = 16 Hz, 4H, THF); -0.74 (s, $w_{1/2}$ = 11 Hz, 4H, THF). ^{13}C NMR (C_6D_6): δ 161.8, 133.9, 39.7 (s, 3- and 5-C pz and *C*Me_3); 91.9 (t, THF); 66.1 (q, C*Me*$_3$); 66.1 (t, CH_2 Et_2O); 51.3 (d, C–H pz); 21.8 (t, THF); 15.6 (q, Me Et_2O); 7.3 (q, Me pz). ^{11}B NMR (C_6D_6): δ -27.2. UV/vis (THF): 409 nm (ε = 600); 563 (ε = 500). Analysis (%) calculated for $C_{34}H_{61}N_6BIO_{2.5}Sm$: C, 46.30; H, 6.97; N, 9.53. Found: C, 46.32; H, 7.18; N, 9.57.

Preparation of $[Tp^{3\text{-}t\text{-}Bu\text{-}5\text{-}Me}YbI(THF)]$ (4.2)

YbI_2 (2.00 g, 4.48 mmol) and $KTp^{3\text{-}t\text{-}Bu\text{-}5\text{-}Me}$ (2.04 g, 4.41 mmol) were mixed in a Schlenk and cooled to -78 °C THF (100 ml) was added. and the mixture was stirred for 12 hr whilst warming to room temperature and then allowed to

settle. The canary yellow solution was filtered and the pale yellow residue extracted with THF (50 ml). Solvent was removed from the combined filtrates under reduced pressure and the resulting yellow solid extracted with diethyl ether (2 × 100 ml). Following filtration, solvent was removed under reduced pressure and the yellow solid dried under dynamic vacuum to yield 2.90 g (3.65 mmol, 83 %) of [$Tp^{3\text{-}t\text{-}Bu\text{-}5\text{-}Me}$YbI(THF)]. The product could be recrystallised by cooling a diethyl ether solution, although this crude material was found to be satisfactory for most applications.

IR (KBr): 2554 cm^{-1} (B–H). ^1H NMR (C_6D_6): δ 5.65 (s, 3H, C–H pz); 3.21 (m, 4H, THF); 2.16 (s, 9H, Me); 1.47 (s, 27H, CMe_3); 1.06 (m, 4H, THF). ^{13}C NMR (C_6D_6): δ 163.7, 145.3 (s, 3- and 5-C pz); 102.9 (d, C–H pz); 69.6 (t, THF); 32.6 (s, *C*Me_3); 32.1 (q, C*Me*$_3$); 25.4 (t, THF); 13.5 (q, Me). Solid state CP MAS ^{13}C NMR: δ 163.4, 144.8 (3- and 5-C pz); 105.3, 104.3, 103.4 (C–H pz); 69.2 (THF); 33.2, 32.5, 31.8 (C*Me*$_3$); 24.4 (THF); 15.4 (Me). ^{11}B NMR (C_6D_6): δ -8.5. UV/vis (THF): 420 nm (ε = 300). Analysis (%) calculated for $C_{28}H_{48}N_6BIOYb$: C, 42.28; H, 6.08; N, 10.56. Found: C, 41.71; H, 5.88; N, 10.36.

Preparation of [$Tp^{3\text{-}t\text{-}Bu\text{-}5\text{-}Me}$SmI] (4.3)

[$Tp^{3\text{-}t\text{-}Bu\text{-}5\text{-}Me}SmI(THF)_2$].$(Et_2O)_{0.5}$ was finely ground and heated under dynamic vacuum at 100 °C for *ca* 1 hr. The ^1H NMR of the resultant dark green solid showed it be [$Tp^{3\text{-}t\text{-}Bu\text{-}5\text{-}Me}$SmI] with a small trace of a diamagnetic $Tp^{3\text{-}t\text{-}Bu\text{-}5\text{-}Me}$ species. The starting material could not be desolvated at room temperature and 10^{-2} torr overnight.

IR (KBr): 2548, 2523 cm^{-1} (B–H). ^1H NMR (C_6D_6): δ 1.80 (s, $w_{1/2}$ = 16 Hz, 27H, CMe_3); 1.09 (s, $w_{1/2}$ = 8 Hz, 3H, C–H pz); 0.86 (s, $w_{1/2}$ = 10 Hz, 9H, Me pz). ^{11}B NMR (C_6D_6): δ -27.0. Analysis (%) calculated for $C_{24}H_{40}N_6BISm$: C, 41.13; H, 5.75; N, 11.99. Found: C, 41.07; H, 5.82; N, 12.10.

Preparation of [$Tp^{3\text{-}t\text{-}Bu\text{-}5\text{-}Me}$YbI] (4.4)

[$Tp^{3\text{-}t\text{-}Bu\text{-}5\text{-}Me}$YbI(THF)] (*ca* 0.070 g, 0.09 mmol) was heated under vacuum (10^{-1} torr) at 180 °C for *ca* 4 hr. The residue was extracted with toluene (1 × 20 ml), filtered, and the solvent removed under reduced pressure to give a yellow powder (*ca* 0.050 g, 0.07 mmol).

^{1}H NMR (C_6D_6): δ 5.67 (s, 3H, C–H pz); 2.20 (s, 9H, Me); 1.47 (s, 27H, CMe_3); all resonances were broad, *ca* 10 to 20 Hz. Analysis (%) calculated for $C_{24}H_{40}N_6BIYb$: C, 39.85; H, 5.57; N, 11.62. Found: C, 37.21; H, 5.24; N, 11.90.

Preparation of [Tp$^{3\text{-}t\text{-Bu-5-Me}}$SmI(py)$_2$] (py = pyridine) (4.5)

[Tp$^{3\text{-}t\text{-Bu-5-Me}}$SmI(THF)$_2$].($Et_2O$)$_{0.5}$ (0.105 g, 0.119 mmol) was dissolved in 2 ml toluene. Pyridine (py; 0.066 g, 0.834 mmol) was added and the dark green solution layered with 10 ml 30/40 petrol. Upon standing, thick black needles of [Tp$^{3\text{-}t\text{-Bu-5-Me}}$SmI(py)$_2$] were formed which were isolated, washed with 30/40 petrol (3 × 2 ml) and dried under dynamic vacuum. Yield: 0.045 g (0.052 mmol, 44 %).

IR (KBr): 2550, 2519 cm^{-1} (B–H). ^{1}H NMR (C_6D_6, 50 mM): δ 5.21 (s, $w_{1/2}$ = 26 Hz, 27H, CMe_3); 3.49 (t, 2H, 4-H py); 3.00 (d, 4H, 3,5-H py); 2.50 (s, 9H, Me); 2.19 (s, $w_{1/2}$ = 16 Hz, 3H, C–H pz); -4.04 (s, $w_{1/2}$ = 29 Hz, 4H, 2,6-H py). ^{13}C NMR (C_6D_6, 50 mM): δ 204.5 (d, $w_{1/2}$ = 26 Hz, 2-C py); 162.6, 137.7 (s, 3- and 5-C pz); 150.7 (d, 4-C py); 105.0 (d, 3-C py); 66.0 (q, CMe_3); 53.9 (d, C–H pz); 38.7 (s, CMe_3); 7.6 (q, Me). ^{11}B NMR (C_6D_6, 50 mM): δ -23.8. UV/vis (Toluene): 436 nm (ε = 400); 504 nm (ε = 400); 717 nm (ε = 200). Analysis (%) calculated for $C_{34}H_{50}N_8BISm$: C, 47.55; H, 5.87; N, 13.05. Found: C, 46.15; H, 5.86; N, 12.68.

Preparation of [Tp$^{3\text{-}t\text{-Bu-5-Me}}$SmI(3,5-Me$_2$py)$_2$] (4.6)

[Tp$^{3\text{-}t\text{-Bu-5-Me}}$SmI(THF)$_2$].($Et_2O$)$_{0.5}$ (0.100 g, 0.113 mmol) was dissolved in 2 ml toluene. 3,5-Dimethylpyridine (3,5-Me_2py; 0.065 g, 0.607 mmol) was added and the dark green solution layered with 10 ml 30/40 petrol. Upon standing, black crystals of [Tp$^{3\text{-}t\text{-Bu-5-Me}}$SmI(3,5-Me$_2$py)$_2$] were formed which were isolated, washed with 30/40 petrol (3 × 2 ml) and dried under dynamic vacuum. Yield: 0.082 g (0.090 mmol, 79 %).

IR (KBr): 2521 cm^{-1} (B–H). ^{1}H NMR (C_6D_6, 20 mM): δ 5.23 (s, $w_{1/2}$ = 30 Hz, 27H, CMe_3); 3.77 (s, 2H, 4-H py); 2.38 (s, $w_{1/2}$ = 26 Hz, 3H, C–H pz); 2.28 (s, 9H, Me); -0.39 (s, 12H, Me py); -3.37 (s, $w_{1/2}$ = 54 Hz, 4H, 2,6-H py). ^{13}C NMR (C_6D_6, 40 mM): δ 200.6 (d, $w_{1/2}$ = 50 Hz, 2-C py); 164.1, 138.7 (s, 3- and 5-C

pz); 151.2 (d, 4-C py); 113.2 (s, 3-C py); 66.4 (q, CMe_3); 55.5 (d, C–H pz); 38.5 (s, CMe_3); 14.8 (q, Me py); 8.0 (q, Me pz). ^{11}B NMR (C_6D_6, 40 mM): δ -22.0. UV/vis (Toluene): 420 nm (ε = 700); 502 nm (ε = 500); 710 nm (ε = 300). Analysis (%) calculated for $C_{38}H_{58}N_8BISm$: C, 49.88; H, 6.39; N, 12.25. Found: C, 49.18; H, 6.52; N, 12.30.

Preparation of [Tp$^{3\text{-}t\text{-Bu-5-Me}}$SmI(4-Bu^{t}py)$_2$] (4.7)

Powdered [Tp$^{3\text{-}t\text{-Bu-5-Me}}$SmI(THF)$_2$].$(Et_2O)_{0.5}$ (0.030 g, 0.034 mmol) was suspended in 30/40 petrol (2 ml). Upon addition of a solution of 4-*tert*-butylpyridine (4-Bu^{t}py; 0.013 g, 0.096 mmol) in 30/40 petrol (2 ml), the solid dissolved to give a dark green solution, which on standing deposited large black crystals of [Tp$^{3\text{-}t\text{-Bu-5-Me}}$SmI(4-Bu^{t}py)$_2$]. The supernatant was decanted and the product washed with 30/40 petrol (2 × 2 ml). Yield: 0.030 g (0.031 mmol, 91 %).

IR (KBr): 2510 cm^{-1} (B–H). ^1H NMR (C_6D_6, 20 mM): δ 5.30 (s, $w_{1/2}$ = 26 Hz, 27H, CMe_3 pz); 3.19 (s, 4H, 3,5-H py); 2.42 (s, 9H, Me); 2.27 (s, $w_{1/2}$ = 21 Hz, 3H, C–H pz); 0.16 (s, 18H, CMe_3 py); -3.99 (s, $w_{1/2}$ = 48 Hz, 4H, 2,6-H py). ^{13}C NMR (C_6D_6): δ 205.7 (d, $w_{1/2}$ = 80 Hz, 2-C py); 176.6 (s, 4-C py); 162.1, 138.3 (s, 3- and 5-C pz); 100.2 (d, 3-C py); 66.2 (q, CMe_3 pz); 54.1 (d, C–H pz); 38.3 (s, CMe_3 pz); 33.5 (q, CMe_3 py); 28.9 (s, CMe_3 py); 7.9 (q, Me). ^{11}B NMR (C_6D_6): δ -22.8. UV/vis (Toluene): 420 nm (ε = 900); 504 nm (ε = 400); 720 nm (ε = 400). Analysis (%) calculated for $C_{42}H_{66}N_8BISm$: C, 51.95; H, 6.85; N, 11.54. Found: C, 51.63; H, 6.84; N, 11.75.

Preparation of [Tp$^{3\text{-}t\text{-Bu-5-Me}}$YbI(py)$_2$] (4.8)

[Tp$^{3\text{-}t\text{-Bu-5-Me}}$YbI(THF)] (0.100 g, 0.126 mmol) was suspended with 30/40 petrol and pyridine (py; 0.040 g, 0.506 mmol) in 30/40 petrol (2 ml) was added drop-wise. The dark red solution/solid was stirred for 5 min and then allowed to settle. The supernatant was decanted, the dark red residue washed with 30/40 petrol (3 × 2 ml) and dried under dynamic vacuum to yield 0.052 g (0.059 mmol, 47 %) of [Tp$^{3\text{-}t\text{-Bu-5-Me}}$YbI(py)$_2$].

IR (KBr): 2553, (2526) cm^{-1} (B–H). ^1H NMR (C_6D_6): δ 8.44 (br s, 4H, 2,6-H py); 6.82 (br s, 2H, 4-H py); 6.49 (br s, 4H, 3,5-H py); 5.63 (s, 3H, C–H pz); 2.27 (s,

9H, Me); 1.30 (s, 27H, CMe_3). ^{13}C NMR (C_6D_6): δ 163.8, 145.2 (s, 3- and 5-C pz); 150.3 (d, 2-C py); 136.2 (d, 4-C py); 123.8 (d, 3-C py); 103.1 (d, C–H pz); 32.5 (s, CMe_3); 31.8 (q, CMe_3); 13.6 (q, Me). ^{11}B NMR (C_6D_6): δ -8.5. UV/vis (Toluene): 421 nm, 480 (sh). Analysis (%) calculated for $C_{34}H_{50}N_8BIYb$: C, 46.32; H, 5.72; N, 12.71. Found: C, 45.51; H, 6.27; N, 11.79.

Preparation of [Tp$^{3\text{-}t\text{-Bu-}5\text{-Me}}$YbI(3,5-Me$_2$py)$_2$] (4.9a)

[Tp$^{3\text{-}t\text{-Bu-}5\text{-Me}}$YbI(THF)] (0.100 g, 0.126 mmol) was placed in a vial and suspended in 30/40 petrol (5 ml). 3,5-Dimethylpyridine (3,5-Me_2py; 0.230 g, 2.15 mmol) was added, the mixture shaken and the yellow solid dissolved to give a dark red solution, which gave red crystals of [Tp$^{3\text{-}t\text{-Bu-}5\text{-Me}}$YbI(Me$_2$py)$_2$] upon standing. The solvent was decanted, the crystals washed with 30/40 petrol (3 × 2 ml) and the product dried under dynamic vacuum. Yield: 0.060 g (0.0640 mmol, 51 %).

IR (KBr): 2548, (2527) cm^{-1} (B–H). ^1H NMR (C_6D_6,): δ 8.17 (s, $w_{1/2}$ = 21 Hz, 4H, 2,6-H py); 6.63 (s, $w_{1/2}$ = 15 Hz, 2H, 4-H py); 5.63 (s, 3H, C–H pz); 2.28 (s, 9H, Me pz); 1.73 (s, 12H, Me py); 1.33 (s, 27H, CMe_3). ^{13}C NMR (C_6D_6): δ 163.8, 145.1 (s, 3- and 5-C pz); 147.9 (d, 2-C py); 137.4 (d, 4-C py); 132.7 (s, 3-C py); 103.0 (d, C–H pz); 32.5 (s, CMe_3); 31.8 (q, CMe_3); 17.9 (q, Me py); 13.5 (q, Me pz). ^{11}B NMR (C_6D_6): δ -8.5. UV/vis (Toluene): 424 nm (ε = 400); 476 nm (sh, ε = 300). Analysis (%) calculated for $C_{38}H_{58}N_8BIYb$: C, 48.67; H, 6.23; N, 11.95. Found: C, 48.56; H, 6.17; N, 11.97.

Preparation of [Tp$^{3\text{-}t\text{-Bu-}5\text{-Me}}$YbI(3,5-Me$_2$py)] (4.9b)

[Tp$^{3\text{-}t\text{-Bu-}5\text{-Me}}$YbI(THF)] (0.100 g, 0.126 mmol) was placed in a vial and dissolved in diethyl ether (8 ml). 3,5-Dimethylpyridine (3,5-Me_2py; 0.015 g, 0.140 mmol) in diethyl ether (2 ml) was added to give a dark red solution. This was layered with 30/40 petrol, the vial capped and the mixture allowed to equilibrate. A small hole was then pierced in the cap allowing the slow evaporation of diethyl ether and subsequent formation of large red/black blocks of [Tp$^{3\text{-}t\text{-Bu-}5\text{-Me}}$YbI(3,5-Me$_2$py)]. The supernatant was decanted and the crystals washed with 30/40 petrol (3 × 2 ml) and dried under dynamic vacuum. Yield: 0.060 g (0.072 mmol, 57 %).

IR (KBr): 2549, (2530) cm^{-1} (B–H). ^1H NMR ($C_6D_5CD_3$, 293 K): δ 7.81 (s, 2H, 2,6-H py); 6.49 (s, 1H, 4-H py); 5.54 (s, 3H, C–H pz); 2.21 (s, 9H, Me pz); 1.61 (s, 6H, Me py); 1.24 (s, 27H, CMe_3). ^1H NMR ($C_6D_5CD_3$, 173 K): δ 9.62 (s, 1H, 2,6-H py); 5.90 (s, 2H, 2,6-H and 4-H py); 5.50 (s, 1H, C–H pz); 5.26 (s, 2H, C–H pz); 2.24 (s, 6H, Me pz); 1.89 (s, 3H, Me pz); 1.79 (s, 9H, CMe_3); 1.46, 1.32 (s, 2 × 3H, Me py); 1.04 (s, 18H, CMe_3). ^{13}C NMR ($C_6D_5CD_3$, 293 K): δ 163.6, 145.0 (s, 3- and 5-C pz); 147.6 (d, 2-C py); 138.3 (d, 4-C py); 133.1 (s, 3-C py); 102.8 (d, C–H pz); 32.4 (s, CMe_3); 31.7 (q, CMe_3); 17.7 (q, Me py); 13.6 (q, Me pz). ^{13}C NMR ($C_6D_5CD_3$, 173 K): δ 162.7, 144.8 (s, 3- and 5-C pz); 147.8 (2 × 2-C py); 138.3 (4-C py); 133.7, 132.3 (2 × 3-C py); 102.6 (3 × C–H pz); 32.5 (3 × CMe_3); 32.3 (3 × CMe_3); 30.8 (6 × CMe_3); 17.6 (2 × Me py); 13.4 (2 × Me pz). ^{11}B NMR (C_6D_6): δ -8.4. UV/vis (Toluene): 428 nm (ε = 500); 480 nm (sh, ε = 400). Analysis (%) calculated for $C_{31}H_{49}N_7BIYb$: C, 44.83; H, 5.95; N, 11.81. Found: C, 45.26; H, 5.98; N, 11.92.

Preparation of [Tp$^{3\text{-}t\text{-Bu-5-Me}}$YbI(4-Bu^{t}py)] (4.10)

[Tp$^{3\text{-}t\text{-Bu-5-Me}}$YbI(THF)] (0.100 g, 0.126 mmol) was placed in a vial and suspended in 30/40 petrol (5 ml). 4-*tert*-Butylpyridine (4-Bu^{t}py; 0.150 g, 0.740 mmol) was added, the mixture shaken and the yellow solid dissolved to give a dark red solution, which gave red crystals of [Tp$^{3\text{-}t\text{-Bu-5-Me}}$YbI(4-Bu^{t}py)] upon standing. The solvent was decanted, the crystals washed with 30/40 petrol (3 × 2 ml) and the product dried under dynamic vacuum. Yield: *ca* 0.040 g (0.047 mmol, 37 %).

IR (KBr): 2549, (2526) cm^{-1} (B–H). ^1H NMR (C_6D_6,): δ 8.30 (d, 2H, 2,6-H py); 6.49 (d, 2H, 3,5-H py); 5.65 (s, 3H, C–H pz); 2.30 (s, 9H, Me pz); 1.33 (s, 27H, CMe_3); 0.78 (s, 9H, CMe_3 py). ^{13}C NMR (C_6D_6): δ 163.8, 145.1 (s, 3- and 5-C pz); 161.7 (s, 4-C py); 149.9 (d, 2-C py); 121.1 (d, 3-C py); 103.1 (d, C–H pz); 34.5 (s, CMe_3 py); 32.5 (s, CMe_3 pz); 31.8 (q, CMe_3 pz); 29.8 (q, CMe_3 py); 13.6 (q, Me pz). ^{11}B NMR (C_6D_6): δ -8.5. UV/vis (Toluene): 423 nm (ε = 500); 472 nm (sh, ε = 400). Analysis (%) calculated for $C_{33}H_{53}N_7BIYb$: C, 46.16; H, 6.22; N, 11.42. Found: C, 46.34; H, 6.31; N, 11.08.

Preparation of [Tp$^{3\text{-}t\text{-Bu-5-Me}}$YbI(CNBu^t)] (4.11)

[Tp$^{3\text{-}t\text{-Bu-5-Me}}$YbI(THF)] (0.100 g, 0.126 mmol) was placed in a vial and diethyl ether (0.5 ml) was added. To this yellow solution/slurry, 0.045 g (0.541 mmol)

of $CNBu^t$ were added to give an orange solution which was layered with 10 ml 30/40 petrol. Orange crystals were formed which were isolated, washed with 30/40 petrol (3 × 2 ml) and dried under dynamic vacuum. Yield: 0.056 g (0.069 mmol, 55 %).

IR (KBr): 2556 cm^{-1} (B–H); 2172 cm^{-1} (C≡N). ^1H NMR (C_6D_6): δ 5.69 (s, 3H, C–H pz); 2.15 (s, 9H, Me); 1.55 (s, 27H, CMe_3 pz); 0.73 (s, 9H, CMe_3 isonitrile). ^{13}C NMR (C_6D_6): δ 163.7, 145.3 (s, 3- and 5-C pz); 102.8 (d, C–H pz); 32.7 (s, CMe_3 pz); 32.2 (q, CMe_3 pz); 30.7 (s, CMe_3 isonitrile); 29.2 (q, CMe_3 isonitrile); 13.4 (q, Me pz). ^{11}B NMR (C_6D_6): 8.7. UV/vis (Toluene): 436 nm (ε = 500). Analysis (%) calculated for $C_{29}H_{49}N_7BIYb$: C, 43.19; H, 6.12; N, 12.16. Found: C, 43.03; H, 6.17; N, 12.06.

Preparation of $[Tp^{3\text{-}t\text{-}Bu\text{-}5\text{-}Me}SmI(CNBu^t)_n]$ (4.12)

$[Tp^{3\text{-}t\text{-}Bu\text{-}5\text{-}Me}SmI]$ (*ca* 4 mg, 0.006 mmol) was reacted with one drop of *tert*-butylisonitrile ($CNBu^t$) in C_6D_6. The colour of the solution changed from dark green to dark green/brown upon addition of the isonitrile. The ^1H NMR spectrum of this reaction mixture showed that a new compound was present in solution, consistent with the formation of $[Tp^{3\text{-}t\text{-}Bu\text{-}5\text{-}Me}SmI(CNBu^t)_n]$. Attempts to carry out this reaction on a preparative scale were unsuccessful due to the ready loss of $CNBu^t$ from the solid compound upon standing.

^1H NMR (C_6D_6,): δ 3.50 (s, 27H, CMe_3 pz); 1.60 (s, 3H, C–H pz); 1.07 (s, 9H, Me); 0.66 (s, 18H , CMe_3 isonitrile).

Preparation of $[Tp^{3\text{-}t\text{-}Bu\text{-}5\text{-}Me}Yb(BH_4)(THF)]$ (4.13)

$[Tp^{3\text{-}t\text{-}Bu\text{-}5\text{-}Me}YbI(THF)]$ (0.200 g, 0.251 mmol) and $NaBH_4$ (0.010 g, 0.264 mmol) were mixed in a Schlenk and cooled to -78 °C. THF (30 ml) was added, the mixture stirred and the temperature allowed to rise to -30 °C. The yellow solution was maintained at approximately this temperature for *ca* 6 hr, during which time stirring was continued. The reaction solvent was then removed under reduced pressure and the residue extracted with 30/40 petrol (30 ml) at room temperature. The resultant yellow solution was filtered and the volume of the filtrate reduced to *ca* 10 ml. Cooling to -25 °C gave 0.086 g (0.126 mmol, 50 %) of small, bright yellow crystals of $[Tp^{3\text{-}t\text{-}Bu\text{-}5\text{-}Me}Yb(BH_4)(THF)]$.

IR (KBr): 2557 cm^{-1} (B–H Tp); 2464, 2397, 2287 (sh), 2222, 2170 (sh) cm^{-1} (B–H BH_4). ^1H NMR (C_6D_6): δ 5.69 (s, 3H, C–H pz); 3.23 (m, 4H, THF); 2.19 (s, 9H, Me); 1.45 (s, 27H, CMe_3); 1.12 (m, 4H, THF). ^{13}C NMR (C_6D_6): δ 163.6, 145.2 (s, 3- and 5-C pz); 103.1 (d, C–H pz); 69.1 (t, THF); 32.2 (s, *C*Me_3); 31.6 (q, C*Me*$_3$); 25.5 (t, THF); 13.5 (q, Me). ^{11}B NMR (C_6D_6): δ -8.3 (Tp), -30.4 (BH_4). UV/vis (THF): 443 nm (ε = 400). Analysis (%) calculated for $C_{28}H_{48}N_6BIOYb$: C, 49.21; H, 7.67; N, 12.30. Found: C, 48.07; H, 7.59; N, 11.89.

Preparation of [Tp$^{3\text{-}t\text{-Bu-5-Me}}$Yb($BH_4$)(3,5-$Me_2$py)$_n$] (4.14)

A solution of [Tp$^{3\text{-}t\text{-Bu-5-Me}}$Yb($BH_4$)(THF)] (*ca* 0.030 g, 0.042 mmol) in 5 ml 30/40 petrol was prepared, and to this five drops of 3,5-dimethylpyridine (3,5-Me_2py) added. Slow evaporation of the solvent through a small hole in the cap of the vial gave dark red crystals of [Tp$^{3\text{-}t\text{-Bu-5-Me}}$Yb($BH_4$)(3,5-$Me_2$py)$_n$] (n ≈1.5).

IR (KBr): 2554, (2523) cm^{-1} (B–H Tp); 2400, 2258, 2221, 2168 cm^{-1} (B–H BH_4). ^1H NMR (C_6D_6): δ 7.95 (br s, 2,6-H py); 6.59 (br s, 4-H py); 5.66 (s, C–H pz); 2.29 (s, Me pz); 1.69 (s, Me py); 1.34 (s, CMe_3). ^{13}C NMR (C_6D_6): δ 163.8, 145.1 (s, 3- and 5-C pz); 147.7 (d, 2-C py); 137.5 (d, 4-C py); 132.8 (s, 3-C py); 103.2 (d, C–H pz); 31.7 (s, *C*Me_3); 31.3 (q, C*Me*$_3$); 17.8 (q, Me py); 13.5 (q, Me pz). ^{11}B NMR (C_6D_6): δ -8.2 (Tp); -30.2 (BH_4). UV/vis (Toluene): 428 nm.

Reaction of [Tp$^{3\text{-}t\text{-Bu-5-Me}}$SmI(THF)$_2$] with Potassium Benzyl

[Tp$^{3\text{-}t\text{-Bu-5-Me}}$SmI(THF)$_2$].($Et_2O$)$_{0.5}$ (0.200 g, 0.23 mmol) was dissolved in THF (30 ml) and a solution of KCH_2Ph (0.038 g, 0.29 mmol) in THF (20 ml) was added drop-wise. The colour of the solution changed from the dark green to dark green/brown during the addition. Stirring was continued for 30 min, after which the reaction solvent was removed under reduced pressure and the solid extracted with 30/40 petrol. The solution was filtered and concentrated, and upon cooling deposited black crystals of [(Tp$^{3\text{-}t\text{-Bu-5-Me}}$)$_2$Sm].

Analysis (%) calculated for $C_{48}H_{80}N_{12}Sm$: C, 57.81; H, 8.09; N, 16.85. Found: C, 58.21; H, 8.51; N, 16.18. ^1H NMR (C_6D_6): δ 7.86 (s, 27H, CMe_3); 4.03 (br s,

9H, Me); 3.05 (s, 3H, C–H); 2.19 (s, 3H, C–H); 1.80 (s, 9H, Me); -1.11 (s, 27H, CMe_3).

Preparation of $[SmI_2(3,5\text{-}Me_2py)_4]$ (A3.1)

SmI_2.1.65THF (0.098 g, 0.187 mmol) was dissolved in THF (5 ml) and 3,5-dimethylpyridine (3,5-Me_2py; *ca* 0.6 g, 5.6 mmol) was added drop-wise to give a dark green solution. This was layered with 30/40 petrol (10 ml) and, after equilibration, black block-like crystals were deposited. Following removal of solvent, the product was washed with 30/40 petrol (3 × 2 ml) to leave 0.116 g (0.139 mmol, 74 %) of $[SmI_2(3,5\text{-}Me_2py)_4]$.

Solid state CP MAS ^{13}C NMR: δ 147, 114 (aromatic C); 13 (Me); (all resonances were broad, *ca* 1000 Hz). UV/vis (KBr): 450 nm; 660 nm (br sh). Analysis (%) calculated for $SmC_{28}H_{36}N_4I_2$: C, 40.38; H, 4.36; N, 6.73. Found: C, 40.22; H, 4.44; N, 6.90.

Preparation of $[YbI_2(3,5\text{-}Me_2py)_4]$ (A3.2)

YbI_2.1.7THF (0.162 g, 0.295 mmol) was dissolved in THF (5 ml). 3,5-Dimethylpyridine (*ca* 0.5 g, 4.7 mmol) was added drop-wise giving an immediate colour change from pale yellow to dark red. The solution was layered with 30/40 petrol (10 ml) and left to equilibrate for several days. Large black block-like crystals were formed, which were washed with 30/40 petrol (3 × 2 ml). Yield: 0.164 g (0.192 mmol, 65 %).

Solid state CP MAS ^{13}C NMR: δ 149.1, 137.8, 133.8 (aromatic C); 20.3 (Me). UV/vis (KBr): 367 nm; 573 nm. Analysis (%) calculated for $YbC_{28}H_{36}N_4I_2$: C, 39.31; H, 4.24; N, 6.55; I, 29.67. Found: C, 39.15; H, 4.33; N, 6.84; I, 29.25.

Preparation of $SmI_2(py)_n$ (A3.3)

SmI_2.1.65THF (0.200 g, 0.382 mmol) was dissolved in THF (20 ml) and pyridine (*ca* 0.60 g, 7.6 mmol) was added drop-wise, giving an immediate colour change from dark blue to dark green. The solution was layered with 30/40 petrol (20 ml) and left to equilibrate for several days. Large black

crystals were formed which desolvated rapidly upon removing the solvent and washing with 30/40 petrol (3 × 2 ml). Yield: *ca* 0.25 g.

Preparation of $YbI_2(py)_n$ (A3.4)

YbI_2 (0.400 g, 0.897 mmol) was dissolved in THF (20 ml) and Yb metal removed by vacuum filtration. Pyridine (py; *ca* 1.0 g, 13 mmol) was then added drop-wise, giving an immediate colour change from pale yellow to dark red. The solution was layered with 30/40 petrol (20 ml) and left to equilibrate for several days. Large black crystals were formed which desolvated and turned dark brown/red on the surface upon removing the solvent and washing with 30/40 petrol (3 × 2 ml). Yield: 0.49 g.

Analysis (%) calculated for $YbC_{17}H_{17}N_{3.4}I_2$ ($YbI_2(py)_{3.4}$): C, 29.35; H, 2.46; N, 6.84. Found: C, 29.31; H, 2.56; N, 6.86.

Preparation of $[SmI_2(4\text{-}Bu^tpy)_4]$ (A3.5)

SmI_2.1.65THF (0.212 g, 0.405 mmol) was dissolved in THF (5 ml) and *tert*-butylpyridine (*ca* 1.0 g, 7.4 mmol) was added. The dark green solution was layered with 30/40 petrol (10 ml) and, after equilibration, large black blocks were deposited which were washed with 30/40 petrol (3 × 2 ml). The surface of the crystals became opaque on standing. Yield: 0.225 g (0.238 mmol, 59 %).

^1H NMR (C_6D_6): δ 4.36 (s, $w_{1/2}$ = 50 Hz, 8H, 2,6-H py); 2.90 (s, $w_{1/2}$ = 21 Hz, 8H, 3,5-H py); -0.27 (s, 36H, CMe_3). ^{13}C NMR (C_6D_6): δ 225.3 (d, $w_{1/2}$ = 16 Hz, 2-C py); 175.0 (s, 4-C py); 103.5 (d, 3-C py); 33.9 (q, CMe_3 py); 28.2 (s, CMe_3 py). UV/vis (Toluene): 381 nm (ε = 700); 443 nm (ε = 700); 642 nm (ε = 500). Analysis (%) calculated for $SmC_{36}H_{52}N_4I_2$: C, 45.76; H, 5.55; N, 5.93. Found: C, 44.13; H, 5.28; N, 5.99.

Preparation of $[YbI_2(4\text{-}Bu^tpy)_4]$ (A3.6)

YbI_2 (0.168 g, 0.385 mmol) was dissolved in THF (5 ml) and Yb metal removed by vacuum filtration. *tert*-Butylpyridine (*ca* 0.5 g, 3.7 mmol) was

added drop-wise, causing an immediate colour change from pale yellow to dark red. The solution was layered with 30/40 petrol (10 ml) and left to equilibrate for several days. Black crystals were formed which were washed with 30/40 petrol (3 × 2 ml) and dried under dynamic vacuum. Yield: 0.210 g (0.217 mmol, 56 %).

^{1}H NMR (C_6D_6): δ 9.73 (s, $w_{1/2}$ = 17 Hz, 8H, 2,6-H py); 6.68 (s, $w_{1/2}$ = 14 Hz, 8H, 3,5-H py); 0.79 (s, 36H, CMe_3). ^{13}C NMR (C_6D_6): δ 161.3 (s, 4-C py); 151.2 (d, 2-C py); 121.1 (d, 3-C py); 34.5 (s, *C*Me_3 py); 30.0 (q, C*Me*$_3$ py). UV/vis (Toluene): 359 nm (ε = 800); 410 nm (ε = 800); 480 nm (ε = 700). Analysis (%) calculated for $YbC_{36}H_{52}N_4I_2$: C, 44.68; H, 5.42; N, 5.79. Found: C, 50.31; H, 5.92; N, 6.51.

Appendix 1 - Crystallographic Details

Except for **3.15** and **3.18**, all measurements were made on a Nicolet R3mV four circle diffractometer using Mo-Kα radiation (λ = 0.71073 Å). Solution and refinement of the data were carried out using the SHELXTL PLUS suite of programs[261] on a MicroVAX II computer. Selected crystals were mounted and sealed in lithium glass (Lindemann) capillaries of diameter 0.3 to 0.7 mm. Following inspection under a polarising microscope, rotation photographs were taken of those crystals which appeared to be well formed and single. At least 28 reflections were measured and used to determine the orientation matrix and the unit cell of the crystal. The dimensions of the unit cell were confirmed by taking axial photographs. Data were collected by ω-2θ scans (or ω scans when one or more of the unit cell axes was greater than 23 Å), with the range of 2θ usually being 5 to 50°. The intensities of three standard reflections were remeasured at intervals of 100 reflections during the data collection - significant crystal decay was not observed for any of the structures presented. The data sets were corrected for Lorentz and polarisation effects, and empirical absorption corrections were applied. Structures were solved initially using either Patterson or direct methods, and the solutions developed using alternating cycles of difference Fourier syntheses and full matrix least-squares procedures. In general, in the final structure, all non-hydrogen atoms were modelled anisotropically, whilst hydrogen atoms were placed in idealised positions, with C–H and B–H bond lengths being fixed at 0.96 Å and the isotropic thermal parameter (U) set to 0.08 Å^2.

For complexes **3.15** and **3.18**, samples of the crystals in the mother liquor were sent in sealed tubes to Dr Mark Elsegood. Measurements were made on a Siemens SMART CCD diffractometer fitted with an area detector and a variable temperature unit. The crystals were examined and mounted in degassed oil which was frozen in a stream of cold nitrogen on the diffractometer.[211] Data collection, and solution and refinement of the structures were all carried out using standard SHELX-93 procedures.

Table A1.1 lists the experimental conditions and results of the refinements for all structures presented in this thesis. There then follow tables of fractional coordinates, bond lengths and bond angles for each structure.

Table A1.1 Crystallographic Collection Data

Compound	$[(Tp^{Me2})_2NdOTf]$ **(2.3)**	$[(Tp^{Me2})_2Yb]^+[OTf]^-$ **(2.6)**	$[(Tp^{Me2})_2Eu]$ **(3.2)**
Structure number	STR384	STR356	STR505
Molecular formula	$C_{31}H_{44}N_{12}B_2F_3O_3S_1Nd_1$	$C_{31}H_{44}N_{12}B_2F_3O_3S_1Yb_1$	$C_{30}H_{44}N_{12}B_2Eu$
Molecular weight	887.79	916.59	746.44
Space group	$P2_1/c$ (No. 14)	$C2/m$ (No. 11)	$R\bar{3}$ (No. 148)
a (Å)	17.629(3)	16.593(7)	11.136(2)
b (Å)	12.740(2)	13.671(5)	11.136(2)
c (Å)	18.163(3)	8.746(2)	25.211(6)
α (°)	90	90	90
β (°)	107.35(1)	91.66(3)	90
γ (°)	90	90	120
U (Å^3)	3893(1)	1983(1)	2707(1)
ρ (calc) Mg m^{-3}	1.51	1.53	1.37
Z	4	2	3
Crystal size (mm)	0.50 × 0.40 × 0.06	0.32 × 0.34 × 0.75	0.60 × 0.3 × 0.85
Crystal colour	Pale blue	White	Orange
F(000)	1804	922	1143
Absorption coefficient μ (Mo K$_\alpha$) (cm^{-1})	14.6	24.6	17.80
Temperature (K)	291	291	303
Radiation (Å)	0.71073	0.71073	0.71073
2θ range (°)	$5 \leq 2\theta \leq 50$	$5 \leq 2\theta \leq 50$	$5 \leq 2\theta \leq 55$
Scan type	$\omega - 2\theta$	$\omega - 2\theta$	ω
Number of reflections	7441	3725	4964
Number of unique reflections	6862	1888	4755
Reflections in final refinement ($I \geq 3\sigma(I)$)	4756	1807	1366
Variables	478	137	69
w^{-1}	$\sigma F^2 + 0.000473(F)^2$	$\sigma F^2 + 0.002663(F)^2$	$\sigma F^2 + 0.002771(F)^2$
R†	0.0456	0.0405	0.0279
R_w§	0.0458	0.0416	0.0290
GOF¶	1.43	0.97	0.707
Largest residual peak (e/Å^3)	0.65	2.20	0.46
$(\Delta/\sigma)_{max}$	0.001	0.011	0.003

† $R = \Sigma||F_o| - |F_c|| / \Sigma|F_o|$

§ $R_w = [\Sigma w(|F_o| - |F_c|)^2 / \Sigma w|F_o|^2]^{1/2}$

¶ $GOF = [\Sigma(|F_o| - |F_c|)^2 / \Sigma(N_{reflns} - N_{params})]^{1/2}$

Table A1.1 Crystallographic Collection Data

Compound	$[(Tp^{Me2})_2Yb]$ **(3.3)**	$[(Tp^{Me2})_2Yb]^+ [TCNE]^-.(THF)_6$ **(3.15)**	$[(\eta^3\text{-}Tp^{Me2})Sm(\eta^3\text{-}(HB(\mu\text{-}O)(pz^{Me2})_2)]_2.(THF)_2$ **(3.18)**
Structure number	STR372	AS1	AS4
Molecular formula	$C_{30}H_{44}N_{12}B_2Yb$	$C_{60}H_{92}N_{16}O_6Yb$	$C_{58}H_{90}B_4N_{20}O_4Sm_2$
Molecular weight	767.52	664.08	1475.44
Space group	$R\bar{3}$ (No. 148)	$P\bar{1}$	$P\bar{1}$
a (Å)	11.063(1)	8.6167(5)	10.1022(5)
b (Å)	11.063(1)	14.1546(9)	13.3623(11)
c (Å)	25.006(4)	14.7438(9)	13.6445(11)
α (°)	90	72.247(2)	87.048(2)
β (°)	90	79.609(2)	74.120(2)
γ (°)	120	79.668(2)	71.865(2)
U (Å^3)	2650(1)	1669.6(2)	1682.4(2)
ρ (calc) Mg m^{-3}	1.44	1.321	1.456
Z	3	2	1
Crystal size (mm)	0.35 × 0.22 × 0.15	0.78 × 0.42 × 0.33	0.43 × 0.18 × 0.14
Crystal Colour	Red/purple	Yellow/orange	Yellow
F(000)	1164	692	754
Absorption coefficient μ (Mo K_α) (cm^{-1})	26.7	14.60	17.87
Temperature (K)	298	180(2)	160(2)
Radiation (Å)	0.71073	0.71073	0.71073
2θ range (°)	$5 \leq 2\theta \leq 50$	$3.58 \leq 2\theta \leq 52.78$	$3.10 \leq 2\theta \leq 50$
Scan type	ω	ω	ω
Number of reflections	3580	9074	8919
Number of unique reflections	1273	6335	5876
Reflections in final refinement ($I \geq 3\sigma(I)$)*	1038	6335	5563
Variables	69	382	435
w^{-1}	$\sigma F^2 + 0.000510(F)^2$	0.0730	0.0384
R†	0.00402	0.0308	0.0293
R_w§	0.00405	0.0829	0.0752
GOF¶	1.423	1.069	1.096
Largest residual peak (e/Å^3)	1.01	0.903	2.86
$(\Delta/\sigma)_{max}$	0.001	0.004	0.014

† $R = \Sigma||F_o| - |F_c|| / \Sigma|F_o|$

§ $R_W = [\Sigma w(|F_o| - |F_c|)^2 / \Sigma w|F_o|^2]^{1/2}$

¶ $GOF = [\Sigma(|F_o| - |F_c|)^2 / \Sigma(N_{reflns} - N_{params})]^{1/2}$

* $I \geq 2\sigma(I)$ for complexes 3.15 and 3.18

Table A1.1 Crystallographic Collection Data

Compound	$[(Tp^{Me_2\text{-}4\text{-}Et})_2Sm(\eta^2\text{-}O_2N)]$ **(3.19)**	$[(Tp^{3\text{-}t\text{-}Bu\text{-}5\text{-}Me})SmI(THF)_2].(Et_2O)_{0.5}$ **(4.1)**	$[(Tp^{3\text{-}t\text{-}Bu\text{-}5\text{-}Me})YbI(THF)]$ **(4.2)**
Structure number	STR503	STR423	STR408
Molecular formula	$C_{42}H_{68}N_{13}B_2O_2Sm$	$C_{34}H_{61}N_6B_1O_3SmI_1$	$C_{28}H_{48}N_6B_1O_1Yb_1I_1$
Molecular weight	790.75	881.1	871.73
Space group	*C*2/*c*	*C*2/*m* (No. 11)	$P2_1/n$
a (Å)	21.435(4)	21.609(3)	11.407(2)
b (Å)	18.639(5)	12.869(2)	16.216(5)
c (Å)	13.416(4)	15.323(3)	18.789(7)
α (°)	90	90	90
β (°)	120.41(2)	98.35(1)	99.44(2)
γ (°)	90	90	90
U (Å^3)	4622(2)	4216(1)	3248(2)
ρ (calc) Mg m^{-3}	1.36	1.39	1.69
Z	4	4	4
Crystal size (mm)	0.40 × 0.22 × 0.10	0.44 × 0.50 × 0.60	0.40 × 0.15 × 0.75
Crystal colour	White	Dark green/black	Yellow
F(000)	1976	1784	1584
Absorption coefficient μ (Mo K$_\alpha$) (cm^{-1})	13.2	21.6	36.5
Temperature (K)	293	291	291
Radiation (Å)	0.71073	0.71073	0.71073
2θ range (°)	$5 \leq 2\theta \leq 50$	$5 \leq 2\theta \leq 50$	$5 \leq 2\theta \leq 50$
Scan type	ω-2θ	$\omega - 2\theta$	ω-2θ
Number of reflections	5628	4951	6872
Number of unique reflections	5321	4739	5986
Reflections in final refinement ($I \geq 3\sigma(I)$)	3810	2917	3961
Variables	272	221	321
w^{-1}	$\sigma F^2 + 0.000315(F)^2$	$\sigma F^2 + 0.000819(F)^2$	$\sigma F^2 + 0.000314(F)^2$
R†	0.0472	0.0408	0.0510
R_w§	0.0450	0.0441	0.0511
GOF¶	1.52	1.33	1.97
Largest residual peak (e/Å^3)	0.65	0.60	1.30
$(\Delta/\sigma)_{max}$	0.001	0.001	0.001

† $R = \Sigma||F_o| - |F_c|| / \Sigma|F_o|$

§ $R_w = [\Sigma w(|F_o| - |F_c|)^2 / \Sigma w|F_o|^2]^{1/2}$

¶ $GOF = [\Sigma(|F_o| - |F_c|)^2 / \Sigma(N_{reflns} - N_{params})]^{1/2}$

Table A1.1 Crystallographic Collection Data

Compound	[(Tp$^{3\text{-}t\text{-Bu-5-Me}}$) YbI(3,5-Me$_2$py)$_2$] (**4.9b**)	[(Tp$^{3\text{-}t\text{-Bu-5-Me}}$) YbI(CNBu^t)] (**4.10**)
Structure number	STR425	STR431
Molecular formula	$C_{38}H_{58}N_8B_1Yb_1I_1$	$C_{29}H_{49}N_7B_1Yb_1$
Molecular weight	937.8	806.5
Space group	*C*2/*c*	$P2_1/n$
a (Å)	40.690(8)	10.581(2)
b (Å)	11.354(1)	21.878(6)
c (Å)	20.769(5)	16.443(4)
α (°)	90	90
β (°)	115.14(2)	90.70(2)
γ (°)	90	90
U (Å^3)	8686(3)	3667(1)
ρ (calc) Mg m^{-3}	1.43	1.53
Z	8	4
Crystal size (mm)	0.14 × 0.85 × 0.65	0.20 × 0.60 × 0.60
Crystal Colour	Red	Orange
F(000)	3760	1600
Absorption coefficient μ (Mo K$_\alpha$) (cm^{-1})	28.8	34.0
Temperature (K)	291	298
Radiation (Å)	0.71073	0.71073
2θ range (°)	5 ≤ 2θ ≤ 50	5 ≤ 2θ ≤ 50
Scan type	ω	$\omega - 2\theta$
Number of reflections	9351	7307
Number of unique reflections	8953	6989
Reflections in final refinement ($I \geq 3\sigma(I)$)	5385	4875
Variables	442	350
w^{-1}	$\sigma F^2 + 0.002024(F)^2$	$\sigma F^2 + 0.000991(F)^2$
R[†]	0.0393	0.0387
R_w[§]	0.0442	0.0408
GOF[¶]	1.03	1.41
Largest residual peak (e/Å^3)	0.62	0.74
$(\Delta/\sigma)_{max}$	0.002	0.108

† $R = \Sigma||F_o| - |F_c|| / \Sigma|F_o|$

§ $R_w = [\Sigma w(|F_o| - |F_c|)^2 / \Sigma w|F_o|^2]^{1/2}$

¶ $GOF = [\Sigma(|F_o| - |F_c|)^2 / \Sigma(N_{reflns} - N_{params})]^{1/2}$

Table A1.1 Crystallographic Collection Data

Compound	$[SmI_2(3,5\text{-}Me_2py)_4]$ **(A3.1)**	$[YbI_2(3,5\text{-}Me_2py)_4]$ **(A3.2)**
Structure number	STR394	STR417
Molecular formula	$C_{28}H_{36}N_4I_2Sm$	$C_{28}H_{36}N_4I_2Yb$
Molecular weight	832.84	855.52
Space group	$I\bar{4}$	$I\bar{4}$
a (Å)	9.834(1)	9.711(1)
b (Å)	9.834(1)	9.711(1)
c (Å)	17.216(3)	17.124(6)
α (°)	90	90
β (°)	90	90
γ (°)	90	90
U (Å^3)	1665(2)	1614(8)
ρ (calc) Mg m^{-3}	1.66	1.76
Z	2	2
Crystal size (mm)	0.55 × 0.25 × 0.40	0.70 × 0.40 × 0.50
Crystal Colour	Black	Black
F(000)	800	816
Absorption coefficient μ (Mo Kα) (cm^{-1})	36.2	48
Temperature (K)	293	293
Radiation (Å)	0.71073	0.71073
2θ range (°)	$5 \leq 2\theta \leq 50$	$5 \leq 2\theta \leq 50$
Scan type	ω-2θ	ω-2θ
Number of reflections	1141	4129
Number of unique reflections	848	2070
Reflections in final refinement ($I \geq 3\sigma(I)$)	559	1691
Variables	40	80
w^{-1}	$\sigma F^2 + 0.000181(F)^2$	$\sigma F^2 + 0.002134(F)^2$
R†	0.0384	0.0260
R_w§	0.0367	0.314
GOF¶	1.39	0.8290
Largest residual peak (e/Å^3)	0.64	1.43
$(\Delta/\sigma)_{max}$	0.086	0.099

† $R = \Sigma||F_o| - |F_c|| / \Sigma|F_o|$

§ $R_W = [\Sigma w(|F_o| - |F_c|)^2 / \Sigma w|F_o|^2]^{1/2}$

¶ $GOF = [\Sigma(|F_o| - |F_c|)^2 / \Sigma(N_{reflns} - N_{params})]^{1/2}$

Crystal Structure of $[(Tp^{Me2})_2NdOTf]$ (2.3)

The data collection was routine, and the initial structure solution was obtained using direct methods.

Table A1.2 Fractional Atomic Coordinates (Å $\times 10^4$) and Equivalent Isotropic Displacement Parameters U_{eq} (Å$^2 \times 10^3$) for $[(Tp^{Me2})_2NdOTf]$ (**2.3**). Esds in Parentheses

Atom	x	y	z	U_{eq}†
Nd(1)	2330(1)	127(1)	2141(1)	29(1)
B(1)	4430(5)	189(7)	2952(5)	38(3)
B(2)	482(5)	-922(6)	2182(5)	40(3)
N(11)	3369(4)	-1164(4)	2986(3)	41(2)
N(12)	4140(3)	-786(5)	3266(3)	37(2)
N(21)	3462(3)	26(4)	1588(3)	40(2)
N(22)	4233(3)	133(4)	2065(3)	38(2)
N(31)	3263(4)	1234(4)	3134(3)	37(2)
N(32)	4061(4)	1175(4)	3209(3)	38(2)
N(41)	865(3)	438(4)	1321(3)	38(2)
N(42)	315(3)	55(4)	1673(3)	38(2)
N(51)	1620(3)	-1591(5)	1685(3)	40(2)
N(52)	901(3)	-1762(4)	1815(3)	36(2)
N(61)	1742(3)	-333(5)	3226(3)	38(2)
N(62)	972(3)	-693(4)	3017(3)	36(2)
C(11)	2620(5)	-2678(7)	3320(5)	64(4)
C(12)	3349(5)	-2021(5)	3414(4)	44(3)
C(13)	4071(5)	-2184(6)	3949(5)	54(3)
C(14)	4551(5)	-1390(6)	3864(5)	47(3)
C(15)	5402(5)	-1174(8)	4323(5)	62(4)
C(21)	2779(5)	-47(7)	193(4)	63(3)
C(22)	3499(5)	43(5)	860(4)	43(3)
C(23)	4282(5)	158(6)	870(4)	53(3)
C(24)	4731(5)	221(6)	1632(5)	49(3)
C(25)	5606(5)	329(9)	1950(6)	80(4)
C(31)	2344(5)	2442(7)	3500(5)	60(4)
C(32)	3154(5)	2123(6)	3469(4)	43(3)
C(33)	3868(5)	2632(7)	3763(5)	57(4)
C(34)	4422(5)	2034(6)	3588(5)	52(3)
C(35)	5303(6)	2237(8)	3734(6)	88(5)
C(41)	813(5)	1568(7)	181(4)	60(4)
C(42)	445(5)	1059(6)	749(4)	45(3)
C(43)	-336(5)	1110(6)	744(5)	50(3)

C(44)	-417(4)	480(6)	1322(4)	43(3)
C(45)	-1119(5)	244(7)	1573(5)	67(4)
C(51)	2557(5)	-2580(7)	1174(6)	66(4)
C(52)	1792(5)	-2482(6)	1366(4)	43(3)
C(53)	1194(5)	-3208(6)	1286(5)	52(3)
C(54)	638(4)	-2739(5)	1571(4)	38(3)
C(55)	-145(5)	-3171(6)	1626(5)	62(4)
C(61)	2839(5)	-22(7)	4465(4)	62(3)
C(62)	2009(5)	-341(6)	3997(4)	46(3)
C(63)	1401(5)	-681(7)	4280(4)	51(3)
C(64)	774(5)	-901(6)	3664(5)	49(3)
C(65)	-45(5)	-1292(8)	3634(6)	74(4)
C(1)	2382(6)	3849(7)	1432(5)	61(4)
F(1)	2823(4)	4638(4)	1300(3)	79(3)
F(2)	1664(3)	3972(4)	941(4)	97(3)
F(3)	2326(5)	4000(4)	2127(4)	111(4)
S(1)	2823(1)	2602(2)	1322(1)	45(1)
O(1)	2306(3)	1851(4)	1573(3)	48(2)
O(2)	3608(3)	2669(5)	1829(3)	64(2)
O(3)	2726(4)	2554(4)	518(3)	60(2)

† Equivalent isotropic U_{eq} defined as one third of the trace of the orthogonalised U_{ij} tensor

Table A1.3 Bond Lengths (Å) for $[(Tp^{Me2})_2NdOTf]$ (**2.3**). Esds in Parentheses

Nd(1)-N(11)	2.595(6)	Nd(1)-N(21)	2.491(7)
Nd(1)-N(31)	2.485(5)	Nd(1)-N(41)	2.598(5)
Nd(1)-N(51)	2.535(6)	Nd(1)-N(61)	2.553(7)
Nd(1)-O(1)	2.421(5)	B(1)-N(12)	1.518(11)
B(1)-N(22)	1.545(10)	B(1)-N(32)	1.551(11)
B(2)-N(42)	1.525(10)	B(2)-N(52)	1.558(11)
B(2)-N(62)	1.534(10)	N(11)-N(12)	1.387(8)
N(11)-C(12)	1.349(10)	N(12)-C(14)	1.352(9)
N(21)-N(22)	1.384(7)	N(21)-C(22)	1.344(10)
N(22)-C(24)	1.345(11)	N(31)-N(32)	1.373(9)
N(31)-C(32)	1.326(10)	N(32)-C(34)	1.347(10)
N(41)-N(42)	1.399(9)	N(41)-C(42)	1.340(9)
N(42)-C(44)	1.368(9)	N(51)-N(52)	1.375(9)
N(51)-C(52)	1.348(10)	N(52)-C(54)	1.355(8)
N(61)-N(62)	1.375(8)	N(61)-C(62)	1.338(9)
N(62)-C(64)	1.348(12)	C(11)-C(12)	1.500(12)
C(12)-C(13)	1.368(10)	C(13)-C(14)	1.357(12)
C(14)-C(15)	1.508(10)	C(21)-C(22)	1.475(10)

C(22)-C(23)	1.382(12)	C(23)-C(24)	1.376(10)
C(24)-C(25)	1.483(11)	C(31)-C(32)	1.501(13)
C(32)-C(33)	1.375(11)	C(33)-C(34)	1.350(13)
C(34)-C(35)	1.519(13)	C(41)-C(42)	1.519(13)
C(42)-C(43)	1.376(12)	C(43)-C(44)	1.362(12)
C(44)-C(45)	1.472(13)	C(51)-C(52)	1.497(14)
C(52)-C(53)	1.377(11)	C(53)-C(54)	1.375(12)
C(54)-C(55)	1.517(12)	C(61)-C(62)	1.513(11)
C(62)-C(63)	1.388(14)	C(63)-C(64)	1.346(10)
C(64)-C(65)	1.513(13)	C(1)-F(1)	1.335(12)
C(1)-F(2)	1.322(11)	C(1)-F(3)	1.309(13)
C(1)-S(1)	1.805(10)	S(1)-O(1)	1.484(6)
S(1)-O(2)	1.418(5)	S(1)-O(3)	1.420(6)

Table A1.4 Bond Angles (°) for $[(Tp^{Me_2})_2NdOTf]$ (**2.3**). Esds in Parentheses

N(11)-Nd(1)-N(21)	72.3(2)	N(11)-Nd(1)-N(31)	74.5(2)
N(21)-Nd(1)-N(31)	83.4(2)	N(11)-Nd(1)-N(41)	147.3(2)
N(21)-Nd(1)-N(41)	123.7(2)	N(31)-Nd(1)-N(41)	131.2(2)
N(11)-Nd(1)-N(51)	80.7(2)	N(21)-Nd(1)-N(51)	101.6(2)
N(31)-Nd(1)-N(51)	151.9(2)	N(41)-Nd(1)-N(51)	68.6(2)
N(11)-Nd(1)-N(61)	77.1(2)	N(21)-Nd(1)-N(61)	149.1(2)
N(31)-Nd(1)-N(61)	84.5(2)	N(41)-Nd(1)-N(61)	85.1(2)
N(51)-Nd(1)-N(61)	77.3(2)	N(11)-Nd(1)-O(1)	138.3(2)
N(21)-Nd(1)-O(1)	77.8(2)	N(31)-Nd(1)-O(1)	73.7(2)
N(41)-Nd(1)-O(1)	74.3(2)	N(51)-Nd(1)-O(1)	134.4(2)
N(61)-Nd(1)-O(1)	125.3(2)	N(12)-B(1)-N(22)	111.0(6)
N(12)-B(1)-N(32)	109.3(7)	N(22)-B(1)-N(32)	111.6(5)
N(42)-B(2)-N(52)	109.4(7)	N(42)-B(2)-N(62)	113.2(6)
N(52)-B(2)-N(62)	110.8(6)	Nd(1)-N(11)-N(12)	116.0(4)
Nd(1)-N(11)-C(12)	136.0(5)	N(12)-N(11)-C(12)	105.1(5)
B(1)-N(12)-N(11)	123.3(5)	B(1)-N(12)-C(14)	127.4(6)
N(11)-N(12)-C(14)	109.2(6)	Nd(1)-N(21)-N(22)	119.9(4)
Nd(1)-N(21)-C(22)	132.6(5)	N(22)-N(21)-C(22)	106.7(6)
B(1)-N(22)-N(21)	122.0(6)	B(1)-N(22)-C(24)	128.5(6)
N(21)-N(22)-C(24)	109.4(6)	Nd(1)-N(31)-N(32)	118.5(4)
Nd(1)-N(31)-C(32)	131.4(5)	N(32)-N(31)-C(32)	106.6(6)
B(1)-N(32)-N(31)	121.6(5)	B(1)-N(32)-C(34)	129.4(7)
N(31)-N(32)-C(34)	108.7(6)	Nd(1)-N(41)-N(42)	113.0(4)
Nd(1)-N(41)-C(42)	139.5(5)	N(42)-N(41)-C(42)	105.2(6)
B(2)-N(42)-N(41)	121.8(6)	B(2)-N(42)-C(44)	126.1(6)
N(41)-N(42)-C(44)	109.6(6)	Nd(1)-N(51)-N(52)	118.1(4)
Nd(1)-N(51)-C(52)	135.6(5)	N(52)-N(51)-C(52)	106.1(6)

B(2)-N(52)-N(51)	122.9(5)
N(51)-N(52)-C(54)	109.4(6)
Nd(1)-N(61)-C(62)	135.5(5)
B(2)-N(62)-N(61)	123.7(7)
N(61)-N(62)-C(64)	108.5(6)
N(11)-C(12)-C(13)	110.7(7)
C(12)-C(13)-C(14)	106.7(7)
N(12)-C(14)-C(15)	123.2(7)
N(21)-C(22)-C(21)	121.6(8)
C(21)-C(22)-C(23)	129.1(8)
N(22)-C(24)-C(23)	107.7(7)
C(23)-C(24)-C(25)	128.1(9)
N(31)-C(32)-C(33)	109.8(8)
C(32)-C(33)-C(34)	106.6(7)
N(32)-C(34)-C(35)	122.1(8)
N(41)-C(42)-C(41)	122.0(7)
C(41)-C(42)-C(43)	127.2(7)
N(42)-C(44)-C(43)	107.0(7)
C(43)-C(44)-C(45)	130.5(7)
N(51)-C(52)-C(53)	110.4(8)
C(52)-C(53)-C(54)	106.0(7)
N(52)-C(54)-C(55)	122.8(7)
N(61)-C(62)-C(61)	124.4(8)
C(61)-C(62)-C(63)	126.9(7)
N(62)-C(64)-C(63)	108.7(8)
C(63)-C(64)-C(65)	129.5(9)
F(1)-C(1)-F(3)	106.0(7)
F(1)-C(1)-S(1)	110.5(8)
F(3)-C(1)-S(1)	113.2(6)
C(1)-S(1)-O(2)	104.1(4)
C(1)-S(1)-O(3)	103.2(4)
O(2)-S(1)-O(3)	117.7(4)

B(2)-N(52)-C(54)	127.7(7)
Nd(1)-N(61)-N(62)	117.3(4)
N(62)-N(61)-C(62)	107.2(7)
B(2)-N(62)-C(64)	127.5(6)
N(11)-C(12)-C(11)	123.8(6)
C(11)-C(12)-C(13)	125.5(7)
N(12)-C(14)-C(13)	108.2(6)
C(13)-C(14)-C(15)	128.6(7)
N(21)-C(22)-C(23)	109.3(6)
C(22)-C(23)-C(24)	107.0(8)
N(22)-C(24)-C(25)	124.3(7)
N(31)-C(32)-C(31)	121.3(7)
C(31)-C(32)-C(33)	128.9(7)
N(32)-C(34)-C(33)	108.3(7)
C(33)-C(34)-C(35)	129.6(8)
N(41)-C(42)-C(43)	110.7(7)
C(42)-C(43)-C(44)	107.5(6)
N(42)-C(44)-C(45)	122.5(7)
N(51)-C(52)-C(51)	120.3(7)
C(51)-C(52)-C(53)	129.3(7)
N(52)-C(54)-C(53)	108.1(7)
C(53)-C(54)-C(55)	129.1(7)
N(61)-C(62)-C(63)	108.7(7)
C(62)-C(63)-C(64)	106.9(8)
N(62)-C(64)-C(65)	121.8(7)
F(1)-C(1)-F(2)	106.3(7)
F(2)-C(1)-F(3)	107.5(9)
F(2)-C(1)-S(1)	112.8(6)
C(1)-S(1)-O(1)	102.1(4)
O(1)-S(1)-O(2)	114.1(3)
O(1)-S(1)-O(3)	113.1(3)
Nd(1)-O(1)-S(1)	141.4(3)

Crystal Structure of $[(Tp^{Me_2})_2Yb]^+[OTf]^-$ (2.6)

The data collection was routine, and the initial structure solution was obtained using direct methods. The triflate anion lies across the mirror plane, and disorder was modelled by allowing the structure to refine with 50 % occupancy of CF_3 and SO_3 in each site.

Table A1.5 Fractional Atomic Coordinates (Å $\times 10^4$) and Equivalent Isotropic Displacement Parameters U_{eq} (Å$^2 \times 10^3$) for $[(Tp^{Me2})_2Yb]^+[OTf]^-$ (**2.6**). Esds in Parentheses

Atom	x	y	z	U_{eq} †
Yb(1)	0	0	0	43(1)
N(11)	653	1082	-1559	69(2)
N(21)	1244	0	1349	58(2)
N(12)	1454	923	-1824	54(1)
N(22)	1925	0	521	45(2)
B(1)	1888	0	-1252	45(2)
C(21)	1490	0	2802	86(4)
C(22)	2311	0	2909	90(4)
C(23)	2569	0	1474	68(3)
C(13)	1751	1694	-2529	83(2)
C(11)	483	1978	-2145	99(3)
C(12)	1150	2361	-2737	108(3)
C(231)	3408	0	932	122(7)
C(211)	901	0	4073	150(10)
C(111)	-351	2371	-2040	151(6)
C(131)	2612	1769	-2936	139(5)
S(1)	5451	0	4485	63(1)
C(1)	5451	0	4485	63(1)
F(1)	5220	0	2920	104(3)
O(1)	5220	0	2920	104(3)
F(2)	5861	814	4851	153(3)
O(2)	5861	814	4851	153(3)

† Equivalent isotropic U_{eq} defined as one third of the trace of the orthogonalised U_{ij} tensor

Table A1.6 Bond Lengths (Å) for $[(Tp^{Me2})_2Yb]^+[OTf]^-$ (**2.6**). Esds in Parentheses

Yb(l)-N(11)	2.304(5)	Yb(1)-N(21)	2.347(5)
Yb(1)-N(11A)	2.304(5)	Yb(1)-N(11B)	2.304(5)
Yb(1)-N(11C)	2.304(5)	Yb(1)-N(21A)	2.347(6)
N(11)-N(12)	1.373(6)	N(11)-C(11)	1.354(10)
N(21)-N(22)	1.360(8)	N(21)-C(21)	1.324(10)
N(12)-B(1)	1.529(6)	N(12)-C(13)	1.324(9)
N(22)-B(1)	1.550(8)	N(22)-C(23)	1.337(9)
B(1)-N(12A)	1.529(6)	C(21)-C(22)	1.364(14)
C(21)-C(211)	1.501(14)	C(22)-C(23)	1.338(12)
C(23)-C(231)	1.482(13)	C(13)-C(12)	1.360(11)
C(13)-C(131)	1.485(10)	C(11)-C(12)	1.341(12)

C(11)-C(111)	1.491(12)
S(1)-O(1)	1.388(8)
S(1)-O(2)	1.345(9)
S(1)-F(2A)	1.345(9)
C(1)-O(1)	1.388(8)
C(1)-O(2)	1.345(9)

S(1)-F(1)	1.388(8)
S(1)-F(2)	1.345(9)
C(1)-F(2A)	1.345(9)
C(1)-F(1)	1.388(8)
C(1)-F(2)	1.345(9)
C(1)-S(1A)	1.793(7)

Table A1.7 Bond Angles (°) for $[(Tp^{Me2})_2Yb]^+[OTf]^-$ (**2.6**). Esds in Parentheses

N(11)–Yb(1)–N(21)	82.8(2)
N(21)–Yb(1)–N(11A)	97.2(2)
N(21)–Yb(1)–N(11B)	97.2(2)
N(11)–Yb(1)–N(11C)	79.9(3)
N(11A)–Yb(1)–N(11C)	100.1(3)
N(11)–Yb(1)–N(21A)	97.2(2)
N(11A)–Yb(1)–N(21A)	82.8(2)
N(11C)–Yb(1)–N(21A)	97.2(2)
Yb(1)–N(11)–C(11)	135.1(4)
Yb(1)–N(21)–N(22)	117.7(4)
N(22)–N(21)–C(21)	105.9(6)
N(11)–N(12)–C(13)	109.1(5)
Nt21)–N(22)–B(1)	121.5(5)
B(1)–N(22)–C(23)	129.2(6)
N(12)–B(1)–N(12A)	111.1(5)
N(21)–C(21)–C(22)	110.2(8)
C(22)–C(21)–C(211)	128.3(8)
N(22)–C(23)–C(22)	108.3(7)
C(22)–C(23)–C(231)	129.0(8)
N(12)–C(13)–C(131)	122.7(7)
N(11)–C(11)–C(12)	109.6(7)
C(12)–C(11)–C(111)	131.3(8)
F(1)–S(1)–O(1)	0.0(1)
O(1)–S(1)–F(2)	111.7(4)
O(1)–S(1)–O(2)	111.7(4)
F(1)–S(1)–S(1A)	107.6(5)
F(2)–S(1)–S(1A)	106.8(4)
F(1)–S(1)–F(2A)	111.7(4)
F(2)–S(1)–F(2A)	111.8(7)
F(1)–C(1)–F(2)	111.7(4)
F(1)–C(1)–O(2)	111.7(4)
O(1)–C(1)–S(1A)	107.6(5)
O(2)–C(1)–S(1A)	106.8(4)
O(1)–C(1)–F(2A)	111.7(4)

N(11)–Yb(1)–N(11A)	180.0(1)
N(11)–Yb(1)–N(11D)	100.1(3)
N(11A)–Yb(1)–N(11B)	79.9(3)
N(21)–Yb(1)–N(11C)	82.8(2)
N(11B)–Yb(1)–N(11C)	180.0(1)
N(21)–Yb(1)–N(21A)	180.0(1)
N(11B)–Yb(1)–N(21A)	82.8(2)
Yb(1)–N(11)–N(12)	118.2(4)
N(12)–N(11)–C(11)	105.7(5)
Yb(1)–N(21)–C(21)	136.5(6)
N(11)–N(12)–B(1)	121.6(4)
B(1)–N(12)–C(13)	129.2(5)
N(21)–N(22)–C(23)	109.3(6)
N(12)–B(1)–N(22)	109.4(3)
N(22)–B(1)–N(12A)	109.4(3)
N(21)–C(21)–C(211)	121.5(8)
C(21)–C(22)–C(23)	106.4(8)
N(22)–C(23)–C(231)	122.8(8)
N(12)–C(13)–C(12)	108.4(S)
C(12)–C(13)–C(131)	128.9(8)
N(11)–C(11)–C(111)	119.1(7)
C(13)–C(12)–C(11)	107.2(8)
F(1)–S(1)–F(2)	111.7(4)
F(1)–S(1)–O(2)	111.7(4)
F(2)–S(1)–O(2)	0.0(1)
O(1)–S(1)–S(1A)	107.6(5)
O(2)–S(1)–S(1A)	106.8(4)
O(1)–S(1)–F(2A)	111.7(4)
O(2)–S(1)–F(2A)	111.8(7)
O(1)–C(1)–F(2)	111.7(4)
O(1)–C(1)–O(2)	111.7(4)
F(2)–C(1)–S(1A)	106.8(4)
F(1)–C(1)–F(2A)	111.7(4)
F(2)–C(1)–F(2A)	111.8(7)

O(2)–C(1)–F(2A)	111.8(7)	S(1A)–C(1)–F(2A)	106.8(4)

Crystal Structure of $[(Tp^{Me2})_2Eu]$ (3.2)

The data collection was routine, and the initial structure solution was obtained using Patterson methods.

Table A1.8 Fractional Atomic Coordinates (Å $\times 10^4$) and Equivalent Isotropic Displacement Parameters U_{eq} (Å$^2 \times 10^3$) for $[(Tp^{Me2})_2Eu]$ (**3.2**). Esds in Parentheses

Atom	x	y	z	U_{eq} †
Eu(1)	0	0	0	38(1)
B(1)	0	0	1422(2)	39(1)
N(1)	358(2)	-1111(2)	1234(1)	39(1)
N(2)	724(2)	-1179(2)	722(1)	45(1)
C(1)	32(4)	-2347(3)	2099(1)	63(1)
C(2)	408(2)	-2100(2)	1529(1)	45(1)
C(3)	831(3)	-2816(3)	1199(1)	53(1)
C(4)	1014(3)	-2199(3)	704(1)	51(1)
C(5)	1460(5)	-2557(5)	193(2)	77(2)

† Equivalent isotropic U_{eq} defined as one third of the trace of the orthogonalised U_{ij} tensor

Table A1.9 Bond Lengths (Å) for $[(Tp^{Me2})_2Eu]$ (**3.2**). Esds in Parentheses

Eu(1)-N(2)	2.598(3)	Eu(1)-N(2A)	2.598(3)
Eu(1)-N(2B)	2.598(2)	Eu(1)-N(2C)	2.598(2)
Eu(1)-N(2D)	2.598(2)	Eu(1)-N(2E)	2.598(2)
B(1)-N(1)	1.552(3)	B(1)-N(1A)	1.552(2)
B(1)-N(1B)	1.552(2)	N(1)-N(2)	1.365(3)
N(1)-C(2)	1.353(4)	N(2)-C(4)	1.328(5)
C(1)-C(2)	1.485(4)	C(2)-C(3)	1.387(5)
C(3)-C(4)	1.389(5)	C(4)-C(5)	1.504(6)

Table A1.10 Bond Angles (°) for $[(Tp^{Me2})_2Eu]$ (**3.2**). Esds in Parentheses

N(2)-Eu(1)-N(2A)	180.0(1)	N(2)-Eu(1)-N(2B)	76.3(1)
N(2A)-Eu(1)-N(2B)	103.7(1)	N(2)-Eu(1)-N(2C)	103.7(1)
N(2A)-Eu(1)-N(2C)	76.3(1)	N(2B)-Eu(1)-N(2C)	180.0(1)
N(2)-Eu(1)-N(2D)	76.3(1)	N(2A)-Eu(1)-N(2D)	103.7(1)
N(2B)-Eu(1)-N(2D)	76.3(1)	N(2C)-Eu(1)-N(2D)	103.7(1)
N(2)-Eu(1)-N(2E)	103.7(1)	N(2A)-Eu(1)-N(2E)	76.3(1)

N(2B)-Eu(1)-N(2E)	103.7(1)
N(2D)-Eu(1)-N(2E)	180.0(1)
N(1)-B(1)-N(1B)	111.1(2)
B(1)-N(1)-N(2)	122.4(2)
N(2)-N(1)-C(2)	109.8(2)
Eu(1)-N(2)-C(4)	132.6(2)
N(1)-C(2)-C(1)	124.1(3)
C(1)-C(2)-C(3)	128.3(3)
N(2)-C(4)-C(3)	110.6(3)
C(3)-C(4)-C(5)	128.6(4)

N(2C)-Eu(1)-N(2E)	76.3(1)
N(1)-B(1)-N(1A)	111.1(2)
N(1A)-B(1)-N(1B)	111.1(2)
B(1)-N(1)-C(2)	127.8(2)
Eu(1)-N(2)-N(1)	117.2(2)
N(1)-N(2)-C(4)	106.7(2)
N(1)-C(2)-C(3)	107.6(2)
C(2)-C(3)-C(4)	105.2(3)
N(2)-C(4)-C(5)	120.8(3)

Crystal Structure of $[(Tp^{Me2})_2Yb]$ (3.3)

The data collection was routine, and the initial structure solution was obtained using Patterson methods.

Table A1.11 Fractional Atomic Coordinates (Å $\times 10^4$) and Equivalent Isotropic Displacement Parameters U_{eq} (Å$^2 \times 10^3$) for $[(Tp^{Me2})_2Yb]$ (**3.3**). Esds in Parentheses

Atom	x	y	z	U_{eq} †
Yb(1)	0	0	0	33(1)
N(1)	763(5)	1895(5)	671(2)	41(2)
N(2)	387(5)	1466(5)	1193(2)	38(2)
B(1)	0	0	1387(4)	37(3)
C(11)	1073(6)	3220(6)	645(2)	46(3)
C(12)	908(6)	3669(7)	1155(3)	50(3)
C(13)	468(6)	2554(6)	1480(2)	44(3)
C(111)	1539(9)	4016(7)	132(3)	71(4)
C(131)	86(7)	2412(8)	2064(3)	58(3)

† Equivalent isotropic U_{eq} defined as one third of the trace of the orthogonalised U_{ij} tensor

Table A1.12 Bond Lengths (Å) for $[(Tp^{Me2})_2Yb]$ (**3.3**). Esds in Parentheses

Yb(1)-N(1)	2.480(4)
Yb(1)-N(1B)	2.480(4)
Yb(1)-N(1D)	2.480(3)
N(1)-N(2)	1.381(5)
N(2)-B(1)	1.534(6)
B(1)-N(2A)	1.534(5)
C(11)-C(12)	1.412(9)

Yb(1)-N(1A)	2.480(4)
Yb(1)-N(1C)	2.480(4)
Yb(1)-N(1E)	2.480(3)
N(1)-C(11)	1.330(9)
N(2)-C(13)	1.364(9)
B(1)-N(2B)	1.534(3)
C(11)-C(111)	1.495(9)

C(12)-C(13)	1.349(9)	C(13)-C(131)	1.506(8)

Table A1.13 Bond Angles (°) for $[(Tp^{Me2})_2Yb]$ (**3.3**). Esds in Parentheses

N(1)-Yb(1)-N(1A)	180.0(1)	N(1)-Yb(1)-N(1B)	79.3(1)
N(1A)-Yb(1)-N(1B)	100.7(1)	N(1)-Yb(1)-N(1C)	100.7(1)
N(1A)-Yb(1)-N(1C)	79.3(1)	N(1B)-Yb(1)-N(1C)	180.0(1)
N(1)-Yb(1)-N(1D)	79.3(1)	N(1A)-Yb(1)-N(1D)	100.7(1)
N(1B)-Yb(1)-N(1D)	79.3(1)	N(1C)-Yb(1)-N(1D)	100.7(1)
N(1)-Yb(1)-N(1E)	100.7(1)	N(1A)-Yb(1)-N(1E)	79.3(1)
N(1B)-Yb(1)-N(1E)	100.7(1)	N(1C)-Yb(1)-N(1E)	79.3(1)
N(1D)-Yb(1)-N(1E)	180.0(1)	Yb(1)-N(1)-N(2)	115.7(3)
Yb(1)-N(1)-C(11)	133.7(4)	N(2)-N(1)-C(11)	106.9(5)
N(1)-N(2)-B(1)	122.5(5)	N(1)-N(2)-C(13)	108.6(5)
B(1)-N(2)-C(13)	128.8(5)	N(2)-B(1)-N(2A)	110.6(4)
N(2)-B(1)-N(2B)	110.6(4)	N(2A)-B(1)-N(2B)	110.6(4)
N(1)-C(11)-C(12)	109.7(5)	N(1)-C(11)-C(111)	120.9(6)
C(12)-C(11)-C(111)	129.4(7)	C(11)-C(12)-C(13)	105.9(6)
N(2)-C(13)-C(12)	108.9(5)	N(2)-C(13)-C(131)	121.8(6)
C(12)-C(13)-C(131)	129.3(7)		

Crystal Structure of $[(Tp^{Me2})_2Yb]^+[TCNE]^-.(THF)_6$ (3.15)

The structure was determined by Dr Mark Elsegood, University of Newcastle.

Table A1.14 Fractional Atomic Coordinates (Å) and Equivalent Isotropic Displacement Parameters U_{eq} ($Å^2$) for $[(Tp^{Me2})_2Yb]^+[TCNE]^-.(THF)_6$ (**3.15**). Esds in Parentheses

Atom	x	y	z	U_{eq}†
B1	0.4284(4)	0.3088(2)	0.4286(2)	0.0357(6)
N1	0.3429(3)	0.3723(2)	0.5772(2)	0.0396(5)
N2	0.3430(3)	0.3000(2)	0.5322(2)	0.0361(4)
C1	0.2587(4)	0.3426(3)	0.6652(2)	0.0462(6)
C2	0.2077(4)	0.2514(3)	0.6767(2)	0.0520(7)
C3	0.2628(4)	0.2268(2)	0.5923(2)	0.0435(6)
C4	0.2322(6)	0.4034(4)	0.7346(3)	0.0650(10)
C5	0.2425(5)	0.1353(3)	0.5671(3)	0.0627(9)
N3	0.6742(3)	0.3701(2)	0.4542(2)	0.0370(5)
N4	0.6107(3)	0.3013(2)	0.4277(2)	0.0370(5)
C6	0.8327(3)	0.3424(2)	0.4466(2)	0.0434(6)
C7	0.8704(4)	0.2567(3)	0.4157(3)	0.0562(8)

C8	0.7277(4)	0.2328(3)	0.4046(3)	0.0506(7)
C9	0.9403(4)	0.4007(3)	0.4699(3)	0.0572(9)
C10	0.6983(5)	0.1474(4)	0.3722(5)	0.083(2)
N5	0.3799(3)	0.4995(2)	0.3709(2)	0.0406(5)
N6	0.3670(3)	0.4090(2)	0.3586(2)	0.0370(5)
C11	0.3159(4)	0.5715(3)	0.2995(2)	0.0493(7)
C12	0.2618(4)	0.5276(3)	0.2411(2)	0.0550(8)
C13	0.2961(4)	0.4253(3)	0.2798(2)	0.0477(7)
C14	0.3112(6)	0.6795(3)	0.2906(3)	0.0668(10)
C15	0.2646(6)	0.3427(4)	0.2446(3)	0.0691(11)
C16	0.9568(5)	0.0415(4)	0.0134(3)	0.0697(11)
C17	0.8795(7)	0.0317(5)	0.1096(3)	0.0815(13)
N7	0.8188(8)	0.0260(5)	0.1851(3)	0.112(2)
C18	0.9449(6)	0.1375(5)	-0.0547(3)	0.0794(14)
N8	0.9344(6)	0.2153(4)	-0.1078(3)	0.097(2)
O1	0.2296(16)	0.5426(11)	0.0003(9)	0.157(5)
C19	0.3682(23)	0.5690(29)	-0.0805(18)	0.291(24)
C20	0.2874(20)	0.6104(15)	-0.1634(9)	0.130(5)
C21	0.1393(27)	0.6444(23)	-0.1417(13)	0.193(11)
C22	0.1041(19)	0.6223(14)	-0.0328(11)	0.143(6)
O1A	0.1394(20)	0.6901(14)	-0.1264(15)	0.156(8)
C19A	0.0859(25)	0.5844(19)	-0.0952(27)	0.174(12)
C20A	0.2243(34)	0.5197(18)	-0.0565(30)	0.204(16)
C21A	0.3474(22)	0.5519(15)	-0.0958(16)	0.113(6)
C22A	0.3203(20)	0.6593(14)	-0.1559(14)	0.110(6)
O2	0.3720(12)	0.9241(8)	0.3143(9)	0.126(4)
C23	0.2132(16)	0.9537(12)	0.2715(12)	0.116(4)
C24	0.1276(15)	1.0328(12)	0.3113(13)	0.119(5)
C25	0.2090(14)	1.0737(8)	0.3455(8)	0.080(3)
C26	0.3670(16)	1.0178(11)	0.3527(11)	0.110(4)
O2A	0.2086(17)	0.9211(11)	0.3301(12)	0.135(5)
C23A	0.1554(21)	1.0083(15)	0.3752(15)	0.125(6)
C24A	0.2793(25)	1.0631(14)	0.3531(14)	0.110(5)
C25A	0.3913(21)	1.0404(16)	0.2912(17)	0.132(7)
C26A	0.3582(24)	0.9615(16)	0.2570(16)	0.130(7)
O3	0.5234(13)	0.1385(9)	-0.0226(9)	0.143(4)
C27	0.5188(15)	0.2380(10)	-0.0018(10)	0.112(4)
C28	0.3515(21)	0.2537(18)	0.0434(17)	0.167(9)
C29	0.2638(14)	0.2207(12)	0.0058(12)	0.125(5)
C30	0.3500(16)	0.1519(11)	-0.0453(11)	0.107(4)
O3A	0.3331(35)	0.1214(18)	0.0364(20)	0.235(13)
C27A	0.4390(45)	0.1785(21)	0.0770(18)	0.203(15)
C28A	0.3912(33)	0.2810(15)	0.0114(19)	0.131(8)
C29A	0.4072(38)	0.2710(18)	-0.0706(17)	0.169(12)

C30A	0.4100(48)	0.1698(23)	-0.0733(18)	0.187(15)

† Equivalent isotropic U_{eq} defined as one third of the trace of the orthogonalised U_{ij} tensor

Table A1.15 Bond Lengths (Å) for $[(Tp^{Me2})_2Yb]^+[TCNE]^-.(THF)_6$ (**3.15**). Esds in Parentheses

Yb1-N5	2.327(2)	Yb1-N1	2.338(2)
Yb1-N3	2.344(2)	B1-N6	1.547(4)
B1-N2	1.551(4)	B1-N4	1.553(4)
N1-C1	1.350(4)	N1-N2	1.377(4)
N2-C3	1.346(4)	C1-C2	1.389(5)
C1-C4	1.492(5)	C2-C3	1.374(5)
C3-C5	1.498(5)	N3-C6	1.346(4)
N3-N4	1.378(3)	N4-C8	1.341(4)
C6-C7	1.387(5)	C6-C9	1.490(4)
C7-C8	1.381(5)	C8-C10	1.504(5)
N5-C11	1.344(4)	N5-N6	1.374(4)
N6-C13	1.348(4)	C11-C12	1.385(5)
C11-C14	1.488(5)	C12-C13	1.382(5)
C13-C15	1.500(5)	C16-C16	1.398(11)
C16-C18	1.421(7)	C16-C17	1.432(6)
C17-N7	1.126(7)	C18-N8	1.140(7)

Table A1.16 Bond Angles (°) for $[(Tp^{Me2})_2Yb]^+[TCNE]^-.(THF)_6$ (**3.15**). Esds in Parentheses

N5-Yb1-N5A	180.0	N5-Yb1-N1	80.65(9)
N5A-Yb1-N1	99.35(9)	N1-Yb1-N1A	180.0
N5-Yb1-N3	81.93(8)	N5A-Yb1-N3	98.07(8)
N1-Yb1-N3	82.74(8)	N1A-Yb1-N3	97.26(8)
N3-Yb1-N3A	180.0	N6-B1-N2	110.7(2)
N6-B1-N4	110.0(2)	N2-B1-N4	109.4(2)
C1-N1-N2	106.6(2)	C1-N1-Yb1	134.9(2)
N2-N1-Yb1	118.1(2)	C3-N2-N1	109.4(2)
C3-N2-B1	129.2(3)	N1-N2-B1	121.5(2)
N1-C1-C2	109.5(3)	N1-C1-C4	121.7(3)
C2-C1-C4	128.8(3)	C3-C2-C1	106.2(3)
N2-C3-C2	108.4(3)	N2-C3-C5	123.5(3)
C2-C3-C5	128.1(3)	C6-N3-N4	106.5(2)
C6-N3-Yb1	135.2(2)	N4-N3-Yb1	118.3(2)
C8-N4-N3	109.7(2)	C8-N4-B1	129.1(3)
N3-N4-B1	121.1(2)	N3-C6-C7	109.6(3)
N3-C6-C9	121.2(3)	C7-C6-C9	129.2(3)

C8-C7-C6	106.1(3)
N4-C8-C10	123.1(3)
C11-N5-N6	107.4(3)
N6-N5-Yb1	118.4(2)
C13-N6-B1	129.4(3)
N5-C11-C12	109.3(3)
C12-C11-C14	129.2(3)
N6-C13-C12	108.2(3)
C12-C13-C15	128.6(3)
C16-C16-C17	120.8(6)
N7-C17-C16	178.7(7)

N4-C8-C7	108.1(3)
C7-C8-C10	128.9(3)
C11-N5-Yb1	134.2(2)
C13-N6-N5	108.9(3)
N5-N6-B1	121.7(2)
N5-C11-C14	121.6(3)
C13-C12-C11	106.2(3)
N6-C13-C15	123.2(3)
C16-C16-C18	120.5(5)
C18-C16-C17	118.8(5)
N8-C18-C16	178.7(6)

Crystal Structure of $[(\eta^3\text{-}Tp^{Me_2})Sm(\eta^3\text{-}(HB(\mu\text{-}O)(pz^{Me_2})_2)]_2.(THF)_2$ (3.18)

The structure was determined by Dr Mark Elsegood, University of Newcastle.

Table A1.17 Fractional Atomic Coordinates (Å) and Equivalent Isotropic Displacement Parameters U_{eq} ($Å^2$) for $[(\eta^3\text{-}Tp^{Me_2})Sm(\eta^3\text{-}(HB(\mu\text{-}O)(pz^{Me_2})_2)]_2.(THF)_2$ (**3.18**). Esds in Parentheses

Atom	x	y	z	U_{eq} †
Sm1	0.57104(2)	0.877289(12)	0.565097(12)	0.01687(7)
N1	0.6832(3)	0.9075(2)	0.6998(2)	0.0223(6)
N2	0.6559(3)	0.8660(2)	0.7946(2)	0.0252(6)
C1	0.7516(4)	0.9776(3)	0.7046(3)	0.0237(7)
C2	0.7683(4)	0.9818(3)	0.8018(3)	0.0321(8)
C3	0.7062(4)	0.9115(3)	0.8568(3)	0.0326(9)
C4	0.7972(4)	1.0383(3)	0.6136(3)	0.0274(8)
C5	0.6903(6)	0.8864(5)	0.9670(3)	0.0539(13)
N3	0.6831(3)	0.6957(2)	0.6380(2)	0.0254(6)
N4	0.6549(3)	0.6862(2)	0.7415(2)	0.0275(7)
C6	0.7540(4)	0.5989(3)	0.5962(3)	0.0296(8)
C7	0.7712(5)	0.5266(3)	0.6725(4)	0.0405(10)
C8	0.7069(5)	0.5835(3)	0.7634(4)	0.0388(10)
C9	0.8029(4)	0.5754(3)	0.4835(3)	0.0347(9)
C10	0.6912(7)	0.5449(4)	0.8701(4)	0.064(2)
N5	0.3831(3)	0.8578(2)	0.7247(2)	0.0245(6)
N6	0.4179(3)	0.8276(2)	0.8147(2)	0.0259(6)
C11	0.2391(4)	0.8924(3)	0.7466(3)	0.0278(8)
C12	0.1800(4)	0.8855(4)	0.8506(3)	0.0366(9)
C13	0.2957(4)	0.8437(3)	0.8912(3)	0.0347(9)

C14	0.1645(4)	0.9293(3)	0.6648(3)	0.0336(9)
C15	0.2951(6)	0.8155(5)	0.9986(3)	0.0548(14)
B1	0.5767(5)	0.7809(3)	0.8179(3)	0.0282(9)
N7	0.5060(3)	0.7614(2)	0.4580(2)	0.0226(6)
N8	0.5468(3)	0.7818(2)	0.3561(2)	0.0217(6)
C16	0.4452(4)	0.6842(3)	0.4651(3)	0.0257(7)
C17	0.4454(4)	0.6557(3)	0.3684(3)	0.0317(8)
C18	0.5104(4)	0.7192(3)	0.3017(3)	0.0276(8)
C19	0.3904(4)	0.6416(3)	0.5662(3)	0.0340(9)
C20	0.5339(5)	0.7249(4)	0.1888(3)	0.0435(10)
N9	0.8085(3)	0.8202(2)	0.4288(2)	0.0212(6)
N10	0.7837(3)	0.8245(2)	0.3337(2)	0.0215(6)
C21	0.9526(4)	0.7801(3)	0.4139(3)	0.0243(7)
C22	1.0203(4)	0.7605(3)	0.3101(3)	0.0281(8)
C23	0.9106(4)	0.7889(3)	0.2618(3)	0.0259(8)
C24	1.0167(4)	0.7593(3)	0.5020(3)	0.0320(8)
C25	0.9201(5)	0.7844(4)	0.1508(3)	0.0407(10)
B2	0.6201(4)	0.8732(3)	0.3274(3)	0.0210(8)
O1	0.5502(2)	0.9503(2)	0.4100(2)	0.0198(5)
O3	1.0163(14)	0.6605(9)	0.8907(9)	0.219(4)
C27	1.1412(30)	0.5705(19)	0.9162(18)	0.190(8)
C28	1.1304(21)	0.4848(13)	0.8735(10)	0.134(6)
C29	1.1075(19)	0.5097(13)	0.7796(11)	0.120(5)
C30	1.0549(12)	0.6220(10)	0.7786(8)	0.137(3)
O3A	1.0163(14)	0.6605(9)	0.8907(9)	0.219(4)
C27A	1.1411(33)	0.6251(29)	0.9370(22)	0.164(10)
C28A	1.2397(36)	0.5669(32)	0.8531(21)	0.152(11)
C29A	1.1789(27)	0.5349(23)	0.7891(20)	0.117(7)
C30A	1.0549(12)	0.6220(10)	0.7786(8)	0.137(3)

† Equivalent isotropic U_{eq} defined as one third of the trace of the orthogonalised U_{ij} tensor

Table A1.18 Bond Lengths (Å) for $[(\eta^3\text{-}Tp^{Me_2})Sm(\eta^3\text{-}(HB(\mu\text{-}O)(pz^{Me_2})_2)]_2.(THF)_2$ (**3.18**). Esds in Parentheses

Sm1-O1A	2.240(2)	Sm1-O1	2.319(2)
Sm1-N1	2.515(3)	Sm1-N7	2.522(3)
Sm1-N9	2.522(3)	Sm1-N5	2.530(3)
Sm1-N3	2.611(3)	N1-C1	1.338(4)
N1-N2	1.373(4)	N2-C3	1.352(5)
N2-B1	1.557(5)	C1-C2	1.388(5)
C1-C4	1.493(5)	C2-C3	1.370(6)
C3-C5	1.500(6)	N3-C6	1.336(5)
N3-N4	1.370(4)	N4-C8	1.359(5)

N4-B1	1.541(6)
C6-C9	1.498(6)
C8-C10	1.502(7)
N5-N6	1.375(4)
N6-B1	1.542(5)
C11-C14	1.493(5)
C13-C15	1.493(6)
N7-N8	1.377(4)
N8-B2	1.596(5)
C16-C19	1.493(5)
C18-C20	1.495(6)
N9-N10	1.383(4)
N10-B2	1.602(5)
C21-C24	1.490(5)
C23-C25	1.495(5)
O1-Sm1	2.240(2)

C6-C7	1.392(6)
C7-C8	1.374(7)
N5-C11	1.333(5)
N6-C13	1.346(5)
C11-C12	1.391(6)
C12-C13	1.379(6)
N7-C16	1.342(4)
N8-C18	1.338(5)
C16-C17	1.392(6)
C17-C18	1.386(6)
N9-C21	1.346(4)
N10-C23	1.345(5)
C21-C22	1.393(5)
C22-C23	1.386(5)
B2-O1	1.436(4)
C29A-C30A	1.46(2)

Table A1.19 Bond Angles (°) for $[(\eta^3\text{-}Tp^{Me_2})Sm(\eta^3\text{-}(HB(\mu\text{-}O)(pz^{Me_2})_2)]_2.(THF)_2$ (**3.18**). Esds in Parentheses

O1-Sm1-O1A	70.67(9)
O1-Sm1-N1	135.06(9)
O1-Sm1-N7	68.10(9)
O1A-Sm1-N9	118.61(9)
N1-Sm1-N9	94.14(9)
O1A-Sm1-N5	84.42(9)
N1-Sm1-N5	79.53(9)
N9-Sm1-N5	155.67(9)
O1-Sm1-N3	139.53(9)
N7-Sm1-N3	81.41(9)
N5-Sm1-N3	73.63(10)
N7-Sm1-Sm1	94.47(7)
N5-Sm1-Sm1	110.91(7)
C1-N1-N2	106.6(3)
N2-N1-Sm1	122.4(2)
C3-N2-B1	129.5(3)
N1-C1-C2	110.0(3)
C2-C1-C4	129.2(3)
N2-C3-C2	108.2(3)
C2-C3-C5	128.5(4)
C6-N3-Sm1	133.6(3)
C8-N4-N3	109.6(3)
N3-N4-B1	123.2(3)
N3-C6-C9	123.4(3)

O1A-Sm1-N1	84.50(9)
O1A-Sm1-N7	121.03(9)
N1-Sm1-N7	152.90(9)
O1-Sm1-N9	68.19(8)
N7-Sm1-N9	81.82(9)
O1-Sm1-N5	131.80(9)
N7-Sm1-N5	93.15(9)
O1A-Sm1-N3	149.79(9)
N1-Sm1-N3	71.49(9)
N9-Sm1-N3	82.08(9)
N1-Sm1-Sm1	112.55(7)
N9-Sm1-Sm1	93.25(6)
N3-Sm1-Sm1	174.14(7)
C1-N1-Sm1	129.8(2)
C3-N2-N1	109.3(3)
N1-N2-B1	121.2(3)
N1-C1-C4	120.8(3)
C3-C2-C1	105.9(3)
N2-C3-C5	123.3(4)
C6-N3-N4	106.8(3)
N4-N3-Sm1	119.0(2)
C8-N4-B1	127.2(3)
N3-C6-C7	109.8(4)
C7-C6-C9	126.8(4)

C8-C7-C6	106.2(4)
N4-C8-C10	123.5(4)
C11-N5-N6	106.9(3)
N6-N5-Sm1	121.8(2)
C13-N6-B1	129.2(3)
N5-C11-C12	109.7(3)
C12-C11-C14	129.4(3)
N6-C13-C12	107.8(3)
C12-C13-C15	128.9(4)
N4-B1-N2	110.7(3)
C16-N7-N8	106.8(3)
N8-N7-Sm1	111.3(2)
C18-N8-B2	133.7(3)
N7-C16-C17	109.6(3)
C17-C16-C19	129.7(3)
N8-C18-C17	108.2(3)
C17-C18-C20	128.6(3)
C21-N9-Sm1	143.2(2)
C23-N10-N9	109.7(3)
N9-N10-B2	117.8(3)
N9-C21-C24	120.8(3)
C23-C22-C21	106.1(3)
N10-C23-C25	122.6(3)
O1-B2-N8	105.6(3)
N8-B2-N10	106.7(3)
B2-O1-Sm1	111.6(2)

N4-C8-C7	107.6(4)
C7-C8-C10	128.9(4)
C11-N5-Sm1	129.9(2)
C13-N6-N5	109.5(3)
N5-N6-B1	121.3(3)
N5-C11-C14	120.9(3)
C13-C12-C11	106.0(3)
N6-C13-C15	123.2(4)
N4-B1-N6	109.9(3)
N6-B1-N2	110.9(3)
C16-N7-Sm1	141.9(2)
C18-N8-N7	109.6(3)
N7-N8-B2	116.6(3)
N7-C16-C19	120.8(3)
C18-C17-C16	105.8(3)
N8-C18-C20	123.1(3)
C21-N9-N10	106.6(3)
N10-N9-Sm1	110.0(2)
C23-N10-B2	132.5(3)
N9-C21-C22	109.7(3)
C22-C21-C24	129.5(3)
N10-C23-C22	108.0(3)
C22-C23-C25	129.4(3)
O1-B2-N10	105.3(3)
B2-O1-Sm1A	139.1(2)
Sm1-O1-Sm1A	109.33(9)

Crystal Structure of $[(Tp^{Me2})_2Sm(\eta^2\text{-}O_2N)]$ (3.19)

The data collection was routine, and the initial structure solution was obtained using Patterson methods.

Table A1.20 Fractional Atomic Coordinates (Å $\times 10^4$) and Equivalent Isotropic Displacement Parameters U_{eq} (Å$^2 \times 10^3$) for $[(Tp^{Me2})_2Sm(\eta^2\text{-}O_2N)]$ (**3.19**). Esds in Parentheses

Atom	x	y	z	U_{eq}[†]
Sm(1)	5000	2917(1)	2500	32(1)
B(1)	5340(3)	2582(3)	5238(5)	35(2)
N(11)	5704(2)	3279(2)	5162(3)	36(2)
N(12)	6012(2)	3340(2)	4470(3)	41(2)
N(21)	5657(2)	1928(2)	4944(3)	35(2)

N(22)	5605(2)	1857(2)	3881(3)	39(2)
N(31)	4502(2)	2598(2)	4445(3)	34(2)
N(32)	4182(2)	2618(2)	3258(3)	35(2)
C(11)	5632(4)	3961(4)	6693(6)	70(4)
C(12)	5896(3)	3850(3)	5868(5)	49(3)
C(13)	6356(4)	4275(3)	5686(5)	57(3)
C(14)	6740(5)	4950(4)	6330(7)	91(5)
C(15)	6353(6)	5576(5)	5699(8)	118(7)
C(16)	6402(3)	3939(3)	4801(5)	47(3)
C(17)	6828(4)	4184(4)	4264(6)	66(4)
C(21)	6089(4)	1227(3)	6778(5)	60(3)
C(22)	5954(3)	1335(3)	5575(4)	40(2)
C(23)	6104(3)	864(3)	4935(5)	43(2)
C(24)	6398(3)	117(3)	5246(6)	61(3)
C(25)	5815(4)	-438(3)	4892(9)	94(5)
C(26)	5877(3)	1214(3)	3884(5)	40(2)
C(27)	5934(3)	939(3)	2889(5)	58(3)
C(31)	4156(3)	2446(4)	5958(5)	58(3)
C(32)	3988(3)	2486(3)	4726(4)	38(2)
C(33)	3323(3)	2423(3)	3729(5)	40(2)
C(34)	2597(3)	2282(3)	3600(5)	55(3)
C(35)	2507(4)	1537(4)	3917(8)	86(5)
C(36)	3472(3)	2507(3)	2835(4)	40(2)
C(37)	2937(3)	2472(4)	1562(5)	61(3)
O(1)	5321(2)	4127(2)	2114(3)	58(2)
N(1)	5000	4504(4)	2500	62(4)

† Equivalent isotropic U_{eq} defined as one third of the trace of the orthogonalised U_{ij} tensor

Table A1.21 Bond Lengths (Å) for $[(Tp^{Me2})_2Sm(\eta^2\text{-}O_2N)]$ (**3.19**). Esds in Parentheses

Sm(1)-N(12)	2.551(4)
Sm(1)-N(32)	2.494(6)
Sm(1)-N(1)	2.958(7)
Sm(1)-N(22A)	2.567(4)
Sm(1)-O(1A)	2.487(4)
B(1)-N(21)	1.541(8)
N(11)-N(12)	1.389(8)
N(12)-C(16)	1.330(7)
N(21)-C(22)	1.342(6)
N(31)-N(32)	1.380(6)
N(32)-C(36)	1.345(7)
C(12)-C(13)	1.380(11)

Sm(1)-N(22)	2.567(4)
Sm(1)-O(1)	2.487(4)
Sm(1)-N(12A)	2.551(4)
Sm(1)-N(32A)	2.494(6)
B(1)-N(11)	1.545(8)
B(1)-N(31)	1.557(7)
N(11)-C(12)	1.344(7)
N(21)-N(22)	1.379(7)
N(22)-C(26)	1.333(7)
N(31)-C(32)	1.347(9)
C(11)-C(12)	1.490(13)
C(13)-C(14)	1.512(9)

C(13)-C(16)	1.389(11)
C(16)-C(17)	1.492(12)
C(22)-C(23)	1.375(9)
C(23)-C(26)	1.398(8)
C(26)-C(27)	1.491(11)
C(32)-C(33)	1.381(6)
C(33)-C(36)	1.397(10)
C(36)-C(37)	1.501(6)
N(1)-O(1A)	1.264(7)

C(14)-C(15)	1.435(11)
C(21)-C(22)	1.501(9)
C(23)-C(24)	1.498(7)
C(24)-C(25)	1.501(10)
C(31)-C(32)	1.504(9)
C(33)-C(34)	1.501(10)
C(34)-C(35)	1.493(10)
O(1)-N(1)	1.264(7)

Table A1.22 Bond Angles (°) for $[(Tp^{Me2})_2Sm(\eta^2\text{-}O_2N)]$ (**3.19**). Esds in Parentheses

N(12)-Sm(1)-N(22)	68.7(1)
N(22)-Sm(1)-N(32)	74.7(2)
N(22)-Sm(1)-O(1)	139.1(1)
N(12)-Sm(1)-N(1)	72.0(1)
N(32)-Sm(1)-N(1)	102.9(1)
N(12)-Sm(1)-N(12A)	144.0(2)
N(32)-Sm(1)-N(12A)	95.0(2)
N(1)-Sm(1)-N(12A)	72.0(1)
N(22)-Sm(1)-N(22A)	79.3(2)
O(1)-Sm(1)-N(22A)	129.8(1)
N(12A)-Sm(1)-N(22A)	68.7(1)
N(22)-Sm(1)-N(32A)	85.4(2)
O(1)-Sm(1)-N(32A)	78.0(2)
N(12A)-Sm(1)-N(32A)	92.9(2)
N(12)-Sm(1)-O(1A)	71.6(1)
N(32)-Sm(1)-O(1A)	78.0(2)
N(1)-Sm(1)-O(1A)	25.0(1)
N(22A)-Sm(1)-O(1A)	139.1(1)
N(11)-B(1)-N(21)	110.2(6)
N(21)-B(1)-N(31)	110.2(4)
B(1)-N(11)-C(12)	127.1(6)
Sm(1)-N(12)-N(11)	102.9(3)
N(11)-N(12)-C(16)	106.1(5)
B(1)-N(21)-C(22)	128.4(5)
Sm(1)-N(22)-N(21)	114.8(3)
N(21)-N(22)-C(26)	106.1(4)
B(1)-N(31)-C(32)	129.0(4)
Sm(1)-N(32)-N(31)	115.9(3)
N(31)-N(32)-C(36)	106.1(5)
N(11)-C(12)-C(13)	108.7(7)
C(12)-C(13)-C(14)	127.4(8)

N(12)-Sm(1)-N(32)	92.9(2)
N(12)-Sm(1)-O(1)	75.9(1)
N(32)-Sm(1)-O(1)	127.9(2)
N(22)-Sm(1)-N(1)	140.4(1)
O(1)-Sm(1)-N(1)	25.0(1)
N(22)-Sm(1)-N(12A)	147.1(1)
O(1)-Sm(1)-N(12A)	71.6(1)
N(12)-Sm(1)-N(22A)	147.1(1)
N(32)-Sm(1)-N(22A)	85.4(2)
N(1)-Sm(1)-N(22A)	140.4(1)
N(12)-Sm(1)-N(32A)	95.0(2)
N(32)-Sm(1)-N(32A)	154.1(2)
N(1)-Sm(1)-N(32A)	102.9(1)
N(22A)-Sm(1)-N(32A)	74.7(2)
N(22)-Sm(1)-O(1A)	129.8(1)
O(1)-Sm(1)-O(1A)	50.0(3)
N(12A)-Sm(1)-O(1A)	75.9(1)
N(32A)-Sm(1)-O(1A)	127.8(2)
N(11)-B(1)-N(31)	112.7(4)
B(1)-N(11)-N(12)	122.7(4)
N(12)-N(11)-C(12)	109.1(5)
Sm(1)-N(12)-C(16)	131.8(4)
B(1)-N(21)-N(22)	121.6(4)
N(22)-N(21)-C(22)	109.8(4)
Sm(1)-N(22)-C(26)	139.1(4)
B(1)-N(31)-N(32)	121.0(5)
N(32)-N(31)-C(32)	109.2(4)
Sm(1)-N(32)-C(36)	137.9(3)
N(11)-C(12)-C(11)	122.6(6)
C(11)-C(12)-C(13)	128.7(6)
C(12)-C(13)-C(16)	105.1(5)

C(14)-C(13)-C(16)	127.5(8)
N(12)-C(16)-C(13)	111.0(7)
C(13)-C(16)-C(17)	126.9(6)
N(21)-C(22)-C(23)	108.5(5)
C(22)-C(23)-C(24)	128.1(6)
C(24)-C(23)-C(26)	126.7(6)
N(22)-C(26)-C(23)	110.6(6)
C(23)-C(26)-C(27)	126.7(5)
N(31)-C(32)-C(33)	109.3(5)
C(32)-C(33)-C(34)	128.9(6)
C(34)-C(33)-C(36)	126.5(4)
N(32)-C(36)-C(33)	110.9(4)
C(33)-C(36)-C(37)	126.7(6)
Sm(1)-N(1)-O(1)	56.2(3)
O(1)-N(1)-O(1A)	112.4(7)

C(13)-C(14)-C(15)	110.8(6)
N(12)-C(16)-C(17)	122.1(6)
N(21)-C(22)-C(21)	124.1(5)
C(21)-C(22)-C(23)	127.4(5)
C(22)-C(23)-C(26)	105.1(5)
C(23)-C(24)-C(25)	112.8(5)
N(22)-C(26)-C(27)	122.7(5)
N(31)-C(32)-C(31)	122.7(4)
C(31)-C(32)-C(33)	128.0(6)
C(32)-C(33)-C(36)	104.5(6)
C(33)-C(34)-C(35)	113.9(5)
N(32)-C(36)-C(37)	122.4(6)
Sm(1)-O(1)-N(1)	98.8(4)
Sm(1)-N(1)-O(1A)	56.2(3)

Crystal Structure of $[Tp^{3\text{-}t\text{-}Bu\text{-}5\text{-}Me}SmI(THF)_2].(Et_2O)_{0.5}$ (4.1)

The data collection was routine, and the initial structure solution was obtained using Patterson methods. The half molecule of Et_2O lies across the mirror plane.

Table A1.23 Fractional Atomic Coordinates (Å $\times 10^4$) and Equivalent Isotropic Displacement Parameters U_{eq} (Å$^2 \times 10^3$) for $[Tp^{3\text{-}t\text{-}Bu\text{-}5\text{-}Me}SmI(THF)_2].(Et_2O)_{0.5}$ (**4.1**). Esds in Parentheses

Atom	x	y	z	U_{eq} †
Sm(1)	7388(1)	5000	1915(1)	35(1)
I(1)	7666(1)	5000	-73(1)	65(1)
B(1)	6986(4)	5000	4059(6)	39(3)
O(1)	7869(2)	6898(3)	1961(3)	57(2)
N(11)	6597(2)	6106(4)	2687(3)	44(2)
N(12)	6717(2)	5991(4)	3593(3)	40(2)
N(21)	8062(3)	5000	3502(4)	39(2)
N(22)	7711(3)	5000	4201(4)	40(2)
C(12)	5303(4)	7145(11)	1472(6)	116(5)
C(13)	6465(3)	6815(6)	3967(4)	55(2)
C(14)	6179(3)	7429(6)	3319(4)	63(3)
C(15)	6261(3)	6982(5)	2534(4)	51(2)
C(16)	6517(5)	6937(7)	4951(5)	110(5)
C(17)	5998(3)	7314(6)	1611(5)	62(3)
C(18)	6111(6)	8465(9)	1516(7)	122(5)

C(19)	6291(5)	6746(8)	911(5)	102(4)
C(22)	7901(5)	5000	5872(6)	75(5)
C(23)	8108(4)	5000	4969(5)	44(3)
C(24)	8711(5)	5000	4772(6)	55(3)
C(25)	8657(4)	5000	3850(6)	44(3)
C(26)	9197(4)	5000	3328(6)	53(3)
C(27)	9602(4)	5962(8)	3567(6)	92(4)
C(28)	8985(4)	5000	2329(6)	65(5)
C(31)	8154(4)	7462(6)	1316(5)	71(3)
C(32)	8526(4)	8290(7)	1782(5)	75(3)
C(33)	8185(5)	8537(7)	2532(6)	93(4)
C(34)	7908(4)	7524(6)	2741(5)	67(3)
O(2)	0	0	5000	157(7)
C(1)	42(17)	519(33)	5856(24)	220(17)
C(2)	66(13)	0	6569(19)	181(10)

† Equivalent isotropic U_{eq} defined as one third of the trace of the orthogonalised U_{ij} tensor

Table A1.24 Bond Lengths (Å) for $[Tp^{3\text{-}t\text{-}Bu\text{-}5\text{-}Me}SmI(THF)_2].(Et_2O)_{0.5}$ (**4.1**). Esds in Parentheses

Sm(1)-I(1)	3.191(1)	Sm(1)-O(1)	2.652(5)
Sm(1)-N(11)	2.632(5)	Sm(1)-N(21)	2.647(6)
Sm(1)-O(1A)	2.652(5)	Sm(1)-N(11A)	2.632(5)
B(1)-N(12)	1.534(7)	B(1)-N(22)	1.550(12)
B(1)-N(12A)	1.534(7)	O(1)-C(31)	1.435(9)
O(1)-C(34)	1.434(8)	N(11)-N(12)	1.383(6)
N(11)-C(15)	1.342(8)	N(12)-C(13)	1.357(9)
N(21)-N(22)	1.399(10)	N(21)-C(25)	1.317(10)
N(22)-C(23)	1.352(10)	C(12)-C(17)	1.502(10)
C(13)-C(14)	1.346(9)	C(13)-C(16)	1.503(10)
C(14)-C(15)	1.368(10)	C(15)-C(17)	1.509(9)
C(17)-C(18)	1.512(14)	C(17)-C(19)	1.511(12)
C(22)-C(23)	1.516(13)	C(23)-C(24)	1.379(14)
C(24)-C(25)	1.400(13)	C(25)-C(26)	1.508(13)
C(26)-C(27)	1.529(11)	C(26)-C(28)	1.533(13)
C(26)-C(27A)	1.529(11)	C(31)-C(32)	1.457(11)
C(32)-C(33)	1.487(14)	C(33)-C(34)	1.490(12)
O(2)-C(1)	1.462(38)	O(2)-C(1A)	1.462(38)
O(2)-C(1B)	1.462(38)	O(2)-C(1C)	1.462(38)
C(1)-C(2)	1.276(45)	C(1)-C(1C)	1.335(84)
C(2)-C(1C)	1.275(45)		

Table A1.25 Bond Angles (°) for $[Tp^{3\text{-}t\text{-}Bu\text{-}5\text{-}Me}SmI(THF)_2].(Et_2O)_{0.5}$ (**4.1**). Esds in Parentheses

I(1)-Sm(1)-O(1)	84.1(1)
O(1)-Sm(1)-N(11)	76.6(2)
O(1)-Sm(1)-N(21)	79.3(1)
I(1)-Sm(1)-O(1A)	84.1(1)
N(11)-Sm(1)-O(1A)	139.8(2)
I(1)-Sm(1)-N(11A)	130.8(1)
N(11)-Sm(1)-N(11A)	65.5(2)
O(1A)-Sm(1)-N(11A)	76.6(2)
N(12)-B(1)-N(12A)	112.4(6)
Sm(1)-O(1)-C(31)	130.8(4)
C(31)-O(1)-C(34)	108.1(5)
Sm(1)-N(11)-C(15)	138.2(4)
B(1)-N(12)-N(11)	124.0(5)
N(11)-N(12)-C(13)	108.2(5)
Sm(1)-N(21)-C(25)	138.2(6)
B(1)-N(22)-N(21)	122.8(6)
N(21)-N(22)-C(23)	108.7(7)
N(12)-C(13)-C(16)	122.0(6)
C(13)-C(14)-C(15)	107.3(7)
N(11)-C(15)-C(17)	121.5(6)
C(12)-C(17)-C(15)	109.0(6)
C(15)-C(17)-C(18)	108.9(6)
C(15)-C(17)-C(19)	112.8(6)
N(22)-C(23)-C(22)	124.1(8)
C(22)-C(23)-C(24)	127.9(8)
N(21)-C(25)-C(24)	110.0(8)
C(24)-C(25)-C(26)	125.2(8)
C(25)-C(26)-C(28)	112.8(7)
C(25)-C(26)-C(27A)	109.5(6)
C(28)-C(26)-C(27A)	108.4(6)
C(31)-C(32)-C(33)	103.6(7)
O(1)-C(34)-C(33)	106.8(6)
C(1)-O(2)-C(1B)	125.7(33)
C(1)-O(2)-C(1C)	54.3(33)
C(1B)-O(2)-C(1C)	180.0(1)
O(2)-C(1)-C(1C)	62.8(16)
C(1)-C(2)-C(1C)	63.1(39)

I(1)-Sm(1)-N(11)	130.8(1)
I(1)-Sm(1)-N(21)	136.2(1)
N(11)-Sm(1)-N(21)	83.9(2)
O(1)-Sm(1)-O(1A)	134.2(2)
N(21)-Sm(1)-O(1A)	79.3(1)
O(1)-Sm(1)-N(11A)	139.8(2)
N(21)-Sm(1)-N(11A)	83.9(2)
N(12)-B(1)-N(22)	111.9(5)
N(22)-B(1)-N(12A)	111.9(5)
Sm(1)-O(1)-C(34)	120.9(4)
Sm(1)-N(11)-N(12)	110.7(3)
N(12)-N(11)-C(15)	106.4(5)
B(1)-N(12)-C(13)	127.0(5)
Sm(1)-N(21)-N(22)	114.6(4)
N(22)-N(21)-C(25)	107.2(6)
B(1)-N(22)-C(23)	128.5(7)
N(12)-C(13)-C(14)	108.4(6)
C(14)-C(13)-C(16)	129.6(7)
N(11)-C(15)-C(14)	109.6(6)
C(14)-C(15)-C(17)	128.8(6)
C(12)-C(17)-C(18)	107.5(8)
C(12)-C(17)-C(19)	110.0(7)
C(18)-C(17)-C(19)	108.4(8)
N(22)-C(23)-C(24)	108.1(7)
C(23)-C(24)-C(25)	106.1(8)
N(21)-C(25)-C(26)	124.8(8)
C(25)-C(26)-C(27)	109.5(6)
C(27)-C(26)-C(28)	108.4(6)
C(27)-C(26)-C(27A)	108.2(8)
O(1)-C(31)-C(32)	107.1(6)
C(32)-C(33)-C(34)	103.8(7)
C(1)-O(2)-C(1A)	180.0(1)
C(1A)-O(2)-C(1B)	54.3(33)
C(1A)-O(2)-C(1C)	125.7(33)
O(2)-C(1)-C(2)	121.3(32)
C(2)-C(1)-C(1C)	58.4(20)

Crystal Structure of [Tp$^{3\text{-}t\text{-Bu-5-Me}}$YbI(THF)] (4.2)

The crystals were somewhat prone to desolvation and were therefore sealed in capillaries with a little of the mother liquor (diethyl ether). The data collection was routine, and the initial structure solution was obtained using direct methods. There was some rotational disorder in the *tert*-butyl group of pyrazolyl ring 3, which was successfully modelled over two sites.

Table A1.26 Fractional Atomic Coordinates (Å $\times$ 10^4) and Equivalent Isotropic Displacement Parameters U_{eq} (Å^2 $\times$ 10^3) for [Tp$^{3\text{-}t\text{-Bu-5-Me}}$YbI(THF)] (**4.2**). Esds in Parentheses

Atom	x	y	z	U_{eq} †
Yb(1)	302(1)	9317(1)	2465(1)	47(1)
I(1)	-2063(1)	9051(1)	1453(1)	90(1)
N(11)	1118(6)	8232(4)	3354(4)	45(3)
N(12)	2178(6)	8452(4)	3801(4)	42(3)
N(21)	889(7)	10052(4)	3597(4)	47(3)
N(22)	2101(6)	10013(4)	3820(4)	40(3)
N(31)	2367(7)	9164(4)	2294(4)	47(3)
N(32)	3194(7)	9254(4)	2907(4)	47(3)
B(1)	2859(10)	9251(6)	3682(7)	48(4)
O(1)	577(7)	10704(4)	1975(4)	72(3)
C(1)	-207(15)	11184(9)	1463(10)	120(5)
C(2)	51(20)	12012(14)	1636(13)	193(10)
C(3)	1326(16)	12027(11)	2234(10)	142(7)
C(4)	1644(12)	11147(7)	2202(8)	84(4)
C(11)	-332(10)	7095(6)	3281(7)	68(5)
C(12)	775(9)	7517(6)	3617(6)	53(4)
C(13)	1590(9)	7277(6)	4220(6)	59(4)
C(14)	2461(9)	7879(6)	4316(5)	50(4)
C(15)	3547(9)	7936(7)	4899(6)	65(4)
C(16)	-1402(12)	7618(9)	3338(10)	115(8)
C(17)	-291(13)	6924(9)	2477(8)	116(7)
C(18)	-434(14)	6267(8)	3638(10)	137(9)
C(21)	-799(10)	10926(6)	3827(6)	57(4)
C(22)	497(9)	10708(6)	3910(5)	49(3)
C(23)	1454(10)	11106(6)	4324(6)	60(4)
C(24)	2433(9)	10654(6)	4264(6)	54(4)
C(25)	3711(10)	10813(7)	4570(8)	95(6)
C(26)	-1020(11)	11845(7)	3719(8)	92(6)
C(27)	-1529(10)	10463(9)	3212(10)	116(8)
C(28)	-1265(14)	10667(10)	4490(9)	135(9)

C(31)	2371(12)	8993(7)	975(7)	74(5)
C(32)	2968(11)	9112(6)	1743(6)	58(4)
C(33)	4160(11)	9176(6)	2003(7)	69(5)
C(34)	4302(9)	9282(6)	2723(7)	57(4)
C(35)	5406(10)	9376(8)	3253(8)	87(6)
C(36)	1049(22)	8881(16)	893(15)	102(8)
C(36A)	1608(34)	8168(22)	971(21)	116(12)
C(37)	2656(23)	9699(14)	533(13)	97(7)
C(37A)	1648(31)	9720(19)	665(19)	95(10)
C(38)	2858(26)	8234(16)	686(15)	113(9)
C(38A)	3334(34)	8817(27)	525(22)	121(13)

† Equivalent isotropic U_{eq} defined as one third of the trace of the orthogonalised U_{ij} tensor

Table A1.27 Bond Lengths (Å) for [$Tp^{3\text{-}t\text{-}Bu\text{-}5\text{-}Me}$YbI(THF)] (**4.2**). Esds in Parentheses

Yb(1)-I(1)	3.065(1)	Yb(1)-N(11)	2.499(7)
Yb(1)-N(21)	2.434(8)	Yb(1)-N(31)	2.442(8)
Yb(1)-O(1)	2.469(7)	N(11)-N(12)	1.401(10)
N(11)-C(12)	1.343(12)	N(12)-B(1)	1.546(12)
N(12)-C(14)	1.343(12)	N(21)-N(22)	1.379(10)
N(21)-C(22)	1.328(12)	N(22)-B(1)	1.554(13)
N(22)-C(24)	1.348(11)	N(31)-N(32)	1.372(11)
N(31)-C(32)	1.334(16)	N(32)-B(1)	1.565(15)
N(32)-C(34)	1.364(14)	O(1)-C(1)	1.431(17)
O(1)-C(4)	1.417(14)	C(1)-C(2)	1.401(27)
C(2)-C(3)	1.687(27)	C(3)-C(4)	1.476(21)
C(11)-C(12)	1.483(14)	C(11)-C(16)	1.504(18)
C(11)-C(17)	1.545(21)	C(11)-C(18)	1.514(18)
C(12)-C(13)	1.398(14)	C(13)-C(14)	1.383(14)
C(14)-C(15)	1.515(13)	C(21)-C(22)	1.503(15)
C(21)-C(26)	1.520(15)	C(21)-C(27)	1.509(18)
C(21)-C(28)	1.493(21)	C(22)-C(23)	1.391(14)
C(23)-C(24)	1.356(15)	C(24)-C(25)	1.499(15)
C(31)-C(32)	1.504(16)	C(31)-C(36)	1.502(29)
C(31)-C(36A)	1.595(39)	C(31)-C(37)	1.483(27)
C(31)-C(37A)	1.501(34)	C(31)-C(38)	1.488(31)
C(31)-C(38A)	1.518(45)	C(32)-C(33)	1.371(17)
C(33)-C(34)	1.347(19)	C(34)-C(35)	1.480(16)
C(36)-C(36A)	1.317(44)	C(36)-C(37A)	1.611(43)
C(36A)-C(38)	1.607(51)	C(37)-C(37A)	1.216(46)
C(37)-C(38A)	1.627(49)	C(38)-C(38A)	1.154(51)

Table A1.28 Bond Angles (°) for [$Tp^{3\text{-}t\text{-}Bu\text{-}5\text{-}Me}$YbI(THF)] (**4.2**). Esds in Parentheses

I(1)-Yb(1)-N(11)	120.6(2)	I(1)-Yb(1)-N(21)	134.3(2)
N(11)-Yb(1)-N(21)	75.1(2)	I(1)-Yb(1)-N(31)	132.4(2)
N(11)-Yb(1)-N(31)	75.8(3)	N(21)-Yb(1)-N(31)	91.8(3)
I(1)-Yb(1)-O(1)	92.8(2)	N(11)-Yb(1)-O(1)	146.6(2)
N(21)-Yb(1)-O(1)	81.2(2)	N(31)-Yb(1)-O(1)	81.9(2)
Yb(1)-N(11)-N(12)	114.3(5)	Yb(1)-N(11)-C(12)	139.0(6)
N(12)-N(11)-C(12)	105.9(7)	N(11)-N(12)-B(1)	122.1(7)
N(11)-N(12)-C(14)	109.7(7)	B(1)-N(12)-C(14)	128.2(7)
Yb(1)-N(21)-N(22)	111.2(5)	Yb(1)-N(21)-C(22)	135.6(6)
N(22)-N(21)-C(22)	107.2(7)	N(21)-N(22)-B(1)	122.9(7)
N(21)-N(22)-C(24)	108.6(7)	B(1)-N(22)-C(24)	127.5(7)
Yb(1)-N(31)-N(32)	115.1(6)	Yb(1)-N(31)-C(32)	137.6(7)
N(32)-N(31)-C(32)	106.7(8)	N(31)-N(32)-B(1)	122.8(8)
N(31)-N(32)-C(34)	109.2(9)	B(1)-N(32)-C(34)	127.8(8)
N(12)-B(1)-N(22)	109.6(8)	N(12)-B(1)-N(32)	110.1(8)
N(22)-B(1)-N(32)	112.3(7)	Yb(1)-O(1)-C(1)	129.9(8)
Yb(1)-O(1)-C(4)	120.3(6)	C(1)-O(1)-C(4)	109.8(9)
O(1)-C(1)-C(2)	106.3(14)	C(1)-C(2)-C(3)	107.1(16)
C(2)-C(3)-C(4)	98.6(13)	O(1)-C(4)-C(3)	107.3(11)
C(12)-C(11)-C(16)	110.8(10)	C(12)-C(11)-C(17)	109.8(11)
C(16)-C(11)-C(17)	109.0(11)	C(12)-C(11)-C(18)	110.0(10)
C(16)-C(11)-C(18)	110.3(12)	C(17)-C(11)-C(18)	106.9(11)
N(11)-C(12)-C(11)	121.3(9)	N(11)-C(12)-C(13)	110.1(8)
C(11)-C(12)-C(13)	128.6(9)	C(12)-C(13)-C(14)	106.1(9)
N(12)-C(14)-C(13)	108.1(8)	N(12)-C(14)-C(15)	123.4(8)
C(13)-C(14)-C(15)	128.5(9)	C(22)-C(21)-C(26)	112.5(9)
C(22)-C(21)-C(27)	111.8(9)	C(26)-C(21)-C(27)	109.1(10)
C(22)-C(21)-C(28)	109.1(9)	C(26)-C(21)-C(28)	108.3(11)
C(27)-C(21)-C(28)	105.8(11)	N(21)-C(22)-C(21)	122.7(8)
N(21)-C(22)-C(23)	109.2(9)	C(21)-C(22)-C(23)	128.1(9)
C(22)-C(23)-C(24)	106.5(9)	N(22)-C(24)-C(23)	108.5(8)
N(22)-C(24)-C(25)	121.8(9)	C(23)-C(24)-C(25)	129.6(9)
C(32)-C(31)-C(36)	113.8(15)	C(32)-C(31)-C(36A)	105.9(16)
C(36)-C(31)-C(36A)	50.2(17)	C(32)-C(31)-C(37)	109.4(12)
C(36)-C(31)-C(37)	110.1(16)	C(36A)-C(31)-C(37)	144.6(18)
C(32)-C(31)-C(37A)	113.9(15)	C(36)-C(31)-C(37A)	64.9(18)
C(36A)-C(31)-C(37A)	113.1(20)	C(37)-C(31)-C(37A)	48.1(18)
C(32)-C(31)-C(38)	108.7(13)	C(36)-C(31)-C(38)	107.0(17)
C(36A)-C(31)-C(38)	62.7(19)	C(37)-C(31)-C(38)	107.8(17)
C(37A)-C(31)-C(38)	136.2(19)	C(32)-C(31)-C(38A)	107.7(17)
C(36)-C(31)-C(38A)	136.6(19)	C(36A)-C(31)-C(38A)	106.5(23)

C(37)-C(31)-C(38A)	65.7(20)
C(38)-C(31)-C(38A)	45.1(20)
N(31)-C(32)-C(33)	109.0(10)
C(32)-C(33)-C(34)	108.4(12)
N(32)-C(34)-C(35)	123.6(11)
C(31)-C(36)-C(36A)	68.5(21)
C(36A)-C(36)-C(37A)	123.5(28)
C(31)-C(36A)-C(38)	55.4(17)
C(31)-C(37)-C(37A)	66.7(20)
C(37A)-C(37)-C(38A)	119.5(27)
C(31)-C(37A)-C(37)	65.2(20)
C(31)-C(38)-C(36A)	61.9(18)
C(36A)-C(38)-C(38A)	128.5(32)
C(31)-C(38A)-C(38)	66.0(26)

C(37A)-C(31)-C(38A)	109.4(22)
N(31)-C(32)-C(31)	122.9(11)
C(31)-C(32)-C(33)	128.1(12)
N(32)-C(34)-C(33)	106.6(9)
C(33)-C(34)-C(35)	129.7(12)
C(31)-C(36)-C(37A)	57.5(16)
C(31)-C(36A)-C(36)	61.2(19)
C(36)-C(36A)-C(38)	110.1(29)
C(31)-C(37)-C(38A)	58.2(18)
C(31)-C(37A)-C(36)	57.6(15)
C(36)-C(37A)-C(37)	119.2(27)
C(31)-C(38)-C(38A)	68.8(26)
C(31)-C(38A)-C(37)	56.1(18)
C(37)-C(38A)-C(38)	118.2(35)

Crystal Structure of $[Tp^{3\text{-}t\text{-}Bu\text{-}5\text{-}Me}YbI(3,5\text{-}Me_2py)_2]$ (4.9a)

The data collection was routine, and the initial structure solution was obtained using Patterson methods.

Table A1.29 Fractional Atomic Coordinates (Å $\times 10^4$) and Equivalent Isotropic Displacement Parameters U_{eq} (Å$^2 \times 10^3$) for $[Tp^{3\text{-}t\text{-}Bu\text{-}5\text{-}Me}YbI(3,5\text{-}Me_2py)_2]$ (**4.9a**). Esds in Parentheses

Atom	x	y	z	U_{eq}[†]
Yb(1)	3712(1)	2337(1)	9201(1)	41(1)
I(1)	3335(1)	37(1)	8403(1)	64(1)
B(1)	4201(3)	4747(8)	10026(4)	54(4)
N(11)	4330(2)	2526(5)	10264(3)	50(2)
N(12)	4348(2)	3661(5)	10505(3)	50(2)
C(12)	4604(3)	4781(10)	11643(5)	100(5)
C(13)	4548(2)	3685(9)	11207(4)	67(4)
C(14)	4668(3)	2568(9)	11424(4)	74(4)
C(15)	4530(2)	1860(8)	10819(3)	55(3)
C(16)	4595(2)	571(8)	10773(4)	70(4)
C(17)	4504(3)	-142(10)	11304(5)	107(7)
C(18)	4996(3)	397(9)	10926(5)	92(5)
C(19)	4365(3)	88(7)	10032(5)	79(5)
N(21)	4131(2)	3661(5)	8898(3)	45(2)
N(22)	4265(2)	4610(5)	9348(3)	50(3)
C(22)	4665(3)	6387(8)	9505(5)	98(6)
C(23)	4465(2)	5291(7)	9117(4)	64(4)

C(24)	4464(2)	4795(7)	8528(4)	64(4)
C(25)	4257(2)	3772(6)	8406(3)	48(3)
C(26)	4178(3)	2897(8)	7812(4)	63(4)
C(27)	4537(3)	2619(8)	7757(5)	85(6)
C(28)	4026(3)	1771(8)	7961(5)	87(5)
C(29)	3906(3)	3465(10)	7112(4)	91(5)
N(31)	3539(2)	4125(5)	9684(3)	49(3)
N(32)	3799(2)	5000(5)	9864(3)	46(2)
C(32)	3850(3)	7187(7)	10062(6)	87(6)
C(33)	3646(2)	6056(6)	9886(4)	59(4)
C(34)	3291(2)	5852(7)	9729(4)	65(4)
C(35)	3229(2)	4647(6)	9599(4)	52(3)
C(36)	2876(2)	4025(8)	9428(5)	67(4)
C(37)	2570(3)	4686(10)	8808(7)	128(7)
C(38)	2789(4)	4034(12)	10048(7)	165(11)
C(39)	2875(3)	2776(7)	9180(6)	78(4)
N(4)	3621(2)	1398(6)	10322(3)	54(3)
C(41)	3754(2)	2021(9)	10926(4)	70(4)
C(42)	3729(3)	1716(9)	11539(4)	75(4)
C(43)	3549(3)	699(10)	11526(5)	77(5)
C(44)	3402(2)	0(7)	10918(4)	64(4)
C(45)	3451(2)	410(7)	10333(4)	60(3)
C(46)	3915(4)	2432(11)	12203(5)	115(7)
C(47)	3201(3)	-1129(9)	10892(5)	91(5)
N(5)	3274(2)	3511(5)	8026(3)	53(3)
C(51)	3297(2)	4681(7)	8059(4)	57(3)
C(52)	3065(3)	5445(7)	7542(4)	68(4)
C(53)	2789(3)	4922(7)	6955(4)	69(4)
C(54)	2762(2)	3734(7)	6893(4)	58(3)
C(55)	3010(2)	3055(7)	7443(4)	60(3)
C(56)	3103(3)	6742(8)	7639(6)	97(6)
C(57)	2469(3)	3175(9)	6262(5)	88(5)

† Equivalent isotropic U_{eq} defined as one third of the trace of the orthogonalised U_{ij} tensor

Table A1.30 Bond Lengths (Å) for $[Tp^{3\text{-}t\text{-}Bu\text{-}5\text{-}Me}YbI(3,5\text{-}Me_2py)_2]$ (**4.9a**). Esds in Parentheses

Yb(1)-I(1)	3.123(1)	Yb(1)-N(11)	2.556(5)
Yb(1)-N(21)	2.545(7)	Yb(1)-N(31)	2.494(6)
Yb(1)-N(4)	2.727(7)	Yb(1)-N(5)	2.684(5)
B(1)-N(12)	1.537(10)	B(1)-N(22)	1.545(12)
B(1)-N(32)	1.551(12)	N(11)-N(12)	1.373(8)
N(11)-C(15)	1.329(9)	N(12)-C(13)	1.336(8)

C(12)-C(13)	1.497(14)
C(14)-C(15)	1.393(11)
C(16)-C(17)	1.535(17)
C(16)-C(19)	1.524(11)
N(21)-C(25)	1.327(11)
C(22)-C(23)	1.517(12)
C(24)-C(25)	1.393(11)
C(26)-C(27)	1.545(17)
C(26)-C(29)	1.546(11)
N(31)-C(35)	1.337(11)
C(32)-C(33)	1.487(12)
C(34)-C(35)	1.398(11)
C(36)-C(37)	1.553(13)
C(36)-C(39)	1.508(12)
N(4)-C(45)	1.321(11)
C(42)-C(43)	1.363(15)
C(43)-C(44)	1.391(12)
C(44)-C(47)	1.509(14)
N(5)-C(55)	1.336(8)
C(52)-C(53)	1.390(11)
C(53)-C(54)	1.355(12)
C(54)-C(57)	1.487(11)

C(13)-C(14)	1.365(14)
C(15)-C(16)	1.498(13)
C(16)-C(18)	1.536(14)
N(21)-N(22)	1.378(7)
N(22)-C(23)	1.351(12)
C(23)-C(24)	1.344(14)
C(25)-C(26)	1.510(11)
C(26)-C(28)	1.506(14)
N(31)-N(32)	1.380(8)
N(32)-C(33)	1.361(10)
C(33)-C(34)	1.359(13)
C(35)-C(36)	1.500(12)
C(36)-C(38)	1.474(21)
N(4)-C(41)	1.338(10)
C(41)-C(42)	1.363(14)
C(42)-C(46)	1.499(14)
C(44)-C(45)	1.393(14)
N(5)-C(51)	1.331(10)
C(51)-C(52)	1.392(10)
C(52)-C(56)	1.486(12)
C(54)-C(55)	1.392(10)

Table A1.31 Bond Angles (°) for $[Tp^{3\text{-}t\text{-}Bu\text{-}5\text{-}Me}YbI(3,5\text{-}Me_2py)_2]$ (**4.9a**). Esds in Parentheses

I(1)-Yb(1)-N(11)	127.5(1)
N(11)-Yb(1)-N(21)	69.3(2)
N(11)-Yb(1)-N(31)	85.8(2)
I(1)-Yb(1)-N(4)	85.0(1)
N(21)-Yb(1)-N(4)	142.3(2)
I(1)-Yb(1)-N(5)	86.9(1)
N(21)-Yb(1)-N(5)	74.8(2)
N(4)-Yb(1)-N(5)	133.7(2)
N(12)-B(1)-N(32)	111.9(7)
Yb(1)-N(11)-N(12)	105.9(4)
N(12)-N(11)-C(15)	107.4(5)
B(1)-N(12)-C(13)	125.4(7)
N(12)-C(13)-C(12)	122.9(8)
C(12)-C(13)-C(14)	129.2(7)
N(11)-C(15)-C(14)	108.6(7)
C(14)-C(15)-C(16)	127.5(7)
C(15)-C(16)-C(18)	108.2(8)
C(15)-C(16)-C(19)	111.6(6)

I(1)-Yb(1)-N(21)	126.3(1)
I(1)-Yb(1)-N(31)	137.4(1)
N(21)-Yb(1)-N(31)	87.2(2)
N(11)-Yb(1)-N(4)	74.7(2)
N(31)-Yb(1)-N(4)	79.1(2)
N(11)-Yb(1)-N(5)	140.7(2)
N(31)-Yb(1)-N(5)	76.7(2)
N(12)-B(1)-N(22)	109.8(7)
N(22)-B(1)-N(32)	113.1(5)
Yb(1)-N(11)-C(15)	135.9(5)
B(1)-N(12)-N(11)	124.9(5)
N(11)-N(12)-C(13)	109.3(6)
N(12)-C(13)-C(14)	107.9(8)
C(13)-C(14)-C(15)	106.8(7)
N(11)-C(15)-C(16)	124.0(6)
C(15)-C(16)-C(17)	111.5(9)
C(17)-C(16)-C(18)	110.0(8)
C(17)-C(16)-C(19)	107.6(8)

C(18)-C(16)-C(19)	107.8(9)
Yb(1)-N(21)-C(25)	139.8(4)
B(1)-N(22)-N(21)	121.7(6)
N(21)-N(22)-C(23)	109.4(7)
N(22)-C(23)-C(24)	108.2(7)
C(23)-C(24)-C(25)	106.5(9)
N(21)-C(25)-C(26)	123.3(7)
C(25)-C(26)-C(27)	108.4(7)
C(27)-C(26)-C(28)	108.9(8)
C(27)-C(26)-C(29)	109.7(8)
Yb(1)-N(31)-N(32)	112.4(5)
N(32)-N(31)-C(35)	106.8(6)
B(1)-N(32)-C(33)	127.6(6)
N(32)-C(33)-C(32)	123.7(8)
C(32)-C(33)-C(34)	129.1(8)
N(31)-C(35)-C(34)	108.9(7)
C(34)-C(35)-C(36)	125.7(8)
C(35)-C(36)-C(38)	110.6(8)
C(35)-C(36)-C(39)	112.9(8)
C(38)-C(36)-C(39)	109.8(9)
Yb(1)-N(4)-C(45)	127.4(5)
N(4)-C(41)-C(42)	125.4(9)
C(41)-C(42)-C(46)	120.9(10)
C(42)-C(43)-C(44)	121.5(10)
C(43)-C(44)-C(47)	122.3(9)
N(4)-C(45)-C(44)	124.6(7)
Yb(1)-N(5)-C(55)	126.8(5)
N(5)-C(51)-C(52)	124.8(6)
C(51)-C(52)-C(56)	121.0(7)
C(52)-C(53)-C(54)	120.8(7)
C(53)-C(54)-C(57)	120.8(7)
N(5)-C(55)-C(54)	123.6(7)

Yb(1)-N(21)-N(22)	114.1(5)
N(22)-N(21)-C(25)	106.0(6)
B(1)-N(22)-C(23)	128.8(6)
N(22)-C(23)-C(22)	123.3(9)
C(22)-C(23)-C(24)	128.4(10)
N(21)-C(25)-C(24)	109.9(7)
C(24)-C(25)-C(26)	126.8(8)
C(25)-C(26)-C(28)	110.7(8)
C(25)-C(26)-C(29)	108.2(7)
C(28)-C(26)-C(29)	110.8(7)
Yb(1)-N(31)-C(35)	135.9(4)
B(1)-N(32)-N(31)	122.8(6)
N(31)-N(32)-C(33)	109.6(6)
N(32)-C(33)-C(34)	107.2(7)
C(33)-C(34)-C(35)	107.4(8)
N(31)-C(35)-C(36)	125.3(7)
C(35)-C(36)-C(37)	108.6(8)
C(37)-C(36)-C(38)	108.3(10)
C(37)-C(36)-C(39)	106.6(7)
Yb(1)-N(4)-C(41)	116.5(6)
C(41)-N(4)-C(45)	116.1(8)
C(41)-C(42)-C(43)	116.7(8)
C(43)-C(42)-C(46)	122.3(10)
C(43)-C(44)-C(45)	115.7(8)
C(45)-C(44)-C(47)	121.9(8)
Yb(1)-N(5)-C(51)	116.3(4)
C(51)-N(5)-C(55)	116.5(6)
C(51)-C(52)-C(53)	116.2(7)
C(53)-C(52)-C(56)	122.8(7)
C(53)-C(54)-C(55)	118.1(7)
C(55)-C(54)-C(57)	121.1(8)

Crystal Structure of [$Tp^{3\text{-}t\text{-}Bu\text{-}5\text{-}Me}$YbI(CNBu^t)] (4.11)

The data collection was routine, and the initial structure solution was obtained using Direct methods. Disorder in the Bu^t group of the isonitrile was modelled over two sites.

Table A1.32 Fractional Atomic Coordinates (Å × 10^4) and Equivalent Isotropic Displacement Parameters U_{eq} (Å^2 × 10^3) for [Tp$^{3\text{-}t\text{-Bu-5-Me}}$YbI(CNBu^t)] (**4.11**). Esds in Parentheses

Atom	x	y	z	U_{eq} †
Yb(1)	277(1)	2239(1)	8535(1)	45(1)
I(1)	2265(1)	1229(1)	8910(1)	64(1)
B(1)	-2295(8)	3093(4)	8084(5)	49(3)
C(1)	1722(8)	3228(5)	8142(5)	68(3)
N(1)	1958(7)	3721(3)	7927(5)	73(3)
C(2)	2181(10)	4360(5)	7608(7)	87(4)
C(3)	3506(15)	4370(8)	7228(10)	107(5)
C(4)	1253(18)	4446(10)	6863(12)	125(6)
C(5)	1980(23)	4818(11)	8244(13)	150(8)
C(3A)	2399(43)	4363(21)	6804(25)	115(13)
C(4A)	838(39)	4630(21)	7597(28)	118(13)
C(5A)	3095(39)	4702(21)	8227(25)	107(12)
N(11)	-547(5)	2587(3)	7232(3)	51(2)
N(12)	-1497(5)	3031(3)	7305(3)	48(2)
C(11)	-2729(12)	3804(5)	6447(6)	101(5)
C(12)	-1704(8)	3324(4)	6571(5)	63(3)
C(13)	-877(9)	3065(4)	6034(5)	69(3)
C(14)	-175(7)	2602(4)	6449(4)	57(3)
C(15)	831(9)	2162(4)	6131(5)	71(3)
C(16)	1915(11)	2557(7)	5760(9)	127(6)
C(17)	325(12)	1818(7)	5402(8)	137(6)
C(18)	1363(12)	1745(6)	6748(7)	134(6)
N(21)	-1977(5)	1969(3)	8628(3)	47(2)
N(22)	-2776(5)	2441(3)	8359(3)	47(2)
C(21)	-5091(8)	2625(5)	8122(6)	77(3)
C(22)	-3984(7)	2241(4)	8376(5)	57(3)
C(23)	-3980(7)	1625(4)	8658(5)	59(3)
C(24)	-2715(7)	1476(3)	8807(4)	54(2)
C(25)	-2166(8)	862(4)	9144(6)	72(3)
C(26)	-1265(10)	984(5)	9840(6)	86(4)
C(27)	-3231(10)	426(5)	9431(8)	102(5)
C(28)	-1440(9)	529(5)	8454(6)	89(4)
N(31)	-638(5)	3155(3)	9222(3)	48(2)
N(32)	-1594(5)	3442(3)	8782(3)	48(2)
C(31)	-2852(11)	4434(5)	8799(7)	114(5)
C(32)	-1867(8)	4011(4)	9120(5)	64(3)
C(33)	-1078(8)	4080(4)	9785(5)	71(3)
C(34)	-336(7)	3549(4)	9833(4)	53(2)
C(35)	665(9)	3396(4)	10452(5)	70(3)

C(36)	171(13)	3487(9)	11295(7)	146(7)
C(37)	1103(14)	2745(6)	10400(9)	144(7)
C(38)	1774(11)	3859(7)	10342(9)	145(7)

† Equivalent isotropic U_{eq} defined as one third of the trace of the orthogonalised U_{ij} tensor

Table A1.33 Bond Lengths (Å) for [$Tp^{3\text{-}t\text{-}Bu\text{-}5\text{-}Me}$YbI(CNBu^t)] (**4.11**). Esds in Parentheses

Yb(1)-I(1)	3.051(1)	Yb(1)-C(1)	2.670(9)
Yb(1)-N(11)	2.416(6)	Yb(1)-N(21)	2.458(5)
Yb(1)-N(31)	2.443(6)	B(1)-N(22)	1.536(10)
B(1)-N(12)	1.549(10)	C(1)-N(1)	1.126(12)
B(1)-N(32)	1.545(10)	C(2)-C(3)	1.542(19)
N(1)-C(2)	1.465(12)	C(2)-C(5)	1.442(24)
C(2)-C(4)	1.571(22)	C(2)-C(4A)	1.530(43)
C(2)-C(3A)	1.345(43)	C(3)-C(3A)	1.356(47)
C(2)-C(5A)	1.571(42)	C(3)-C(5A)	1.843(44)
N(11)-N(12)	1.379(8)	N(11)-C(14)	1.353(9)
N(12)-C(12)	1.372(9)	C(11)-C(12)	1.496(14)
C(12)-C(13)	1.364(12)	C(13)-C(14)	1.399(12)
C(14)-C(15)	1.512(12)	C(15)-C(16)	1.549(16)
C(15)-C(17)	1.493(16)	C(15)-C(18)	1.451(15)
N(21)-N(22)	1.374(8)	N(21)-C(24)	1.334(9)
N(22)-C(22)	1.347(9)	C(21)-C(22)	1.479(11)
C(22)-C(23)	1.379(11)	C(23)-C(24)	1.394(10)
C(24)-C(25)	1.521(11)	C(25)-C(26)	1.503(14)
C(25)-C(27)	1.533(14)	C(25)-C(28)	1.547(14)
N(31)-N(32)	1.376(8)	N(31)-C(34)	1.338(9)
N(32)-C(32)	1.355(10)	C(31)-C(32)	1.464(14)
C(32)-C(33)	1.376(12)	C(33)-C(34)	1.369(11)
C(34)-C(35)	1.495(11)	C(35)-C(36)	1.500(14)
C(35)-C(37)	1.452(15)	C(35)-C(38)	1.538(16)

Table A1.34 Bond Angles (°) for [$Tp^{3\text{-}t\text{-}Bu\text{-}5\text{-}Me}$YbI(CNBu^t)] (**4.11**). Esds in Parentheses

Yb(1)-C(1)-N(1)	157.9(7)	Yb(1)-N(11)-C(14)	138.2(5)
Yb(1)-N(11)-N(12)	112.6(4)	Yb(1)-N(21)-C(24)	139.9(5)
Yb(1)-N(21)-N(22)	113.9(4)	Yb(1)-N(31)-C(34)	138.1(5)
Yb(1)-N(31)-N(32)	113.3(4)	I(1)-Yb(1)-C(1)	101.4(2)
I(1)-Yb(1)-N(11)	129.1(1)	I(1)-Yb(1)-N(21)	119.6(1)
I(1)-Yb(1)-N(31)	137.2(1)	N(11)-C(14)-C(13)	108.8(7)
N(11)-C(14)-C(15)	121.9(7)	N(11)-N(12)-C(12)	109.8(6)

N(11)-Yb(1)-N(21)	77.6(2)
N(12)-B(1)-N(22)	110.7(6)
N(12)-C(12)-C(11)	122.2(7)
N(12)-N(11)-C(14)	106.7(6)
N(21)-C(24)-C(25)	121.4(6)
N(21)-Yb(1)-N(31)	76.4(2)
N(22)-C(22)-C(21)	124.9(7)
N(22)-N(21)-C(24)	105.9(5)
N(31)-C(34)-C(35)	122.6(7)
N(32)-C(32)-C(31)	123.1(8)
N(32)-N(31)-C(34)	106.9(5)
B(1)-N(12)-N(11)	122.3(5)
B(1)-N(22)-N(21)	122.5(5)
B(1)-N(32)-N(31)	121.7(5)
C(12)-C(13)-C(14)	107.7(7)
C(14)-C(15)-C(16)	109.5(8)
C(14)-C(15)-C(18)	113.5(8)
C(16)-C(15)-C(18)	108.5(9)
C(21)-C(22)-C(23)	127.5(7)
C(22)-C(23)-H(23A)	127.0(4)
C(24)-C(25)-C(26)	111.6(7)
C(24)-C(25)-C(28)	108.0(7)
C(26)-C(25)-C(28)	108.7(8)
C(31)-C(32)-C(33)	130.1(8)
C(33)-C(34)-C(35)	128.0(7)
C(34)-C(35)-C(37)	112.8(8)
C(36)-C(35)-C(37)	106.9(10)
C(37)-C(35)-C(38)	110.4(9)
C(1)-Yb(1)-N(11)	75.5(2)
C(1)-Yb(1)-N(31)	74.1(2)
C(3)-C(2)-C(5)	115.3(13)
C(3A)-C(2)-C(5A)	121.6(25)
C(4A)-C(2)-C(5A)	113.6(24)
N(1)-C(2)-C(3A)	112.8(21)
N(1)-C(2)-C(4A)	101.1(18)
N(1)-C(2)-C(5A)	106.8(17)

N(11)-Yb(1)-N(31)	91.7(2)
N(12)-B(1)-N(32)	113.1(6)
N(12)-C(12)-C(13)	107.0(7)
N(21)-C(24)-C(23)	110.5(6)
N(21)-N(22)-C(22)	110.3(6)
N(22)-B(1)-N(32)	111.4(6)
N(22)-C(22)-C(23)	107.6(6)
N(31)-C(34)-C(33)	109.4(6)
N(31)-N(32)-C(32)	109.4(6)
N(32)-C(32)-C(33)	106.8(7)
B(1)-N(12)-C(12)	127.4(6)
B(1)-N(22)-C(22)	127.2(6)
B(1)-N(32)-C(32)	128.5(6)
C(11)-C(12)-C(13)	130.7(8)
C(13)-C(14)-C(15)	129.2(7)
C(14)-C(15)-C(17)	109.2(8)
C(16)-C(15)-C(17)	101.9(9)
C(17)-C(15)-C(18)	113.6(10)
C(22)-C(23)-C(24)	105.6(6)
C(23)-C(24)-C(25)	128.1(7)
C(24)-C(25)-C(27)	110.0(7)
C(26)-C(25)-C(27)	109.3(8)
C(27)-C(25)-C(28)	109.1(8)
C(32)-C(33)-C(34)	107.5(7)
C(34)-C(35)-C(36)	110.5(8)
C(34)-C(35)-C(38)	108.6(8)
C(36)-C(35)-C(38)	107.6(10)
C(1)-N(1)-C(2)	175.6(9)
C(1)-Yb(1)-N(21)	139.0(2)
C(3)-C(2)-C(4)	104.2(11)
C(3A)-C(2)-C(4A)	99.0(27)
C(4)-C(2)-C(5)	113.1(13)
N(1)-C(2)-C(3)	108.0(9)
N(1)-C(2)-C(4)	106.5(10)
N(1)-C(2)-C(5)	109.3(12)

Crystal Structure of $[SmI_2(3,5\text{-}Me_2py)_4]$ (A3.1)

The data collection was routine, and the initial structure solution was obtained using direct methods. Only the Sm and I atoms were refined anisotropically.

Table A1.35 Fractional Atomic Coordinates (Å $\times 10^4$) and Equivalent Isotropic Displacement Parameters U_{eq} (Å$^2 \times 10^3$) for $[SmI_2(3,5\text{-}Me_2py)_4]$ (**A3.1**). Esds in Parentheses

Atom	x	y	z	U_{eq} †
Sm(1)	0	5000	2500	33(1)
I(1)	0	5000	629(1)	58(2)
N(1)	947(10)	2422(10)	2598(10)	37(3)
C(2)	1210(29)	1851(29)	1871(16)	41(8)
C(3)	1729(24)	490(24)	1746(13)	34(7)
C(4)	2022(14)	-171(14)	2399(14)	47(5)
C(5)	1753(33)	449(32)	3104(15)	59(11)
C(6)	1201(34)	1681(31)	3217(18)	55(10)
C(31)	2192(26)	-135(36)	1099(15)	82(10)
C(51)	1828(25)	-271(29)	3993(13)	61(7)

† Equivalent isotropic U_{eq} defined as one third of the trace of the orthogonalised U_{ij} tensor

Table A1.36 Bond Lengths (Å) for $[SmI_2(3,5\text{-}Me_2py)_4]$ (**A3.1**). Esds in Parentheses

Sm(1)-I(1)	3.221(1)	Sm(1)-N(1)	2.706(9)
Sm(1)-I(1A)	3.221(1)	Sm(1)-N(1A)	2.706(9)
Sm(1)-N(1B)	2.706(9)	Sm(1)-N(1C)	2.706(9)
N(1)-C(2)	1.396(32)	N(1)-C(6)	1.315(34)
C(2)-C(3)	1.448(37)	C(3)-C(4)	1.331(31)
C(3)-C(31)	1.351(37)	C(4)-C(5)	1.383(35)
C(5)-C(6)	1.342(44)	C(5)-C(51)	1.688(35)

Table A1.37 Bond Angles (°) for $[SmI_2(3,5\text{-}Me_2py)_4]$ (**A3.1**). Esds in Parentheses

I(1)-Sm(1)-N(1)	93.6(4)	I(1)-Sm(1)-I(1A)	180.0(1)
N(1)-Sm(1)-I(1A)	86.4(4)	I(1)-Sm(1)-N(1A)	86.4(4)
N(1)-Sm(1)-N(1A)	90.2(1)	I(1A)-Sm(1)-N(1A)	93.6(4)
I(1)-Sm(1)-N(1B)	93.6(4)	N(1)-Sm(1)-N(1B)	172.9(7)
I(1A)-Sm(1)-N(1B)	86.4(4)	N(1A)-Sm(1)-N(1B)	90.2(1)
I(1)-Sm(1)-N(1C)	86.4(4)	N(1)-Sm(1)-N(1C)	90.2(1)
I(1A)-Sm(1)-N(1C)	93.6(4)	N(1A)-Sm(1)-N(1C)	172.9(7)
N(1B)-Sm(1)-N(1C)	90.2(1)	Sm(1)-N(1)-C(2)	112.6(14)
Sm(1)-N(1)-C(6)	129.4(16)	C(2)-N(1)-C(6)	117.9(19)
N(1)-C(2)-C(3)	124.7(22)	C(2)-C(3)-C(4)	113.7(20)
C(2)-C(3)-C(31)	131.4(24)	C(4)-C(3)-C(31)	113.7(23)
C(3)-C(4)-C(5)	119.0(19)	C(4)-C(5)-C(6)	127.1(26)

C(4)-C(5)-C(51)	127.0(24)
N(1)-C(6)-C(5)	117.4(26)

C(6)-C(5)-C(51)	105.4(23)

Crystal Structure of $[YbI_2(3,5\text{-}Me_2py)_4]$ (A3.2)

The data collection was routine, and the initial structure solution was obtained using direct methods.

Table A1.38 Fractional Atomic Coordinates (Å $\times 10^4$) and Equivalent Isotropic Displacement Parameters U_{eq} (Å$^2 \times 10^3$) for $[YbI_2(3,5\text{-}Me_2py)_4]$ (**A3.2**). Esds in Parentheses

Atom	x	y	z	U_{eq}†
Yb(1)	0	5000	2500	28(1)
I(1)	0	5000	671(1)	46(1)
N(1)	923(3)	2503(3)	2482(6)	41(1)
C(2)	1228(6)	1813(6)	1831(4)	40(2)
C(3)	1748(8)	513(8)	1799(6)	52(3)
C(4)	1991(5)	-126(4)	2482(9)	50(1)
C(5)	1725(6)	525(7)	3191(5)	42(2)
C(6)	1175(6)	1855(6)	3168(6)	49(2)
C(31)	2014(11)	-172(9)	1020(5)	67(3)
C(51)	1969(12)	-174(12)	3963(8)	88(5)

† Equivalent isotropic U_{eq} defined as one third of the trace of the orthogonalised U_{ij} tensor

Table A1.39 Bond Lengths (Å) for $[YbI_2(3,5\text{-}Me_2py)_4]$ (**A3.2**). Esds in Parentheses

Yb(1)-I(1)	3.132(1)
Yb(1)-I(1A)	3.132(1)
N(1)-C(6)	1.355(12)
C(3)-C(4)	1.345(17)
C(4)-C(5)	1.393(16)
C(5)-C(51)	1.506(15)

Yb(1)-N(1)	2.585(3)
N(1)-C(2)	1.333(10)
C(2)-C(3)	1.361(10)
C(3)-C(31)	1.513(13)
C(5)-C(6)	1.398(9)

Table A1.40 Bond Angles (°) for $[YbI_2(3,5\text{-}Me_2py)_4]$ (**A3.2**). Esds in Parentheses

I(1)-Yb(1)-N(1)	89.3(2)
N(1)-Yb(1)-I(1A)	90.7(2)
N(1)-Yb(1)-N(1B)	178.6(4)

I(1)-Yb(1)-I(1A)	180.0
N(1)-Yb(1)-N(1A)	90.0
I(1A)-Yb(1)-N(1B)	90.7(2)

Yb(1)-N(1)-C(2)	123.9(5)
C(2)-N(1)-C(6)	116.8(4)
C(2)-C(3)-C(4)	117.3(8)
C(4)-C(3)-C(31)	122.3(7)
C(4)-C(5)-C(6)	117.8(8)
C(6)-C(5)-C(51)	120.1(8)

Yb(1)-N(1)-C(6)	119.2(5)
N(1)-C(2)-C(3)	125.6(7)
C(2)-C(3)-C(31)	120.5(8)
C(3)-C(4)-C(5)	121.0(6)
C(4)-C(5)-C(51)	122.1(7)
N(1)-C(6)-C(5)	121.5(8)

Table A2.1 IR Absorption Bands for Complexes **2.3**, **2.5** and Related Compounds (ν cm^{-1}, intensities in parentheses)†

Assignment[160-162]	Calculated for Triflate Anion[160]	$[Bu_4N]^+[OTf]^-$[162]	$[(Tp^{Me_2})_2Dy]^+[OTf]^-$ (**2.5**)	$(\mu\text{-}H)_2Os_3(CO)_9(\mu,\eta^2\text{-}O_2CCH_3)(\eta^1\text{-}OTf)$[163]	$[(Tp^{Me_2})_2Nd(\eta^1\text{-}OTf)]$ (**2.3**)
Tp			457 (m), 457 (m)		454 (m), 458 (m), 464 (m)
$\nu_{S\text{-}O(bd)}$, $\nu_{C\text{-}F(bd)}$	509 (17)	517 (m)	518 (m)		515 (m), 519 (m)
$\nu_{C\text{-}F(bd)}$, $\nu_{S\text{-}O(bd)}$	571 (10)	572 (m)	572 (w)		581 (w)
$\nu_{S\text{-}O(bd)}$, $\nu_{C\text{-}S(st)}$, $\nu_{C\text{-}F(bd)}$	641 (172)	637 (vs)	638 (vs), 643 (sh)		632 (vs)
Tp			652 (s), 666 (sh), 668 (m), 698 (s)		646 (s), 652 (s), 665 (m), 670 (m), 696 (s), 702 (s)
$\nu_{C\text{-}F(st)}$, $\nu_{C\text{-}S(st)}$	757 (14)	751 (m)	752 (w)		759 (m), 765 (m)
Tp			803 (vs,br), 835 (s), 855 (sh), 988 (m)		775 (s), 783 (s), 790 (s), 806 (s, sh), 812 (s), 833 (s), 849 (w), 982 (s, br)
$\nu_{S\text{-}O(st)}$				995	1013 (vs)
Tp			1036 (vs)		1034 (vs,br)
$\nu_{S\text{-}O(st)}$, Tp	1046 (10)	1032 (vs)	1047 (vs)		1045 (vs)
Tp			1071 (vs), 1096 (sh,br), 1127 (m)		1068 (s), 1075 (s), 1120 (w), 1125 (m)
$\nu_{C\text{-}F(st)}$	1214 (140)	1145 (vs)	1146 (vs)	1164	1161 (m,sh), 1166 (vs)
Tp, $\nu_{C\text{-}F(st)}$			1188 (vs,br)	1185	*ca* 1185 (vs,sh)
$\nu_{S\text{-}O}$				1202	1204 (vs,br)
$\nu_{C\text{-}F(st,bd)}$, $\nu_{C\text{-}S(st)}$	1284 (80)	1223 (s)	1226 (m)		
$\nu_{C\text{-}F(st)}$				1232	1234 (vs)
$\nu_{S\text{-}O(st)}$	1310 (368)	1269 (vs)	1276 (vs)		
$\nu_{S\text{-}O(st)}$				1343	1331 (vs)
Tp			1328 (m,br), 1356 (vs), 1382 (s), *ca* 1499 (m,br), 1419 (vs), 1442 (vs), 1538 (vs)		1359 (vs,br), 1377 (s), 1383 (s), 1417 (vs,br), 1441 (vs,br), *ca* 1496 (m,br), 1544 (vs,br)
Tp ($\nu_{B\text{-}H}$)			2566 (m)		2565 (m)
Tp			2931 (m), 2964 (m), 3128 (m)		2929 (m), 2975 (m), 3110 (w)

† Tp = band due to Tp^{Me_2} ligand, bd = bend, st = stretch; vs = strong, s = strong, m = medium, w = weak, sh = shoulder, br = broad

Appendix 3 - Synthesis and Characterisation of Pyridine Derivatives of the Lanthanide Diiodides

During one attempt to displace the THF from $[Tp^{3\text{-}t\text{-}Bu\text{-}5\text{-}Me}SmI(THF)_2]$ (**4.1**), a large excess of 3,5-dimethylpyridine (3,5-Me_2py) was added to a solution of this complex in toluene. Slow diffusion of 30/40 petrol into this solution gave black crystals (**A3.1**), and IR spectroscopy of this product showed that it no longer contained a pyrazolylborate ligand. The X-ray crystal structure of this complex was determined; details of the data collection, together with tables of fractional coordinates, bond lengths and bond angles are given in Appendix 1 (Tables A1.1 and A1.35 to A1.37). The molecular structure of **A3.1** (shown in Figure A3.1) confirmed that the $Tp^{3\text{-}t\text{-}Bu\text{-}5\text{-}Me}$ ligand had been displaced from the metal, which now had two iodide ions and four 3,5-Me_2py ligands in the first coordination sphere.

Figure A3.1 The Molecular Structure of $[SmI_2(3,5\text{-}Me_2py)_4]$ (**A3.1**)†

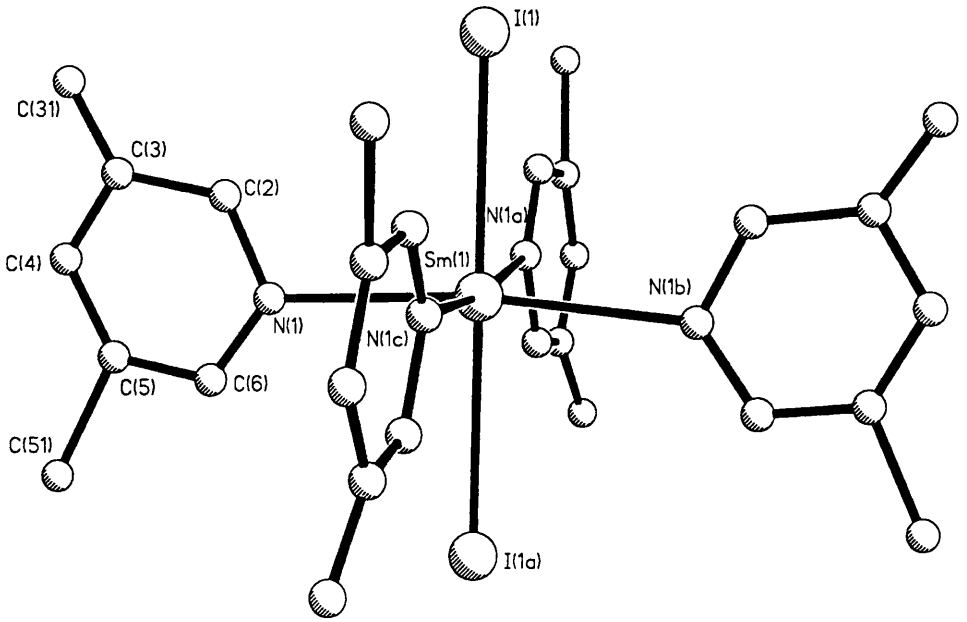

The structural characterisation of a number of Lewis base adducts of Ln^{2+} ions with iodide or other anionic ligands have been reported.[237-239,245,268-270] The area is of particular interest due to the implications the structures of these complexes have for the use of divalent lanthanide compounds as

† Hydrogen atoms omitted for clarity

reducing agents in organic synthesis. **A3.1** had crystallised in the space group $I\bar{4}$; the metal centre lies both on an inversion centre and, along with the two iodide ions, on a four-fold axis. In this highly symmetrical structure, the Sm(1)–I(1) bond length is 3.221(1) Å, compared with 3.191(1) Å in $[Tp^{3\text{-}t\text{-}Bu\text{-}5\text{-}Me}SmI(THF)_2]$ (**4.1**) and 3.242(1) Å in $[Sm(NCBu^t)_2(\mu\text{-}I)_2]_\infty$.[268] The Sm–I distance in the analogous HMPA complex, $[SmI_2(HMPA)_4]$, is much longer at 3.390(2) Å and has been attributed to the very strong σ-donor properties of the HMPA ligand.[238] The Sm–N bond lengths in **A3.1** are 2.706(9) Å, similar to those observed in $[SmI(\mu\text{-}I)(N\text{-}MeIm)_3]$ (2.621(7) to 2.641(6) Å; *N*-MeIm = *N*-Methylimidazole).[237]

The complex **A3.1** can be prepared directly by reaction of SmI_2 in THF with an excess of 3,5-Me_2py, and precipitates as black crystals upon diffusion of 30/40 petrol into this solution. The corresponding Yb compound, **A3.2**, was prepared similarly, and the crystal structure of this complex was determined and found to be isomorphous with **A3.1**. Details of the data collection, together with tables of fractional coordinates, bond lengths and bond angles are given in Appendix 1 (Tables A1.1 and A1.38 to A1.40); Figure A1.2 shows a space filling model of **A3.2**.

Figure A3.2 A Space Filling Model of $[YbI_2(3,5\text{-}Me_2py)_4]$ (**A3.2**)†

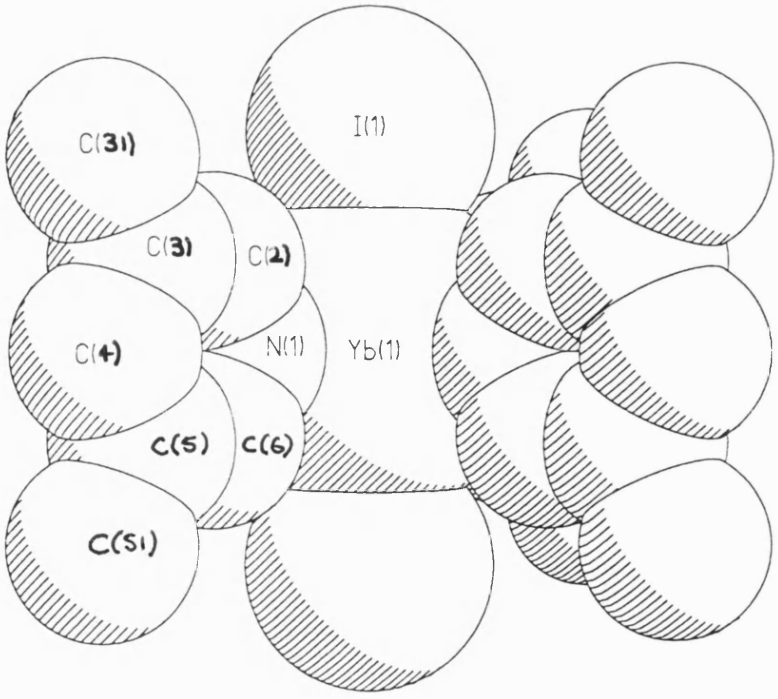

† Hydrogen atoms omitted for clarity

The Yb–I bond length in **A3.2** (3.132(1) Å) is shorter than that observed in **A3.1**, consistent with the smaller ionic radius of the Yb^{2+} ion over Sm^{2+}. The corresponding Yb–I distance in $[YbI_2(THF)_4]$ (3.103(1) Å) is similar to that in **A3.2**. The Yb–N bond length in **A3.2** (2.585(4) Å) is comparable with those in other six coordinate pyridine complexes of Yb^{2+}: $[Yb(EPh)_2(py)_4]$ (E = S, 2.565(7) and 2.529(7) Å; E = Se, 2.502(4) and 2.563(5) Å; E = Te, 2.62(1) Å)[245] and $[(C_5H_5N)_5Yb(CH_3CN)_2]^{2+}$ (2.52(2) to 2.55(2) Å).[270]

We have also synthesised other pyridine adducts of LnI_2 in a manner analogous to that outlined above. When unsubstituted pyridine (py) was used, black crystals were obtained which desolvated very rapidly upon removal from the solvent. Thus, elemental analyses were poor for these products. However, in the light the report by Evans and coworkers of the structure of a seven coordinate THF adduct of SmI_2 - $[SmI_2(THF)_5]$[239§] - we tentatively assign these complexes the formulae $[LnI_2(py)_5]$ (Ln = Sm, **A3.3**; Ln = Yb, **A3.4**). The corresponding reactions of LnI_2 in THF with an excess of 4-*tert*-butylpyridine (4-Bu^{t}py) gives black crystals after diffusion of 30/40 petrol into the solution. The elemental analysis of the Sm^{2+} complex was consistent with this compound (**A3.5**) having the composition $[SmI_2(Bu^tpy)_4]$. We were unable to obtain a reasonable analysis for the Yb complex; however, a preliminary X-ray crystal structure of this compound (**A3.6**) indicates that it has the formula $[YbI_2(Bu^tpy)_4]$. Both **A3.5** and **A3.6** are soluble in aromatic solvents and were characterised by ^1H and ^{13}C NMR.

Complexes **A3.1** and **A3.2** are extremely insoluble in most solvents (they dissolve in THF to give $LnI_2(THF)_n$ as shown by UV spectroscopy). We suppose that this provided the driving force for the original synthesis of **A3.1**, the other product from this ligand redistribution reaction presumably being $[(Tp^{3\text{-}t\text{-}Bu\text{-}5\text{-}Me})_2Sm]$ (Equation A3.1).

Equation A3.1

$$2\,[Tp^{3\text{-}Bu^t\text{-}5\text{-}Me}SmI(THF)_2] + 4\;\;3,5\text{-}Me_2py \xrightarrow[\text{excess } 3,5\text{-}Me_2py]{THF} [SmI_2(3,5\text{-}Me_2py)_4]\;(A3.1) + [(Tp^{3\text{-}Bu^t\text{-}5\text{-}Me})_2Sm]\;?$$

§ Desolvation of $SmI_2(THF)_5$ was reported to extremely facile and no elemental analysis was reported

Appendix 4 - Variable Temperature ^{1}H NMR Experiment for [Tp$^{3\text{-}t\text{-Bu-5-Me}}$YbI(3,5-dimethylpyridine)] (4.9b) [246]

The rigorous analysis of temperature dependent NMR spectra, to extract activation energies and transition state parameters, requires empirical computer simulation of the line shapes. This is particularly so when the exchange process involves more than two sites. However, approximate methods are available which can be used to estimate these parameters, and it is this approach that will be followed here.

Two dynamic processes may be responsible for the fluxional behaviour of [Tp$^{3\text{-}t\text{-Bu-5-Me}}$YbI(3,5-Me$_2$py)] (**4.9b**). The first involves hindered rotation of the 3,5-Me$_2$py ligand about the Yb–N bond, such that in the low temperature ^{1}H NMR spectrum, the two Me substituents on this ligand become inequivalent. The second process concerns the rearrangement of the coordination environment of the Yb^{2+} ion, so that at room temperature the three pyrazolyl rings are equivalent but in the slow exchange limit they become split in the ratio 2:1. This inequivalence is presumed, on the basis of the solid state structure of the THF analogue **4.2**, to be due to coordination of 3,5-Me$_2$py in the cleft between two of the Bu^t substituents of the Tp$^{3\text{-}t\text{-Bu-5-Me}}$ ligand. These processes may be linked, with some concerted rearrangement of the Yb^{2+} coordination sphere being responsible for the equivalence both of the pyrazolyl rings and the Me substituents on the pyridine. Equally, we may be observing the rapid dissociation/recoordination of the pyridine ligand at room temperature, which again could account for the observed equivalencies.

The variable temperature ^{1}H NMR spectra of **4.9b** are shown in Figure A4.1; an expansion of the methyl region of the spectrum is shown in Figure A4.2.

When the populations (p_A and p_B) of two exchanging sites (A and B) are equal, an approximation to the rate constant (k_c) for the exchange process at the coalescence temperature (T_c) is given by

$$k_c = \frac{\pi \Delta \nu}{\sqrt{2}}$$

Figure A4.1 The Variable ^1H NMR Spectra of [$Tp^{3\text{-}t\text{-}Bu\text{-}5\text{-}Me}$YbI($Me_2$py)] **(4.9b)**

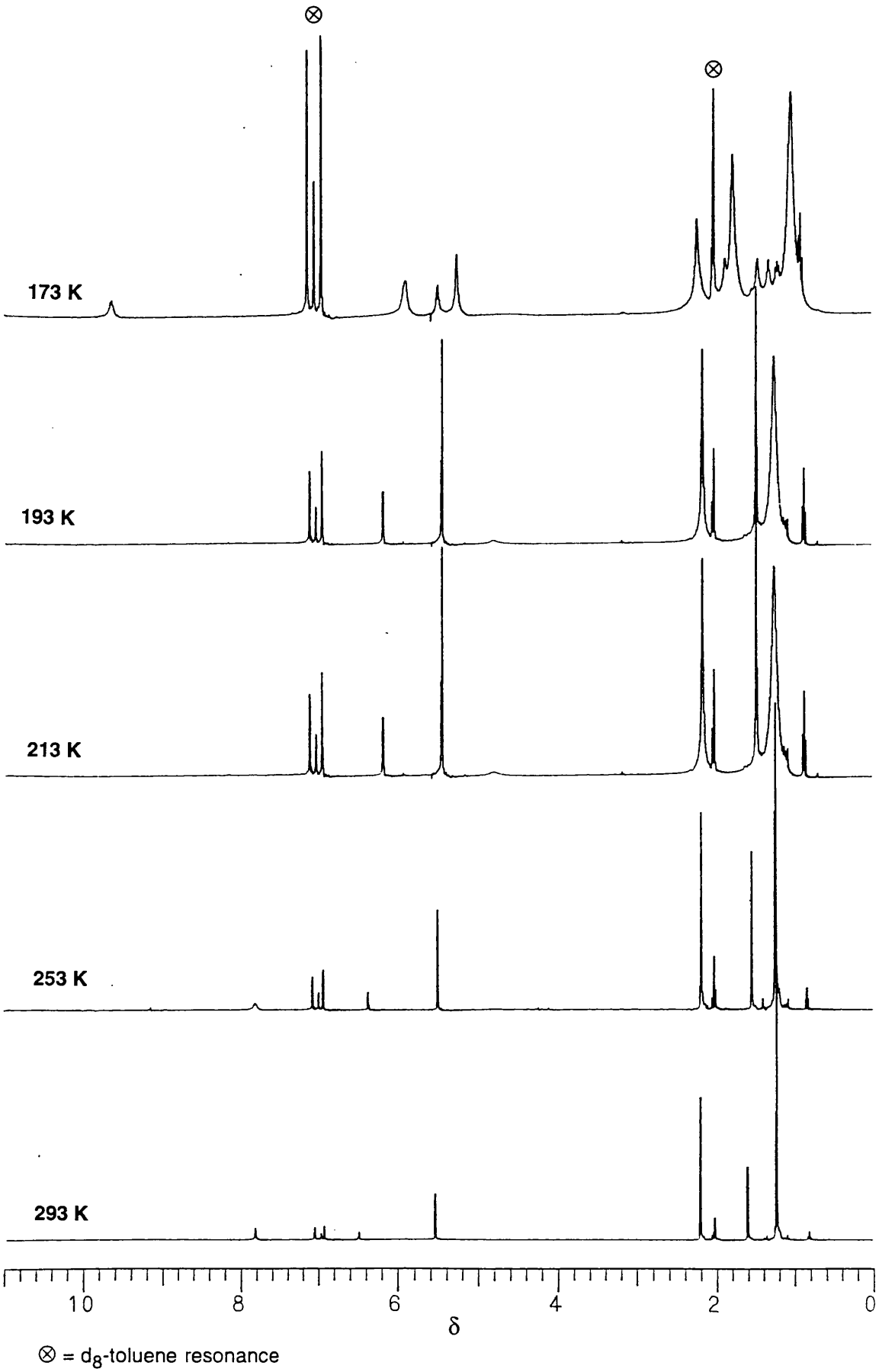

⊗ = d_8-toluene resonance

Figure A4.2 An Expansion of the Methyl Region of the Variable ^{1}H NMR Spectra of $[Tp^{3\text{-}t\text{-}Bu\text{-}5\text{-}Me}YbI(Me_2py)]$ **(4.9b)**

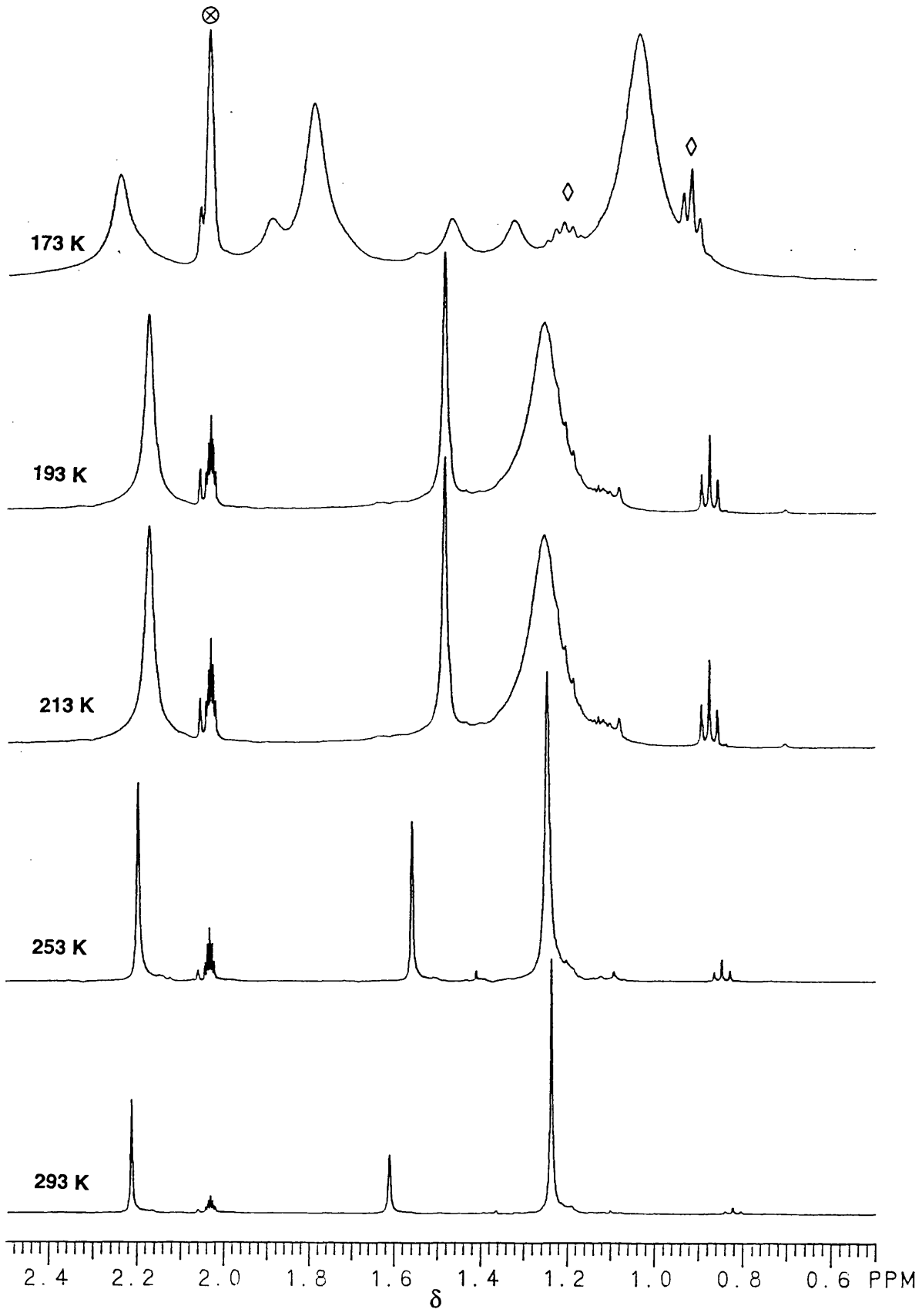

⊗ = d_8-toluene resonance; ◊ = 30/40 petrol resonance

where $\Delta\nu$ is the frequency separation of the two resonances in the 'static' spectrum. The value of k_c can than be substituted into the Eyring equation to obtain a value for the free energy of activation ($\Delta G^{\ddagger}$) for the transition state (R is the universal gas constant, 8.31 J K^{-1}):

$$\Delta G^{\ddagger} = RT_c\{23.76 - \ln(k_c/T_c)\}$$

The data obtained for the exchange of the substituents in 3,5-Me_2py and the calculated values of $\Delta G^{\ddagger}$ are given in Table A4.1.

Table A4.1 The Free Energies of Activation for the Hindered Rotation of the 3,5-Me_2py Ligand in [$Tp^{3\text{-}t\text{-}Bu\text{-}5\text{-}Me}$YbI(3,5-$Me_2$py)] (**4.9b**) Calculated from Coalescence Temperatures

Resonance	$\delta^{\dagger}$ (293 K)	$\delta^{\dagger}$ (173 K)	$\Delta\nu$ (Hz)	k_c (s^{-1})	T_c (K)	$\Delta G^{\ddagger}$ (kJ mol^{-1})
2,6-H	7.81 (2H)	9.62 (1H) 5.90 (2H)	1490	3640	208±10	36±2
3,5-Me	1.61 (6H)	1.46 (3H) 1.32 (3H)	56	130	188±5	37.5±2

Another method for extracting information from variable temperature NMR spectra is by a simple analysis of line width. In the fast exchange spectra at temperatures approaching that at which coalescence occurs, the rate constant is given by the equation

$$k_A = \frac{4\pi p_A p_B^2 \Delta\nu^2}{\Delta_e}$$

in which Δ_e is the broadening of the peak due to exchange.[§] Once values of the rate constant have been obtained at different temperatures, these may then be used to determine the activation enthalpy ($\Delta H^{\ddagger}$) and entropy ($\Delta S^{\ddagger}$) by plotting $\ln(k_A/T)$ against reciprocal temperature

† Integration of the peaks in parentheses. The 2-H 3,5-Me_2py resonance at δ 5.90 in the spectrum of **4.9a** at 173 K overlaps with the 4-H peak and hence integrates as two protons

§ Obtained by subtracting $w_{1/2}$ of a non-dynamic peak (*eg* that of the NMR solvent) from $w_{1/2}$ of the resonance under consideration

$$\ln(k_A/T) = 23.76-(\Delta H^{\ddagger}/RT)+(\Delta S^{\ddagger}/R)$$

The results of this 'exchange broadening' analysis for the 2,6-H_2 and 3,5-Me_2 resonances of the 3,5-Me_2py ligand in **4.9b** are given in Table A4.2 and Figure A4.3. The analysis was also carried out for the 3-Bu^t and 5-Me peaks and the these results are shown in Table A4.3 and Figure A4.4.

Table A4.2 The Results of Exchange Broadening Analysis of the 3,5-Me_2py Resonances in the ^{1}H NMR Spectra of [Tp$^{3\text{-}t\text{-Bu-5-Me}}$YbI(3,5-$Me_2$py)] (**4.9b**)

2,6-H_2 Resonance ($\Delta\nu$ = 1490 Hz)		
T	**Δ_e**	**k_A**
253	8	436000
233	45	77500
223	90	38700
$\Delta H^{\ddagger}$ = 36 kJ mol^{-1}		
$\Delta S^{\ddagger}$ = 8 J mol^{-1}		
$\Delta G^{\ddagger}$ = 34 kJ mol^{-1} (at 208 K)		

3,5-Me_2 Resonance ($\Delta\nu$ = 56 Hz)		
T	**Δ_e**	**k_A**
213	3.7	1330
203	7.3	675
193	28	175
$\Delta H^{\ddagger}$ = 33 kJ mol^{-1}		
$\Delta S^{\ddagger}$ = -26 J mol^{-1}		
$\Delta G^{\ddagger}$ = 38 kJ mol^{-1} (at 208 K)		

Table A4.3 The Results of Exchange Broadening Analysis of the Pyrazolyl Resonances in the ^{1}H NMR Spectra of [Tp$^{3\text{-}t\text{-Bu-5-Me}}$YbI(3,5-$Me_2$py)] (**4.9b**)

3-Bu^t Resonance ($\Delta\nu$ = 300 Hz)		
T	**Δ_e**	**k_A†**
233	7.3	11500
223	13.3	6300
213	31.3	2680
203	97.3	860
$\Delta H^{\ddagger}$ = 32 kJ mol^{-1}		
$\Delta S^{\ddagger}$ = -26 J mol^{-1}		
$\Delta G^{\ddagger}$ = 37 kJ mol^{-1} (at 208 K)		

5-Me Resonance ($\Delta\nu$ = 140 Hz)		
T	**Δ_e**	**k_A†**
223	4.7	3880
213	8	2280
203	22.3	818
193	58	314
$\Delta H^{\ddagger}$ = 32 kJ mol^{-1}		
$\Delta S^{\ddagger}$ = -27 J mol^{-1}		
$\Delta G^{\ddagger}$ = 38 kJ mol^{-1} (at 208 K)		

† k_A in this case is calculated with respect to the doubly degenerate site, *ie* p_A = 2/3

Figure A4.3 A Plot of $\ln(k_A/T)$ Against Reciprocal Temperature for the 3,5-Me_2py Resonances in the ^1H NMR Spectra of [$Tp^{3\text{-}t\text{-}Bu\text{-}5\text{-}Me}$YbI(3,5-$Me_2$py)] (**4.9b**)

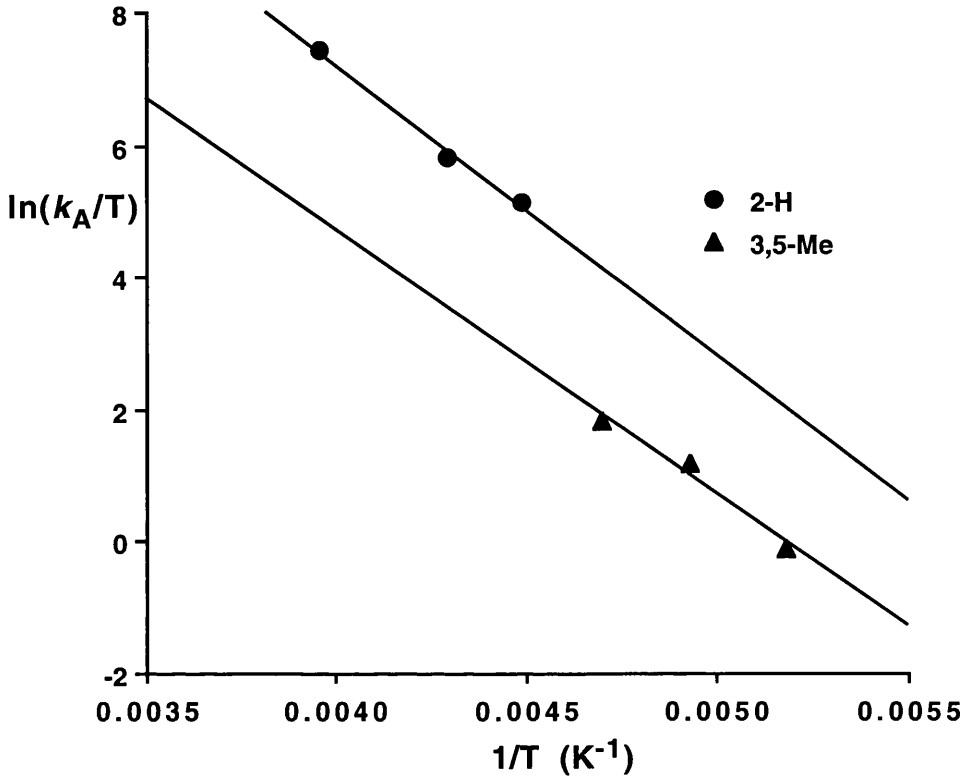

The activation parameters determined by the line shape analysis for exchange of the pyrazolyl rings in **4.9b**, are consistent for the 3-Bu^t and the 5-Me resonances. On the other hand, those determined for the rotation of 3,5-Me_2py are not: the apparent rate constant for exchange of the 2,6-H_2 sites in this molecule is an order of magnitude greater than that for the 3,5-Me_2 groups (resulting in vastly different calculated activation entropies). This discrepancy may be caused by the 2,6-H_2 and 3,5-Me_2 protons having very different transverse (T_2) relaxation times, which are important in determining the line widths of the resonances. In addition, accurate determination of line widths and peak separations are complicated by the slight temperature dependence of the chemical shifts. Hence, it is not possible to determine whether a single process is responsible for the fluxionality both of the pyrazolyl rings and the pyridine substituents. Despite this, the range of values of $\Delta G^{\ddagger}$ (at 208 K) obtained from these analyses is relatively small (34 to 38 kJ mol^{-1}).

Figure A4.4 A Plot of $\ln(k_A/T)$ Against Reciprocal Temperature for the Pyrazolyl Resonances in the ^1H NMR Spectra of $[Tp^{3\text{-}t\text{-}Bu\text{-}5\text{-}Me}YbI(3,5\text{-}Me_2py)]$ (**4.9b**)

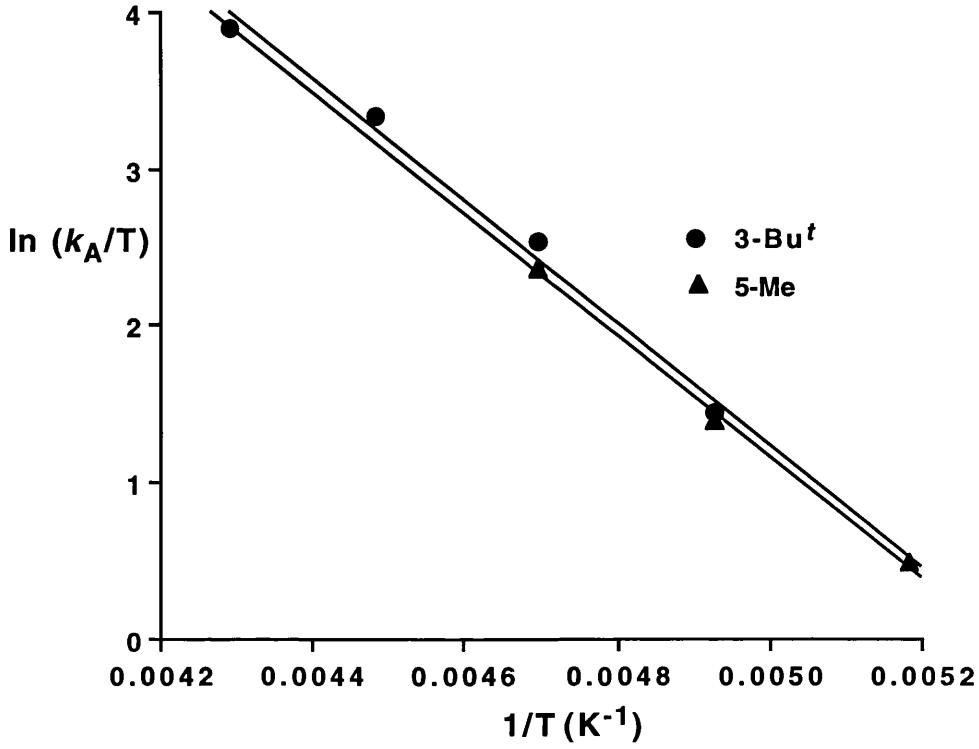

At 293 K, $\Delta G^{\ddagger}$ for the rearrangement of the Yb^{2+} coordination sphere in **4.9b** is probably 40±1 kJ mol^{-1}.†

† This neglects the value of $\Delta G^{\ddagger}$ calculated from exchange broading of the 2,6-H resonance of the 3,5-Me_2py ligand; the positive value of $\Delta S^{\ddagger}$ which was obtained from this analysis suggests that the activation parameters are unreliable

References

1. Maunder, G. H.; Sella, A.; Tocher, D. A. *J. Chem. Soc., Chem. Commun.* **1994**, 885-886.
2. Liu, S.-Y.; Maunder, G. H.; Sella, A.; Stevenson, M.; Tocher, D. A. *Inorg. Chem.* **1995**, *35*, 76-81.
3. Maunder, G. H.; Sella, A.; Tocher, D. A. *J. Chem. Soc., Chem. Commun.* **1994**, 2689-2690.
4. Moeller, T. in *Comprehensive Inorganic Chemistry*; J. C. Bailar, H. J. Emeléus, R. Nyholm and A. F. Trotman-Dickenson, Ed.; Pergamon Press: Oxford, 1973; Vol. 4; Chap. 44; pp 1-101.
5. Greenwood, N. N.; Earnshaw, A. *Chemistry of the Elements*; first ed.; Pergamon Press: Oxford, 1986; Chap. 30; pp 1423-1449.
6. Mellor, J. W. *A Comprehensive Treatise on Inorganic and Theoretical Chemistry*; first ed.; Longmans, Green and Co: London, 1924; Vol. 7; Chap. 44; pp 174-253.
7. Tompkins, E. R.; Khym, J. X.; Cohn, W. E. *J. Am. Chem. Soc.* **1947**, *69*, 2769-2777.
8. Spedding, F. H.; Voigt, A. F.; Gladrow, E. M.; Sleight, N. R. *J. Am. Chem. Soc.* **1947**, *69*, 2777-2781.
9. Peppard, D. F.; Faris, J. P.; Gray, P. R.; Mason, G. W. *J. Phys. Chem.* **1953**, *57*, 294-301.
10. Marinsky, J. A.; Glendenin, L. E.; Coryell, C. D. *J. A. Chem. Soc.* **1947**, *69*, 2781-2785.
11. Freeman, A. J. *Physica* **1980**, *102B*, 3-11.
12. Johnson, D. A. *Some Thermodynamic Aspects of Inorganic Chemistry*; second ed.; Cambridge University Press: Cambridge, 1982; Chap. 6.8; pp 158-168.
13. Connick, R. E. *J. Chem. Soc., Suppl.* **1949**, 235-241.
14. Freeman, A. J.; Watson, R. E. *Phys. Rev.* **1962**, *127*, 2058-2075.
15. Shannon, R. D. *Acta Cryst.* **1976**, *A32*, 751-767.
16. McClure, D. S.; Kliss, Z. *J. Chem. Phys.* **1963**, *39*, 3251-3257.
17. Mikheev, N. B.; Kamenskaya, A. N. *Coord. Chem. Rev.* **1991**, *109*, 1-59.
18. Kamenskaya, A. N.; Mikheev, N. B.; Kholmogorova, N. P. *Russ. J. Inorg. Chem.* **1983**, *28*, 1420-1423.
19. Mikeev, N. B. *Naturwissenschaften* **1989**, *76*, 107-113.
20. Molander, G. A. *Chem. Rev.* **1992**, *92*, 29-68.
21. Greco, A.; Cesca, S.; Bertolini, G. *J. Organomet. Chem.* **1976**, *113*, 321-330.
22. Edelmann, F. T. *New J. Chem.* **1995**, *19*, 535-550.
23. Wedler, M.; Recknagel, A.; Edelmann, F. T. *J. Organomet. Chem.* **1990**, *395*, C26-C29.
24. Evans, W. J. *Polyhedron* **1987**, *6*, 803-835.
25. Cloke, F. G. N.; de Lemos, H. C.; Sameh, A. A. *J. Chem. Soc., Chem. Commun.* **1986**, 1344-1345.
26. Bochkarev, M. N.; Trifonov, A. A.; Cloke, F. G. N.; Dalby, C. I.; Matsunaga, P. T.;

Andersen, R. A.; Schumann, H.; Loebel, J.; Hemling, H. *J. Organomet. Chem.* **1995**, *486*, 177-182.

27. Cloke, F. G. N. *Abs. Am. Chem. Soc.* **1995**, *207 Part 1*, INOR 403.
28. Brennan, J. G.; Cloke, F. G. N.; Sameh, A. A.; Zalkin, A. *J. Chem. Soc., Chem. Commun.* **1987**, 1668-1669.
29. Anderson, D. M.; Cloke, F. G. N.; Cox, P. A.; Edelstein, N.; Green, J. C.; Pang, T.; Sameh, A. A.; Shalimoff, G. *J. Chem. Soc., Chem. Commun.* **1989**, 53-55.
30. Cloke, F. G. N. *Chem. Soc. Rev.* **1993**, 17-24.
31. Burns, C. J.; Bursten, B. E. *Comments Inorg. Chem.* **1989**, *9*, 61-93.
32. Wilkinson, G.; Birmingham, J. M. *J. Am. Chem. Soc.* **1954**, *76*, 6210.
33. Birmingham, J. M.; Wilkinson, G. *J. Am. Chem. Soc.* **1956**, *78*, 42-44.
34. Raymond, K. N.; Eigenbrot, C. W., Jr. *Acc. Chem. Res.* **1980**, *13*, 276-283.
35. Andersen, R. A.; Boncella, J. M.; Burns, C. J.; Green, J. C.; Hohl, D.; Rösch, N. *J. Chem. Soc., Chem. Commun.* **1986**, 405-407.
36. Green, J. C.; Hohl, D.; Rösch, N. *Organometallics* **1987**, *6*, 712-720.
37. Boudreaux, E. A.; Baxter, E. *Int. J. Quant. Chem.* **1994**, *Quant. Chem. Symp. 28*, 565-569.
38. Green, J. C.; Kelly, M. R.; Long, J. A.; Kanellakopulos, B.; Yarrow, P. I. W. *J. Organomet. Chem.* **1981**, *212*, 329-340.
39. Di Bella, S.; Gulino, A.; Lanza, G.; Fragalà, I.; Stern, D.; Marks, T. J. *Organometallics* **1994**, *13*, 3810-3815.
40. Min, X. M. *Acta Chim. Sinica* **1992**, *50*, 449-455.
41. Min, X. M. *Acta Chim. Sinica* **1992**, *50*, 1098-1104.
42. Min, X. M. *Acta Chim. Sinica* **1994**, *52*, 996-1001.
43. Green, J. C. *Structure and Bonding* **1981**, *43*, 37-112.
44. Brown, D. *Halides of the Lanthanides and Actinides*; Wiley-Interscience: London, 1968.
45. Bradley, D. C.; Ghotra, J. S.; Hart, F. A.; Hursthouse, M. B.; Raithby, P. R. *J. Chem. Soc., Dalton Trans.* **1977**, 1166-1172.
46. Hitchcock, P. B.; Lappert, M. F.; Smith, R. G.; Bartlett, R. A.; Power, P. P. *J. Chem. Soc., Chem. Commun.* **1988**, 1007-1009.
47. Schaverien, C. J.; Orpen, A. G. *Inorg. Chem.* **1991**, *30*, 4968-4978.
48. Evans, W. J.; Hughes, L. A.; Hanusa, T. P. *J. Am. Chem. Soc.* **1984**, *106*, 4270-4272.
49. Evans, W. J.; Hughes, L. A.; Hanusa, T. P. *Organometallics* **1986**, *5*, 1285-1291.
50. Andersen, R. A.; Boncella, J. M.; Burns, C. J.; Blom, R.; Haaland, A.; Volden, H. V. *J. Organomet. Chem.* **1986**, *312*, C49-C52.
51. Burns, C. J. PhD Thesis, University of California, Berkeley, 1987.
52. Williams, R. A.; Hanusa, T. P.; Huffman, J. C. *Organometallics* **1990**, *9*, 1128-1134.
53. Andersen, R. A.; Blom, R.; Burns, C. J.; Volden, H. V. *J. Chem. Soc., Chem. Commun.* **1987**, 768-769.
54. Jutzi, P.; Holtmann, U.; Kanne, D.; Krüger, C.; Blom, R.; Gleiter, R.; Hyla-Kryspin, I. *Chem. Ber.* **1989**, *122*, 1629-1639.
55. Jutzi, P.; Kohl, F.; Hofman, P.; Krüger, C.; Tsay, Y.-H. *Chem. Ber.* **1980**, *113*, 757-769.

56. Atwood, J. L.; Hunter, W. E.; Cowley, A. H.; Jones, R. A.; Stewart, C. A. *J. Chem. Soc., Chem. Commun.* **1981**, 925-927.
57. Almlöf, J.; Fernholt, L.; Fægri, K., Jr.; Haaland, A.; Schilling, B. E. R.; Seip, R.; Taugbøl, K. *Acta Chem. Scand.* **1983**, *37A*, 131-140.
58. Rittner, E. S. *J. Chem. Phys.* **1951**, *19*, 1030-1035.
59. Guido, M.; Gigli, G. *J. Chem. Phys.* **1976**, *65*, 1397-1402.
60. Hollis, T. K.; Burdett, J. K.; Bosnich, B. *Organometallics* **1993**, *12*, 3385-3386.
61. Bosnich, B. *Chem. Soc. Rev.* **1994**, *23*, 387-395.
62. Timofeeva, T. V.; Lii, J.-H.; Allinger, N. L. *J. Am. Chem. Soc.* **1995**, *117*, 7452-7459.
63. Kaupp, M.; Schleyer, P. V.; Dolg, M.; Stoll, H. *J. Am. Chem. Soc.* **1992**, *114*, 8202-8208.
64. King, W. A.; Marks, T. J.; Anderson, D. M.; Duncalf, D. J.; Cloke, F. G. N. *J. Am. Chem. Soc.* **1992**, *114*, 9221-9223.
65. King, W. A.; Dibella, S.; Lanza, G.; Khan, K.; Duncalf, D. J.; Cloke, F. G. N.; Fragala, I. L.; Marks, T. J. *J. Am. Chem. Soc.* **1996**, *118*, 627-635.
66. Drago, R. S. *Physical methods for Chemists;* second ed.; Saunders: Philadelphia, 1992.
67. Bursten, B. E.; Kaltsoyannis, N. *J. Organomet. Chem.* **1996**, submitted.
68. Bovey, F. A. *Nuclear Magnetic Resonance Spectroscopy;* second ed.; Academic Press: London, 1988.
69. Dobson, C. M.; Levine, B. A. *New Techniques in Biophysics and Cell Biology*; first ed.; R. H. Pain and B. J. Smith, Ed.; Wiley: London, 1976; Vol. 3; Chap. 2; pp 19-91.
70. Eaton, D. R. in *Physical Methods in Advanced Inorganic Chemistry*; H. A. O. Hill and P. Day, Ed.; Wiley Interscience: New York, 1968; Chap. pp 462-537.
71. Bleaney, B. *J. Mag. Res.* **1972**, *8*, 91-100.
72. Stainer, M. V. R.; Takats, J. *J. Am. Chem. Soc.* **1983**, *105*, 410-415.
73. Aime, S.; Botta, M.; Ermondi, G. *Inorg. Chem.* **1992**, *31*, 4291-4299.
74. Werner, J.; Yünlü, K.; Oroschin, W.; Amberger, H.-D.; Fischer, R. D. *Inorg. Chim. Acta* **1984**, *95*, 85-104.
75. Fischer, F. O.; Fischer, H. *J. Organomet. Chem.* **1965**, *3*, 181-187.
76. Maginn, R. E.; Manastyrskyj, S.; Dubeck, M. *J. Am. Chem. Soc.* **1963**, *85*, 672-676.
77. Marks, T. J. *Prog. Inorg. Chem.* **1978**, *24*, 51-107.
78. Lappert, M. F.; Singh, A.; Atwood, J. L.; Hunter, W. E. *J. Chem. Soc., Chem. Commun.* **1981**, 1190-1191.
79. Watson, P. L.; Parshall, G. W. *Acc. Chem. Res.* **1985**, *18*, 51-56.
80. Holton, J.; Lappert, M. F.; Ballard, D. G. H.; Pearce, R.; Atwood, J. L.; Hunter, W. E. *J. Chem. Soc., Dalton Trans.* **1979**, 54-61.
81. Evans, W. J.; Drummond, D. K.; Hanusa, T. P.; Doedens, R. J. *Organometallics* **1987**, *6*, 2279-2285.
82. Namy, J. L.; Girard, P.; Kagan, H. B. *Nouv. J. Chim.* **1981**, *5*, 479-484.
83. Deacon, G. B.; Koplick, A. J.; Tuong, T. D. *Polyhedron* **1982**, *1*, 423-424.
84. Zinnen, H. A.; Pluth, J. J.; Evans, W. J. *J. Chem. Soc., Chem. Commun.* **1980**, 810-812.

85. Evans, W. J.; Ulibarri, T. A.; Ziller, J. W. *J. Am. Chem. Soc.* **1988**, *110*, 6877-6879.
86. Burns, C. J.; Andersen, R. A. *J. Am. Chem. Soc.* **1987**, *109*, 915-917.
87. Burns, C. J.; Andersen, R. A. *J. Am. Chem. Soc.* **1987**, *109*, 941-942.
88. Evans, W. J. *New J. Chem.* **1995**, *19*, 525-533.
89. Edelmann, F. T. *Angew. Chem. Int. Ed. Eng.* **1995**, *34*, 2466-2488.
90. Tilley, T. D.; Zalkin, A.; Andersen, R. A.; Templeton, D. H. *Inorg. Chem.* **1981**, *20*, 551-554.
91. Deacon, G. B.; Hitchcock, P. B.; Holmes, S. A.; Lappert, M. F.; MacKinnon, P.; Newnham, R. H. *J. Chem. Soc., Chem. Commun.* **1989**, 935-937.
92. van den Hende, J. R.; Hitchcock, P. B.; Lappert, M. F. *J. Chem. Soc., Chem. Commun.* **1994**, 1413-1414.
93. Çetinkaya, B.; Hitchcock, P. B.; Lappert, M. F.; Smith, R. G. *J. Chem. Soc., Chem. Commun.* **1992**, 932-934.
94. Cary, D. R.; Arnold, J. *Inorg. Chem.* **1994**, *33*, 1791-1796.
95. Cloke, F. G. N.; Dalby, C. I.; Hitchcock, P. B.; Karamallakis, H.; Lawless, G. A. *J. Chem. Soc., Chem. Commun.* **1991**, 779-781.
96. Bochkarev, L. N.; Makarov, V. M.; Hrzhanovskaya, Y. N. *J. Organomet. Chem.* **1994**, *467*, C3-C5.
97. Nief, F.; Ricard, L. *J. Chem. Soc., Chem. Commun.* **1994**, 2723-2724.
98. Eaborn, C.; Hitchcock, P. B.; Izod, K.; Smith, J. D. *J. Am. Chem. Soc.* **1994**, *116*, 12071-12072.
99. Trofimenko, S. *Acc. Chem. Res.* **1971**, *4*, 17-22.
100. Trofimenko, S. in *Progress In Inorganic Chemistry*; S. J. Lippard, Ed.; Wiley-Interscience: 1986; Vol. 34; Chap. pp 115-210.
101. Niedenzu, K.; Trofimenko, S. *Top. Curr. Chem.* **1986**, *131*, 1-37.
102. Trofimenko, S. *Chem. Rev.* **1993**, *93*, 943-979.
103. Trofimenko, S. *J. Am. Chem. Soc.* **1966**, *88*, 1842-1844.
104. Trofimenko, S.; Calabrese, J. C.; Kochi, J. K.; Wolowiec, S.; Hulsbergen, F. B.; Reedijk, J. *Inorg. Chem.* **1992**, *31*, 3943-3950.
105. Cano, M.; Heras, J. V.; Trofimenko, S.; Monge, A.; Gutierrez, E.; Jones, C. J.; McCleverty, J. A. *J. Chem. Soc., Dalton Trans.* **1990**, 3577-3582.
106. Wilkinson, G.; Pauson, P. L.; Birmingham, J. M.; Cotton, F. A. *J. Am. Chem. Soc.* **1953**, *75*, 1011-1012.
107. Jesson, J. P.; Trofimenko, S.; Eaton, D. R. *J. Am. Chem. Soc.* **1967**, *89*, 3148-3158.
108. Trofimenko, S. *J. Am. Chem. Soc.* **1967**, *89*, 3170-3177.
109. Jutzi, P.; Leffers, W.; Müller, G. *J. Organomet. Chem.* **1987**, *334*, C24-C26.
110. Beachley, O. T., Jr; Lees, J. F.; Glassman, T. E.; Churchill, M. R.; Buttrey, L. A. *Organometallics* **1990**, *9*, 2488-2492.
111. Dias, H. V. R.; Jin, W. *Inorg. Chem.* **1996**, *35*, 267-268.
112. Fischer, E. O.; Bittler, K. *Z. Naturforsch.* **1962**, *17B*, 274.
113. Steyn, M. M. d. V.; Singleton, E.; Hietkamp, S.; Liles, D. C. *J. Chem. Soc., Dalton Trans.* **1990**, 2991-2997.

114. Reger, D. L.; Swift, C. A.; Lebioda, L. *Inorg. Chem.* **1984**, *23*, 349-354.
115. Ball, R. G.; Edelmann, F.; Matisons, J. G.; Takats, J.; Marques, N.; Marçalo, J.; Pires de Matos, A.; Bagnall, K. W. *Inorg. Chim. Acta* **1987**, *132*, 137-143.
116. Bielawski, J.; Hodgkins, T. G.; Layton, W. J.; Niedenzu, K.; Niedenzu, P. M.; Trofimenko, S. *Inorg. Chem.* **1986**, *25*, 87-90.
117. Tolman, C. A. *J. Am. Chem. Soc.* **1970**, *92*, 2956-2965.
118. Tolman, C. A. *Chem. Rev.* **1977**, *77*, 313-348.
119. Maitlis, P. M. *Chem. Soc. Rev.* **1981**, *10*, 1-48.
120. Rheingold, A. L.; Ostrander, R. L.; Haggerty, B. S.; Trofimenko, S. *Inorg. Chem.* **1994**, *33*, 3666-3676.
121. Calabrese, J. C.; Domaille, P. J.; Trofimenko, S.; Long, G. J. *Inorg. Chem.* **1991**, *30*, 2795-2801.
122. Trofimenko, S.; Calabrese, J. C.; Thompson, J. S. *Inorg. Chem.* **1987**, *26*, 1507-1514.
123. Trofimenko, S.; Calabrese, J. C.; Domaille, P. J.; Thompson, J. S. *Inorg. Chem.* **1989**, *28*, 1091-1101.
124. Chan, M. K.; Armstrong, W. H. *Inorg. Chem.* **1989**, *28*, 3777-3779.
125. Niedenzu, K.; Nöth, H.; Serwatowska, J.; Serwatowska, J. *Inorg. Chem.* **1991**, *30*, 3249-3254.
126. Atwood, V. O.; Atwood, D. A.; Cowley, A. H.; Trofimenko, S. *Polyhedron* **1992**, *11*, 711-713.
127. Kitajima, N.; Tolman, W. B. *Prog. Inorg. Chem.* **1995**, *43*, 419-531.
128. Parkin, G. *Adv. Inorg. Chem.* **1995**, *42*, 291-393.
129. Bagnall, K. W.; Tempest, A. C.; Takats, J.; Masino, A. P. *Inorg. Nucl. Chem. Letts.* **1976**, *12*, 555-557.
130. Santos, I.; Marques, N. *New J. Chem.* **1995**, *19*, 551-571.
131. Stainer, M. V. R.; Takats, J. *Inorg. Chem.* **1982**, *21*, 4050-4053.
132. Domingos, A.; Marcalo, J.; Marques, N.; Dematos, A. P.; Galvao, A.; Isolani, P. C.; Vicentini, G.; Zinner, K. *Polyhedron* **1995**, *14*, 3067-3076.
133. Masino, A. P. PhD Thesis, University of Alberta, 1978.
134. Reger, D. L.; Lindeman, J. A.; Lebioda, L. *Inorg. Chim. Acta* **1987**, *139*, 71-73.
135. Reger, D. L.; Lindeman, J. A.; Lebioda, L. *Inorg. Chem.* **1988**, *27*, 3923-3929.
136. Reger, D. L.; Knox, S. J.; Lindeman, J. A.; Lebioda, L. *Inorg. Chem.* **1990**, *29*, 416-419.
137. Moffat, W. D.; Stainer, M. V. R.; Takats, J. *Inorg. Chim. Acta* **1987**, *139*, 75-78.
138. Moss, M. A. J.; Jones, C. J. *Polyhedron* **1989**, *8*, 555-558.
139. Moss, M. A. J.; Jones, C. J. *J. Chem. Soc., Dalton Trans.* **1990**, 581-591.
140. Moss, M. A. J.; Jones, C. J.; Edwards, A. J. *Polyhedron* **1988**, *7*, 79-81.
141. Moss, M. A. J.; Jones, C. J.; Edwards, A. J. *J. Chem. Soc., Dalton Trans.* **1989**, 1393-1400.
142. Moss, M. A. J.; Jones, C. J. *Polyhedron* **1989**, *8*, 2367-2370.
143. Kilimann, U.; Edelmann, F. T. *J. Organomet. Chem.* **1994**, *469*, C5-C9.
144. Kilimann, U.; Edelmann, F. T. *J. Organomet. Chem.* **1993**, *444*, C15-C17.

145. Bruin, P.; Booij, M.; Teuben, J. H.; Oskam, A. *J. Organomet. Chem.* **1988**, *350*, 17-23.
146. Schumann, H.; Köhn, R. D.; Reier, F.-W.; Dietrich, A.; Pickardt, J. *Organometallics* **1989**, *8*, 1388-1392.
147. Moss, M. A. J.; Jones, C. J. *Polyhedron* **1990**, *9*, 697-702.
148. Schaverien, C. J. *Adv. Organomet. Chem.* **1994**, *36*, 283-362.
149. Trofimenko, S. *J. Am. Chem. Soc.* **1967**, *89*, 6288-6294.
150. Hamidi, M. E. M.; Pascal, J.-L. *Polyhedron* **1994**, *13*, 1787-1792.
151. Lawrance, G. A. *Chem. Rev.* **1986**, *86*, 17-34.
152. Schumann, H.; Meese-Marktscheffel, J. A.; Dietrich, A. *J. Organomet. Chem.* **1989**, *377*, C5-C8.
153. Schumann, H.; Meese-Marktscheffel, J. A.; Dietrich, A.; Görlitz, F. H. *J. Organomet. Chem.* **1992**, *430*, 299-315.
154. Stehr, J.; Fischer, R. D. *J. Organomet. Chem.* **1992**, *430*, C1-C4.
155. Kilimann, U.; Schafer, M.; Herbstirmer, R.; Edelmann, F. T. *J. Organomet. Chem.* **1994**, *469*, C10-C14.
156. Liu, S.-Y. PhD Thesis, University College London, 1996.
157. Reger, D. L.; Mason, S. S.; Reger, L. B.; Rheingold, A. L.; Ostrande, R. L. *Inorg. Chem.* **1994**, *33*, 1811-1816.
158. Eschaverien, A. M.; Stille, J. K. *J. Am. Chem. Soc.* **1987**, *109*, 5478-5486.
159. Horrocks, W. de W. *J. Am. Chem. Soc.* **1974**, *96*, 3022-3024.
160. Gejji, S. P.; Hermansson, K.; Lindgren, J. *J. Phys. Chem.* **1993**, *97*, 3712-3715.
161. Huang, W.; Wheeler, R. A.; Frech, R. *Spectrochimica Acta* **1994**, *50A*, 985-996.
162. Johnston, D. H.; Shriver, D. F. *Inorg. Chem.* **1993**, *32*, 1045-1047.
163. Frauenhoff, G. R.; Wilson, S. R.; Shapley, J. R. *Inorg. Chem.* **1991**, *30*, 78-85.
164. Clark, E. P. *Ind. Eng. Chem. Ed.* **1941**, *13*, 820.
165. Anderson, O. P.; Packard, A. B. *Inorg. Chem.* **1979**, *18*, 1129-1132.
166. Thewalt, U.; Lasser, W. *Z. Naturforsch.* **1983**, *38B*, 1501-1505.
167. Takats, J.; Zhang, X. W., personal communication.
168. Zhang, X. W. PhD Thesis, University of Alberta, 1995.
169. Marques, N., personal communication.
170. Han, R.; Parkin, G. *Organometallics* **1991**, *10*, 1010-1020.
171. Han, R.; Parkin, G. *J. Am. Chem. Soc.* **1992**, *114*, 748-757.
172. Parkin, G., personal communication.
173. Moss, M. A.; Kresinski, R. A.; Jones, C. J.; Evans, W. J. *Polyhedron* **1993**, *12*, 1953-1955.
174. Tilley, T. D.; Andersen, R. A.; Spencer, B.; Ruben, H.; Zalkin, A.; Templeton, D. H. *Inorg. Chem.* **1980**, *19*, 2999-3003.
175. Tilley, T. D.; Andersen, R. A.; Spencer, B.; Zalkin, A. *Inorg. Chem.* **1982**, *21*, 2647-2649.
176. Wayda, A. L.; Dye, J. L. *Organometallics* **1984**, *3*, 1605-1610.
177. Evans, W. J.; Grate, J. W.; Choi, H. W.; Bloom, I.; Hunter, W. E.; Atwood, J. L. *J. Am. Chem. Soc.* **1985**, *107*, 941-946.

178. Evans, W. J.; Ulibarri, T. A. *Polyhedron* **1989**, *8*, 1007-1014.
179. Swamy, S. J.; Loebel, J.; Pickardt, J.; Schumann, H. *J. Organomet. Chem.* **1988**, *353*, 27-34.
180. Takats, J.; Zhang, X. W.; Day, V.; Eberspacher, T. A. *Organometallics* **1993**, *12*, 4286-4288.
181. Sohrin, Y.; Marsui, M.; Hata, Y.; Hasegawa, H.; Kokusen, H. *Inorg. Chem.* **1994**, *33*, 4376-4383.
182. Dutremez, S. G.; Leslie, D. B.; Streib, W. E.; Chisholm, M. H.; Caulton, K. G. *J. Organomet. Chem.* **1993**, *462*, C1-C2.
183. Belderraín, T.; Contreras, L.; Paneque, M.; Carmona, E.; Monge, A.; Ruiz, C. *J. Organomet. Chem.* **1994**, *474*, C5-C7.
184. Reger, D. L.; Huff, M. F.; Rheingold, A. L.; Haggerty, B. S. *J. Am. Chem. Soc.* **1992**, *114*, 579-584.
185. Reger, D. L.; Mason, S. S.; Rheingold, A. L.; Ostrander, R. L. *Inorg. Chem.* **1993**, *32*, 5216-5222.
186. Oliver, J. D.; Mullica, D. F.; Hutchinson, B. B.; Milligan, W. O. *Inorg. Chem.* **1980**, *19*, 165-169.
187. Sohrin, Y.; Hokusen, H.; Kihara, S.; Matsui, M.; Kushi, Y.; Shiro, M. *J. Am. Chem. Soc.* **1993**, *115*, 4128-4136.
188. Cotton, F. A.; Wilkinson, G. *Advanced Inorganic Chemistry;* fourth ed.; Wiley Interscience: New York, 1980.
189. Evans, W. J.; Ulibarri, T. A.; Chamberlain, L. R.; Ziller, J. W.; Alvarez, D. *Organometallics* **1990**, *9*, 2124-2130.
190. Burns, C. J.; Andersen, R. A. *J. Chem. Soc., Chem. Commun.* **1989**, 136-137.
191. Dönges, E. in *Handbook of Preparative Inorganic Chemistry*; second ed.; G. Brauer, Ed.; Academic Press: New York, 1963; Vol. 1; Chap. 16; pp 877-878.
192. Taylor, E. C.; Hawks, G. H., III; McKillop, A. *J. Am. Chem. Soc.* **1968**, *90*, 2421-2422.
193. Jeffrey, J. C.; Kurek, S. S.; McCleverty, J. A.; Psillakis, E.; Richardson, R. M.; Ward, M. D.; Wlodarczyk, A. *J. Chem. Soc., Dalton Trans.* **1994**, 2559-2564.
194. Amoroso, A. J.; Thompson, A. M. C.; Jeffery, J. C.; Jones, P. L.; McCleverty, J. A.; Ward, M. D. *J. Chem. Soc., Chem. Commun.* **1994**, 2751-2752.
195. Amoroso, A. J.; Jeffery, J. C.; Jones, P. L.; McCleverty, J. A.; Rees, L.; Rheingold, A. L.; Sun, Y. M.; Takats, J.; Trofimenko, S.; Ward, M. D.; Yap, G. P. A. *J. Chem. Soc., Chem. Commun.* **1995**, 1881-1882.
196. Martin, W. C.; Zalubas, R.; Hagan, L. *Atomic Energy Levels - the Rare Earth Elements, the Spectra of Lanthanum, Cerium, Praseodymium, Neodymium, Promethium, Samarium, Europium, Gadolinium, Terbium, Dysprosium, Holmium, Erbium, Thulium, Ytterbium and Lutetium*; NSRDS-NBS 60: 1978.
197. Longley, K. Part II Thesis, University of Oxford, 1994.
198. Eland, J. H. D. *Photoelectron Spectroscopy;* second ed.; Butterworths: London, 1984.
199. Koopmans, T. *Physica* **1934**, *1*, 104-113.
200. Cox, P. A. *Structure and Bonding* **1975**, *24*, 59-81.

201. Yeh, J. J.; Lindau, I. *Atomic Data and Nuclear Data Tables* **1985**, *32*, 1-55.
202. Bruno, G.; Centineo, G.; Ciliberto, E.; Di Bella, S.; Fragalà, I. *Inorg. Chem.* **1984**, *23*, 1832-1836.
203. Lovell-Smith Part II Thesis, University of Oxford, 1986.
204. Evans, W. J.; Grate, J. W.; Hughes, L. A.; Zhang, H.; Atwood, J. L. *J. Am. Chem. Soc.* **1985**, *107*, 3728-3730.
205. Nolan, S. P.; Marks, T. J. *J. Am. Chem. Soc.* **1989**, *111*, 8538-8540.
206. Evans, W. J.; Ulibarri, T. A.; Ziller, J. W. *J. Am. Chem. Soc.* **1990**, *112*, 219-223.
207. Chappell, J. S.; Bloch, A. N.; Bryden, W. A.; Maxfield, M.; Poehler, T. O.; Cowan, D. O. *J. Am. Chem. Soc.* **1981**, *103*, 2442-2443.
208. van Duyne, R. P.; Cape, T. W.; Suchanski, M. R.; Siedle, A. R. *J. Phys. Chem.* **1986**, *90*, 739-743.
209. Miller, J. S. *Science* **1987**, *235*, 871-873.
210. Miller, J. S.; Calabrese, J. C.; Rommelmann, H.; Chittapeddi, S. R.; Zhang, J. H.; Reiff, W. M.; Epstein, A. J. *J. Am. Chem. Soc.* **1987**, *109*, 769-781.
211. Hope, H. *Prog. Inorg. Chem.* **1992**, *41*, 1-19.
212. Becker, P.; Coppens, P.; Ross, F. K. *J. Am. Chem. Soc.* **1973**, *95*, 7604-7609.
213. Miller, F. A.; Sala, O.; Devlin, P.; Overend, J.; Lippert, E.; Lüder, W.; Moser, H.; Varchmin, J. *Spectrochimica Acta* **1964**, *20*, 1233-1247.
214. Dixon, D. A.; Calabrese, J. C.; Miller, J. S. *J. Am. Chem. Soc.* **1986**, *108*, 2582-2588.
215. Dixon, D. A.; Miller, J. S. *J. Am. Chem. Soc.* **1987**, *109*, 3656-3664.
216. Kaim, W.; Moscherosch, M. *Coord. Chem. Rev.* **1994**, *129*, 157-193.
217. Mason, S. J.; Hill, C. M.; Murphy, V. J.; O'Hare, D.; Watkin, D. J. *J. Organomet. Chem.* **1995**, *485*, 165-171.
218. Carvalho, A.; Domingos, A.; Gaspar, P.; Marques, N.; Pires de Matos, A.; Santos, I. *Polyhedron* **1992**, *11*, 1481-1488.
219. Liu, S.-Y.; Sella, A.; Day, V. W., unpublished work.
220. Liu, S.-Y.; Sella, A.; Elsegood, M., unpublished work.
221. Zhang, X. W.; Loppnow, G. R.; McDonald, R.; Takats, J. *J. Am. Chem. Soc.* **1995**, *117*, 7828-7829.
222. Goodgame, D. M. L.; Hitchman, M. A. *Inorg. Chem.* **1965**, *4*, 721-725.
223. Finney, A. J.; Hitchman, M. A.; Raston, C. L.; Rowbottom, G. L.; White, A. H. *Aust. J. Chem.* **1981**, *34*, 2159-2176.
224. Wu, Z. Z.; Xu, Z. N.; You, X. Z.; Wang, H. Q.; Zhou, X. G.; Sheng, F. R.; Hu, J. P. *J. Organomet. Chem.* **1993**, *455*, 93-97.
225. Kay, M. I.; Frazer, B. C. *Acta Cryst.* **1961**, *14*, 56-57.
226. Weston, R. E., Jr; Brodasky, T. F. *J. Chem. Phys.* **1957**, *27*, 683-689.
227. Ruggierio, C. E.; Carrier, S. M.; Tolman, W. B. *Angew. Chem. Int. Ed. Engl.* **1994**, *33*, 895-897.
228. Evans, W. J.; Grate, J. W.; Bloom, I.; Hunter, W. E.; Atwood, J. L. *J. Am. Chem. Soc.* **1985**, *107*, 405-409.
229. Evans, W. J.; Drummond, D. K.; Chamberlain, L. R.; Doedens, R. J.; Bott, S. G.; Zhang,

H.; Atwood, J. L. *J. Am. Chem. Soc.* **1988**, *110*, 4983-4994.
230. Hillier, A.; Sella, A., work in progress.
231. Hillier, A.; Liu, S.-Y.; Sella, A.; Zekria, O.; Elsegood, M. *J. Organomet. Chem.* **1996**, submitted.
232. Swamy, S. J.; Schumann, H. *J. Organomet. Chem.* **1987**, *334*, 1-7.
233. Evans, W. J.; Drummond, D. K.; Zhang, H. M.; Atwood, J. L. *Inorg. Chem.* **1988**, *27*, 575-579.
234. Duncalf, D. J.; Hitchcock, P. B.; Lawless, G. A. *J. Chem. Soc., Chem. Comm.* **1996**, 269-271.
235. Hasinoff, L.; Takats, J.; Zhang, X. W.; Bond, A. H.; Rogers, R. D. *J. Am. Chem. Soc.* **1994**, *116*, 8833-8834.
236. Evans, W. J.; Foster, S. E. *J. Organomet. Chem.* **1992**, *433*, 79-94.
237. Evans, W. J.; Rabe, G. W.; Ziller, J. W. *Inorg. Chem.* **1994**, *33*, 3072-3078.
238. Hou, Z.; Wakatsuki, Y. *J. Chem. Soc., Chem. Commun.* **1994**, 1205-1206.
239. Evans, W. J.; Gummersheimer, T. S.; Ziller, J. W. *J. Am. Chem. Soc.* **1995**, *117*, 8999-9002.
240. van den Hende, J. R.; Hitchcock, P. B.; Holmes, S. A.; Lappert, M. F.; Leung, W.-P.; Mak, T. C. W.; Prashar, S. *J. Chem. Soc., Dalton Trans.* **1995**, 1427-1433.
241. Berry, R. S. *J. Chem. Phys.* **1960**, *32*, 933-938.
242. Reger, D. L.; Tarquine, M. E. *Inorg. Chem.* **1983**, *22*, 1064-1068.
243. Zhang, X. W.; McDonald, R.; Takats, J. *New J. Chem.* **1995**, *19*, 573-585.
244. Watson, P. L. *J. Chem. Soc., Chem. Commun.* **1980**, 652-653.
245. Brewer, M.; Khasnis, D.; Buretea, M.; Berardini, M.; Emge, T. J.; Brennan, J. G. *Inorg. Chem.* **1994**, *33*, 2743-2747.
246. Günther, H. *NMR Spectroscopy;* second ed.; Wiley: Chichester, 1995.
247. Santos, I.; Marques, N.; Pires de Matos, A. *Inorg. Chim. Acta* **1987**, *139*, 89-90.
248. Santos, I.; Marçalo, J.; Marques, N.; Pires de Matos, A. *Inorg. Chim. Acta* **1987**, *134*, 315-320.
249. Domingos, A.; Marçalo, J.; Pires de Matos, A. *Polyhedron* **1992**, *11*, 909-915.
250. Domingos, A.; Pires de Matos, A.; Santos, I. *Polyhedron* **1992**, *11*, 1601-1606.
251. Dolphin, D.; Wick, A. E. *Tabulation of Infrared Spectral Data*; Wiley: New York, 1977.
252. Elschenbroich, C.; Salzer, A. in ; VCH: Weinheim, 1992; Chap. 14; pp 240-241.
253. Evans, W. J.; Drummond, D. K. *Organometallics* **1988**, *7*, 797-802.
254. Evans, W. J.; Drummond, D. K.; Hughes, L. A.; Zhang, H. M.; Atwood, J. L. *Polyhedron* **1988**, *7*, 1693-1703.
255. Fischer, E. O.; Fischer, H. *J. Organomet. Chem.* **1966**, *6*, 141-148.
256. von Ammon, R.; Fischer, R. D.; Kanellakopulos, B. *Chem. Ber.* **1971**, *104*, 1072-1087.
257. Burns, J. H.; Baldwin, W. H. *J. Organomet. Chem.* **1976**, *120*, 361-368.
258. Han, R.; Looney, A.; Parkin, G. *J. Am. Chem. Soc.* **1989**, *111*, 7276-7278.
259. *Experimental Organometallic Chemistry: A Practicum in Synthesis and Characterisation*; McNally, S.; Cooper, N. J., Ed.; American Chemical Society: Washington DC, 1987; Vol. 357, ACS Symposium Series.

260. Shriver, D. F.; Drezdon, M. A. *The Manipulation of Air-Sensitive Compounds;* second ed.; Wiley: New York, 1986.
261. Sheldrick, G. M. In University of Göttingen, Germany, 1986; pp .
262. Girard, P.; Namy, G. L.; Kagan, H. B. *J. Am. Chem. Soc.* **1980**, *102*, 2693-2698.
263. *Inorg. Synth.*; A. P. Ginsberg, Ed.; Wiley-Interscience: New York, 1990; Vol. 27; Chap. 4; pp 137-181.
264. Swamer, F. W.; Hauser, C. R. *J. Am. Chem. Soc.* **1950**, *72*, 1352-1356.
265. Cloke, F. G. N., personal communication.
266. Hitchcock, P. B.; Lappert, M. F.; Leung, W.-P.; Diansheng, L.; Shun, T. *J. Chem. Soc., Chem. Commun.* **1993**, 1386-1387.
267. Shun, T. DPhil Thesis, University of Sussex, 1995.
268. Chebolu, V.; Whittle, R. R.; Sen, A. *Inorg. Chem.* **1985**, *24*, 3082-3085.
269. Sen, A.; Chebolu, V.; Rheingold, A. L. *Inorg. Chem.* **1987**, *26*, 1821-1823.
270. White, J. P., III; Deng, H.; Boyd, E.; Gallucci, J.; Shore, S. G. *Inorg. Chem.* **1994**, *33*, 1685-1694.